August 4, 2006

To the Graduate School:

This dissertation entitled "Field Measurements and Wind Tunnel Simulation of Hurricane Wind Loads on Single Family Dwellings" and written by Zhuzhao Liu is presented to the Graduate School of Clemson University. I recommend that it be accepted in partial fulfillment of the requirements for the degree of Doctor of Philosophy with a major in Civil Engineering.

_____
Dr. David O. Prevatt, Dissertation Advisor

We have reviewed this dissertation
and recommend its acceptance:

_____
Dr. Timothy A. Reinhold

_____
Dr. C. Hsein Juang

_____
Dr. Ronald D. Andrus

Accepted for the Graduate School:

_____

FIELD MEASUREMENTS AND WIND TUNNEL SIMULATION OF HURRICANE WIND LOADS ON SINGLE FAMILY DWELLINGS

A Dissertation

Presented to

the Graduate School of

Clemson University

In Partial Fulfillment

of the Requirements for the Degree

Doctor of Philosophy

Civil Engineering

---

by

Zhuzhao Liu

August 2006

Advisor: Dr. David O. Prevatt

ABSTRACT

Recent damage occurring during hurricane activity has demonstrated the urgent need to improve the hurricane-resistance of constructed facilities, particularly for residential buildings which continue to bear a disproportionately high portion of the economic losses. The economic losses due to hurricanes can be mitigated by improving the structural performance of buildings, and this requires us to improve our understanding of hurricane wind loads on houses.

In response to this need, through the Florida Coastal Monitoring Program (FCMP), a residential building, named as House FL-27, was instrumented during Tropical Storm Isidore (2002) and Hurricane Ivan (2004). The wind pressure instrumentation successfully recorded high-resolution wind pressures on this single family house from two storms. This dissertation presents the methods developed to analyze the extreme wind loads measured on House FL-27. The uncertainties of the full-scale measurement system associated with corrections for reference pressures, temperature variations, and calibration errors are analyzed. Once corrected, the full-scale test results are used to evaluate the ability of the wind tunnel simulation methods to reproduce model-scale wind pressure results comparable to full-scale extreme wind loads. Probability density functions of wind pressure fluctuations and the effects of spatial and time averaging on the peak wind loads are investigated based on full-scale and wind tunnel test results. Through comparison of full-scale and wind tunnel test results with the provisions of the current wind load design code, ASCE 7-05, the design wind

loads on the critical roof corner areas of the subject house are assessed. The effects of terrain exposures and surrounding houses on wind loads are also investigated as part of this study.

DEDICATION

I dedicate this thesis to my father Yuxin Liu, my mother Zhen Liu, and my wife Lingrong Gu.

ACKNOWLEDGEMENTS

I would like to express my gratitude to everyone who has dedicated time and effort to the completion of my research and dissertation. First and foremost, I would like to thank Dr. David O. Prevatt and Dr. Timothy A. Reinhold for offering me the opportunity to study at Clemson University and for their guidance, support, and patience throughout this entire research effort. Thanks also go to Dr. Hsein Juang and Dr. Ronald D. Andrus for their advice on my thesis and for serving on my committee.

I also wish to thank Dr. Kurt R. Gurley of the University of Florida, Dr. Quan Yong of the Tokyo Polytechnic University, Dr. Rujin Ma of the Tongji University, and Dr. Xianfei He of the University of California at San Diego. Their advice greatly enriched my work. Many thanks are extended to Mr. Scott Kaufman, Mr. Cos Gardner and my follow Wind Load Test Facility student Bo Cui, Peter Datin, Kenneth Hill, Kalin Bost at Clemson University. I also want to extend my appreciation to Mr. Luis Aponte who is from the University of Florida for his support.

Finally, I would like to gratefully acknowledge support from the National Institute of Standards and Technology (NIST), the South Carolina Sea Grant Consortium, and the Florida Coastal Monitoring Program, which is funded by the Florida Department of Community Affairs.

TABLE OF CONTENTS

Page

TITLE PAGE..... i

ABSTRACT..... ii

DEDICATION..... iv

ACKNOWLEDGEMENTS v

LIST OF TABLE..... ix

LIST OF FIGURES xii

CHAPTERS

1. INTRODUCTION..... 1

1.1 General background..... 1
1.2 Research Objectives..... 6
1.3 Dissertation Structure..... 7

2. LITERATURE REVIEW..... 8

2.1 Full-Scale Tests of Wind Loads on Low-rise Buildings..... 8
2.2 Validation of Wind Tunnel Methodologies for Simulating Wind Loads on Low-rise Buildings..... 18
2.3 Wind Tunnel Tests of Extreme Wind Loads on Low-rise Buildings..... 20
2.4 Wind Load Code for Low-rise Buildings..... 24

3. WIND TUNNEL SETTINGS AND MEASUREMENT INSTRUMENTS..... 26

3.1 Wind Load Test Facility at Clemson University..... 26
3.2 Wind Tunnel Configurations of 1:50 Open and Suburban Terrain Exposure..... 27
3.3 Data Acquisition System..... 28
3.4 Flow Characteristics of Wind Tunnel Exposure Configurations 31
3.5 Procedures of Calculating Pressure Coefficients..... 37

Table of Contents (Continued)

Page

4. FIELD MEASUREMENT OF HURRICANE WIND LOADS ON HOUSE FL-27 42

4.1 Description of Experimental Building and Site 42
4.2 Signal Detection and Preconditioning 46
4.3 Analysis Methodology of Wind Loads Recorded by the House Instrumentation System 48
4.4 Wind Speeds and Wind Directions at Mean Roof Height of FL-27 House 52
4.5 Determination of Extreme Wind Loads on FL-27 House Roof 57
4.6 Turbulence Intensity, Integral Length Scale and Wind Velocity Spectra 61
4.7 Summary 68

5. VALIDATION OF FULL-SCALE TEST RESULTS OF HOUSE FL-27 69

5.1 Sensitivity Analysis for Basic Parameters 69
5.2 Uncertainty Analysis of Wind Loads Measured by the House Instrumentation System 74
5.3 Effects of the Choice of Mobile Tower Records as the Reference Pressure 78
5.4 Probability Density Function (PDF) of the Fluctuating Wind Pressures 80
5.5 Spatial and Time-Averaged Effects on Peak Pressures Peak Pressures 84
5.6 Summary 93

6. WIND TUNNEL SIMULATION OF HURRICANE WIND LOAD ON HOUSE FL-27 94

6.1 House Model and Wind Tunnel Setting 97
6.2 Wind Tunnel Simulation Results of House FL-27 Model 99
6.3 Comparison of Wind Tunnel Simulation with Field Measurement Results 104
6.4 Influences of Neighborhood Houses and Terrain Exposures on Wind Loads 113
6.5 Design Wind loads on House FL-27 116
6.6 Summary 126

Table of Contents (Continued)

Page

7. INVESTIGATION OF THE INFLUENCES OF TERRAIN EXPOSURES AND NEIGHBORHOODS ON WIND LOADS ON LOW-RISE BUILDINGS..... 128

7.1 Experimental Models and Set-up..... 129
7.2 The Influences of Terrain Exposures..... 136
7.3 The Influence of Surrounding Houses..... 139
7.4 Summary..... 145

8. CONCLUSIONS AND RECOMMENDATIONS..... 146

8.1 Conculsion..... 146
8.2 Recommendations for Future Research..... 148

APPENDICES..... 150

A. Lists of 15-minute Records of House FL-27 Full-scale Tests during Tropical Storm (2002) and Hurricane Ivan (2004)..... 151
B. Source Program for Analyzing Full-scale Records of the House Instrumentation System..... 156
C. Uncertainty Analysis of the Wind Loads Measured during Hurricane Ivan..... 160
D. Measured and Predicted 15-minute PDF of Pressure coefficient of Individual Channels Measured in Hurricane Ivan..... 166
E. Effect of Averaging Period on the Peak Factors of Individual Channels..... 177
F. Comparison of Area-Averaged Negative Peak Pressure Coefficients to the Corresponding Values of Individual Channels..... 188
G. Area-averaged Pressure Coefficients of Critical Roof Corner Areas..... 195

BIBLIOGRAPHY..... 206

LIST OF TABLES

Table Page

1.1 2004 and 2005 US Hurricane Losses 2

3.1 Surface Roughness Categories, Extension and Typical Values (Simiu and Scanlan, 1992) 32

3.2(a) Expected Values of Integral Length Scale 36

3.2(b) Integral Length Scale of Turbulence in 1:50 Open Country Setting 36

3.2(c) Integral Length Scale of Turbulence in 1:50 Suburban Terrain Setting 36

3.3 Values of β Corresponding to Various Roughness Lengths (Simiu and Scanlan, 1992) 39

3.4 Coefficient of $C(t)$ (Simiu and Scanlan, 1992 39

3.5 Ratio of Mean Wind Speed and 3-second Gust Wind Speed at Mean Roof Heights 39

3.6 Adjustment Factors ϕ for 1:50 Suburban Terrain Exposure Setting 41

3.7 Adjustment Factor ϕ for 1:50 Open Country Exposure Setting Exposure Setting 41

4.1(a) The Calculation of 3-second Gust Wind Speed $U_{3-\sec}$ at Mean Roof Height Based on 15-minute Mean Wind Speed Measured by The House Anemometers 56

4.1(b) The Calculation of 3-second Gust Wind Speed $U_{3-\sec}$ at Mean Roof Height Based on 15-minute Mean Wind Speed at 10 m Height Measured by The Mobile Towers 56

List of Tables (Continued)

Table Page

4.2 Main Parameters Used in the Process of House Instrumentation System Records..... 57

4.3(a) Turbulence Intensities Measured by the House Instrumentation Systems the House Instrumentation Systems..... 63

4.3(b) The Turbulence Intensities Measured by the Mobile Tower Systems near House FL-27..... 63

4.4 The Integral Length Scales Measured by the Mobile Tower Systems near House FL-27 63

5.1 Summary of Sensitivity Factors of Random Variables in the Calculation of Wind Pressure $p_{i-15\min}$ by the House Instrumentation System..... 73

5.2 Summary of Mean and Standard Deviation of Random Variables in the Calculation of Wind Pressure $p_{i-15\min}$ by the House Instrumentation System..... 73

5.3 Summary of Channel Numbers of Each Roof Corner Divisions Divisions..... 88

6.1 Measurement Configurations and Data Acquisition of Wind Tunnel Model Study of House FL-27..... 99

6.2(a) 15-minute Mean Incident Wind Directions and Wind Speeds at House FL-27 Roof Height in Tropical Storm Isidore..... 100

6.2(b) 15-minute Mean Incident Wind Directions and Wind Speeds at House FL-27 Roof Height in Hurricane Ivan..... 100

6.3 Averaged Difference across All Taps of the Mean, Peak Minimum and Maximum Pressure Coefficients between the Model and House FL-27..... 108

List of Tables (Continued)

Table Page

6.4 ASCE 7-05 Design Wind Loads on House FL-27 Critical Corner Areas..... 122

6.5 Summary of Methods for Calculating External Design Wind Loads on House FL-27 Roof Corner Areas..... 124

7.1 Main Test Parameters of Wind Tunnel Tests for the Investigation of the Influences of Terrain Exposures..... 130

7.2 Main Test Parameters of Wind Tunnel Tests for the Investigation of the Influences of Surrounding Houses..... 130

7.3 Dimensionless Ratio A_f / s of Roughness Element Spacing Density for Different Density of Surrounding Houses..... 140

7.4 Dimensionless Ratio A_f / s of Roughness Element Spacing Density for Three Sets of Surrounding Houses for Eight Wind Directions..... 141

C.1 Simulated Mean Values and Standard Deviations of Peak Negative Wind Pressure Measured in Hurricane Ivan Considering the Effects of Random Variables..... 160

C.2 Simulated Mean Values and Standard Deviations of Mean Wind Pressure Measured in Hurricane Ivan Considering the Effects of Random Variables..... 162

C.3 Simulated Mean Values and Standard Deviations of Peak Positive Wind Pressure Measured in Hurricane Ivan Considering the Effects of Random Variables..... 164

LIST OF FIGURES

Figure		Page
2.1	Aylesbury Experimental Building and Pressure Transducer Locations (Sill et al, 1989, Holmes, 2001).....	10
2.2	The WERFL Building and the Meteorological Tower (Levitan and Mehta, 1992).....	12
2.3	The FCMP Mobile Tower Systems (FCMP Website, 2005).....	15
2.4	The FCMP House Instrumentation System (FCMP Website, 2005).....	16
2.5	Locations of FCMP participant homes in Florida (Gurley et al, 2005).....	17
3.1(a)	Wind Tunnel Settings of 1:50 Open Country.....	27
3.1(b)	Wind Tunnel Settings of 1:50 Suburban Terrain.....	28
3.2	Photo of ZOC33/64Px Model (Scanivalve Corporation, 2004).....	29
3.3	Photo of RAD3200 with 8 A/D modules (Scanivalve Corporation, 2004)	30
3.4	RAD3200 System with Extended USB (Scanivalve Corporation, 2004)	31
3.5(a)	Velocity and Turbulence Intensity Profile for 1:50 Open Country Wind Tunnel Setting.....	33
3.5(b)	Velocity and Turbulence Intensity Profile for 1:50 Suburban Terrain Wind Tunnel Setting.....	33
3.6	Determination of Longitudinal Integral Length Scale	35
4.1	Aerial View of House FL-27(top), Mobile Tower T1 (Hurrican Ivan, 2004-Bottom Right) and Mobile Tower T2 (Tropical Storm Isidore, 2002-Bottom Left)	43

List of Figures (Continued)

Figure Page

4.2(a) House FL-27 Photos..... 44

4.2(b) House FL-27 Roof Plan..... 45

4.3 The Power Spectrum Density of the Fluctuation Component of the Original 15-minute Records of Channel 9 and Channel 10 Measured in The Hurricane Ivan (A 15-minute House Record No.137)..... 47

4.4 The Power Spectrum Density of the Fluctuation Component of the Filtered 15-minute Records of Channel 9 and Channel 10 Measured in The Hurricane Ivan (A 15-minute House Record No.137)..... 47

4.5 Flow Chart of Program to Analyze Full-scale Data Recorded by The House Instrumentation System..... 51

4.6(a) 15-minute Mean Wind Speeds and Mean Wind Directions Measured by the House Instrumentation System during Tropical Storm Isidore..... 53

4.6(b) 15-minute Mean Wind Speeds and Mean Wind Directions Measured by the Mobile Tower System during Tropical Storm Isidore..... 53

4.7(a) 15-minute Mean Wind Speeds and Mean Wind Directions Measured by the House Instrumentation System during Hurricane Ivan..... 54

4.7(b) 15-minute Mean Wind Speeds and Mean Wind Directions Measured by the Mobile Tower System during Hurricane Ivan..... 54

4.8(a) Peak Negative Pressure Coefficients on FL-27 House Roof Measured in Tropical Storm Isidore (The Data Sets Recorded from (Sampling frequency = 100Hz and Low-passed: 25 Hz)..... 58

List of Figures (Continued)

Figure Page

4.8(b) Peak Positive Pressure Coefficients on FL-27 House Roof Measured in Tropical Storm Isidore (Sampling frequency = 100Hz and Low-passed: 25 Hz)…… 59

4.9(a) Peak Negative Pressure Coefficients on FL-27 House Roof Measured in Hurricane Ivan (Sampling frequency = 100Hz and Low-passed: 25 Hz)…… 59

4.9(b) Peak Postive Pressure Coefficients on FL-27 House Roof Measured in Hurricane Ivan (Sampling frequency = 100Hz and Low-passed: 25 Hz) …… 60

4.10(a) Normalized Spectrum of the Longitudinal Velocity Component Recorded by the 5 m Gill Anemometer of the Mobile Tower T2 in Tropical Storm Isidore and the Corresponding Von Karman Spectrum…… 64

4.10(b) Normalized Spectrum of the Lateral Velocity Component Recorded by the 5 m Gill Anemometer of the Mobile Tower T2 in Tropical Storm Isidore and the Corresponding Von Karman Spectrum…… 64

4.10(c) Normalized Spectrum of the Longitudinal Velocity Component Recorded by the 10 m Gill Anemometer of the Mobile Tower T2 in Tropical Storm Isidore and the Corresponding Von Karman Spectrum…… 65

4.10(d) Normalized Spectrum of the Lateral Velocity Component Recorded by the 10 m Gill Anemometer of the Mobile Tower T2 in Tropical Storm Isidore and the Corresponding Von Karman Spectrum…… 65

4.11(a) Normalized Spectrum of the Longitudinal Velocity Component Recorded by the 5 m Gill Anemometer of the Mobile Tower T1 in Hurricane Ivan and the Corresponding Von Karman Spectrum…… 66

List of Figures (Continued)

Figure Page

4.11(b) Normalized Spectrum of the Lateral Velocity Component Recorded by the 5 m Gill Anemometer of the Mobile Tower T1 in Hurricane Ivan and the Corresponding Von Karman Spectrum..... 66

4.11(c) Normalized Spectrum of the Longitudinal Velocity Component Recorded by the 10 m Gill Anemometer of the Mobile Tower T1 in Hurricane Ivan and the Corresponding Von Karman Spectrum..... 67

4.11(d) Normalized Spectrum of the Lateral Velocity Component Recorded by the 10 m Gill Anemometer of the Mobile Tower T1 in Hurricane Ivan and the Corresponding Von Karman Spectrum..... 67

5.1 Normal Probability Distribution for 15-Minute Mean and Peak Wind Pressure of Channel 2..... 76

5.2 Worst Negative and Positive Wind Pressure Coefficients with the Confidence Level of 95% on the FL-27 House Measured (Sampling frequency = 100Hz, Low-pass = 25 Hz)..... 76

5.3 Comparison of Peak Wind Pressure Coefficients by Using the House Instrumentation System and the Mobile Tower System Records (Sampling frequency = 100Hz, Low-pass = 25 Hz)..... 79

5.4 Probability Density Function for *u* Component of Velocity Measured on House FL-27 Roof Height by the House Instrumentation System in Hurricane Ivan..... 81

5.5 Measured and Predicted 15-minute PDF of Pressure Coefficient of Chan_02 and Chan-28 Measured in Hurricane Ivan..... 83

5.6(a) Effect of Averaging Period on the Peak Factor of Channel 3..... 85

5.6(b) Effect of Averaging Period on the Peak Factor of Channel 20..... 86

List of Figures (Continued)

Figure Page

5.6(c) Effect of Averaging Period on the Peak Factor of Channel 28 86

5.7 Locations of Areas for Analyzing the Area-Averaged Effects 88

5.8(a) Comparison of Area-averaged Negative Peak Pressure Coefficients to the Corresponding Values of Individual Channels within Area 1 89

5.8(b) Comparison of Area-averaged Negative Peak Pressure Coefficients to the Corresponding Values of Individual Channels within Area 2 90

5.8(c) Comparison of Area-averaged Negative Peak Pressure Coefficients to the Corresponding Values of Individual Channels within Area 3 90

5.9(a) Effect of Averaging Period on the Peak Factor of Area 1 91

5.9(b) Effect of Averaging Period on the Peak Factor of Area 2 92

5.9(c) Effect of Averaging Period on the Peak Factor of Area 3 92

6.1 Arrangement of Taps on House FL-27 Model Roof 96

6.2 Photo of 1:50 Scale Model of House FL-27 96

6.3 House FL-27 Model within Simulated Surrounding Houses under 1:50 Suburban Terrain Exposure 97

6.4(a) Pressure Coefficients of the House FL-27 Model Test to Simulate the Wind Load of Tropical Storm Isidore 102

6.4(b) Pressure Coefficients of the House FL-27 Model Test to Simulate the Wind Load of Hurricane Ivan 102

List of Figures (Continued)

Figure Page

6.5 Peak Negative Pressure Coefficients on House FL-27 Model Roof..... 103

6.6(a) Comparison of Pressure Coefficients of Full-scale Tests (Tropical Storm Isidore) with Wind Tunnel Tests at Wind Incident Direction = 125° 105

6.6(b) Comparison of Pressure Coefficients of Full-scale Tests (Hurricane Ivan) with Wind Tunnel Tests at Wind Incident Direction = 125° 105

6.7(a) Linear Regression Analyses of Peak Negative Pressure Coefficients of Full-Scale and Wind Tunnel Simulation Tests..... 106

6.7(b) Linear Regression Analyses of Mean Pressure Coefficients of Full-Scale and Wind Tunnel Simulation Tests..... 106

6.7(c) Linear Regression Analyses of Peak Positive Pressure Coefficients of Full-Scale and Wind Tunnel Simulation Tests..... 107

6.7(d) Linear Regression Analyses of RMS of Pressure Coefficients of Full-Scale and Wind Tunnel Simulation Tests..... 107

6.8(a) Comparison of Adjusted Pressure Coefficients of Full-scale Tests (Tropical Storm Isidore) with Wind Tunnel test at Wind Incident Direction = 125° 110

6.8(b) Comparison of Adjusted Pressure Coefficients of Full-scale Tests (Hurricane Ivan) with Wind Tunnel test at Wind Incident Direction = 125° 111

6.9(a) Comparison of PDF of Channel 2 of Full-scale Test (Hurricane Ivan) with Wind Tunnel test at Wind Incident Direction = 125° 111

6.9(b) Comparison of PDF of Channel 3 of Full-scale Test (Hurricane Ivan) with Wind Tunnel test at Wind Incident Direction = 125° 112

6.9(c) Comparison of PDF of Channel 9 of Full-scale Test (Hurricane Ivan) with Wind Tunnel test at Wind Incident Direction = 125° 112

List of Figures (Continued)

Figure Page

6.10(a) Comparison of Largest Peak Pressure Coefficients Measured under 1:50 Suburban Terrain Exposure with and without Surrounding Houses for All Directions 114

6.10(b) Comparison of Peak Pressure Coefficients Measured under 1:50 Suburban Terrain Exposure with and without Surrounding Houses for Wind Incident Directions = 125° 115

6.11 Comparison of Largest Peak Pressure Coefficients for All Directions Measured under 1:50 Suburban Terrain and Open Country Exposures 115

6.12 Comparison of Largest Peak Pressures of Twenty Four Sensors of Full-scale Test Results with ASCE 7-05 Provision Values 118

6.13(a) Comparison of Area-averaged Peak Pressures of the Specific Areas (Tropical Storm Isidore) with ASCE 7-05 Provision Values..... 119

6.13(b) Comparison of Area-averaged Peak Pressures of the Specific Areas (Hurricane Ivan) with ASCE 7-05 Provision Values..... 120

6.14 Comparison of Largest Peak Pressures of Twenty Four Sensors for All Directions (Wind tunnel tests) with ASCE 7-05 Provision Values..... 121

6.15 Division of Critical Roof Corner Areas of House FL-27 Model..... 122

6.16 Comparison of the External Negative Simulated Design Wind Loads on Roof Corner Areas with ASCE 7-05 Design Load..... 125

7.1(a) Photo, Arrangement of Test Points and Divisions of Roof of 1:50 Scale FIU Model 1 (Model Basic Size: $L \times W \times H$ = 371 mm $\times$ 218 mm $\times$ 114 mm, and 445 Test Points Arranged on the Model Roof)..... 131

List of Figures (Continued)

Figure Page

7.1(b) Photo, Arrangement of Test Points and Divisions of Roof of 1:50 Scale FIU Model 2 (Model Basic Size: L × W × H = 340 mm × 267 mm × 218 mm, and 218 Test Points Arranged on the Model Roof) 132

7.1(c) Photo, Arrangement of Test Points and Divisions of Roof of 1:50 Scale FIU Model 2 (Model Basic Size: L × W × H = 366 mm × 257 mm × 122 mm, and 404 Test Points Arranged on the Model Roof) 133

7.2(a) Arrangement of Turntable for High Density Surrounding Houses..... 134

7.2(b) Arrangement of Turntable for Medium Density Surrounding Houses..... 134

7.2(c) Arrangement of Turntable for Low Density Surrounding Houses..... 135

7.3(a) Comparisons and Linear Regression Analysis of Peak Negative Pressure Coefficients on Zone 3 of FIU Series House Models 137

7.3(b) Comparisons and Linear Regression Analysis of Peak Negative Pressure Coefficients on Zone 2 of FIU Series House Models..... 137

7.3(c) Comparisons and Linear Regression Analysis of Peak Negative Pressure Coefficients on Zone 1 of FIU Series House Models..... 138

7.4 Comparisons and Linear Regression Analysis of Peak Positive Pressure Coefficients on Roofs of FIU Series House Models..... 138

7.5(a) Envelope Line of $\bar{\phi}$ of the Negative Peak Pressure Coefficients against the Dimensionless Ratio A_f / s for Zone 3 of FIU Series House Models..... 142

List of Figures (Continued)

Figure Page

7.5(b) Envelope Line of $\bar{\phi}$ of the Negative Peak Pressure Coefficients against the Dimensionless Ratio A_f / s for Zone 2 of FIU Series House Models..... 142

7.5(c) Envelope Line of $\bar{\phi}$ of the Negative Peak Pressure Coefficients against the Dimensionless Ratio A_f / s for Zone 1 of FIU Series House Models..... 143

7.6 Envelope Line of $\bar{\phi}$ of the Positive Peak Pressure Coefficients against the Dimensionless Ratio A_f / s for Roof Areas of FIU Series House Models..... 143

CHAPTER 1

INTRODUCTION

1.1 General Background

With the development of the economy and society of the south-east United States, the migration of the population towards coastal regions is continuously increasing the population density of these regions. Since 1992, the coastal population has increased by 28% (Crossett et al, 2004). Recent hurricane seasons have shown that the south-east regions are vulnerable to damage from hurricanes. For a number of reasons, the majority of wind damage occurs to low-rise residential construction, particularly to single-family wood frame construction.

Hurricanes are intense tropical cyclones capable of producing extreme wind velocities and a storm surge that can cause massive damage to a large area. In the North Atlantic Ocean, hurricanes typically occur between June and November and they can affect the Caribbean islands, the south-east coastal regions of the United States, Central America, and Mexico. Historical records of hurricane activity show annual occurrence varies with some periodicity and it is predicted that the south-east United States will experience a period of increased hurricane activity for several decades to come (Klotzbach and Gray, 2006).

From the 1970s to the present, coastal areas in the south-east United States have suffered damage from several strong hurricanes, such as Hurricanes Hugo (1989), Andrew (1992) and Katrina (2005). During the 2004 and 2005 hurricane seasons, eight hurricanes made landfall along the eastern and Gulf Coast states of the United States. The

high winds and storms surge from Hurricanes Charley, Frances, Ivan, Jeanne, Dennis, Katrina, Rita and Wilma caused billions of dollars in economic losses. In August 2005, Hurricane Katrina became the most costly and one of the deadliest hurricanes in US history, resulting in more than $40 billion in insurance claims and over 1,300 deaths (King, 2005). Table 1.1 summarizes the 2004 and 2005 US hurricane losses.

Table 1.1 2004 and 2005 US Hurricane Losses

Name	Dates	Hurricane Category* (Landfall)	Insurance Loss ($ Billions*)
Katrina	23–30 Aug, 2005	4	40.6
Wilma	15–25 Oct, 2005	3	8.4
Rita	18–26 Sep, 2005	3	5.0
Charley	9-15 Aug, 2004	4	7.7
France	25 Aug - 9 Sept, 2004	4	4.8
Ivan	2-24 Sept, 2004	4	7.4
Jeanne	13-28 Sept, 2004	3	3.8
Source: *Insurance Information Institute			

In Hurricane Hugo, the majority of hurricane damage occured to low-rise buildings, especially residential houses (Sparks, 1994). The 1989 Hurricane Hugo, which made landfall in Bulls Bay, South Carolina, resulted in $3 billion in insurance costs, 58 percent of which was paid to repair housing damage (Sparks et al, 1994; Smith, 2005). In 1992, the Hurricane Andrew resulted in insured losses exceeding $13 billion and overall economic losses of almost $30 billion (AIR Report, 2002). Hurricane Andrew made landfall in Homestead, Florida with sustained winds of 138 mph. Twenty-five thousand homes in Dade County, Florida were destroyed and 100,000 more were damaged. Field investigations continue to show that houses are particularly vulnerable to damage from extreme wind events (Gurley et al, 2005). With the predicted increase in frequency and

intensity of hurricanes over the next few decades, mitigating hurricane damage has become the special concern of the populations in coastal communities. There is an urgent need for the engineering and research communities to help reduce wind damage to and vulnerability of low-rise buildings in hurricane-prone areas.

Post-hurricane field investigations have revealed that most wind damage to houses was restricted to the building envelope (Sparks et al, 1994; Uematsu and Isyamov, 1998; Gurley et al, 2005, Smith, 2005). An improvement in wind resistance of the building envelopes of these structures can mitigate much of the economic losses due to hurricanes. Therefore, it is important to improve our understanding of the impact of hurricane wind loads on houses, and in particular, the roofs which experience the most damage. To satisfy these requirements, a number of full-scale experiments have been performed (Eaton and Mayne, 1975; Richardson, et al, 1990; Levitan and Mehta, 1992). These tests provided researchers with information on the characteristics of the atmospheric surface layer and the natural wind interaction with low-rise buildings. These test results are also accepted as the benchmarks for validating wind tunnel results on model-scale buildings. The validated wind tunnel techniques have been widely applied in generic model studies. These efforts have furthered the understanding of wind/structure interactions and continue to improve wind load codes to accurately express wind load on low-rise buildings. According to the investigation of hurricane damages of the 2004 and 2005 hurricane seasons, Reinhold (2005) summarized that strengthening building codes and design standards works in preventing substantial hurricane damage. He specially noted that design standards for manufactured housing had changed substantially since

1976 and especially after 1994 with “clearly superior performance” for housing built under post-1994 standards.

Though there is evidence that engineered houses based on the current design code have improved structural performance in hurricanes, questions remain about the adequacy of the building code. The wind load code has been strengthened since Hurricane Andrew in 1992, however, there continue to be failures of residential roof structures in hurricanes. These damages occur in roofs that have been designed and constructed according to the code. This has led to some suspicion that that the current wind load design code may not account for such factors as terrain exposure and surrounding houses (Dearhart, 2003; Reinhold, 2005). First, most of the full-scale experiments were performed on isolated buildings with simple gable or flat roof shapes and the buildings were located in a uniform (i.e. flat, open) terrain. In addition, the buildings were subjected to extra-tropical (frontal type) winds rather than hurricanes. Thus, the current wind load design codes were developed by utilizing the data sets collected in wind tunnel tests of generic models, and these wind tunnel studies were undertaken by simulating wind flow fields that were validated by the previous full-scale studies (Stathopoulos, 1979; Ho et al, 2005). Previous full-scale wind load studies focused on extra-tropical storms rather than hurricanes (Eaton and Mayne, 1975; Richardson et al, 1990; Levitan and Mehta, 1992). Masters (Masters, 2004) proposed that the wind flow characteristics of extra-tropical storms are different from the wind flows generated by hurricane cases, and he found that hurricanes produce gustier winds and more turbulence than extra-tropical storms. Considering the difference of wind flow fields between hurricanes and extra-tropical storms and higher turbulence meaning higher

pressure at peak, the current wind load design codes may not be adequate for quantifying the hurricane wind loads on low-rise buildings.

Until recently, there has been no comprehensive full-scale study of hurricane wind loads on low-rise buildings. In response to this need for full-scale hurricane wind and load data, the Florida Coastal Monitoring Program (FCMP) was initiated in 1998 with funding from the Florida Department of Community Affairs and FEMA. This program uses technology developed at Clemson University's Wind Load Test Facility. The consortium of research partners includes Clemson University, the University of Florida, the Florida International University, Florida Institute of Technology, and the Institute for Business and Home Safety. The thrust of the FCMP research pertinent to this research is to collect field hurricane wind speeds and gust characteristics plus wind pressure data on the residential roof structures. The FCMP has successfully recorded multiple high-resolution datasets of wind pressure on single family houses since 2002. Several of these datasets include homes subjected to sustained hurricane level winds. The data from FCMP full-scale test results offer the ability to validate current wind tunnel simulation method and ASCE prescriptive wind loads.

1.2 Research Objectives

The focus of this research is on the collection and analysis of wind pressure data taken from a low-rise single-family home in the Florida panhandle during both Tropical Storm Isidore (2002) and Hurricane Ivan (2004). The full-scale tests are described, and full-scale wind pressure data is presented. Wind tunnel studies of a scale model of the subject house were conducted in the Boundary Layer Wind Tunnel at Clemson University's Wind Load Test Facility. The major objectives of this study are:

1) To establish a methodology for analyzing full-scale wind pressure data to determine external pressure coefficients;
2) To investigate measurement system uncertainties associated with reference pressures, temperature variations, calibration errors, and the spatial and time averaged effects of wind loads;
3) To compare full-scale results with wind tunnel tests to determine the ability of wind tunnel to reproduce full-scale test results;
4) To evaluate the wind design provisions of ASCE 7-05 in comparison with full-scale and wind tunnel test results, to see if it is conservative for hurricane wind loads on low-rise buildings; and
5) To investigate terrain exposure and neighboring surrounding house effects on wind loads on low-rise buildings.

1.3 Dissertation Structure

A literature review is presented in Chapter 2 that discusses prior research in wind engineering on low-rise buildings. Chapter 3 describes the measurement instruments used at the Wind Load Test Facility at Clemson University, the wind tunnel setup and the simulation of the wind field used for this dissertation. Chapter 4 presents the experimental setup to collect full-scale data and the methods of analyzing full-scale test records from a residential house during both Tropical Storm Isidore (2002) and Hurricane Ivan (2004). Uncertainty analyses of full-scale test results are presented in Chapter 5. In addition, by analyzing full-scale data, the probability density function of wind loads and the spatial and time-averaged effects on wind loads are described in Chapter 5. Chapter 6 presents results of wind tunnel tests on a 1:50 scale model of the prototype house and compares of full-scale and wind tunnel test results with ASCE 7-05 design values. Chapter 7 describes a study of the investigation of the influences of terrain exposures and surrounding buildings on components and cladding wind loads for low-rise buildings. Finally, my conclusions and recommendations for future research are in Chapter 8.

CHAPTER 2

LITERATURE REVIEW

In the past three decades, a large amount of research has been performed to study extreme wind loads on low-rise buildings. Stathopoulos (1984), Surry (1999), and Uematsu and Isyumov (1999) provide a comprehensive review of the evolution of research on extreme wind loads on low-rise buildings. The papers about the research of extreme wind loads on low-rise buildings can be divided into four categories (Uematsu and Isyumov, 1999)

a) Full-scale tests of extreme wind loads on low-rise buildings;

b) Validation of wind tunnel methodologies for simulating wind loads on low-rise buildings;

c) Wind tunnel tests of extreme wind loads on low-rise buildings; and

d) Codification of wind loads on low-rise buildings.

2.1 Full-Scale Tests of Wind Loads on Low-rise Buildings

To quantify the characteristics of the wind field around low-rise buildings and the extreme wind loads on low-rise buildings, extensive full-scale tests have been conducted during the past several decades. The knowledge gained from these full-scale tests has furthered the understanding of the wind / structure interaction, and improved wind tunnel simulation methods.

2.1.1 Aylesbury Experiment

The Aylesbury experimental building was built in Aylesbury, England, in the early 1970's. This two-story building was 13.3 m long by 7.0 m wide and 5.0 m high to the eave with an adjustable slope roof, which could alter the roof pitch from 5 degree to 45 degrees (Eaton and Mayne, 1975). A total of seventy-two differential pressure sensors were mounted on roof and wall surfaces to collect wind loads on the experimental building. A pressure sensor stationed within a manhole east of the building was used to determine the reference pressure on site during testing (Sill et al, 1989). The reference pressure was designed to describe the local barometric pressure by continuous venting of the manhole to atmospheric pressure (Holmes, 1982). Wind load data obtained in the Aylesbury experiment indicates that wind pressure with highly fluctuating and high peak wind pressures distribute along the roof ridge and eaves and near the wall corners (Holmes, 2001).

A large number of wind tunnel tests have been performed on the Aylesbury experimental building, with geometric scaling ratios varying from 1:500 to 1:25 (Holmes, 1982). To estimate tunnel-to-tunnel differences in pressure measurements on low-rise structures, the corresponding wind tunnel studies of the Aylesbury experimental building (the International Association for Wind Engineering Aylesbury comparative experiment) were conducted at seventeen laboratories around the world using an identical 1:100 model of this building (Sill et al, 1989, 1992). The comparison showed there were significant differences in the pressure coefficients measured by different laboratories. Sill summarized that the significant differences could be caused by the poor response of static pressure tubes in turbulent flow, leaks in reference tubing, along-wind gradients of static

pressure, model blockage, model proximity effects, or variation in reference location (Sill et al, 1989).

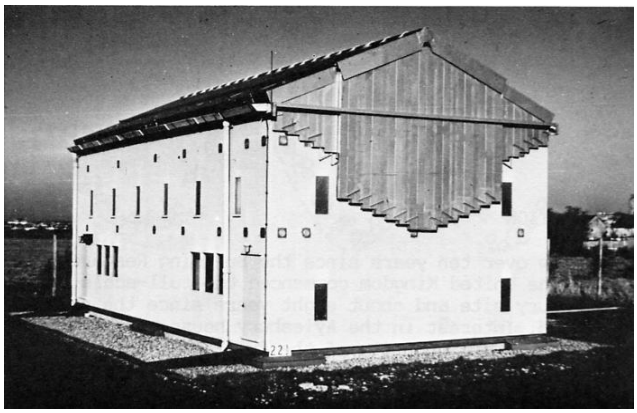

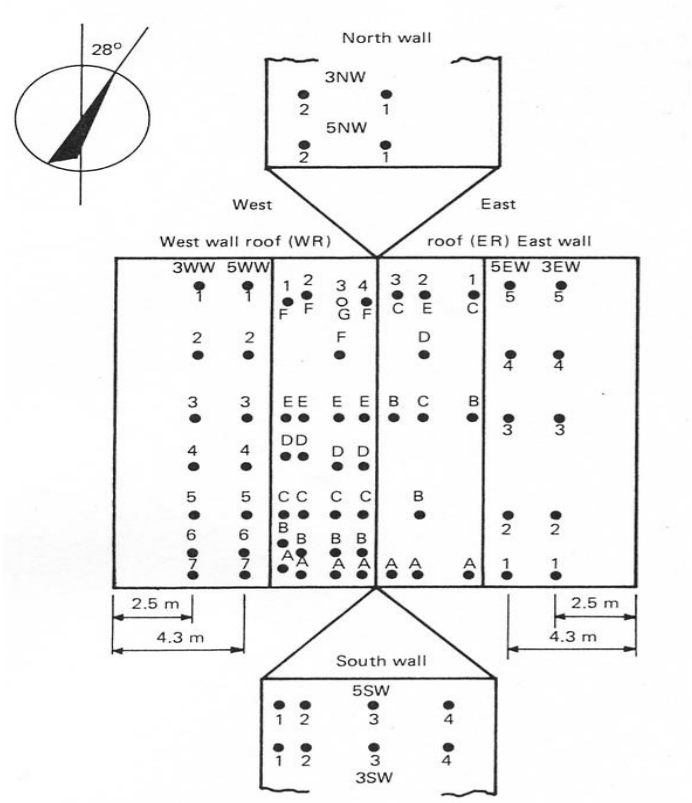

Figure 2.1 Aylesbury Experimental Building and Pressure Transducer Locations (Sill et al, 1989, Holmes, 2001)

2.1.2 Silsoe Structure Building

The Silsoe Structure Building was constructed in Wrest Park, Silsoe, England in the late 1980's. The Silsoe Structure Building was a large steel portal-framed structure with 24.0 m long by 12.9 m wide and 5.3 m high with a 10 degree roof pitch, located in open country (Richardson and Surry, 1992). A total of seventy-seven differential pressure sensors were mounted on roof and wall surfaces to collect wind loads on the experimental building. Twelve strain gauges were also installed along the building's central portal frame to measure the structural response to wind loads on the building (Richardson and Surry, 1992).

In the full-scale tests of the Silsoe Structure Building, measurements of wind pressures were taken at several locations on the building envelope and the strains were measured in some structural members. The full-scale test results were used to verify the wind tunnel simulation tests and numerical simulations in following studies, which were performed by the Building Research Establishment (BRE) and the University of Western Ontario (UWO) (Richardson and Blackmore, 1995). The comparison of results shows that wind tunnel results from BRE underestimate the peak suctions while wind tunnel results from UWO overestimate the peak suctions (Stathopoulos and Saathoff, 1991). The strains measured in the portal frame were found to be consistent with the simulated results from a structural analysis computer program (Holmes, 2001).

2.1.3 Texas Tech University (TTU) Building

The TTU Building is located in Lubbock, Texas. This building is 12.2 m long by 9.1 m wide and 4.0 m high with an almost flat roof. The TTU Building is constructed on a turntable which allows it to be rotated to vary the angle of attack of the approaching wind (Levitan and Mehta, 1992). Wind speeds at the site are measured by gill anemometers mounted on a meteorological tower at heights of 1, 2.5, 4, 10, 21, and 49 m. Barometric sensors are also installed at a 4 m height on the meteorological tower to collect the data of atmosphere pressure, temperature, and relative humidity (Levitan and Mehta, 1992). In TTU building tests, researchers used 204 differential pressure transducers, which were distributed on all surfaces of the experimental building, to measure simultaneously the external and internal pressures caused by incident speeds around the experimental building (Levitan and Mehta, 1992).

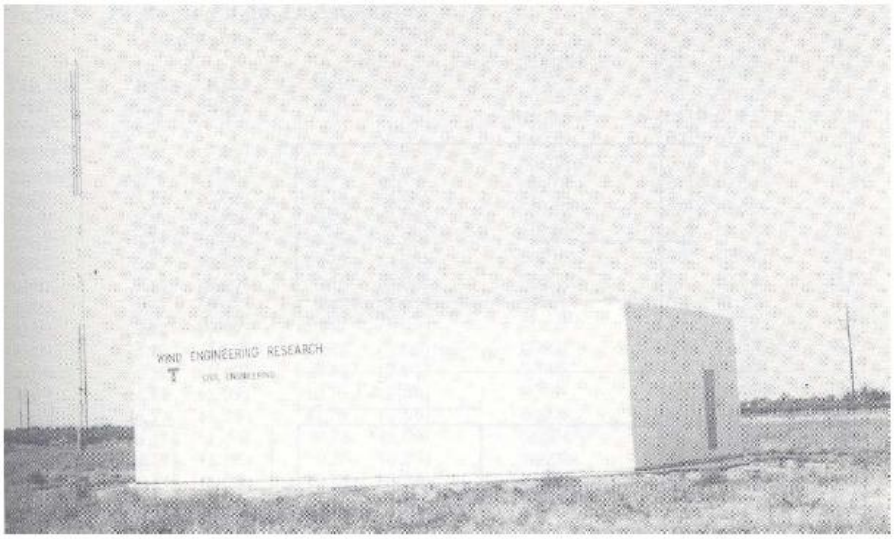

Figure 2.2 The WERFL Building and The Meteorological Tower
(Levitan and Mehta, 1992)

Extreme wind pressures were found at the windward roof corner when the incident wind angle was approximately 45 degree. The worst external wind pressures measured by TTU full-scale tests were greater than the results from the corresponding 1:100 scale wind tunnel model tests (Holmes, 2001).

The TTU building tests have provided the most comprehensive and reliable full-scale measurements of wind loads on low-rise buildings to date. TTU full-scale test results were extensively recognized as the benchmark to validate wind tunnel simulations (Surry, 1991; Cochran and Cermak, 1992; Tieleman et al, 1997; Cheung et al, 1997). Comparison of wind tunnel and TTU full-scale tests contributed to a significant improvement in wind tunnel simulation techniques (Holmes, 2001).

2.1.4 Full-scale Tests of the Florida Coastal Monitoring Program (FCMP)

The Florida Coastal Monitoring Program (FCMP) was initiated in 1998 using technology developed at Clemson University with funding from the Florida Department of Community Affairs. Over the years the program has been supported by funding from the Florida Department of Community Affairs, the South Carolina Sea Grant Consortium, the Institute of Business and Home Safety, and the Florida Sea Grant. The consortium of research partners now includes Clemson University, the University of Florida, Florida International University, Florida Institute of Technology, and the Institute for Business and Home Safety. The thrust of the FCMP research is to collect in-field hurricane wind speed and gust structure data plus pressure data on the roofs of residential structures. The FCMP has successfully recorded multiple high-resolution datasets of wind pressure on single family houses since 2002. Several of these datasets include homes subjected to

sustained hurricane level winds. The data from FCMP full-scale test results offer the ability to validate current wind tunnel simulation methods for hurricane extreme wind loads on low-rise buildings and ASCE prescriptive wind loads.

The FCMP has developed two independent systems that are used to quantify the hurricane wind field and wind loads on full-scale low-rise buildings. These are respectively the Mobile Tower System and the House Instrumentation System. The objectives of the FCMP are to:

a) conduct measurements of hurricane wind velocities using the portable 10-m tall Mobile Tower Systems;

b) conduct measurements of wind-induced pressures on critical roof areas of residential buildings using the House Instrumentation System;

c) conduct wind tunnel studies at Clemson University's Wind Load Test Facility and compare the full-scale pressures with wind tunnel results; and

d) evaluate the effectiveness of inexpensive retrofit measures.

The Mobile Tower System (see Figure 2.3), described in several FCMP published papers (Masters, 2004; Aponte, 2004; Gurley, et al 2005), is designed to collect wind velocity data at 5 and 10 m heights, barometric pressure, temperature, and relative humidity. The House Instrumentation System, described by Michot (1999) and Reinhold et al (2005) and shown in Figure 2.4, uses anemometers to collect approximate wind speed data at the house roof and absolute pressure transducers to measure hurricane wind pressures at critical roof areas. The pressure transducers are Microswitch 142 PC 15-A absolute pressure transducers. The linearity and accuracy of the pressure sensors and the signal conditioning combination were evaluated in a controlled laboratory setting. The

target of operating range of the absolute pressure transducers is between 825 mb to 1017 mb (-375 psf to +25 psf relative to 1005 mb) which covers the pressure range associated with both atmospheric pressure drops and the wind-induced suction pressures occurring during extreme storm events. The transducers and circuit combination produce voltage signals that have an overall accuracy of ±0.5 psf, and the data acquisition system collects the sensor output at 100 Hz.

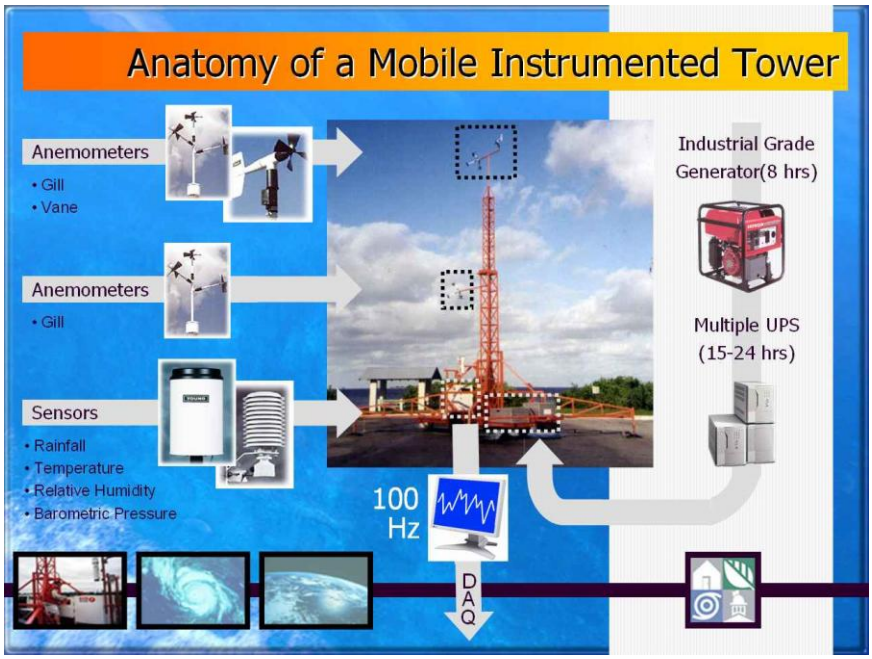

Figure 2.3 The FCMP Mobile Tower Systems (FCMP Website, 2005)

Figure 2.4 The FCMP House Instrumentation System (FCMP Website, 2005)

There are currently 32 residential houses in Florida that participated in the FCMP and are located along Florida's Atlantic Coastal and Gulf Coastal areas, as shown in Figure 2.4. Each house has had brackets installed on the roof to allow teams to fasten pressure sensors just prior to storm land fall. The locations for the sensors are selected to reflect the most likely extreme pressure regions (corners, edges and ridge lines). The Mobile Tower Systems are typically located near to the instrumented homes (within 1.6 to 4.8 km), providing additional wind velocity and turbulence information as the storm approaches.

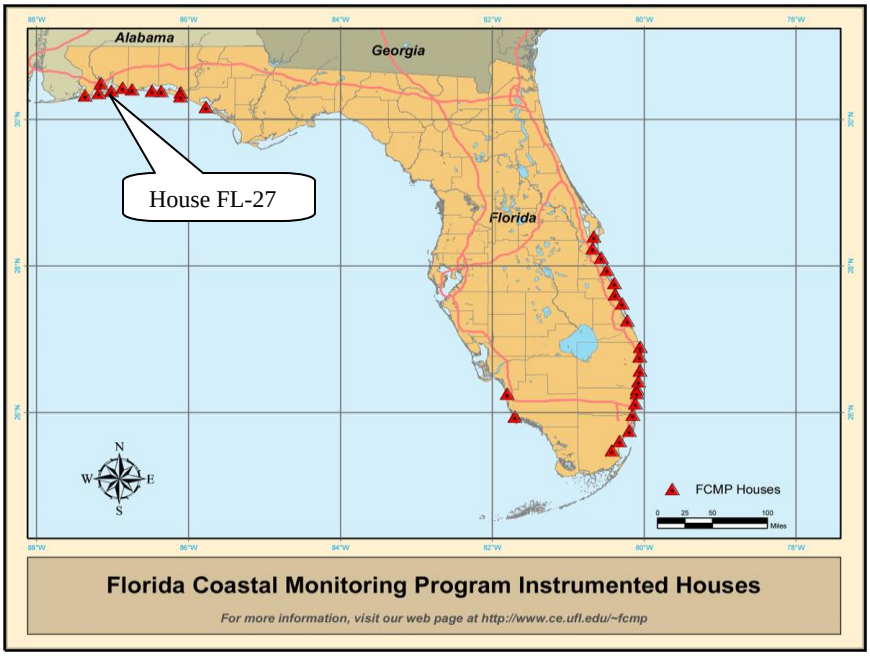

Fig 2.5 Locations of FCMP participant homes in Florida (Gurley et al, 2005)

Dearhart (2003) performed a preliminary analysis of full-scale records of two residential buildings located in suburban settings near the coast of Florida during Tropical Storm Isidore, in September 2002. The corresponding wind tunnel model test results were compared with full-scale values. The comparison of full-scale and model test results shows that model tests produced pressure fluctuations with similar characteristics to those observed for the full-scale structures while model test results underestimate the peak negative pressure coefficients. However, Dearhart's research only focused on analyzing peak pressure coefficients obtained from one storm (the Tropical Storm Isidore) and didn't investigate the systematic error of measurement system. Therefore, in the study, one purpose is, by referring Dearhart's analysis procedures, to establish a general methodology for analyzing full-scale wind pressure data of FCMP and assess hurricane wind loads on low-rise buildings.

2.2 Validation of Wind Tunnel Methodologies for Simulating Wind Loads on Low-rise Buildings

Wind tunnel testing has been extensively applied in the practice of civil engineering to study wind effects on structures (Cermak, 2003). Wind tunnel techniques in structural engineering practice are discussed in greater detail by Cermak (1975), Reinhold (1982) and American Society of Civil Engineers (1999). These discussions provide the comprehensive information on requirements for boundary-layer wind tunnel simulation, model construction, and test of procedures. Two factors which need to be considered during wind tunnel studies on low-rise buildings are the determination of geometric scale and the determination the appropriate modeling of the atmospheric boundary layer to ensure the similar of wind flow characteristics between full-scale and wind tunnel tests (Uematsu and Isyumov, 1999).

2.2.1 Simulation of the Atmospheric Boundary Layer

In order to reproduce wind loads on low-rise buildings in a wind tunnel, a proper flow-simulation of the atmospheric boundary layer is required. The atmospheric boundary layer is referred to as the region of the atmosphere near the ground surface in which the air flow is affected by friction at the earth's surface (Holmes, 2001). Buildings and structures are located in this layer. Usually, wind tunnel tests for wind loads on low-rise buildings are performed in homogeneous surface layer flows. In homogeneous surface layer flows, turbulent exchange of momentum, heat and moisture between a flat, horizontally homogeneous surface and the atmosphere is well described by the Monin-Obukhov (MO) similarity theory (Monin and Obukhov, 1954). To simulate the aerodynamic forces in wind tunnel model tests, the equality of Reynolds number and

geometric similarity are required to be achieved (Tieleman, 2003). Reynolds number is the ratio of inertial to viscous forces. In many cases of low-rise building tests, Reynolds number similarity can be neglected because scaled model buildings with sharp edges produce separation points on the model that are independent of Reynolds number. To achieve theoretical geometric similarity, the geometric scaling ratio for the models should be equal to the ratio of the roughness length and the integral scales (Tieleman, 2003). The roughness length, z_0, is defined as *"a measure of the aerodynamic roughness of a surface, which affects the boundary-layer flow over it"* (Holmes, 2001). The integral scale is defined as "*a measure of the average size of the turbulent eddies of the flow.*" (Simiu and Scanlan, 1992). The Jensen number, H / z_0, is the ratio of the building height H to roughness length z_0, and is historically considered as the most important parameter. Jensen (1965) identified that having model/full-scale equality of the Jensen number is sufficient to simulate the flow in the surface layer (Tieleman, 2003). Some wind tunnel tests show that using the Jensen number as the representative scaling length for wind tunnel model studies can guarantee excellent agreement for mean pressure coefficients between model and field data (Jensen and Franck, 1965). However, results from comparisons of full-scale and wind tunnel tests show that the fluctuation of pressure cannot be simulated thoroughly (Tieleman et al, 1998; Surry, 1999; Cook, 2002). The geometric similarity based on Jensen's law may benefit simulating the velocity profile, but it is not sufficient to simulate turbulence intensities of the horizontal velocity components (Tieleman, 1991). Tieleman et al (1998) found that inadequate simulation of the horizontal fluctuations, the integral scale and small scale turbulence components of

flow account for the discrepancies of the pressure fluctuation between the full-scale and the wind tunnel tests (Tieleman, 1991; Tieleman et al, 1998).

2.2.2 Model Scaling of Wind Tunnel Tests for Low-rise Buildings

The current wind tunnel techniques use a variety of means to simulate the scaled atmospheric boundary layer flow. By varying the floor roughness and using trip boards and vertical spires, a 0.5 m - 1.5 m scaled atmospheric boundary layer can be generated (Tieleman, 2003). In the practice of wind engineering, the simulated gradient height of the neutral atmospheric boundary layer flow varies between 275 m and 550 m (Davenport, 1960). Therefore, model scales should be around 1:400 to match the overall scale of the simulated atmospheric boundary layer in a typical sized wind tunnel. However, the scale of 1:400 is too small for models of low-rise buildings, which could result in tiny models incapable of accommodating a large number of pressure taps (Tieleman, 2003). Thus, in order to embody the structural details in the model and arrange as many test points as possible, 1:50 and 1:100 scales of model are the practical model sizes used for wind tunnel studies of low-rise buildings. Additionally, at 1:50 or 1:100 scales only the lower portion of the atmospheric boundary layer can be simulated in wind tunnel tests.

2.3 Wind Tunnel Tests on Low-rise Buildings

Wind tunnel tests have been performed on scale models of low-rise buildings in order to better predict wind loads. Past researches investigated the characteristics of wind pressures on low-rise buildings (Stathopoulos, 1979; Ho,1992), wind tunnel simulation of

wind loads observed in full-scale tests (Tieleman, 2003), and investigation and development of design wind codes for low-rise buildings (St. Pierre et al, 2005; Ho, 2005).

2.3.1 Fluctuation of Wind Loads on Low-rise Buildings

Several factors that may influence wind load fluctuations on low-rise buildings in wind tunnel tests include: (Krishna, 1995)

a) the atmospheric boundary layer simulation;

b) vertical and horizontal turbulence intensities;

c) proximity of pressure ports to edges and corners;

d) spacing of pressure ports; and

e) area averaging and time averaging of wind loads.

It is necessary to ensure wind tunnel test accurately model these factors in order to reproduce full-scale test data. In one study, extensive wind tunnel tests were performed to investigate the fluctuation of wind loads on low-rise buildings by Stathopoulos (1979). He found that high fluctuations of wind loads occurred on the windward walls, the separated-reattaching flow regions on the side walls, and the roof corner and ridge areas.

The standard deviation of wind pressure coefficients, which is related to turbulence intensities ($I = \frac{\sigma}{\overline{U}}$), is used to measure the general level of pressure fluctuation. Higher standard deviations of wind pressure coefficients correspond to higher instantaneous peak pressures. So far the worst negative peak factor, which is defined as the peak pressure coefficient minus the mean pressure coefficient divided by the standard deviation of the pressure fluctuation expressed in coefficient form, is up to 26 that were

observed on the house roof in the TTU full-scale tests (Holmes, 2001). This high suction has not been duplicated yet by wind tunnel tests (Surry, 1999; Cook, 2002). Researchers found that the highest negative peak pressures are associated with conical vortices when the flow approaches the roof corners (Stathopoulos, 1984; Banks et al, 2000). Comparison research of full-scale and wind tunnel tests show that it is important to reproduce the level of turbulence at model scale in order to duplicate the high suction pressures observed on prototype low-rise buildings (Tieleman et al, 1998).

2.3.2 Spatial and Temporal Effects on Peak Wind Pressures

Wind pressures on low-rise building surface are constantly changing in time and space. Components and cladding elements may be affected by localized pressures (e.g. the wind load on a fastener may be affected by wind pressure acting on its/immediate small areas. The wind load on larger structural elements is affected by larger surface areas). It was found that wind pressure is more correlated on smaller areas, usually in higher pressure on small areas (Surry and Stathopoulos, 1977). In addition, wind pressure correlates in time.

Two area-averaging approaches have been developed to assess wind load effects on structures, pneumatic averaging and using synchronous pressure time history. Pneumatic averaging method uses an tube manifold that combines several pressure taps to measure the area-averaged wind pressure. This method assigns equal weight (area) to each pressure tap and was first used by Surry and Stathopoulos (1977), and the theoretical model of this method was developed by Gumley (1981, 1983). The second method uses the synchronous pressure time history records of individual pressure taps to

determine the area-averaged pressure. Tributary area for each pressure tap can be assigned for use in the analysis.

Researchers found that it is too conservative to use the individual pressure measurement results to represent the wind load on an area because the results of point pressures are unsuitable to effectively estimate the response of structural members (Marshall, 1977; Surry and Stathopoulos, 1977; Davenport et al, 1978; Holmes and Best, 1981). This conclusion is also supported by TTU full-scale tests (Mehta et al, 1992). Usually, area-averaged pressures are regarded as a suitable way to describe the wind load on an area since it is based on an accumulation of point pressures and since it is more normally distributed than individual pressures (Uematsu and Isyumov, 1998). Nevertheless, some structural elements, such as fasteners, likely respond to local pressure acting over small areas. As a result, the design wind loads presented in the current wind code ASCE 7-05 begins with point pressure coefficients which are then reduced as the tributary area increases above 1.0 square meter.

The peak wind pressures on low-rise buildings are also affected by the duration time of loads. Uematsu and Isyumov (1998) investigated the relationship of the effects of spatial and temporal averaging on the peak pressures on low-rise buildings. They found that severe suction pressures, which occurred in the leading edge and corner regions, typically last for 0.2 to 0.3 seconds. In general, the severe suction pressures are concentrated on a small area less than 1 square meter. The spatial and temporal averages of pressure fluctuations lead to a significant reduction in the effective peak suction.

2.4 Wind Load Code for Low-rise Buildings

Low-rise buildings are defined by the American Society of Civil Engineers Standard for Minimum Design Loads for Buildings and Other Structures (ASCE 7-05, Section 6.2) as "*structures with a mean roof height less than the least horizontal dimension and less than 18m (60ft)*" (ASCE 7-05, 2005). In general, low-rise buildings can be categorized as rigid-structures because they have high fundamental frequencies of vibration. Therefore, dynamic amplification effects of wind load on low-rise buildings can be neglected.

Three methods defined by ASCE 7-05 are used to estimate the wind loads on low-rise buildings. They are referred to as Method 1-simplified procedure, Method 2-analytical procedure, and Method 3-wind tunnel procedure. In the practice of engineering, Method 2 is widely applicable for analyzing the design wind loads on low-rise buildings.

In ASCE 7-05, design criteria for low-rise buildings are divided into two sections for the main wind force-resisting system (MWFRS) and the components and cladding system (C&C system). The main wind force-resisting system, which transfers wind load received by the components to the ground and provides support and stability for the overall structure, includes structural elements like shear walls, roof-trusses, roof diaphragms or the assemblage of structural elements. The components and cladding system is defined as elements of the building envelope that do not qualify as part of the main wind force resisting system. Components typically receive wind loads directly, or they receive wind loads from cladding and transfer the load to the main wind force resisting system.

The study presented in this dissertation will focus on hurricane wind loads on the components and cladding system of low-rise buildings, and so the procedures to determine design loads are described here. Cladding includes curtain wall, exterior window (fixed or operable), doors and overhead doors. Components include purlins, roof decking, roof trusses, fasteners, parapets and studs. The design wind loads for components is considered to be the load carried by an effective area which is used to determine peak wind pressure coefficient GC_p. The effective area corresponds to the tributary area of the component being considered. The effective area for a cladding panel and a cladding faster will be different as load carried by the cladding panel acts over an area equal to the total area of the panel while the load on a cladding fastener is the area of cladding secured by a single fastener.

Analytical procedures for the determination of design wind loads on components and cladding involves the determination of wind directionality, velocity pressure, topographic features, and wind pressure coefficients. The procedure allows for consideration of structural reliability, different wind exposures and topographical features and also differentiates between rigid and flexible buildings and other structures. In ASCE 7, the pressure coefficients of components and cladding systems are the peak pressure coefficients derived by an envelope approach. This method encompasses all of the worst values associated with a number of parameters, such as height, roof slope, size and other building features. The peak pressure coefficient is denoted as GC_p.

CHAPTER 3

WIND TUNNEL SETTINGS AND MEASUREMENT INSTRUMENTS

Wind tunnel tests for this study were conducted in the boundary layer wind tunnel at Wind Load Test Facility at Clemson University. This chapter describes Wind Load Test Facility at Clemson University, the data collection system, wind tunnel layout of wind pressure tests, and the analysis procedures of wind tunnel pressure test records.

3.1 Wind Load Test Facility at Clemson University

Wind Load Test Facility (WLTF) at Clemson University holds a 3.0 m wide by 2.0 m high open return boundary layer wind tunnel, which is powered by a pair of 1.8 m diameter fans controlled by a variable frequency inverter. Wind flow driven by the two fans passes through a honeycomb grill and a set of screens to generate a uniform flow. To simulate the appropriate turbulent boundary layer at the center of the turntable where the experimental models are mounted, a specific combination of spires and trip boards and a series of roughness elements were arranged along the 16 meters test section. Uniform flow entering the test section is modified by the roughness elements to generate aerodynamic parameters that are consistence with the desired type of terrain and model scale.

3.2 Wind Tunnel Configurations of 1:50 Open and Suburban Terrain Exposures

In this research, the wind tunnel was set up to simulate 1:50 scale wind velocity and turbulence profile from two terrain exposure, open country exposure and suburban exposure, as shown in Figure 3.1. The 1:50 open country exposure was established by using a combination of three spire boards (240 mm wide at top and 406 mm wide at the base), a trip board (20 mm thickness and 191 mm height), four 30 degree slant boards (20 mm thickness and 191 mm in height) and 75 mm and 25 mm cube roughness elements installed along the wind tunnel floor. The detailed description of the flow simulation for 1:50 open country can be found in Monroe (1996) and Chen (2000). For this study the 1:50 sparse suburban terrain exposure (see Figure 3.1b) was simulated using a combination of three spire boards (240 mm wide at top and 406 mm wide at the base), a trip board (20 mm thickness and 191 mm height) and 75 mm cube roughness elements installed along the wind tunnel floor.

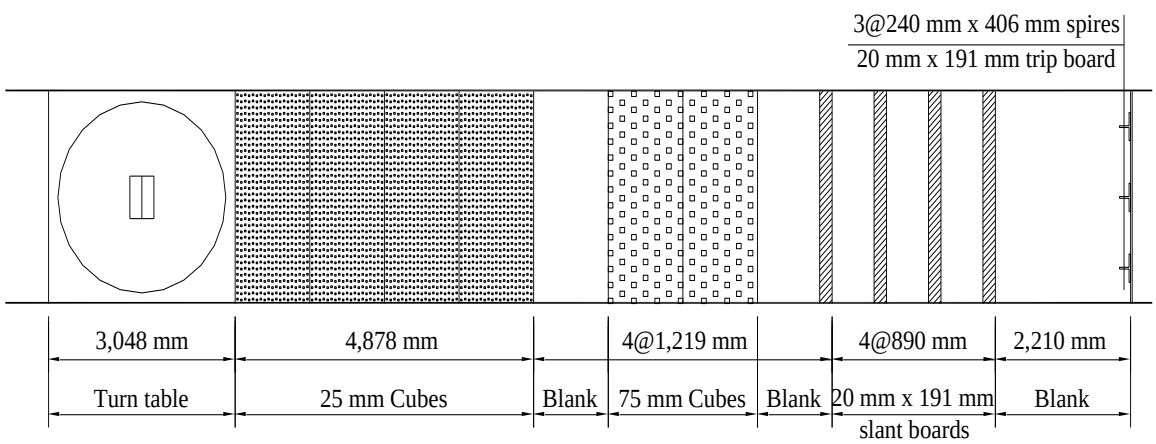

Figure 3.1(a) Wind Tunnel Settings of 1:50 Open Country

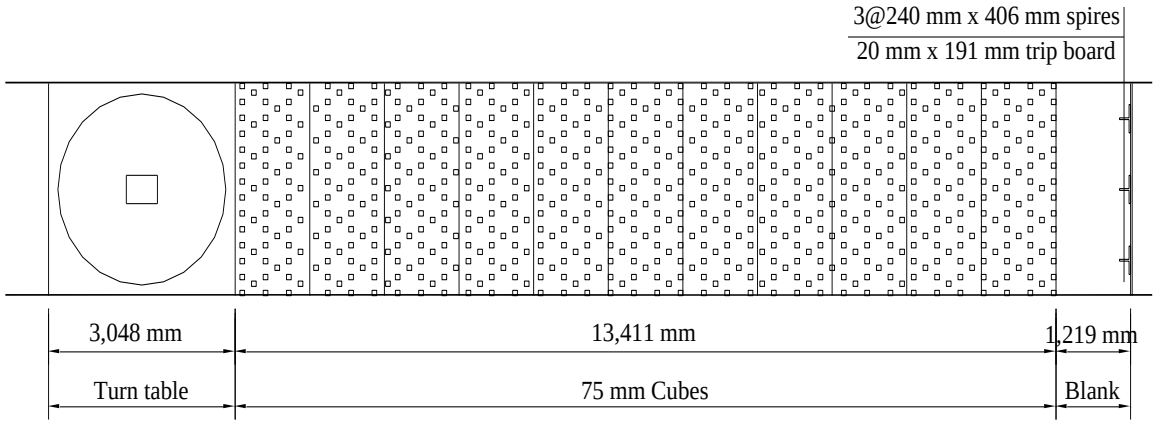

Figure 3.1(b) Wind Tunnel Settings of 1:50 Suburban Terrain

3.3 Data Acquisition System

The data acquisition system used in wind tunnel pressure tests for this research is the RAD3200 system produced by Scanivalve Corp. This system is a combination of both hardware and software and consists of eight ZOC33/64Px pressure-scanning modules used to measure the pressure signals. The remote RAD3200 A/D (Analog-to-Digital Converter) unit is used to convert the amplified analog signals from the ZOC33/64Px pressure scanners to the digital values for input to a PC via a USB extended cable.

The ZOC33/64Px unit shown in Figure 3.2 consists of an electronic pressure scanner that accepts 64 pneumatic inputs directed to 64 silicon pressure sensors, which convert the changes in pressures to an electrical signal that can be read by the analog to digital converter. Each module is equipped with a calibration valve, a high speed (50 kHz) multiplexer and instrumentation amplifier. Each pressure channel can be sampled at 250-500 Hz per channel, per second. (Scanivalve Corporation, 2004).

Figure 3.2 Photo of ZOC33/64Px Model (Scanivalve Corporation, 2004).

Remote RAD3200 unit shown in Figure 3.3 consists of a miniature set of 16-bit A/D (Analog-to-Digital Converter). Each 16-bit A/D accepts the amplified analog signal from one ZOC33/64Px module. The signals are then digitized and sent out to the PC via a USB extended cable. The RAD3200 is located below the wind tunnel turntable in close proximity to the ZOC33/64Px pressure scanners. The high density ZOC33/64Px analog pressure scanners are located in or under the test model and each pressure port is connected using plastic tubing to the measurement ports. The RAD3200 can accept a maximum of 8 64-channel ZOC33/64Px pressure scanner (total 512 pressure scanner channels) at the same time. The tubing system is of modest length (300 mm) and included in the Scanivalve RAD3200 system, however the frequency response of this tubing system is not considered in this study. In fact, a tubing system with an improved frequency response does not alter the peaks greatly (Surry, 1991).

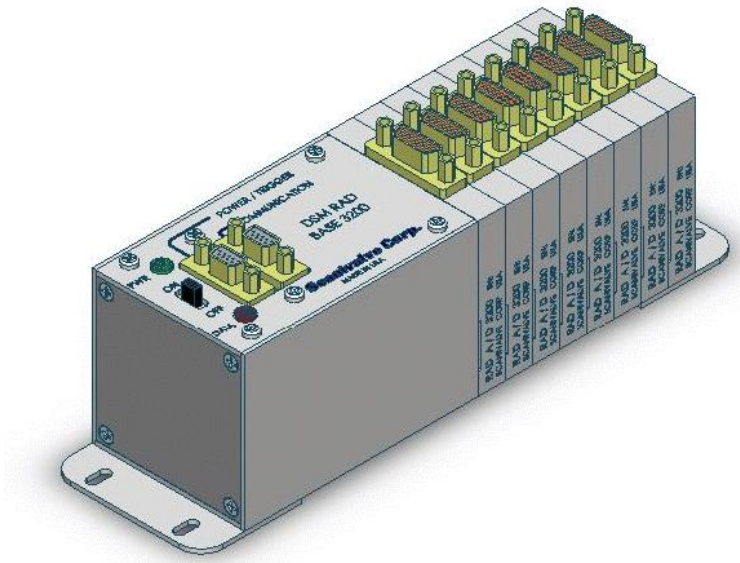

Figure 3.3 Photo of RAD3200 with 8 A/D modules (Scanivalve Corporation, 2004)

The data acquisition computer, which is a P4 1.5GHz CPU with 512Megs of memory, uses the Windows XP operation system. The RAD executable software runs on the data acquisition computer PC and also contains the ZOC33/64Px pressure sensor characterization tables. The raw counts signal from the RAD3200, transmitted via the USB cable, is then converted into Engineering Units of psi. The measured data can either be stored in a file or output from the PC Ethernet TCP/IP. Figure 3.4 shows the configuration of the RAD3200 system used in a standard USB system.

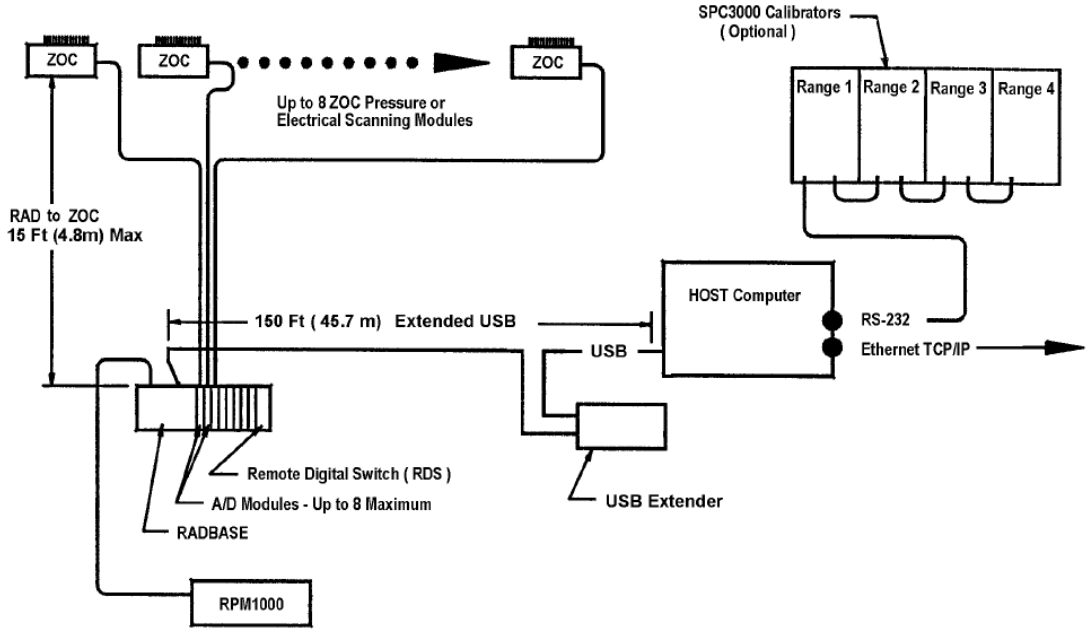

Figure 3.4 RAD3200 System with Extended USB (Scanivalve Corporation, 2004)

3.4 Flow Characteristics of Wind Tunnel Exposure Configurations

The wind flow aerodynamic characteristics of these two wind tunnel settings are measured by using a Thermal System Incorporated (TSI) IFA300 constant temperature hot-film anemometer system. Wind velocities were measured using cross hot films. When the cross hot films were positioned vertically, longitudinal component u and vertical component w of velocities were measured. When the cross hot films were positioned horizontally, the longitudinal component along wind direction u and lateral component v of velocities were measured. The velocity profiles fit to Log-Law profiles are calculated by Equation (3-1) and (3-2).

$$U(z) = 2.5u^{*} \ln(z / z_0) \tag{3-1}$$

$$\frac{U(z)}{U(z_{ref})} = \frac{\ln(z/z_0)}{\ln(z_{ref}/z_0)} \tag{3-2}$$

where, $U(z)$ is mean velocity at height z above the ground; u^* is the shear or friction velocity; z is equivalent full-scale height above the ground; and z_0 is the surface roughness length. The surface roughness length and typical values are listed in Table 3.1.

Table 3.1 Surface Roughness Categories, Extension and Typical Values (Simiu and Scanlan, 1992)

Exposure Category	Lower Limit of z_0 (m)	Typical Value of z_0, (m)	Upper Limit of z_0, (m)
Urban Areas	$0.7 \leq z_0$	2	--
Suburban Terrain	$0.15 \leq z_0$	0.3	$z_0 < 0.7$
Open Country	$0.01 \leq z_0$	0.02	$z_0 < 0.15$
Coastal Areas	--	0.005	$z_0 < 0.01$

Applying the least squares procedure, the best fitting values of the surface roughness length z_0 are calculated. For 1:50 open country exposure, the best fitting value of z_0 equals to 0.047m and, for 1:50 sparse suburban terrain exposure, the best fitting value of z_0 equals to 0.22m. Their corresponding wind profile curves are shown in Figure 3.5(a) and (b).

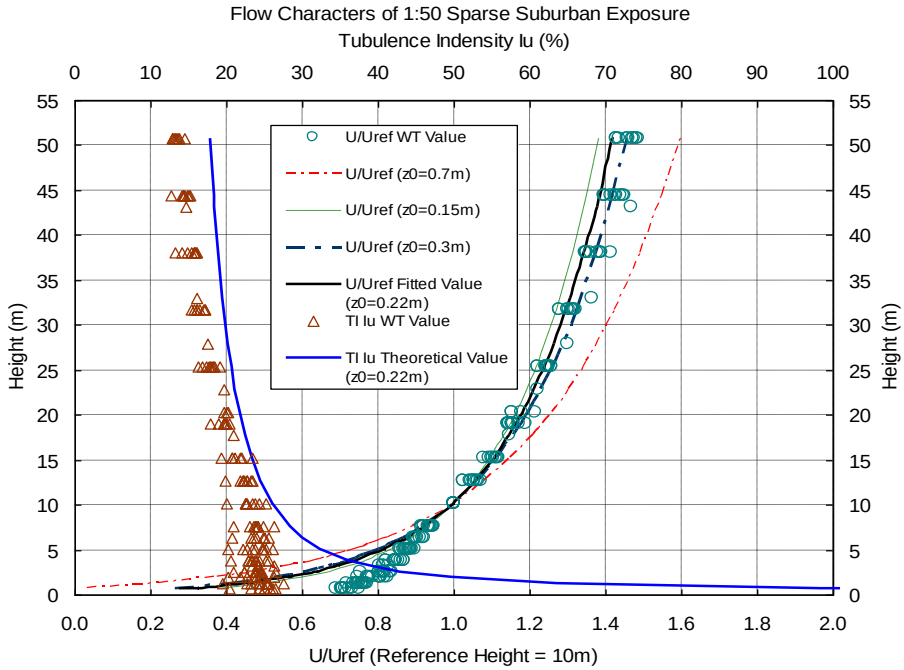

Figure 3.5(a) Velocity and Turbulence Intensity Profiles for 1:50 Suburban Terrain Wind Tunnel Setting

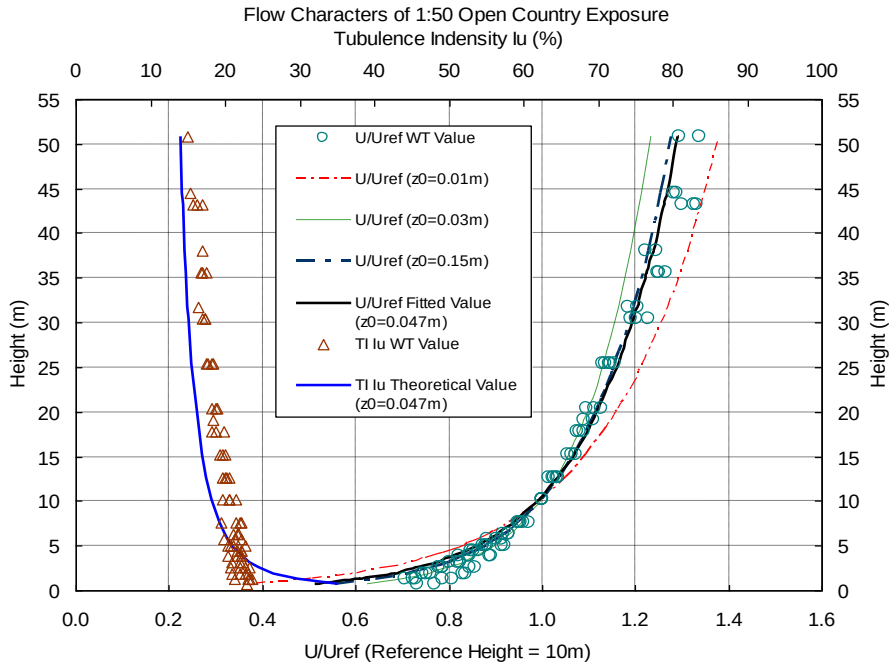

Figure 3.5(b) Velocity and Turbulence Intensity Profiles for 1:50 Open Country Wind Tunnel Setting

The horizontal turbulence intensities I_u are calculated by the Equation (3-3) (Simiu and Scanlan, 1992).

$$I_u = \frac{\sqrt{\beta}}{2.5\ln(z/z_0)} \tag{3-3}$$

For 1:50 open country exposure setting, the fitted equivalent surface roughness length z_0 equals to 0.047m. For 1:50 suburban terrain exposure, the fitted equivalent surface roughness length z_0 equals to 0.22m. The profiles of horizontal turbulence intensities I_u are also plotted in Figure 3.5.

The integral length scale of turbulence is one of the three standard turbulence length scales that are measures of the largest separation distance over which components of the eddy velocities at two distinct points are correlated. They characterize the energy-containing range of eddy length scales. In the most general form, the integral scales (expressed here as a tensor) are functions of position and are defined in terms of the normalized two-point velocity correlations (American Meteorological Society, 2005). Nine integral scales of turbulence are used for measuring three dimensions of eddies associated with the longitudinal, lateral and vertical components of fluctuating velocities u', v' and w'.

In this dissertation, only the longitudinal integral scale L_u^x is calculated. The power spectrum of u' and the von Karman spectrum (von Karman, 1948) was plotted in non-dimensional format of $f^* S(f)/\sigma_u^2$ vs. $f^* L_u^x / U$ in log-log scales, L_u^x is changed until the measured spectrum curve is above the von Karman spectrum in low frequency range.

$$\frac{fS(f)}{u^{*2}} = \frac{4\beta \dfrac{fL_u^x}{U}}{\left[1 + 70.8\left(\dfrac{fL_u^x}{U}\right)^2\right]^{5/6}} \tag{3-4}$$

Here, f is frequency (Hz); $S(f)$ is power spectrum (m^2/s^2); u^* is the shear or friction velocity (m/s); β is a factor that is defined by $\sigma_u^2 = \beta u^{*2}$. Therefore, the von Karman spectrum can be also expressed as

$$\frac{fS(f)}{\sigma_u^2} = \frac{4 \dfrac{fL_u^x}{U}}{\left[1 + 70.8\left(\dfrac{fL_u^x}{U}\right)^2\right]^{5/6}} \tag{3-5}$$

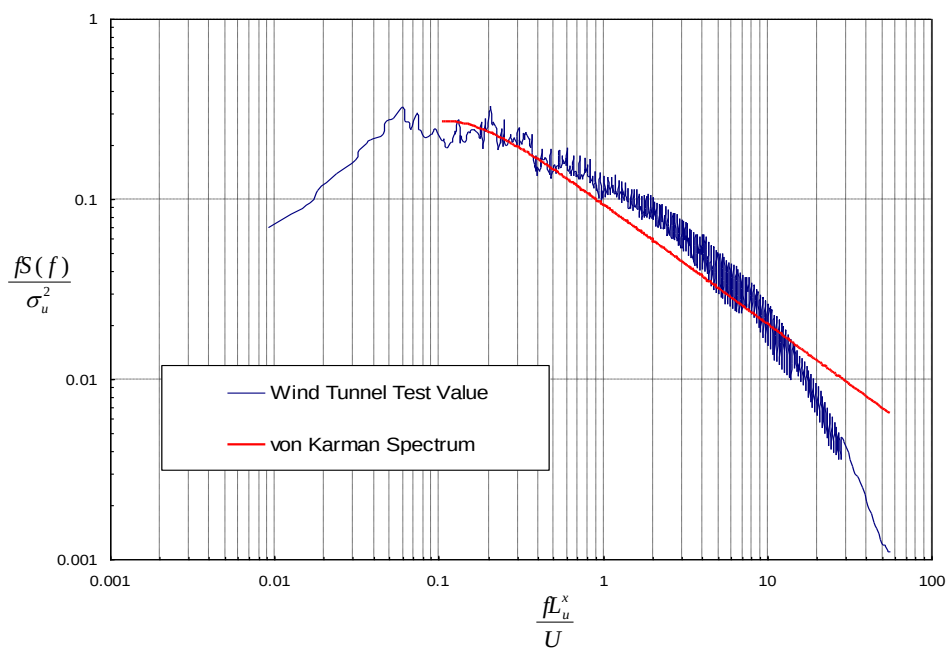

Figure 3.6 Determination of Longitudinal Integral Length Scale L_u^x

Counihan (1975) proposed an empirical expression of the integral length scales for the height range 10-240 m. Expected values for integral length scales of turbulence at 10 and 20-meter height above ground for typical terrain exposures and these expected values are summarized in Table 3.2(a). The measured integral length scales of turbulence at some heights above the wind tunnel floor under 1:50 open country and suburban terrain exposure settings are listed in Table 3.2(b) and Table 3.2(c).

Table 3.2(a) Expected Values of Integral Length Scale

Height (m)	Open Country (z_0 = 0.047 m)			Suburban Terrain (z_0 = 0.22 m)		
	L_u^x (m)	L_v^x (m)	L_w^x (m)	L_u^x (m)	L_v^x (m)	L_w^x (m)
10	120	60	40	90	45	30
20	137	68	46	110	55	36

Table 3.2(b) Integral Length Scale of Turbulence in 1:50 Open Country Setting

Height		L_u^x (m)		L_v^x (m)		L_w^x (m)	
Model (mm)	Full-scale (m)	Wind Tunnel	Full-scale	Wind Tunnel	Full-scale	Wind Tunnel	Full-scale
50.8	2.5	0.55	27.5	0.5	25	0.08	4
101.6	5	0.55	27.5	0.5	25	0.13	6.5
203.2	10	0.8	40	0.5	25	0.13	6.5
406.4	20	0.8	40	0.6	30	0.25	12.5

Table 3.2(c) Integral Length Scale of Turbulence in 1:50 Suburban Terrain Setting

Height		L_u^x (m)		L_v^x (m)		L_w^x (m)	
Model (mm)	Full-scale (m)	Wind Tunnel	Full-scale	Wind Tunnel	Full-scale	Wind Tunnel	Full-scale
50.8	2.5	0.4	20	0.2	10	0.08	4
101.6	5	0.5	25	0.2	10	0.10	5
203.2	10	0.6	30	0.2	10	0.12	6
406.4	20	0.6	30	0.25	12.5	0.15	7.5

3.5 Procedures of Calculating Pressure Coefficients

This section describes the method for determining the pressure coefficients in the wind tunnel tests of WLFT at Clemson University. The laboratory setup with wind tunnel includes a scale model building, differential pressure-scanning transducers, and a pitot tube. Pressure measurement taken at each port is sequentially compound with reference pressure of the pitot tube which is located 1.5 m above wind tunnel floor. The instantaneous external pressure coefficients referenced to the mean dynamic pressure of the reference pitot tube are expressed as the followed equation:

$$C_{p.Pitot}^{Tunnel}(t) = \frac{P_{Taps}(t) - P_{Static.Pitot}(t)}{P_{Dynamics.Pitot.Mean}} = \frac{P_{Taps}(t) - P_{Static.Pitot}(t)}{1/2\rho V_{Pitot.Mean}^2} \tag{3-6}$$

$P_{Taps} - P_{Static.Pitot}$ and $P_{Pitot} - P_{Static.Pitot}$ are measured by the RAD3200 system directly. The statistical properties (mean value, maximum value, minimum value and standard deviation) of the wind pressure coefficients can be calculated by instantaneous pressure coefficients records.

$$\overline{C}_{p.Pitot}^{Tunnel} = mean(C_{p.Pitot}^{Tunnel}(t)) \tag{3-7a}$$

$$\widehat{C}_{p.Pitot}^{Tunnel} = \max(C_{p.Pitot}^{Tunnel}(t)) \tag{3-7b}$$

$$\breve{C}_{p.Pitot}^{Tunnel} = \min(C_{p.Pitot}^{Tunnel}(t)) \tag{3-7c}$$

$$RMS = std(C_{p.Pitot}^{Tunnel}(t)) \tag{3-7d}$$

However, the current wind load design code ASCE 7-05 defines wind pressure coefficients in terms of peak 3-second gust wind speed at mean roof height. The code suggests dividing coefficients based on mean wind speeds at mean roof height by 1.53^2 to reflect the reduced pressure coefficient values associated with a three-second gust speed.

An adjustment factor is used to convert pressure coefficients with reference to the mean wind speed at the reference pitot height $C_{p.Pitot}^{Tunnel}$ to pressure coefficients based on 3-second gust wind speed at mean roof height $(GC_p)_{eq}$. Therefore, the pressure coefficients based on 3-second gust wind speed at mean roof height resulted from wind tunnel tests can be expressed as

$$\overline{C}_{p.Roof.Gust}^{Tunnel} = mean(\phi \cdot C_{p.Pitot}^{Tunnel}(t)) \tag{3-8a}$$

$$\widehat{C}_{p.Roof.Gust}^{Tunnel} = \max(\phi \cdot C_{p.Pitot}^{Tunnel}(t)) \tag{3-8b}$$

$$\breve{C}_{p.Roof.Gust}^{Tunnel} = \min(\phi \cdot C_{p.Pitot}^{Tunnel}(t)) \tag{3-8c}$$

$$RMS = std(\phi \cdot C_{p.Pitot}^{Tunnel}(t)) = \phi^2 \cdot std(C_{p.Pitot}^{Tunnel}(t)) \tag{3-8d}$$

As shown as the Equations (3-9), the adjustment factor ϕ is expressed as the square of the ratio between the gust wind speed at mean roof height and mean wind speed at pitot height.

$$\frac{1}{2}\rho V_{Roof.Gust}^2 (GC_p)_{eq} = \frac{1}{2}\rho V_{Pitot.Mean}^2 (C_{p.Pitot}^{Tunnel}) \tag{3-9a}$$

$$\phi = \frac{(GC_p)_{eq}}{C_{p.Pitot}^{Tunnel}} = \frac{\frac{1}{2}\rho V_{Pitot.Mean}^2}{\frac{1}{2}\rho V_{Roof.,3\sec gust}^2} = \frac{V_{Pitot.Mean}^2}{V_{Roof.,Gust}^2} \tag{3-9b}$$

There are two methods to calculate the ratio of gust wind speed at mean roof height and mean wind speed at the pitot height. One is the theoretical method and the other is based on hot-film anemometry test results.

(a) Theoretical Calculation

The ratio of gust wind speed at mean roof height and mean wind speed at pitot height is expressed by Equation (3-10). The ratio of mean wind speed at mean roof height

and pitot height can be evaluated from the mean wind speed profile of wind tunnel settings, as shown as Figure 3.5. The ratio of mean wind speed and 3-second gust wind speed at mean roof height can be calculated by Equation (3-11). Some ratios of mean wind speed and 3-second gust wind speed at different mean roof heights are listed in Table 3.5.

$$\frac{V_{Pitot.Mean}^2}{V_{Roof.,Gust}^2} = \left(\frac{V_{Pitot.Mean}}{V_{Roof.Mean}} \cdot \frac{V_{Roof.Mean}}{V_{Roof.Gust}} \right)^2 \tag{3-10}$$

$$\frac{V_{Roof.Mean}}{V_{Roof.,Gust}} = 1 / \left(1 + C(3\sec) \left(\frac{\sqrt{\beta}}{2.5 \ln(\frac{z_{Roof}}{z_0})} \right) \right) \tag{3-11}$$

Table 3.3 Values of β Corresponding to Various Roughness Lengths (Simiu and Scanlan, 1992)

z_0	0.005	0.07	0.3	1	2.5
β	6.5	6	5.25	4.85	4

Table 3.4 Coefficient of $C(t)$ (Simiu and Scanlan, 1992)

T(s)	1	10	20	30	50	100	200	300	600	1000	3600
$C(t)$	3.00	2.32	2.00	1.73	1.35	1.02	0.70	0.54	0.36	0.16	0.00

Table 3.5 Ratio of Mean Wind Speed and 3-second Gust Wind Speed at Mean Roof Height

Mean Roof Height		β		$C(t)$	$V_{Roof.Mean} / V_{Roof.Gust}$	
Model (mm)	Full-Scale (m)	$z_0 = 0.047\,m$	$z_0 = 0.22\,m$		Open Country	Suburban Terrain
71.1	3.56	6.18	5.51	2.85	0.655	0.519
76.2	3.81	6.18	5.51	2.85	0.658	0.525
82.6	4.13	6.18	5.51	2.85	0.662	0.532
88.9	4.45	6.18	5.51	2.85	0.665	0.539
95.3	4.76	6.18	5.51	2.85	0.668	0.544
101.6	5.08	6.18	5.51	2.85	0.670	0.550

(b) Calculation Based on Hot-film Anemometry Test Results

To model structures for wind effects and achieve similarity between model and prototype, the reduced frequencies should be kept equality (Holmes, 2001). This concept is expressed as

$$\left(\frac{nB}{V}\right)_m = \left(\frac{nB}{V}\right)_p \tag{3-12}$$

where, n is frequency which is equal to the inverse of period of the wind gust T, B is characteristic model dimension, and V is mean wind speed. Using Equation (3-12), the corresponding model sampling time is determined.

For example, assuming the model scale is 1:50 and the design 3-second gust wind speed at 10-meter height is 130 mph (mean hourly wind speed at mean roof height is 35 m/s). The model is tested under 1:50 suburban exposure wind tunnel setting, and the wind tunnel mean wind speed at mean roof height is about 5 m/s. The corresponding wind gust period (T_m) for the wind tunnel test can be calculated based on Equation (3-12).

$$\frac{1/T_m\,(1)}{5} = \frac{1/(3s)\,(50)}{35} \quad \text{and} \quad T_m = 0.42s \tag{3-13}$$

Consequently, if the hot-film test samples at 2000 Hz, the equivalent 3-second gust wind speed can be produced by averaging 0.42×2000 samples together. The adjustment factor ϕ can be calculated by using equivalent 3-second gust wind speed at mean roof height and mean wind speed at pitot height.

For severe hurricane events, the hurricane mean winds tend to stay fairly uniform for 15-minute periods (Reinhold, 2000) and full-scale data used in this study was based

on 15-minute records. Therefore, 15-minute mean wind speed of full-scale tests should be used in Equation (3-12) to determine the corresponding model sampling time to create equivalent 15-minute records. Adjustment factors ϕ used in this dissertation are listed in Table 3.6 and Table 3.7. This research focuses on the hurricane wind load on low-rise buildings, thus the adjustment factors ϕ determined by 15-minute mean wind speed are adopted in this dissertation.

Table 3.6 Adjustment Factors ϕ for 1:50 Suburban Terrain Exposure Setting

Model Mean Roof Height (mm)	Adjustment Factors ϕ			$V_{Pitot.Mean}$ (m/s)	Design Wind Speed $V_{10m.Gust}$ (m/s)
	Method 1	Method 2			
		1 Hour	15-min		
71.1	1.51	1.56	1.60	11.2	62.6
76.2	1.51	1.51	1.53		
82.6	1.47	1.47	1.50		
88.9	1.43	1.44	1.48		
95.3	1.39	1.42	1.44		
101.6	1.38	1.39	1.41		

Table 3.7 Adjustment Factor ϕ for 1:50 Open Country Exposure Setting

Model Mean Roof Height (mm)	Adjustment Factors ϕ			$V_{Pitot.Mean}$ (m/s)	Design Wind Speed $V_{10m.Gust}$ (m/s)
	Method 1	Method 2			
		1 Hour	15-min		
71.1	1.30	1.39	1.40	11.2	62.6
76.2	1.28	1.36	1.37		
82.6	1.23	1.32	1.34		
88.9	1.22	1.30	1.31		
95.3	1.20	1.27	1.29		
101.6	1.19	1.23	1.25		

CHAPTER 4

FIELD MEASUREMENT OF HURRICANE WIND LOADS ON HOUSE FL-27

The data recorded by the House Instrumentation System of the Florida Coastal Monitoring Program on a single family house (named as House FL-27 by the FCMP) in two storms, Tropical Storm Isidore (2002) and Hurricane Ivan (2004), are used to calculate external pressure coefficients. 165 sequential 15-minute data records during Tropical Storm Isidore and 211 data records during Hurricane Ivan were successfully collected by the House Instrumentation System. These data sets are summarized in Appendix A. This chapter presents the methodology of this procedure used to measure and analyze extreme wind loads on the subject house.

4.1 Description of Experimental Building and Site

The instrumented house FL-27 is located in Gulf Breeze, Florida, situated in flat terrain approximately 8.0 m above mean sea level and about 0.8 km from the Gulf of Mexico coastline. The house is surrounded by similarly sized residential buildings, and the entire residential community is nearly surrounded by forests to the east, west and south sides. House FL-27 is located in suburban terrain exposure in accordance to ASCE 7-05 wind design provisions. Figure 4.1 provides an aerial view of the subject house (courtesy of Google Earth), as well as views of the locations of the Mobile Tower Systems used to monitor the wind field of both Tropical Storm Isidore and Hurricane Ivan.

Figure 4.1 Aerial View of House FL-27(top), Mobile Tower T1 (Hurrican Ivan, 2004-bottom right) and Mobile Tower T2 (Tropical Storm Isidore, 2002-bottom left)

House FL-27 is 20.7 m in long by 19.5 m wide and 6.1 m high to the ridge with a roof slope of approximately 20° degrees (Figure 4.2(a)). A total of 24 pressure sensors were mounted on the roof with two sensors installed in the attic of the house to measure internal pressure (Figure 4.2(b)). If the house remains enclosed, the attic sensors have been found to provide results that closely follow the atmospheric pressure. An additional atmospheric reference pressure sensor was located on the property, but not mounted to

the house. Additionally, the Mobile Tower Systems are typically located near to the instrumented homes, 1.6 km (Tropical Strom Isidore) and 4.8 km (Hurricane Ivan), providing additional wind velocity and turbulence information as the storm approaches. The towers also had an atmospheric pressure sensors. Two three-cup anemometers were installed at 1.4 m above the roof ridge to record wind speed. The data acquisition system was set up to record wind pressure data with a sampling rate of 100Hz and the wind speed at 1/3 Hz.

Figure 4.2(a) House FL-27 Photos

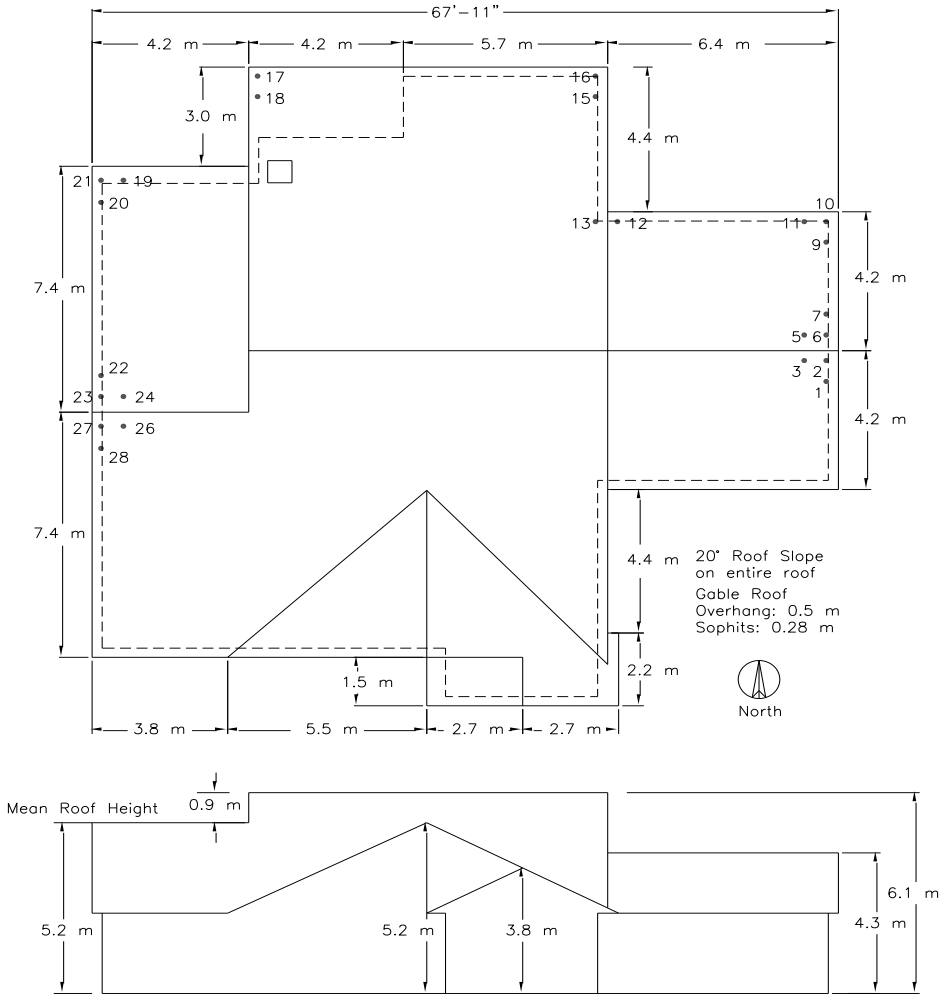

Figure 4.2(b) House FL-27 Roof Plan

4.2 Signal Detection and Preconditioning

Before analyzing full-scale test data, signal detection and preconditioning were preformed to check and remove spurious and degraded signals from the data sets. These signals occurred due to excessive noise, signal dropouts, and transducer malfunctions.

Frequency domain analyses of the fluctuation components of each of the 15-minute signal records of each sensor were executed. By estimating the power spectrum density of the fluctuation components of the 15-minute signal records, the abnormal frequency components were expressed directly. For example, Figure 4.3 presents the power spectrum density of the fluctuation components of the 15-minute records of Channel 9 and Channel 10 measured during Hurricane Ivan. It is obvious that there are narrow-bandwidth peak components in the high frequency region (40Hz ~ 50Hz). These peak components in the high frequency region are estimated to be derived from the AC power supply.

In order to eliminate the spurious and degraded signals displayed in the high frequency region, a digital filter was designed to effectively block the abnormal frequency components without losing desired information. In general, low-rise buildings are categorized as rigid-structures with a high fundamental frequency, and the dynamic amplification effects of wind loads can be neglected. Therefore, in this study, the raw records of sensors were filtered with a 25Hz low-pass filter. The power spectrum density of the fluctuation components of the filtered signals of Channel 9 and Channel 10 measured during Hurricane Ivan are displayed in Figure 4.4.

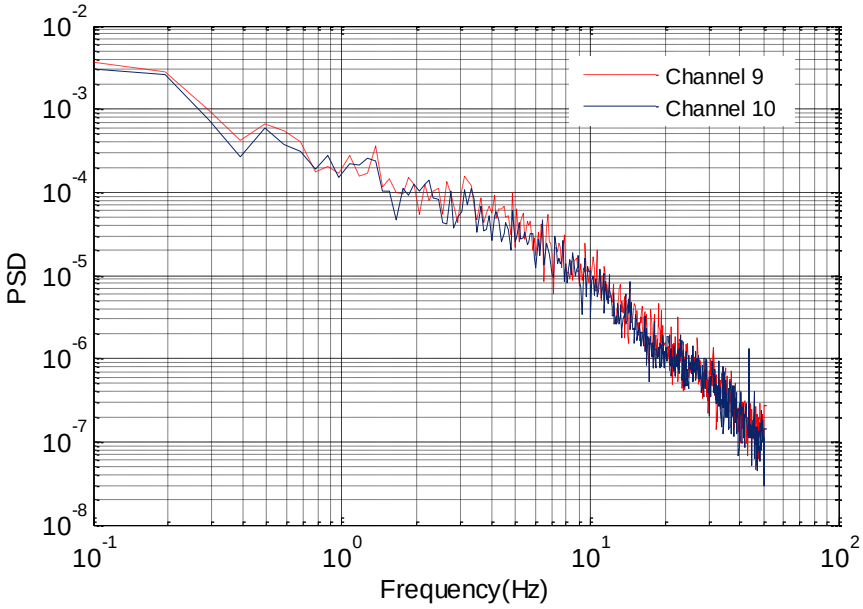

Figure 4.3 Power Spectrum Density of the Fluctuation Component of the Original 15-minute Records of Channel 9 and Channel 10 Measured in Hurricane Ivan (A 15-minute House Record: No. 137)

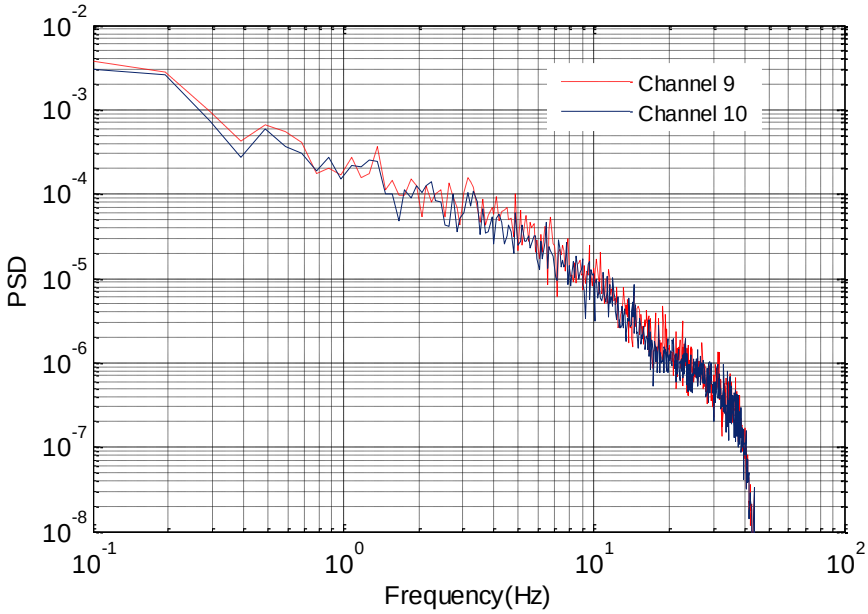

Figure 4.4 Power Spectrum Density of the Fluctuation Component of the Filtered 15-minute Records of Channel 9 and Channel 10 Measured in Hurricane Ivan (A 15-minute House Record: No. 137)

4.3 Analysis Methodology of Wind Loads Recorded by the House Instrumentation System

The House Instrumentation System saves data in 15-minute records with a gap of approximately 8~9 seconds between each 15-minute record. The differential wind pressure measured by the House Instrumentation System is expressed by the following equation:

$$P_i(t) = p_i(t) - p_0(t) \tag{4-1a}$$

where, $P_i(t)$ is the differential (local absolute minus atmospheric reference absolute) wind pressure of channel i at time t, $p_i(t)$ is the absolute pressure measured by channel i at time t (roof sensor), $p_0(t)$ is the absolute atmospheric pressure measured by a reference channel that records atmospheric pressure at time t (attic or atmospheric or Mobile Tower sensor). The analysis uses calibrated output voltage to provide engineering units in psf to each sensor. The absolute pressure measured by sensors is calculated by using the differential voltage from a given senor between calm pre-storm winds and the voltage measured during high winds. Therefore, $P_i(t)$ can be written by:

$$P_i(t) = [p_i(t) - p_i'] - [p_0(t) - p_0'] + (p_i' - p_0') \tag{4-1b}$$

where p_i' is the mean value of absolute pressure measured by channel i in calm pre-storm conditions, p_0' is the mean value of the absolute pressure measured by a reference channel in calm pre-storm conditions (where $p_i' \approx p_0'$), and $P_i(t)$ is finally given by

$$P_i(t) = (\Delta p_i(t) - \Delta p_0(t)) + (p_i' - p_0') \approx \Delta p_i(t) - \Delta p_0(t) \tag{4-1c}$$

where $\Delta p_i(t)$ is the pressure difference between storm and calm conditions on a given roof sensor ($p_i(t)$ and p_i') for channel i, $\Delta p_0(t)$ is the pressure difference between

storm and calm conditions for the reference atmospheric pressure ($p_0(t)$ and p_0') for the reference channel; and i is the channel number for roof, wall and soffit sensors (i = 1,2,…, 28). Equation 4-1c ultimately expresses the difference between local roof and atmospheric pressure, where each is expressed as a differential between pre-storm calm and storm conditions. In this manner, the slope of the calibration curve relating voltage to psf is needed for each sensor and is easily produced in a controlled laboratory pressure chamber, while the y-intercept (offset) of the calibration is not needed as this will vary depending on a number of factors. However, the temperature of the sensor must be accounted for to use this differential analysis scheme.

Changes in temperature will affect the electrical components within the pressure transducer, with a resulting change in the y-intercept (offset) of the calibration curve relating voltage to psf. Therefore temperature differences between calm pre-storm conditions and storm conditions must be accounted for to properly evaluate Equation 4-1c. Ambient temperature differences during hurricane events can be determined by the records of the Mobile Tower Systems located near the experimental house or from hourly temperature data reported by the Asheville National Climatic Data Center. Considering the effect of ambient temperature, the wind pressure measured by the House Instrumentation System can be expressed as:

$$P_i(t) = [\Delta p_i(t) + \Delta p_{i-Temp}] - [\Delta p_0(t) + \Delta p_{0-Temp}] \qquad \text{(4-1d)}$$

where, Δp_{i-Temp} is the indicated difference in pressure of Channel i caused by the change in ambient temperature, Δp_{0-Temp} is the indicated difference in pressure of the reference channel caused by the change in ambient temperature. The relative change in voltage to psf as a function of temperature is also easily produced in a controlled laboratory setting

and is consistent for all sensors used in the House Instrumentation System. A review of Equations 4-1a, b, c, and d reveals the complete set of information necessary to estimate the instantaneous differential pressure at the given roof sensor. This list includes the slope of the calibration curve for each sensor (linear), the effect of temperature on the sensor voltage to psf conversion (changes y-intercept only, not slope), the fluctuating voltage measured at each roof and atmospheric reference sensor for both pre-storm calm and storm conditions, and the mean temperature during both of these time frames.

Finally, a reference 3-second peak wind speed is needed for a given 15-minute record under analysis. The non-dimensional pressure coefficients can now be calculated by the followed equation:

$$C_p(t) = \frac{P_i(t)}{0.00256 \cdot U_{3-\sec}^2} \tag{4-2}$$

where, U_{3s} is the peak 3-second gust wind speed estimated at mean roof height. This value is estimated in several ways and is the subject of Section 4.4 of this chapter.

Based on Equation 4-1d and Equation 4-2, a MATLAB program is developed to process the data collected by the House Instrumentation System and the source program is presented in Appendix A. A flow chart of this program is displayed in Figure 4.5.

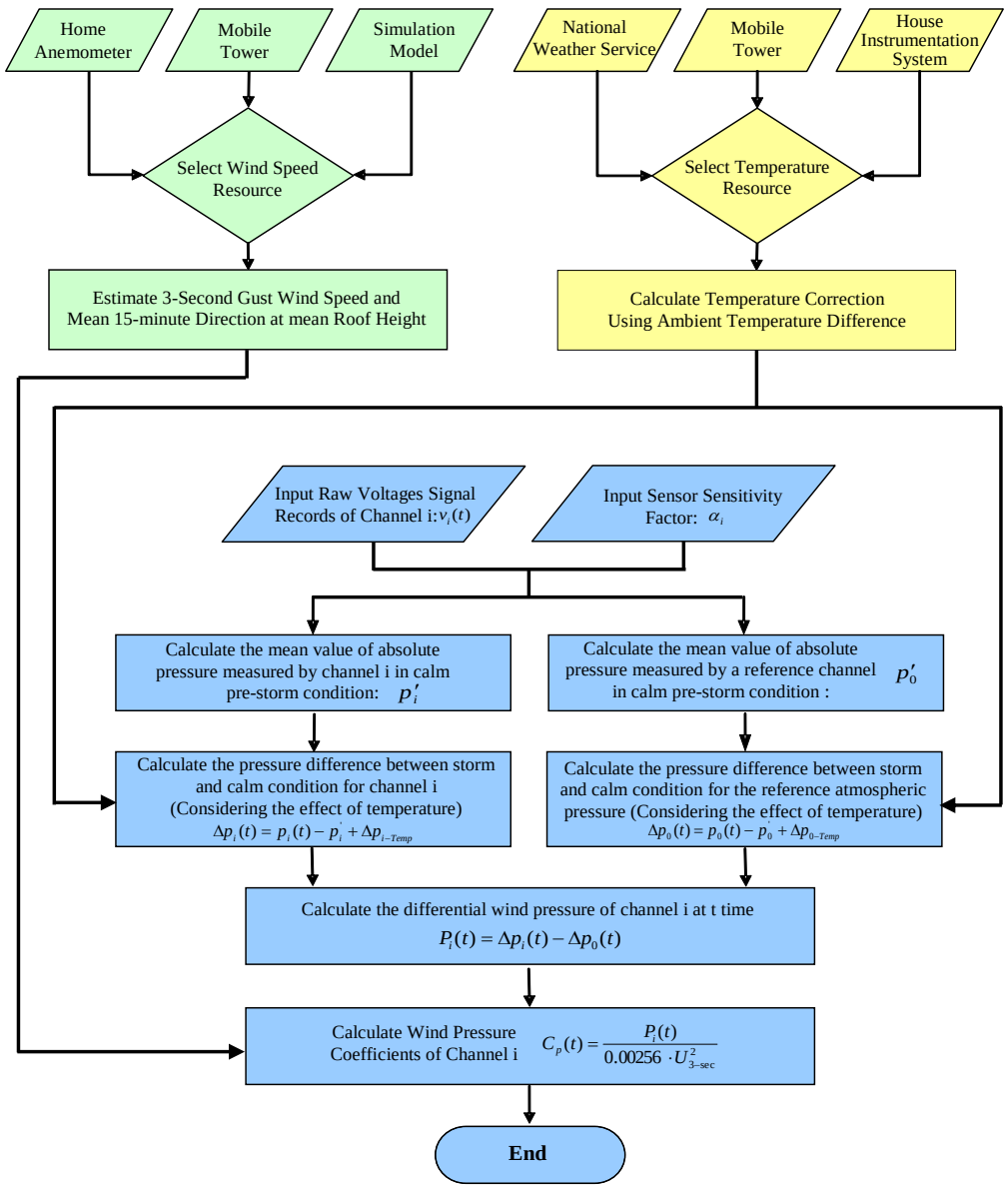

Figure 4.5 Flow Chart of Program to Analyze Full-scale Data Recorded by The House Instrumentation System

4.4 Wind Speeds and Wind Directions at Mean Roof Height of FL-27 House

Wind speed and direction measurements were made using two 3-cup anemometers mounted approximately 1.4 m above the roof ridge (6.5 m above ground). In addition, corroboratory wind speed and wind direction recordings were collected form nearby mobile towers. In Tropical Storm Isidore, the tower was located at the shore in an open parking lot, surrounded by trees to the north, east, and west. In Hurricane Ivan, the tower was located at the Pensacola airport and in open country terrain (see Figure 4.1). A comparison of the data recorded from both the Mobile Tower System and House Instrumentation System enabled the extrapolation of mean wind speed and wind direction at mean roof height. Figures 4.6 (a) and (b) and Figures 4.7(a) and (b) summarize the mean wind speeds and wind directions collected by the Mobile Tower System and House Instrumentation System during Tropical Storm Isidore and Hurricane Ivan. Referring Figure 4.1 and Figure 4.6(b), the wind direction corresponding to the highest winds during Tropical Storm Isidore was out of the southeast, which provides a coastal exposure.

Although house anemometer records were unavoidably disturbed by both the experimental house itself and the surrounding structures, however, the incident wind flow information around House FL-27 recorded by the House Instrumentation System can be verified by comparing with the corresponding mobile tower records. The comparisons of 15-minute mean speeds and wind directions show a coincidental tendency of change in wind speeds and wind directions recorded by both the Mobile Tower System and House Instrumentation System that indicates the House Instrumentation System effectively gauged the wind speeds and wind directions impacting the house at the height of roof.

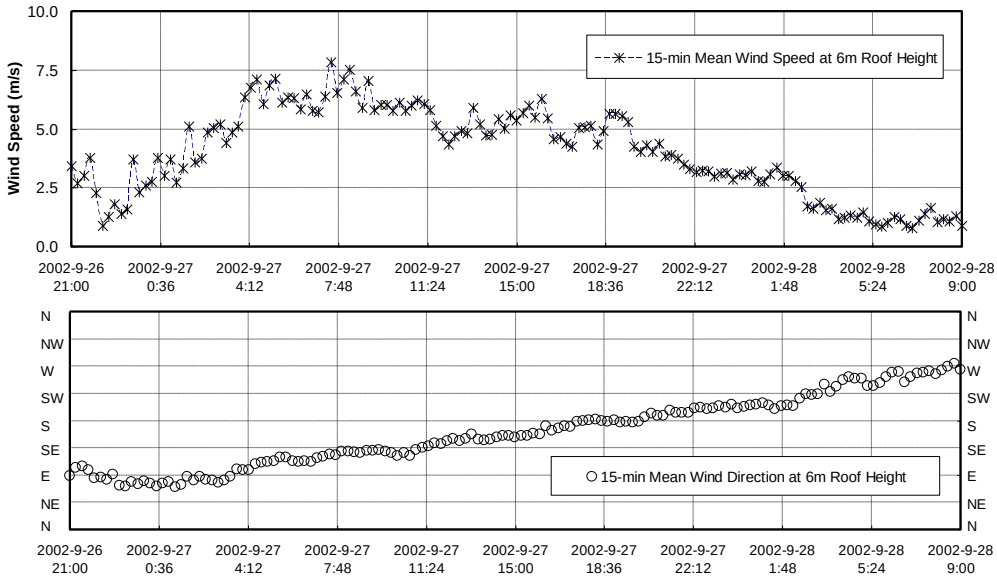

Figure 4.6(a) 15-minute Mean Wind Speeds and Mean Wind Directions Measured by the House Instrumentation System during Tropical Storm Isidore

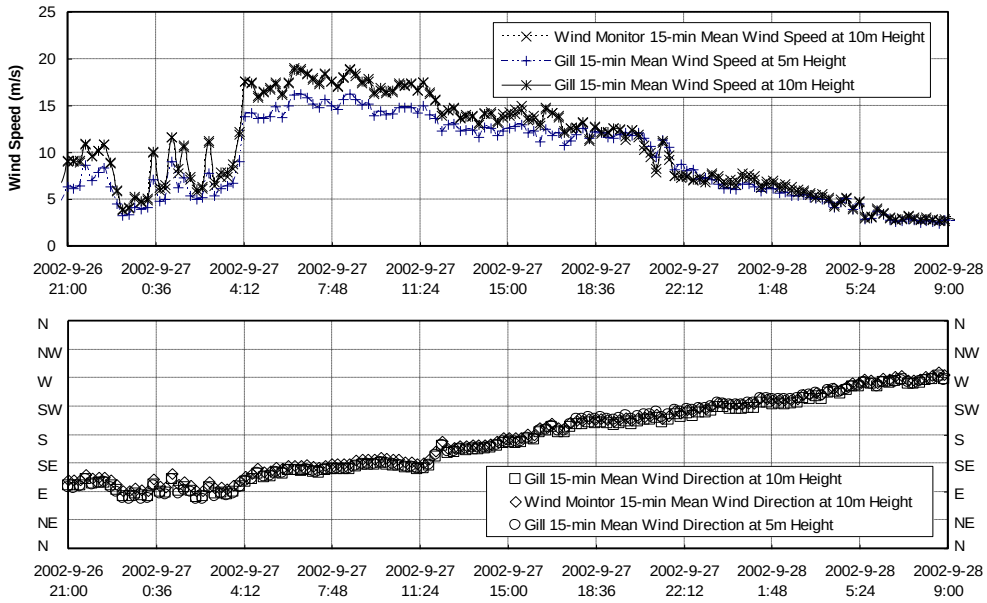

Figure 4.6(b) 15-minute Mean Wind Speeds and Mean Wind Directions Measured by the Mobile Tower System during Tropical Storm Isidore

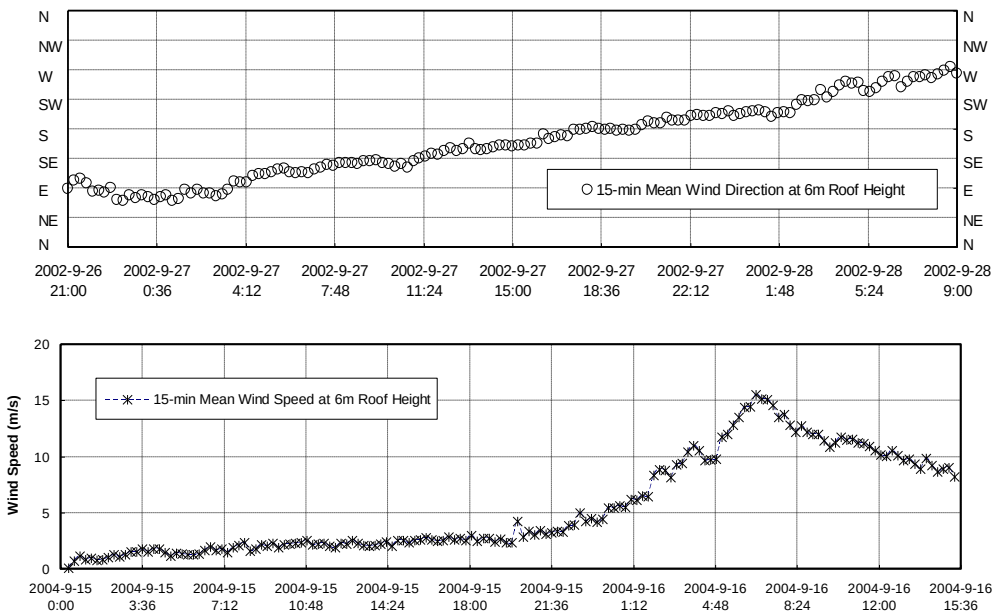

Figure 4.7(a) 15-minute Mean Wind Speeds and Mean Wind Directions Measured by the House Instrumentation System during Hurricane Ivan

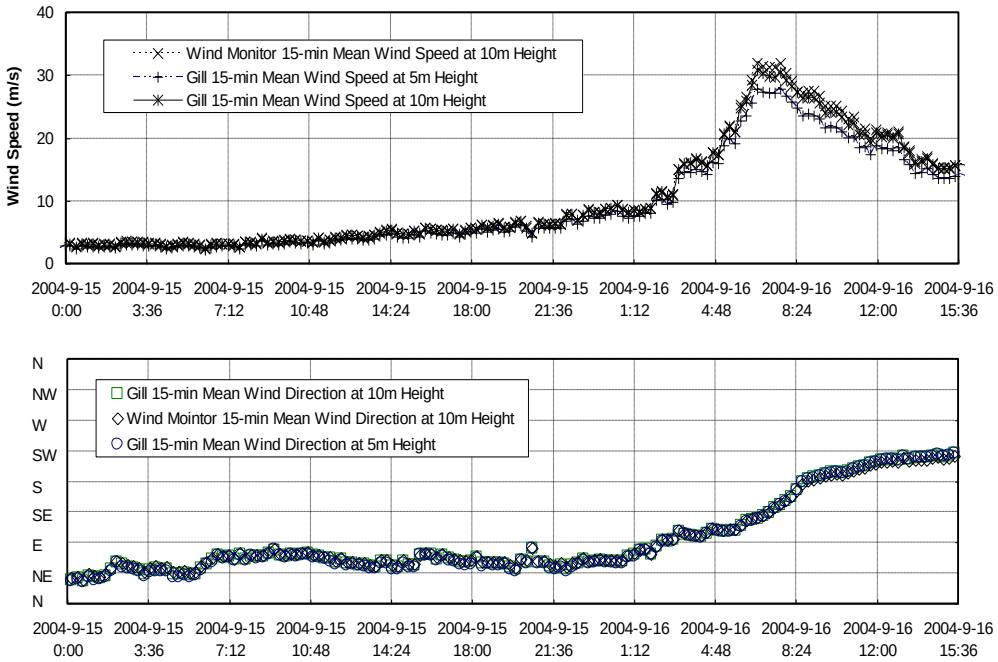

Figure 4.7(b) 15-minute Mean Wind Speeds and Mean Wind Directions Measured by the Mobile Tower System during Hurricane Ivan.

Equation (4-2) uses the 3-second gust wind speed $U_{3-\sec}$ at mean roof height. This peak gust wind speed is typically the expected peak value calculated by the mean wind speed and according to the terrain exposure of the test sites, rather than a direct measure of the peak value for a given record. The relationship between the wind speed averaged over t seconds U_t and the mean hourly wind speed $\overline{U}_h$ can be expressed as Equation (4-3a), and the relationship of the mean hourly wind speed between different terrain exposures can be expressed as Equation (4-3b) (Simiu and Scalan, 1992). Equations (4-3a) and (4-3b) are used to the extrapolate 15-minute mean wind speed $\overline{U}_{15-\min}$ recorded by the house anemometers or the mobile towers to 3-second gust wind speed $U_{3-\sec}$ at mean roof height.

$$U_t = \overline{U}_h \cdot [1 + C(t) \cdot (\sqrt{\beta} / 2.5 \ln(z / z_{0-House}))] \tag{4-3a}$$

$$\overline{U}_h = \overline{U}_{10m-Tower} \cdot \frac{2.5 u_{*House}}{2.5 u_{*Tower}} \cdot \frac{\ln(z / z_{0-House})}{\ln(10 / z_{0-Tower})} \tag{4-3b}$$

where, $\overline{U}_h$ is the mean hourly wind speed at house roof height; the coefficients $C(t)$ and β are listed in the Table 3.3 and Table 3.4, respectively; z is the anemometer height; $z_{0-House}$ and $z_{0-Tower}$ are the roughness length of the full-scale test site and the mobile tower location, respectively; u_{*House} and u_{*Tower} are the friction velocity of the full-scale test site and the mobile tower location, respectively.

House FL-27 is surrounded by similarly sized residences, and the entire community is nearly surrounded by forest to the east, west and south (see Figure 4.1). The exposure of the site can be categorized as suburban terrain exposure, and the corresponding roughness length and the friction velocities are listed in the Table 3.3 and

Table 3.4, respectively. Based on the 15-minute mean wind speeds measured by house anemometers and mobile towers, the 3-second gust wind speeds $U_{3-\sec}$ at mean roof height were calculated and summarized in Table 4.1(a) and Table 4.1(b), respectively. In this study, the 3-second gust wind speeds $U_{3-\sec}$ derived from the mean wind speed provided by the house anemometers were used for calculating wind pressure coefficients on the roof of House FL-27.

Table 4.1(a): The Calculation of 3-second Gust Wind Speed $U_{3-\sec}$ at Mean Roof Height Based on 15-minute Mean Wind Speed Measured by the House Anemometers

	Tropical Storm Isidore	**Hurricane Ivan**
The Maximum 15-minuteMean Wind Speed Measured by House Anemometers (m/s)	7.8	15.5
The Roughness Length $z_{0-House}$(m)	1.0	1.0
3-second Gust Wind Speeds at Mean Roof Height $U_{3-\sec}$(m/s)	16.6	33.0

Table 4.1(b): The Calculation of 3-second Gust Wind Speed $U_{3-\sec}$ at Mean Roof Height Based on 15-minute Mean Wind Speed Measured by the Mobile Towers

	Tropical Storm Isidore	**Hurricane Ivan**
The Maximum 15-minute Mean Wind Speed at 10m Height Measured by Mobile Towers (m/s)	18.9 (Coastal Terrain)	37.1 (Open Country)
The Roughness Length $z_{0-House}$(m)	1.0	1.0
The Roughness Length $z_{0-Tower}$(m)	0.005	0.07
The Ratio of The Friction Velocity u_{*House}/u_{*Tower}	1.60	1.33
3-second Gust Wind Speeds at Mean Roof Height $U_{3-\sec}$(m/s)	16.9	34.8

4.5 Determination of Extreme Wind Load on House FL-27 Roof

The House Instrumentation System successfully collected 165 sequential 15-minute data records during Tropical Storm Isidore and 211 data records during Hurricane Ivan. Each data record contains the pressure sensor and wind speed and direction data. Temperature records were taken from a nearby mobile tower in each case. The wind pressure coefficients were determined by Equation 4.2 and three-second gust wind speeds listed in Table 4.1(a) were determined from conversion of the 15-minute mean wind speed recorded by the house anemometers. Table 4.4 summarizes the main parameters used to process the wind data collected at House FL-27.

Table 4.2 Main Parameters Used in The Process of House Instrumentation System Records

House Name	FL-27
Upstream Exposure	Suburban Terrain Exposure
Sampling Frequency	100 Hz
Sampling Period	15 Minutes
Low-passed Frequency	25 Hz
Reference Pressure	House Instrumentation System Records
Changes of Temperature	Mobile Tower Records
Wind Speed	15-Minute Mean Wind Speed Recorded by House Instrumentation System
Incident Wind Direction	15-Minute Mean Wind Direction Recorded by House Instrumentation System
House Record Number	Tropical Storm Isidore: No.43 – No.49 Hurricane Ivan: No.135 – No.140

The mean, peak negative, peak positive and standard deviation of pressure coefficients recorded during each 15-minute period were calculated based on Equation 4.2 and Equation 4.3. The peak negative and positive pressure coefficients observed during the highest wind speed time sections of the two extreme wind events are displayed

in Figures 4.8 and 4.9. Each column in these figures represents results at a given pressure tap (see Figure 4.2(b) for tap locations by number). Each data point within a given column represents the coefficient resulting from one 15-minute record of full-scale data.

Each plot also includes the components and cladding coefficient value provided in the ASCE 7-05 wind load provisions as a reference point. A thorough probabilistic analysis of the sources and effects of various uncertainties on the estimated full-scale Cp values is presented at the next chapter to provide accurate confidence limits. The wind pressure coefficients observed from full-scale House FL-27 tests are compared with both code values and wind tunnel model studies of these houses in Chapter 6.

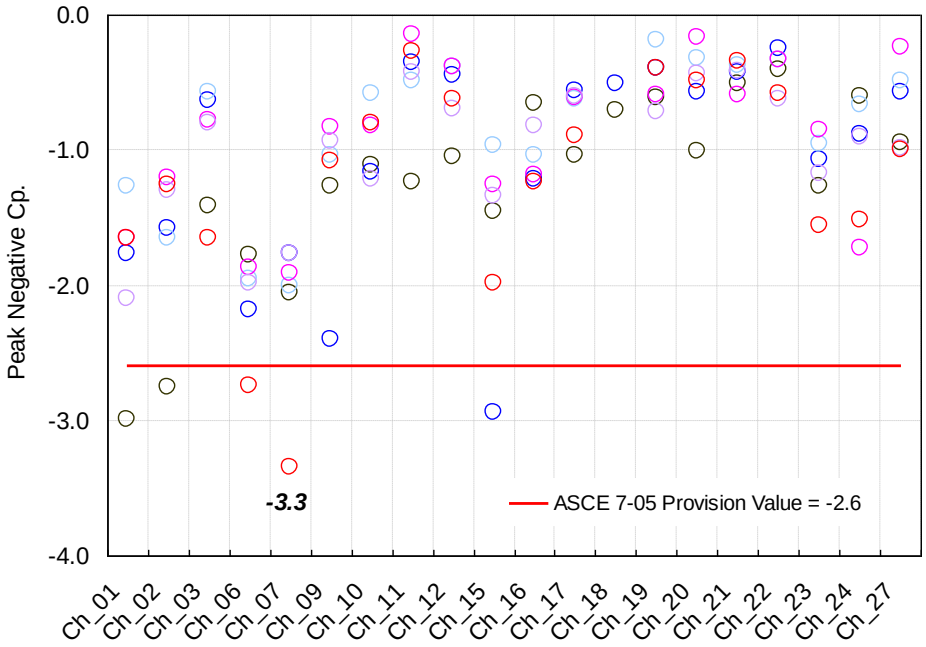

Figure 4.8(a) Peak Negative Pressure Coefficients on FL-27 House Roof Measured in Tropical Storm Isidore (Sampling Frequency: 100 Hz and Low-passed: 25 Hz)

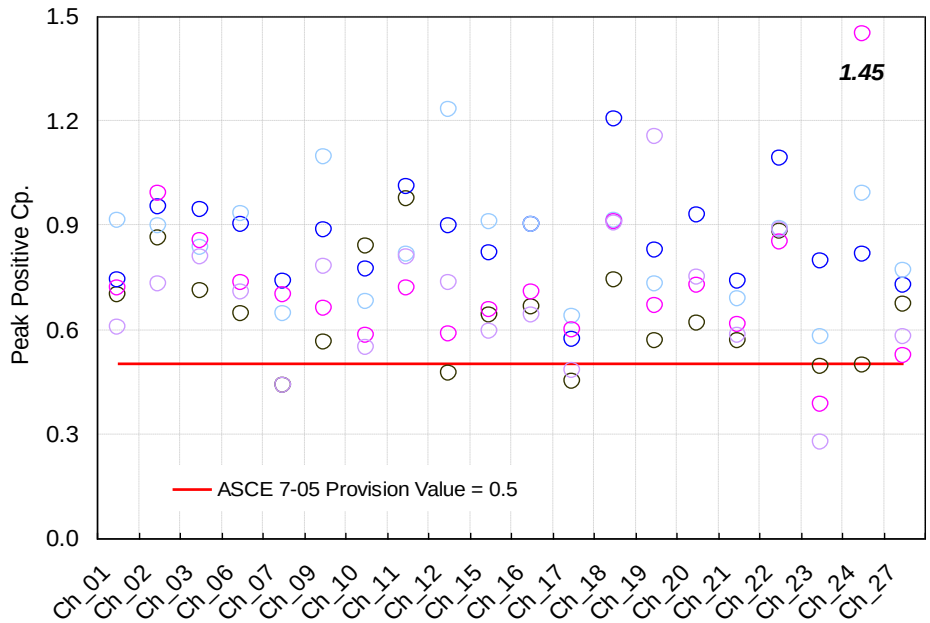

Figure 4.8(b) Peak Positive Pressure Coefficients on FL-27 House Roof Measured in Tropical Storm Isidore (Sampling Frequency: 100 Hz and Low-passed: 25 Hz)

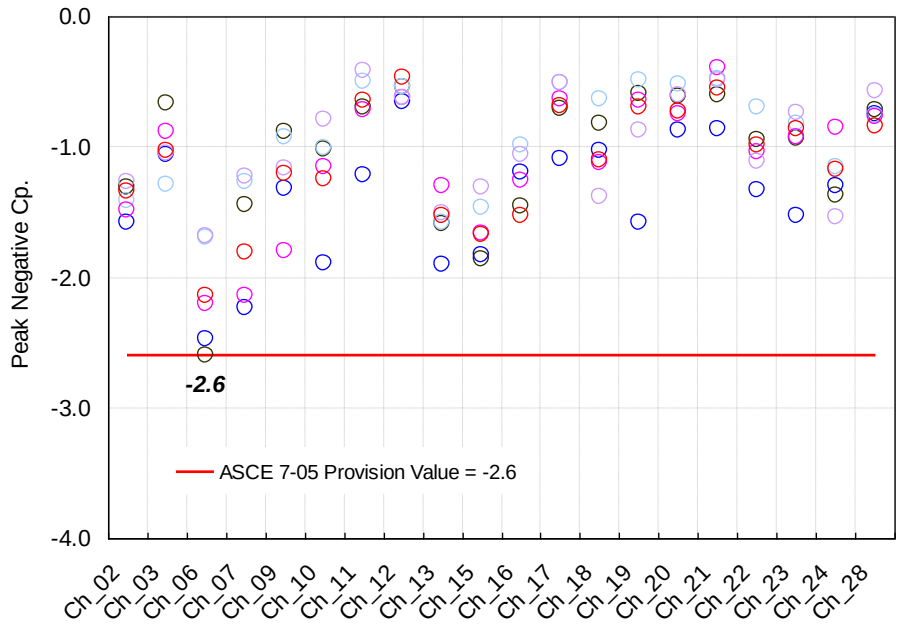

Figure 4.9(a) Peak Negative Pressure Coefficients on FL-27 House Roof Measured in Hurricane Ivan (Sampling Frequency: 100 Hz and Low-passed: 25 Hz)

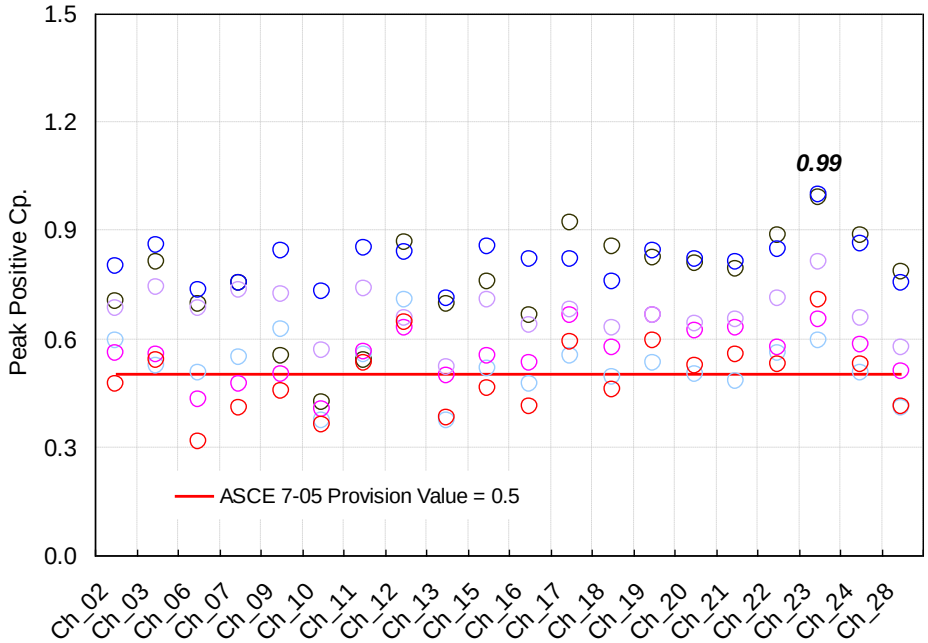

Figure 4.9(b) Peak Positive Pressure Coefficients on FL-27 House Roof Measured in Hurricane Ivan (Sampling Frequency: 100 Hz and Low-passed: 25 Hz)

4.6 Turbulence Intensity, Integral Length Scale and Wind Velocity Spectra

Turbulence intensities for two components, the longitudinal turbulence intensity I_u and the lateral turbulence intensity I_v, are defined as $\sigma_{u'}/\overline{U}$ and $\sigma_{v'}/\overline{U}$, respectively. Here $\overline{U}$ is the 15-minute longitudinal mean wind speed; $\sigma_{u'}$ is the standard deviation of the longitudinal wind velocity fluctuation u'; $\sigma_{v'}$ is the standard deviation of the lateral wind velocity fluctuation v'.

The longitudinal and lateral components of the integral length scale L_u^x and L_v^x are defined by the followed equations, respectively (Simiu and Scalan, 1992):

$$L_u^x = \frac{1}{\sigma_{u'}^2}\int_0^\infty R_{u_1'u_2'}(x)dx \quad \text{and} \quad L_v^x = \frac{1}{\sigma_{v'}^2}\int_0^\infty R_{v_1'v_2'}(x)dx \qquad (4\text{-}4)$$

where $\sigma_{u'}$ is the standard deviation of the longitudinal wind velocity fluctuation u'; $\sigma_{v'}$ is the standard deviation of the lateral wind velocity fluctuation v'; $R_{u'u'}$ is the cross-covariance function of the longitudinal wind velocity fluctuation u' and $R_{v'v'}$ is the cross-covariance function of the lateral wind velocity fluctuation v'.

If it is assumed that flow disturbance travels with velocity $\overline{U}$ and based on Taylor's hypothesis, the longitudinal and lateral components of the integral length scale L_u^x and L_v^x are also expressed as (Simiu and Scalan, 1992)

$$L_u^x = \frac{\overline{U}}{\sigma_{u'}^2}\int_0^\infty R_u(\tau)d\tau \quad \text{and} \quad L_v^x = \frac{\overline{U}}{\sigma_{v'}^2}\int_0^\infty R_v(\tau)d\tau \qquad (4\text{-}5)$$

where, $R_u(\tau)$ and $R_v(\tau)$ are the auto-covariance functions of the fluctuations $u'(x_1,t)$ and $v'(x_1,t)$. The length of record from which $R_u(\tau)$ and $R_v(\tau)$ are estimated is also 15 minutes.

Wind velocity spectra are used to describe the distribution of turbulence with frequency. The longitudinal wind velocity spectrum $S_u(n)$ can be expressed as Equation (4-6) (Holmes, 2001):

$$\sigma_{u'}^2 = \int_0^\infty S_u(n)dn \tag{4-6}$$

In engineering practice, Von Karman's power spectrum is often used to describe the wind velocity spectrum. Von Karman's power spectrum (von Karman, 1948) of the longitudinal velocity fluctuation is given by the following equation:

$$S_u(n) = \frac{2\sigma_{u'}^2 L_u^x}{\overline{U}[1+2(2cnL_u^x/\overline{U})^2]^{5/6}} \tag{4-7}$$

where, $\overline{U}$ is 15-minute mean wind speed; L_u^x is the longitudinal integral length scale; $\sigma_{u'}$ is the standard deviation of the longitudinal wind velocity fluctuation u'; and the coefficient c=2.5.

The turbulence intensities derived from the House Instrumentation System and the Mobile Tower System records measured in Tropical Storm Isidore and Hurricane Ivan were listed at Table 4.3 (a) and (b). The integral length scales derived from the Mobile Tower System records are listed at Tables 4.4. Figures 4.10 and Figures 4.11 present the longitudinal wind velocity spectrum derived from the Mobile Tower System records with the corresponding Von Karman's power spectrum.

Table 4.3(a) Turbulence Intensities Measured by The House Instrumentation Systems

	Tropical Storm Isidore	**Hurricane Ivan**
The Maximum 15-minute Mean Wind Speed at the House Anemometers Height (m/s)	7.8	15.5
The Longitudinal Turbulence Intensities I_u (%)	30~39	32~40
The Lateral Turbulence Intensities I_v (%)	39~49	37~55

Table 4.3(b) Turbulence Intensities Measured by The Mobile Towers near House FL-27

	Tropical Storm Isidore Mobile Tower T2		Hurricane Ivan Mobile Tower T1	
	5m Gill	10m Gill	5m Gill	10m Gill
The Maximum 15-minute Mean Wind Speed at the Mobile Tower Anemometers Height (m/s)	16.3	18.9	27.8	37.1
The Longitudinal Turbulence Intensities I_u (%)	13~17	12~17	16~23	14~23
The Lateral Turbulence Intensities I_v (%)	9 ~ 13	7~ 12	12~16	11~16
Terrain Exposure of Mobile Tower Locations	Coastal Terrain		Open Country	

Table 4.4 Integral Length Scales Measured by the Mobile Towers near House FL-27

	Tropical Storm Isidore Mobile Tower T2		Hurricane Ivan Mobile Tower T1	
	5m Gill	10m Gill	5m Gill	10m Gill
The Maximum 15-minute Mean Wind Speed at the Mobile Tower Anemometers Height (m/s)	16.3	18.9	27.8	30.8
The Mean Longitudinal Integral Length Scales L_u^x (m)	204	325	170	206
The Mean Lateral Integral Length Scales L_v^x (m)	105	125	145	165
Terrain Exposure of Mobile Tower Locations	Coastal Terrain		Open Country	

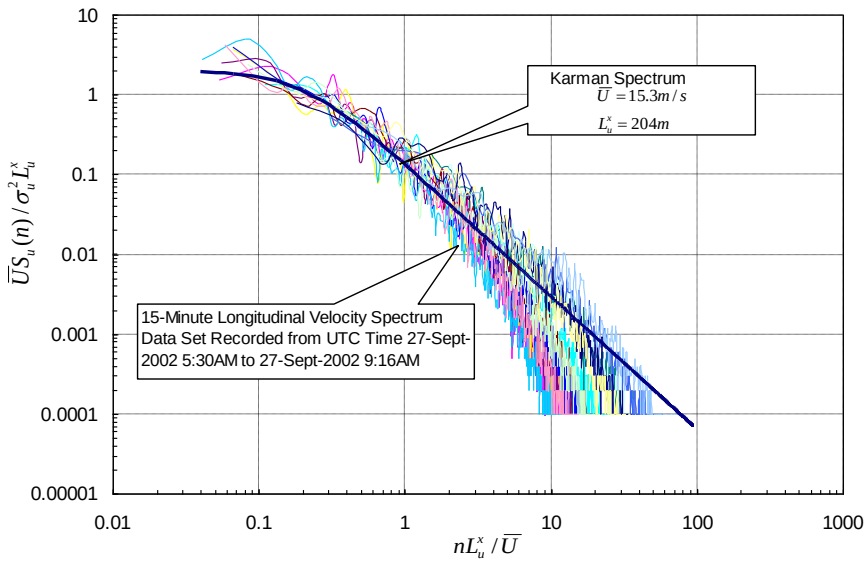

Figure 4.10(a) Normalized Spectrum of the Longitudinal Velocity Component Recorded by the 5 m Gill Anemometer of the Mobile tower T2 in Tropical Storm Isidore and the Corresponding Von Karman Spectrum

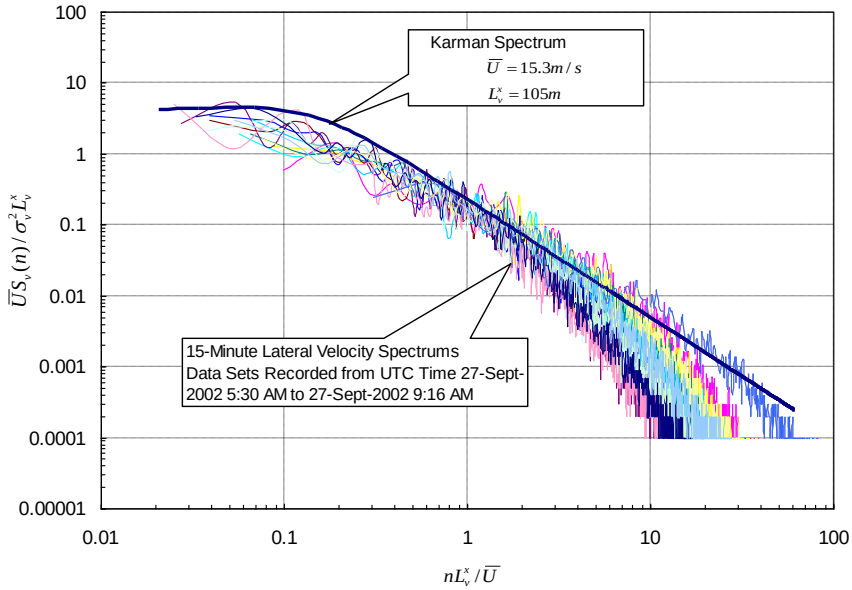

Figure 4.10(b) Normalized Spectrum of the Lateral Velocity Component Recorded by the 5 m Gill Anemometer of the Mobile Tower T2 in Tropical Storm Isidore and the Corresponding Von Karman Spectrum

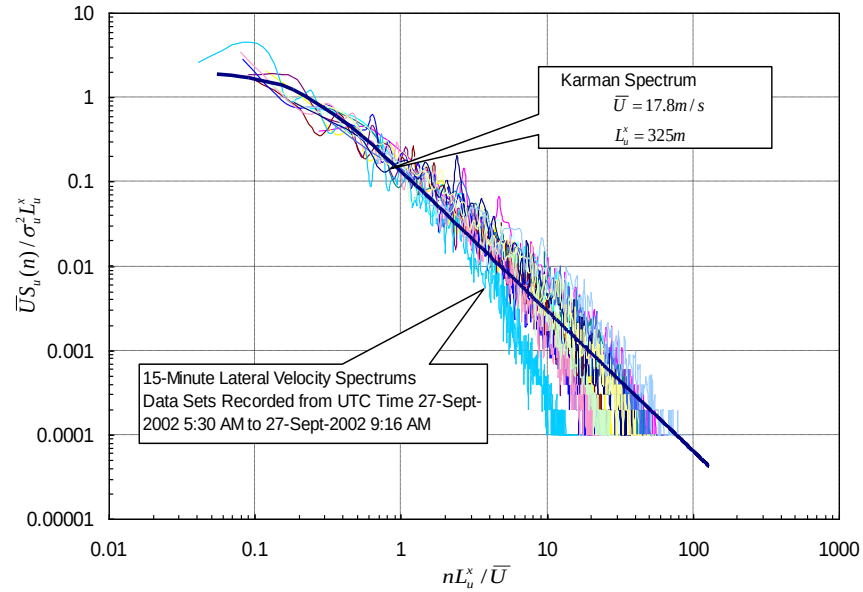

Figure 4.10(c) Normalized Spectrum of the Longitudinal Velocity Component Recorded by the 10 m Gill Anemometer of the Mobile tower T2 in Tropical Storm Isidore and the Corresponding Von Karman Spectrum

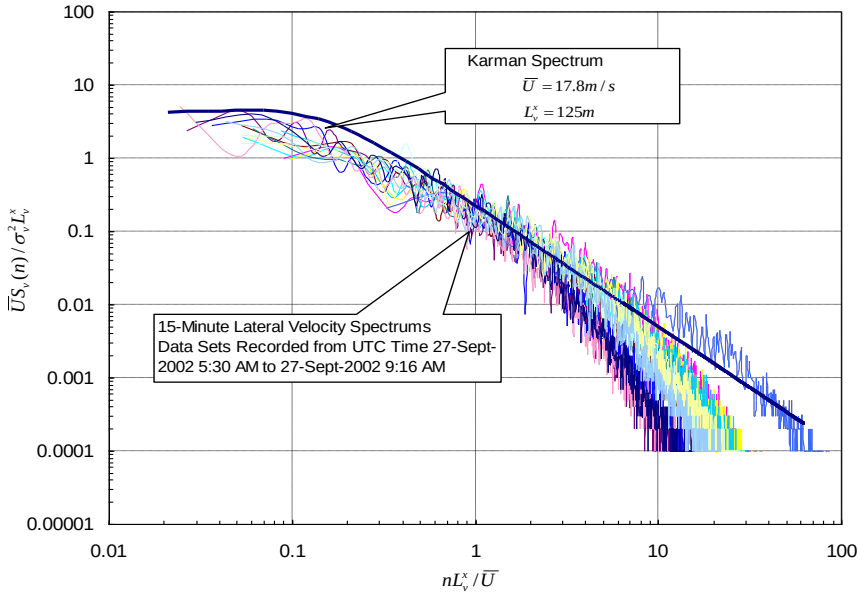

Figure 4.10(d) Normalized Spectrum of the Lateral Velocity Component Recorded by the 10 m Gill Anemometer of the Mobile Tower T2 in Tropical Storm Isidore and the Corresponding Von Karman Spectrum

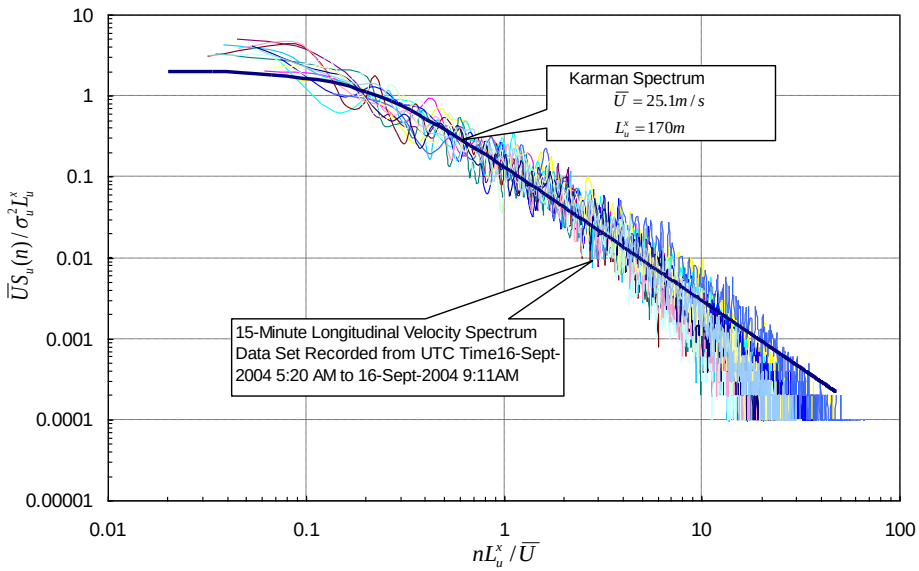

Figure 4.11(a) Normalized Spectrum of the Longitudinal Velocity Component Recorded by the 5 m Gill Anemometer of the Mobile tower T1 in Hurricane Ivan and the Corresponding Von Karman Spectrum

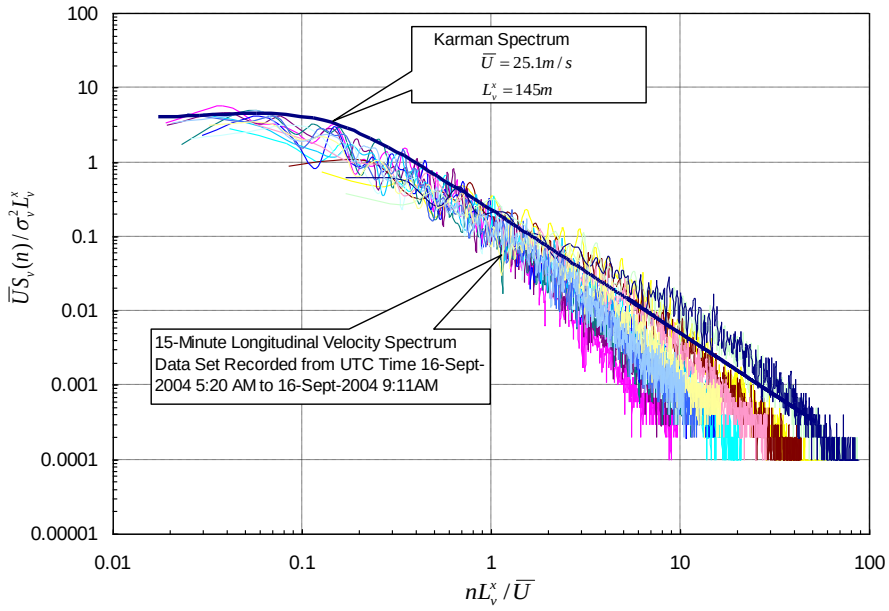

Figure 4.11(b) Normalized Spectrum of the Lateral Velocity Component Recorded by the 5 m Gill Anemometer of the Mobile Tower T1 in Hurricane Ivan and the Corresponding Von Karman Spectrum

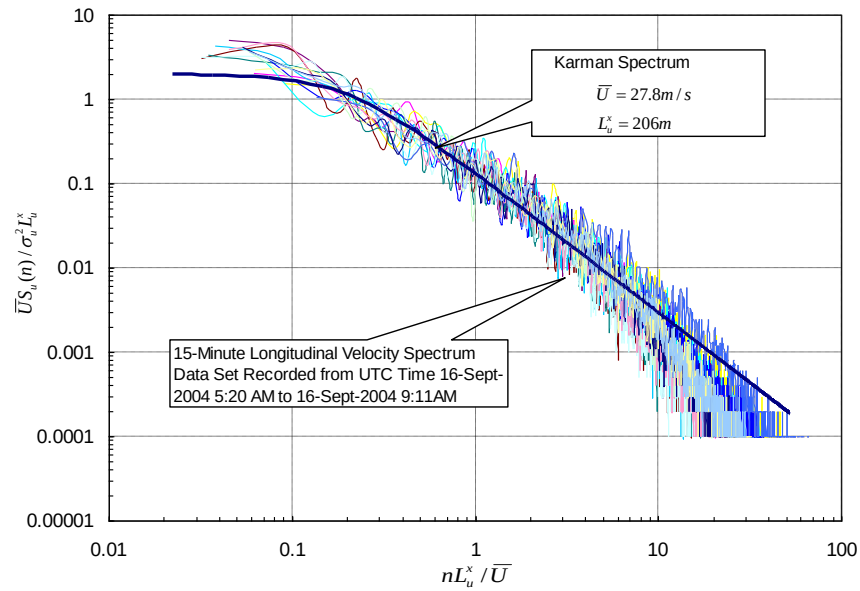

Figure 4.11(c) Normalized Spectrum of the Longitudinal Velocity Component Recorded by the 10 m Gill Anemometer of the Mobile tower T1 in Hurricane Ivan and the Corresponding Von Karman Spectrum

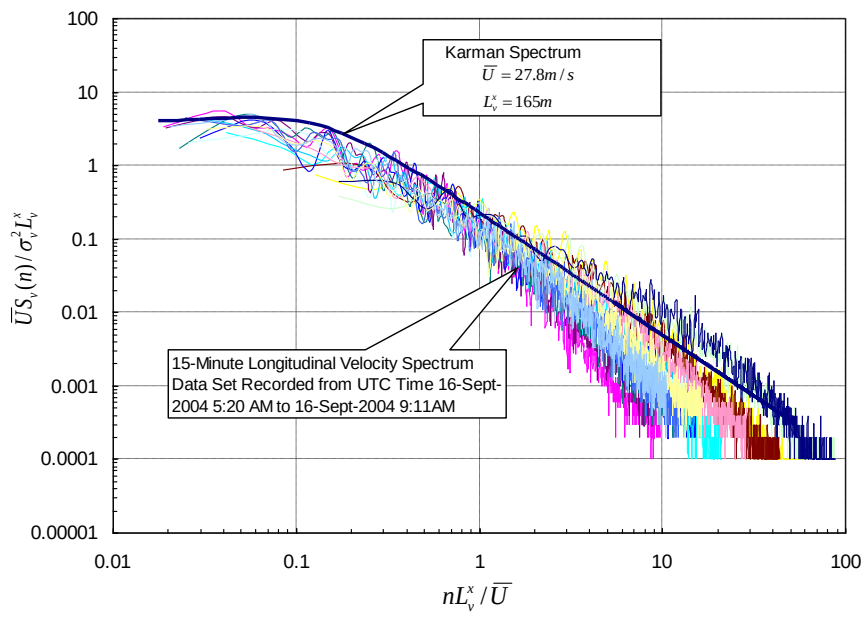

Figure 4.11(d) Normalized Spectrum of the Lateral Velocity Component Recorded by the 10 m Gill Anemometer of the Mobile Tower T1 in Hurricane Ivan and the Corresponding Von Karman Spectrum

4.7 Summary

This chapter presented the methodology for determining extreme wind loads on House FL-27 measured by the House Instrumentation System of FCMP. The preliminary results provided the peak negative and positive pressure coefficients during the highest wind speed time sections of two storms.

The worst peak negative pressure coefficient observed in the Tropical Storm Isidore is -3.3, which value exceeds ASCE 7-05 code value of -2.6 by 26%; and the worst peak positive pressure coefficient observed in the Tropical Storm Isidore is 1.45, which value exceeds ASCE 7-05 code value of 0.5 by 190%.

The worst peak negative pressure coefficient observed in the Hurricane Ivan is -2.6, which value equals to ASCE 7-05 code value of -2.6; and the worst peak positive pressure coefficient observed in the Hurricane Ivan is 0.99, which value exceeds ASCE 7-05 code value of 0.5 by 98%.

These preliminary results in this chapter are reported without consideration of potential systematic errors of the measurement system. The next chapter presents analysis and results to assess the uncertainty of full-scale test data.

CHAPTER 5

VALIDATION OF FULL-SCALE TEST RESULTS OF HOUSE FL-27

Wind pressure coefficients measured by the House Instrumentation System are affected by several variables including temperature difference before and during the storm, the atmospheric pressure, sensitivity factors of pressure transducers, and wind speed at mean roof height.

Chapter 4 presented the analysis method used to determine full-scale pressure coefficients. However, the errors (systematic and random) in the data were not established. This chapter will present a reliability analysis to determine the systematic errors in the results. The purpose of this work is to establish confidence level in the full-scale test results. In addition, the probabilistic properties of wind loads and the effects of spatial and time averaging on the peak wind loads are also investigated.

5.1 Sensitivity Analysis for Basic Parameters

The analysis method for wind loads recorded by the House Instrumentation System is described in the Figure 4.5. It can be expressed as the followed equation:

$$p_i(t) = [\Delta p_i(t) + \Delta p_{i-Temp}] - [\Delta p_0(t) + \Delta p_{0-Temp}] \tag{5-1}$$

where, Δp_{i-Temp} is the indicated difference in pressure of Channel i caused by the change in ambient temperature, Δp_{0-Temp} is the indicated difference in pressure of the reference channel caused by the change in ambient temperature. The relative change in voltage to

psf as a function of temperature is also easily reproduced in a controlled laboratory setting, and is consistent for all sensors used in the House Instrumentation System.

In order to compare the full-scale test with the wind tunnel simulation, the pressure differences between storm and calm conditions for the reference atmospheric pressure $\Delta p_0(t)$ at time t were substituted by the 15-minute mean pressure difference $\Delta\overline{p}_0$. The 15-minute mean pressure difference $\Delta\overline{p}_0$ can be expressed as the followed equation:

$$\Delta\overline{p}_0 = (\overline{v}_0 - v_{0_ref}) \cdot \alpha_0 \tag{5-2}$$

where, $\overline{v}_0$ is the mean voltage of the reference channel for a 15-minute record during storm, and v_{0_ref} is the voltage record of the reference channel for a 15-minute record before the storm.

Wind pressure p_i of channel i at time t in the full-scale records of the House Instrumentation System can be calculated by:

$$p_i(t) = \left(v(t)_i - v_{i_ref} + \Delta T \cdot \frac{0.0144}{20.6} \cdot \alpha_i \right) \cdot \alpha_i - \left(\overline{v}_0 - v_{0_ref} + \Delta T \cdot \frac{0.0144}{20.6} \cdot \alpha_0 \right) \cdot \alpha_0 \tag{5-3}$$

where, $v(t)_i$ is the voltage record for channel i at time t for a 15-minute record during torm; v_{i_ref} is the voltage record for channel i for a 15-minute record before storm; ΔT is the ambient temperature differences between calm pre-storm and in-storm conditions; α_i is the sensitivity factor of channel i.

Therefore, the negative peak pressure $\check{p}_{i-15\min}$, the mean pressure $\bar{p}_{i-15\min}$ and the positive peak pressure $\hat{p}_{i-15\min}$ in a 15-minute period during storm can be calculated as following equations, respectively:

$$\check{p}_{i-15\min} = \left(\check{v}_i - v_{i_ref} + \Delta T \cdot \frac{0.0144}{20.6} \cdot \alpha_i\right) \cdot \alpha_i - \left(\bar{v}_0 - v_{0_ref} + \Delta T \cdot \frac{0.0144}{20.6} \cdot \alpha_0\right) \cdot \alpha_0 \tag{5-4a}$$

$$\bar{p}_{i-15\min} = \left(\bar{v}_i - v_{i_ref} + \Delta T \cdot \frac{0.0144}{20.6} \cdot \alpha_i\right) \cdot \alpha_i - \left(\bar{v}_0 - v_{0_ref} + \Delta T \cdot \frac{0.0144}{20.6} \cdot \alpha_0\right) \cdot \alpha_0 \tag{5-4b}$$

$$\hat{p}_{i-15\min} = \left(\hat{v}_i - v_{i_ref} + \Delta T \cdot \frac{0.0144}{20.6} \cdot \alpha_i\right) \cdot \alpha_i - \left(\bar{v}_0 - v_{0_ref} + \Delta T \cdot \frac{0.0144}{20.6} \cdot \alpha_0\right) \cdot \alpha_0 \tag{5-4c}$$

where, $\check{v}_i$ is the minimum voltage of a 15-minute record for channel *i* during storm; $\bar{v}_i$ is the mean voltage of a 15-minute record for channel *i* during storm; $\hat{v}_i$ is the maximum voltage of a 15-minute record for channel *i* during storm.

Wind pressures $p_{i-15\min}$ are characterized by negative peak wind pressure $\check{p}_{i-15\min}$, mean wind pressure $\bar{p}_{i-15\min}$, and positive peak wind pressure $\hat{p}_{i-15\min}$ in a 15-minute segment during storm are linear functions with the variables v_{i_ref}, $\bar{v}_{0_ref}$, ΔT, α_i and α_0.

$$\check{p}_{i-15\min} = f(v_{i_ref}, v_{0_ref}, \Delta T, \alpha_i, \alpha_0; \check{v}_i) \tag{5-5a}$$

$$\bar{p}_{i-15\min} = f(v_{i_ref}, v_{0_ref}, \Delta T, \alpha_i, \alpha_0; \bar{v}_i) \tag{5-5b}$$

$$\hat{p}_{i-15\min} = f(v_{i_ref}, v_{0_ref}, \Delta T, \alpha_i, \alpha_0; \hat{v}_i) \tag{5-5c}$$

The accuracy of assessment of the wind pressure coefficients measured by the House Instrumentation System depends on the accuracies of these variables. These variables can be treated as random variables. For each variable, the sensitivity factor is used to evaluate the effect of the variable on wind pressures $p_{i-15\min}$. The sensitivity factor of one variable in the linear functions is equal to the partial derivative of this variable. The absolute values of the sensitivity factors indicate the degree of variation in wind pressures $p_{i-15\min}$ due to the change in that variable. If the sensitivity factor of a variable is close to zero, then this variable can be treated as a deterministic variable rather than a random variable and the effect of the random changes of this variable on wind pressure can be neglected.

The sign of the sensitivity factor indicates the tendency of the wind pressure changes to follow the changes of a variable. A "+" value of sensitivity factor indicates that increasing the variable leads to an increase in wind pressure, and a "-" value of the sensitivity factor indicates that increasing the variable leads to a decrease in wind pressure. Table 5.1 summarizes the sensitivity factors of random variables used in Equation (5-5), and the estimated values of sensitivity factors can be approximately calculated with the variables listed on Table 5.2.

Apparently, wind pressure $p_{i-15\min}$ is sensitive to variables v_{0_ref} and v_{i_ref}. If the pressure sensor, which is used to monitor the pressure changes of the reference channel, is the same type of sensor used to measure wind pressure on a house. The calibration factor of pressure sensors α_i should be close to the calibration factor of the reference

sensor, and the sensitivity factor of ΔT should be close to zero. Therefore, the random variable ΔT can be treated as a deterministic variable.

Table 5.1 Summary of sensitivity factors of random variables in the calculation of wind pressure $p_{i-15\min}$ by the House Instrumentation System

Variable Name	Sensitivity Factor	Estimation Value	
		Isidore	Ivan
v_{0_ref}	α_0	20.6	34.2
v_{i_ref}	$-\alpha_i$	-34.4	-34.2
α_i	$v_i - v_{i_ref} + 2\cdot\Delta T\cdot\frac{0.0144}{20.6}\cdot\alpha_i$	-0.4	-3.3
α_0	$-(\bar{v}_0 - v_{0_ref} + 2\cdot\Delta T\cdot\frac{0.0144}{20.6}\cdot\alpha_0)$	0.9	2.7
ΔT	$\frac{0.0144}{20.6}\cdot(\alpha_i^2 - \alpha_0^2)$	0.6	0

Table 5.2 Summary of mean and standard deviation of random variables in the calculation of wind pressure $p_{i-15\min}$ by the House Instrumentation System

Variable Name		Mean Value $E(\cdot)$	Coefficient of Variation (%)
v_{0_ref} (voltage)	Ivan	5.15	0.08
	Isidore	7.90	0.08
v_{i_ref} (voltage)	Ivan	4.87 ~ 5.54	0.10
	Isidore	4.52 ~ 5.31	0.10
α_i (psf /voltage)	Ivan	34.0 ~ 34.7	1.10
	Isidore	34.3 ~ 34.7	1.10
α_0 (psf /voltage)	Ivan	34.27	1.10
	Isidore	20.60	1.10
15-minute ΔT (F°) During Storm	Ivan	-2.0 ~ -5.7	10.0
	Isidore	2.5 ~ 2.5	10.0

5.2 Uncertainty Analysis of the Wind Loads Measured by the House Instrumentation System

Negative peak pressure $\check{p}_{i-15\min}$, mean pressure $\bar{p}_{i-15\min}$, and positive peak pressure $\hat{p}_{i-15\min}$ in a 15-minute period during storm are described by the function of the variables v_{i_ref}, $\bar{v}_{0_ref}$, ΔT, α_i, and α_0, shown as Equation (5-5). Considering the random of these variables, the wind pressure $p_{i-15\min}$ should be treated as a random variable.

Wind pressures $p_{i-15\min}$ are characterized by negative peak wind pressure $\check{p}_{i-15\min}$, mean wind pressure $\bar{p}_{i-15\min}$, and positive peak wind pressure $\hat{p}_{i-15\min}$ in 15-minute period during storm and they are linear functions with random variables v_{i_ref}, $\bar{v}_{0_ref}$, ΔT, α_i and α_0. When the sensors for measuring wind pressure on house roof are the same type of the sensor for measuring reference pressure, the sensitivity of parameter of a random variable ΔT is close to zero. It indicates that the effect of random variable ΔT can be treated as a deterministic variable.

The Monte Carlo simulation analysis (Melchers, 1999) is utilized to investigate the statistic characteristics of wind pressure $p_{i-15\mathrm{m}}$. The mean values and the coefficient of variations of random variables including v_{i_ref}, $\bar{v}_{0_ref}$, α_i and α_0 are summarized in Table 5.2. The standard deviations of these variations are small. The smaller the standard deviations of these variations are, the weaker the effect of the probability distribution of random variables is when generating the random data by using the Monte Carlo simulation method. Therefore, the probability distributions of random variables v_{i_ref},

$\bar{v}_{0_ref}$, α_i and α_0 are supposed to follow the normal distribution in this research. Using the random number generator in MATLAB, 16 random numbers of each random variable v_{i_ref}, $\bar{v}_{0_ref}$, α_i, and α_0 are simulated based on the statistic values described on Table 5.2. Each simulated random numbers of each variable is input into Equation (5-4) separately and form sets of mean and peak wind pressures. A set of wind pressures consists of 65536 (16^4) simulated values. The mean values and standard deviations of each set of peak and mean simulation wind pressures on House FL-27 during Hurricane Ivan are summarized in Appendix C.

The variances of wind pressure $p_{i-15\min}$ caused by random variables v_{i_ref}, $\bar{v}_{0_ref}$, α_i, and α_0 change spatially and temporally. The simulation results listed in Appendix B show that the standard deviations of the mean and peak wind pressures of each channel vary between 0.71 and 1.33 psf. The analysis results of a 15-minute record of Channel 2 (House Record: No.138) show that the normal distribution can effectively describe the probability density function of random variables $p_{i-15\min}$ (see Figure 5.1). According to the mean value and the standard deviation of a random variable $p_{i-15\min}$ which follows the normal distribution, the range of the random variable $p_{i-15\min}$ with 95% confidence level can be calculated. A $\pm 2\sigma$ (up to ±2.7 psf) of mean values can achieve a confidence level of 95%. The worst peak wind pressure coefficients with the confidence level of 95% measured in the full-scale test of House FL-27 during Hurricane Ivan (House Records: No.135-No.140) are shown in the Figure 5.2.

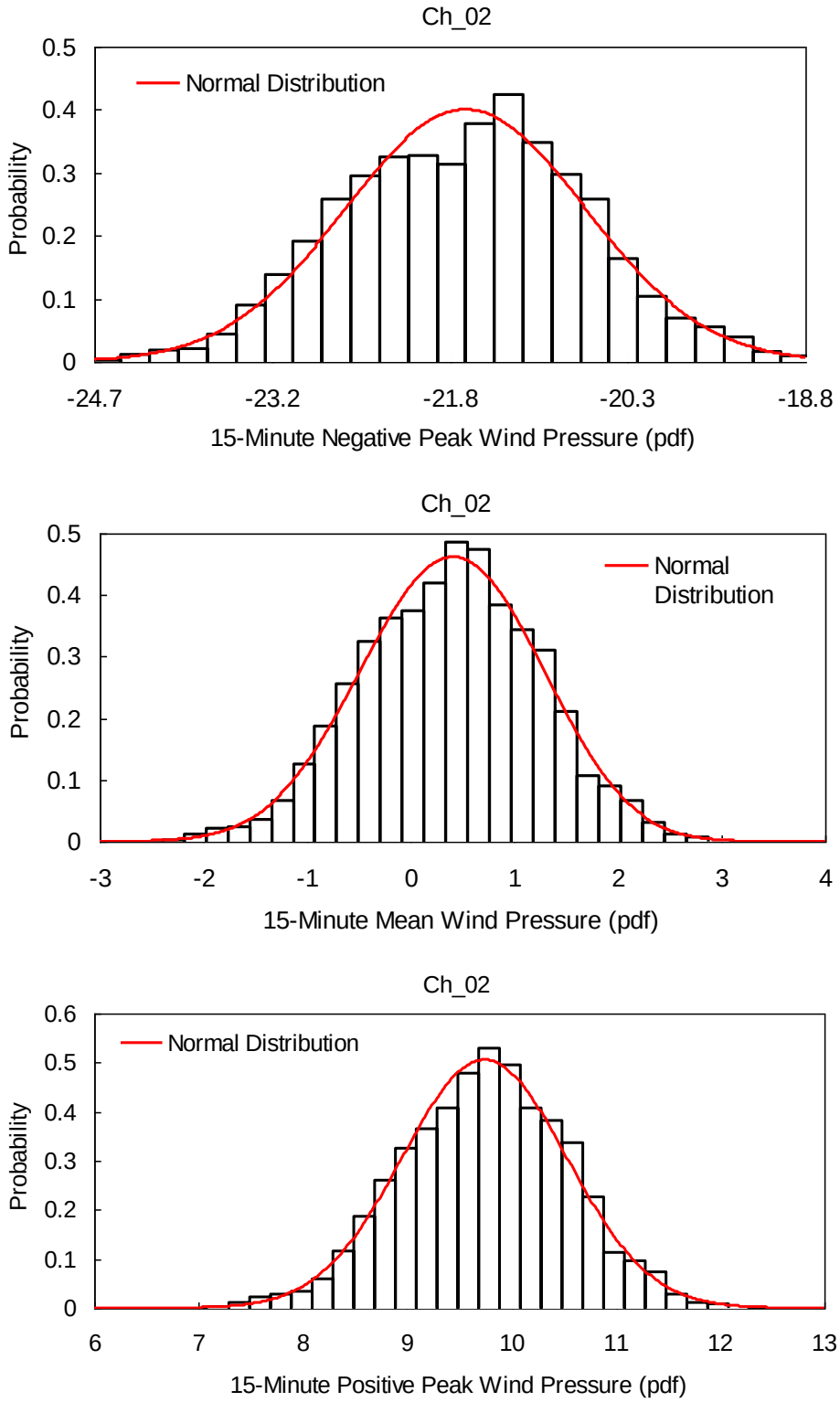

Figure 5.1 Probability Distribution of 15-Minute Mean and Peak Wind Pressure of Channel 2

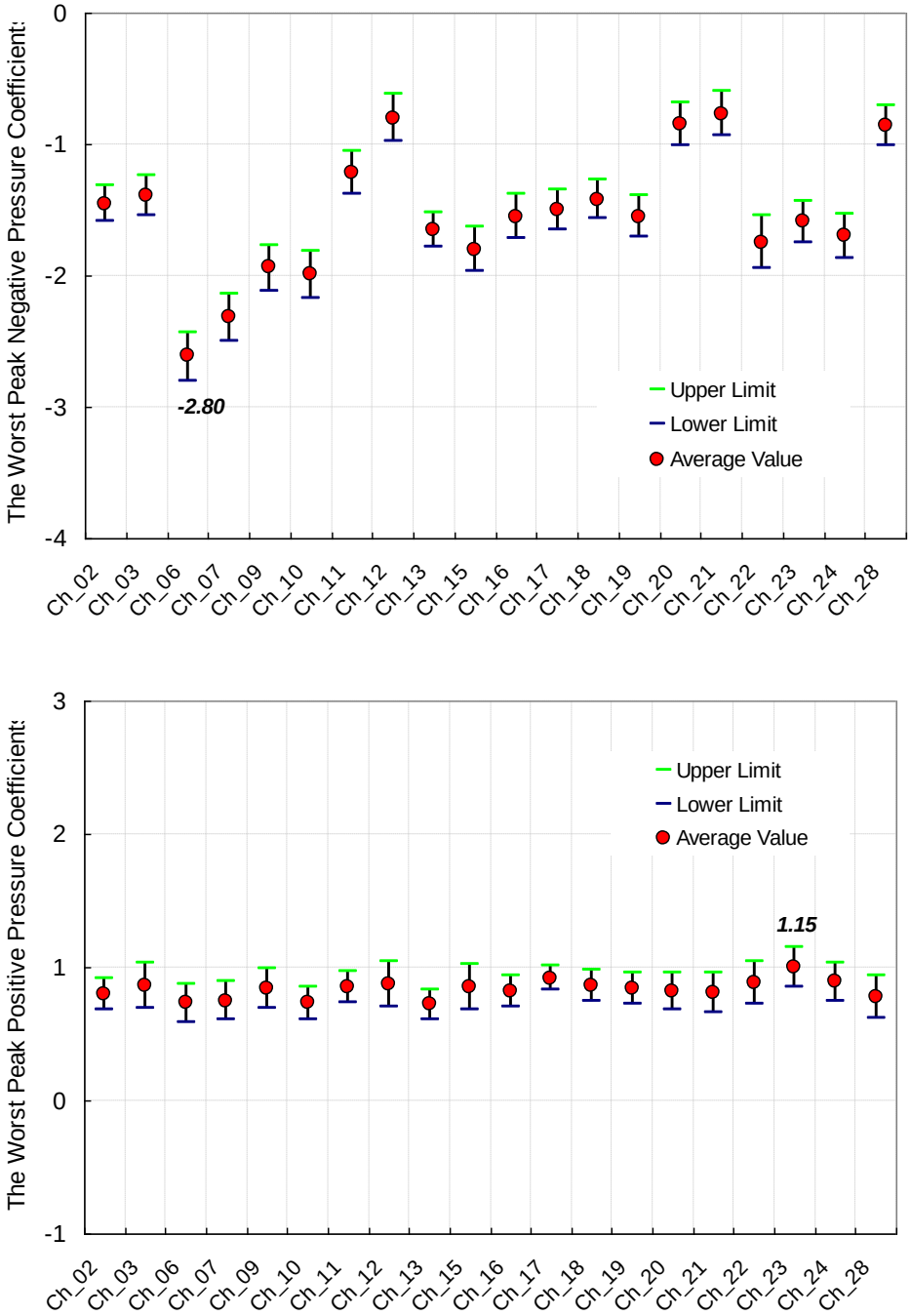

Figure 5.2 Peak Negative and Positive Wind Pressure Coefficients with The Confidence Level of 95% on The FL-27 House Measured in Hurricane Ivan (Sampling Frequency = 100 Hz, Low-pass = 25 Hz)

5.3 Effects of the Choice of Mobile Tower Records as the Reference Pressure

Full-scale tests of the FCMP use two instrumentation systems, namely the House Instrumentation System and the Mobile Tower System. The atmospheric pressure sensors of the Mobile Tower System are used as the backups if the House Instrumentation System fails to record the changes of reference atmospheric pressure. The reference atmospheric pressure is used to calculate wind load on House FL-27. To evaluate the effect of the different atmospheric reference pressure sources on pressure coefficients, atmospheric pressure data obtained from the Mobile Tower System was used to determine pressure coefficients on the roof in Hurricane Ivan.

The peak negative and positive pressure coefficients were calculated using Equation (5-4). For the peak negative pressure coefficients, it was found that the difference of 6% in the worst external pressure coefficient occurred at Channel 6 using the mobile tower reference pressure records and the house instrumentation records (see Figure 5.3). For the peak positive pressure coefficients, the largest difference of 30% in the worst external pressure coefficient occurred at Channel 23 using the mobile tower reference pressure records and the house instrumentation records.

The comparison in Figure 5.3 shows that using atmospheric pressure data obtained from the Mobile Tower System for calculating peak negative pressure coefficients can cause an average difference of less than 10%. This relatively low difference level indicates that the results from the Mobile Tower System can still be used to supplement the ones from the House Instrumentation System for cases when the House Instrumentation System data are not available.

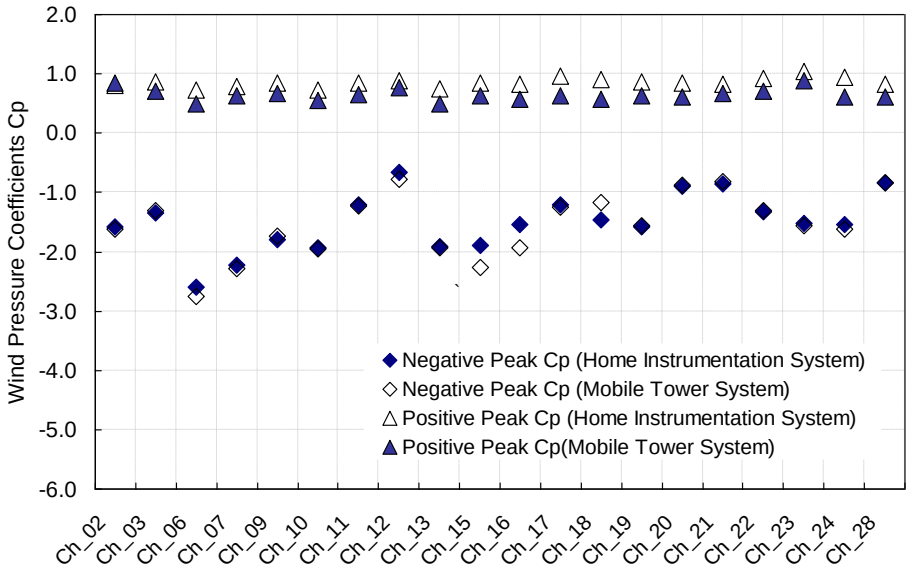

Figure 5.3 Comparisons of Peak Wind Pressure Coefficients by Using the House Instrumentation System and The Mobile Tower System Records (House Records: No.135 - No.140) (Sampling Frequency = 100 Hz, Low-pass = 25 Hz)

5.4 Probability Density Function (PDF) of Fluctuating Wind Pressures

Knowledge of the probability density function (PDF) of fluctuating wind pressures on buildings is important in the design of structural components. The PDF of the fluctuating wind pressures represents the rate of change of probability with the fluctuating wind pressure value. In this section, PDFs of wind pressure coefficient collected from full-scale tests of House FL-27 in Hurricane Ivan are investigated. Four 15-minute full-scale record sections (listed in Table 5.3) collected in Hurricane Ivan were analyzed.

In general, low-rise buildings, which have high fundamental frequency, are categorized as the rigid structures (fundamental frequency is greater than or equal to 1 Hz) and dynamic amplification effects of wind actions on them can be neglected. Based on the quasi-steady assumption, the fluctuating pressures on structures are assumed to follow wind turbulence and wind pressure variations corresponding to wind velocity fluctuations (Holmes, 2001). Thus, the instantaneous dynamic pressure, $p(t)$, can be written:

$$p(t) = \frac{1}{2}\rho \cdot u^2(t) \tag{5-6}$$

where, ρ is the air density; $u(t)$ is the longitudinal component of wind speed fluctuation at time t. The non-dimensional pressure coefficient $C_p(t)$ for low-rise buildings is as follows:

$$C_p(t) = \frac{p(t)}{\frac{1}{2}\rho\overline{U}^2} = \frac{\frac{1}{2}\rho u^2(t)}{\frac{1}{2}\rho\overline{U}^2} \tag{5-7}$$

where, $\overline{U}$ is the mean (time-averaged) wind speed at reference height.

The PDF's of 15-minute longitudinal velocity component $u(t)$, which were measured for House FL-27 roof height by the House Instrumentation System in Hurricane Ivan, are calculated and compared with normal distributions in Figure 5.3. The Figure 5.3 shows that the measured data are generally fitted well with the normal distribution, though it is poor match at some areas.

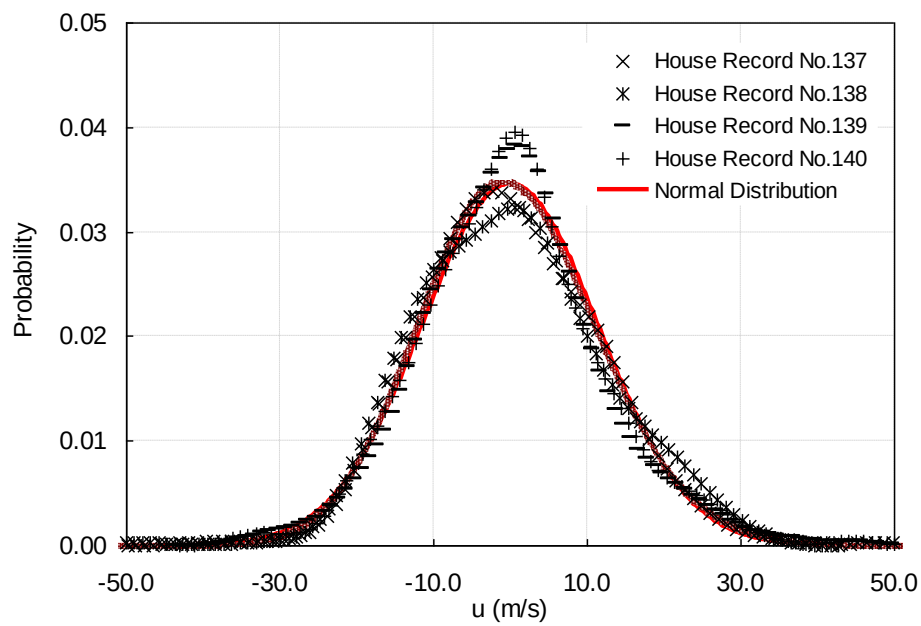

Figure 5.4 Probability Density Function for u Component of Velocity Measured on House FL-27 Roof Height by the House Instrumentation System in Hurricane Ivan

Assuming that the wind velocity components follow the normal distribution, the PDF for u can then be written by:

$$f_u(u) = \frac{1}{\sqrt{2\pi}\sigma_u} \exp\left(\frac{-u^2}{2\sigma_u^2}\right) \tag{5-8}$$

where, σ_u is standard deviation of the u component of velocity. Therefore, the PDF of $C_p(t)$ is given by (Ang and Tang, 1975):

$$f_{Cp}(C_p) = \left|\frac{du}{dC_p}\right| \left\{ f_u(\overline{U} \cdot \sqrt{C_p}) + f_u(-\overline{U} \cdot \sqrt{C_p}) \right\} \tag{5-9a}$$

Using the turbulence intensity I_u to substitute $\frac{\sigma_u}{\overline{U}}$, the PDF of $C_p(t)$ can be written by (Holmes, 2001) when $C_p(t)$ is larger than zero .

For $C_p > 0$

$$f_{Cp}(C_p) = \left(\frac{1}{\sqrt{2\pi C_p} \cdot 2I_u}\right) \cdot \left\{ \exp\left[\left(-\frac{1}{2}\right) \cdot \left(\frac{\sqrt{C_p} - 1}{I_u}\right)^2\right] + \exp\left[\left(-\frac{1}{2}\right) \cdot \left(\frac{\sqrt{C_p} + 1}{I_u}\right)^2\right] \right\} \tag{5-9b}$$

and for $C_p < 0$, the PDF of $C_p(t)$ can be express as following equation:

$$f_{Cp}(C_p) = \left(\frac{1}{\sqrt{-2\pi C_p} \cdot 2I_u}\right) \cdot \left\{ \exp\left[\left(-\frac{1}{2}\right) \cdot \left(\frac{\sqrt{-C_p} - 1}{I_u}\right)^2\right] + \exp\left[\left(-\frac{1}{2}\right) \cdot \left(\frac{\sqrt{-C_p} + 1}{I_u}\right)^2\right] \right\} \tag{5-9c}$$

Four measured 15-minute PDF's of pressure coefficients for each channel of House FL-27 full-scale test in Hurricane Ivan are calculated. Equation (5-9) is also evaluated numerically and shown with the measured distribution of pressures in Figures 5.5 and figures of Appendix C. All of the figures in Appendix C indicate that Equation (5-9c) match closely the negative tails of the measured PDF of wind pressure on House FL-27 in Hurricane Ivan.

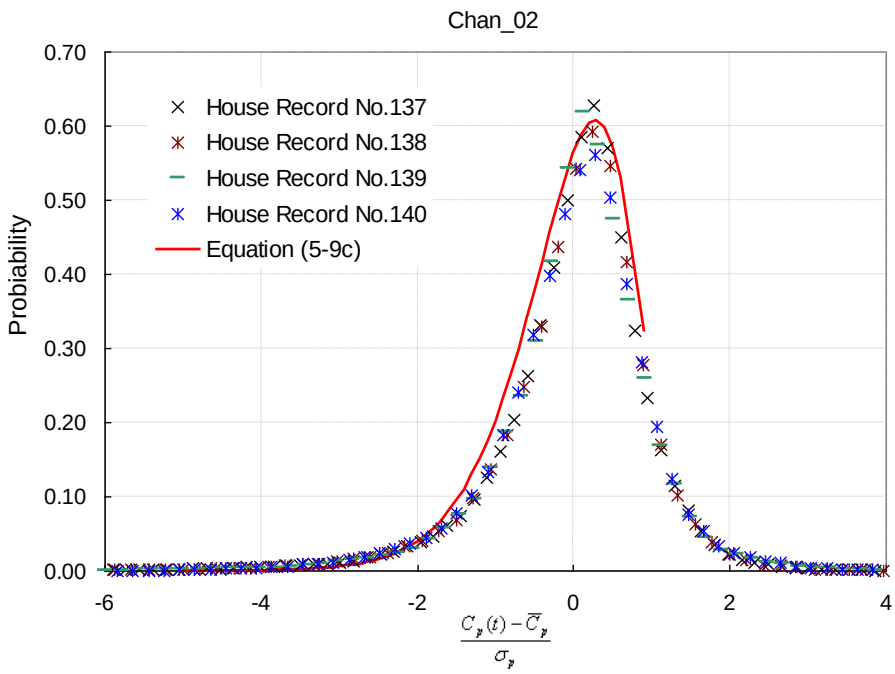

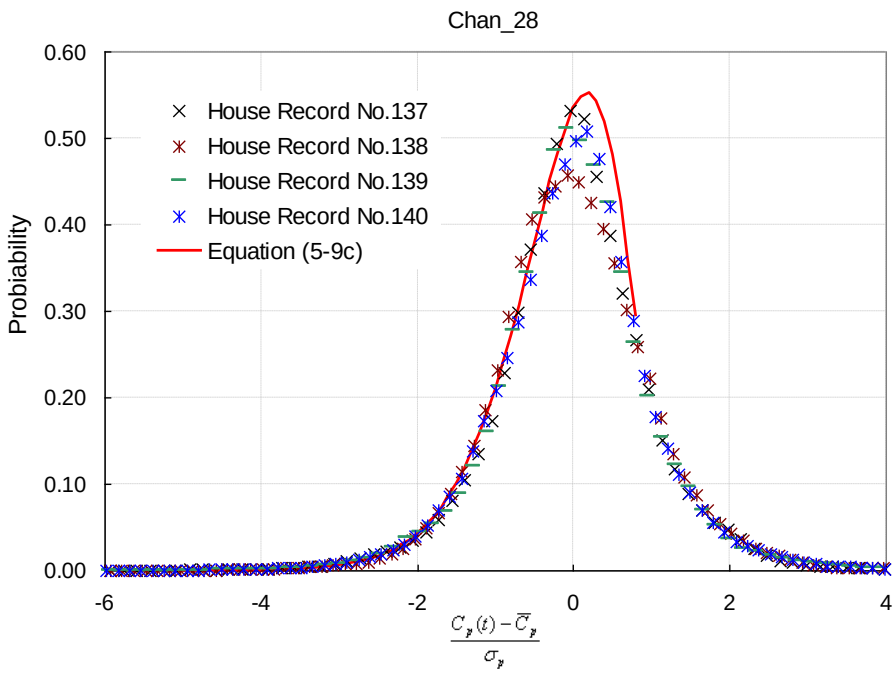

Figure 5.5 Measured and Predicted 15-minute PDFs of Pressure coefficient of Chan_02 and Chan_28 Measured in Hurricane Ivan

5.5 Spatial and Time-Averaged Effects on Peak Pressure

Wind pressure on low-rise buildings varies with space and time. In general, the longer the load duration, the smaller the peak pressure coefficients because wind pressures are better correlated over small area. The duration of peak wind load action is a significant factor that affects structural behavior. It was found that the peak value of pressures averaged simultaneously over the area is smaller than the corresponding peak pressure at individual tap locations. In this section, data from four 15-minute record sections (House records: No.137-No.140) collected in full-scale tests of House FL-27 in Hurricane Ivan is analyzed for investigation of the spatial and time-averaged effects on peak pressure.

5.5.1 Time-Averaged Peak Pressure

Using the peak-factor approach (Holmes, 2001), the peak pressure coefficient $\hat{C}_p$ can be expressed by:

$$\hat{C}_p = \overline{C}_p \pm g\sigma_{Cp} \tag{5-10}$$

where, g represents a peak factor; $\overline{C}_p$ is mean pressure coefficient, and σ_{Cp} is standard deviation of pressure coefficient. The effect of time-average on peak factor g was investigated. For each channel, 15-minute peak gust factors of 25Hz data, which are filtered from 100Hz full-scale test records, are chosen as the reference value and named as $g(0)$. The peak gust factors $g(T)$ of each channel for special averaging period T are calculated and compared with the reference value $g(0)$ that has no moving average. In

the Figure 5.5 and figures of Appendix C, the ratio of the peak factors $g(T)$ to the reference value $g(0)$ of a channel is plotted against the averaging period T.

As shown in the figures mentioned above, the ratio of $g(T)$ to $g(0)$ generally decreases with increasing of averaging period T. The gust factor $g(0)$ of Channel 28, as shown in Figure 5.6(c), is unity up to an averaging time of 1 second. This means that the negative peak wind pressure frequently had a duration of about 1 second at the sensor location of Channel 28.

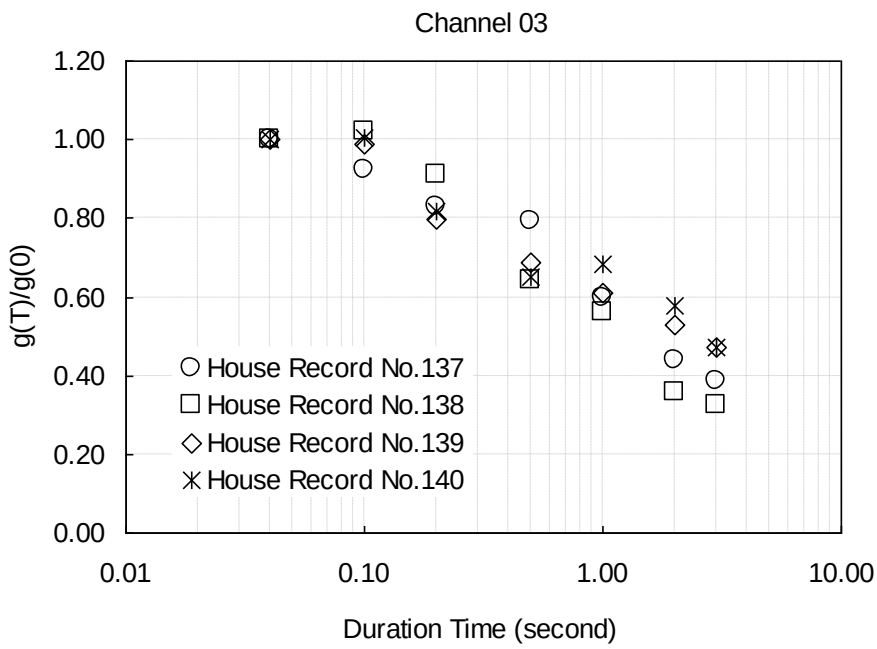

Figure 5.6(a) Effect of Averaging Period on the Peak Factor of Channel 3

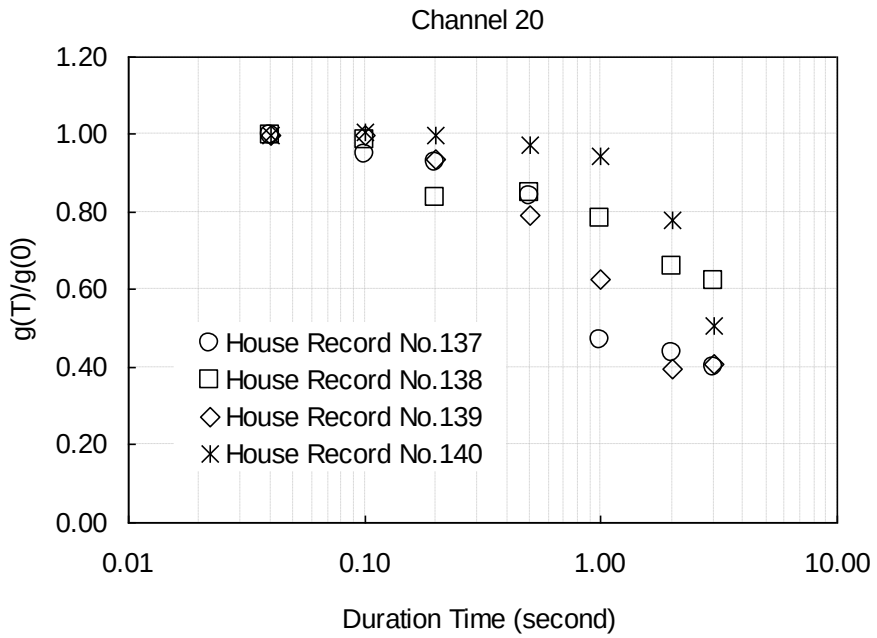

Figure 5.6(b) Effect of Averaging Period on the Peak Factor of Channel 20

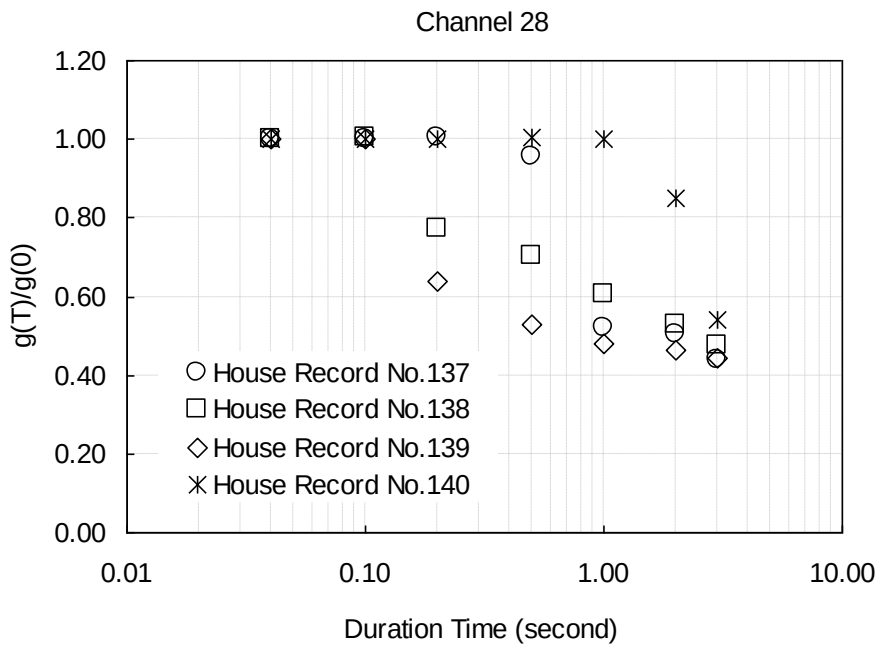

Figure 5.6(c) Effect of Averaging Period on the Peak Factor of Channel 28

5.5.2 Area-Averaged Peak Pressure Coefficients

In engineering practice, area-averaged wind loads, which differ from individual point wind load, are considered to logically represent wind loads acting over an area because area-averaged pressure account for the spatial and temporal correlations of the measured instantaneous point wind pressure in this area. The Area-averaged wind pressure $p_A(t)$ at time t over an area can be calculated by using an area-averaged pressure and is written by:

$$p_A(t) = \frac{1}{2}\rho \overline{U}^2 C_{pA}(t) \tag{5-11}$$

where, ρ is the density of air, $\overline{U}$ is the mean (time-averaged) wind speed at reference height, and $C_{pA}(t)$ is the area-averaged pressure coefficient at time t. To obtain the area-averaged pressure coefficient $C_{pA}(t)$ over an area, pressure coefficient time series of each point within this area are multiplied by the weighting factor and summed together. Therefore, the area-averaged pressure coefficient $C_{pA}(t)$ is given by:

$$C_{pA}(t) = \sum_{i=1}^{n} \delta_i C_{pi}(t) \tag{5-12}$$

where, $C_{pi}(t)$ is the point pressure coefficient at time t for tap i, and δ_i is the weighting factor of tap i. The weighting factor δ_i for tap i is given by:

$$\delta_i = \frac{A_i}{\sum_{j=1}^{n} A_j} \tag{5-13}$$

where, A_i is the tributary area for tap i, A_j is the tributary area for tap j, and $\sum_{j=1}^{n} A_j$ is the total area.

To evaluate area-averaged effect on wind loads, the measurement records of House FL-27 full-scale tests in Hurricane Ivan are analyzed. The area-averaged pressure coefficients of three corner areas are calculated, and these areas are shown in Figure 5.7. Table 5.3 summaries the division of areas channel numbers of each roof corner areas.

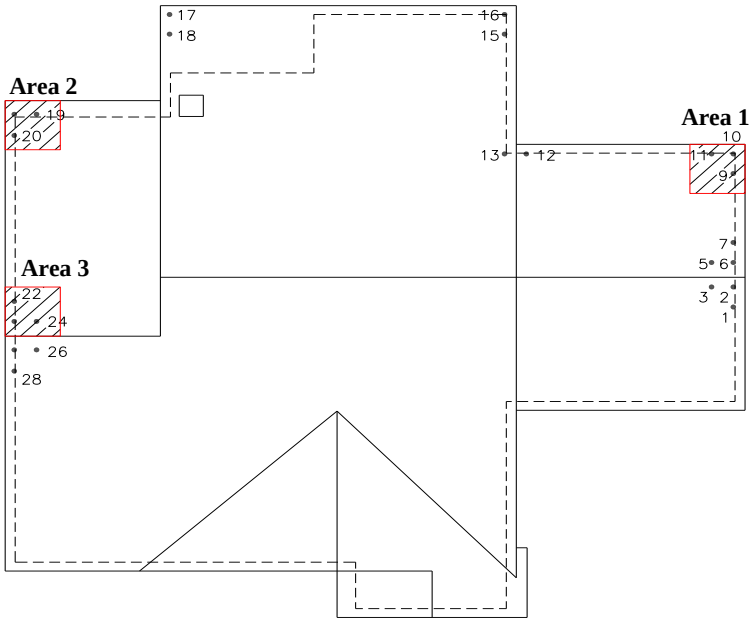

Figure 5.7 Locations of Areas for Analyzing the Area-Averaged Effects

Table 5.3 Summary of Channel Numbers of Each Roof Corner Divisions.

Area Name	Channels in Area	Sampling Frequency
Area 1	Chan_09, Chan_10, and Chan_11	100Hz and Low-pass filtered with 25Hz
Area 2	Chan_19, Chan_20, and Chan_21	
Area 3	Chan_22, Chan_23, and Chan_24	

The area-averaged negative peak pressure coefficients of Area 1, Area 2, and Area 3 are compared with the negative peak pressure coefficients of corresponding individual channels in Figures 5.8 and Appendix E. The results show that the area-averaged negative peak pressure coefficient for an area is apparently less than the corresponding worst value of the individual peak negative pressure coefficients of channels within this area. In addition, the results show, with increasing averaging period T, the difference of the peak negative pressure coefficient between area-averaged and individual values decreases. When averaging periods are bigger than 1 second, the area-averaged peak negative pressure coefficients approach the corresponding individual values. This means that the area-averaged effect can be neglected if the averaging period is larger than 1 second.

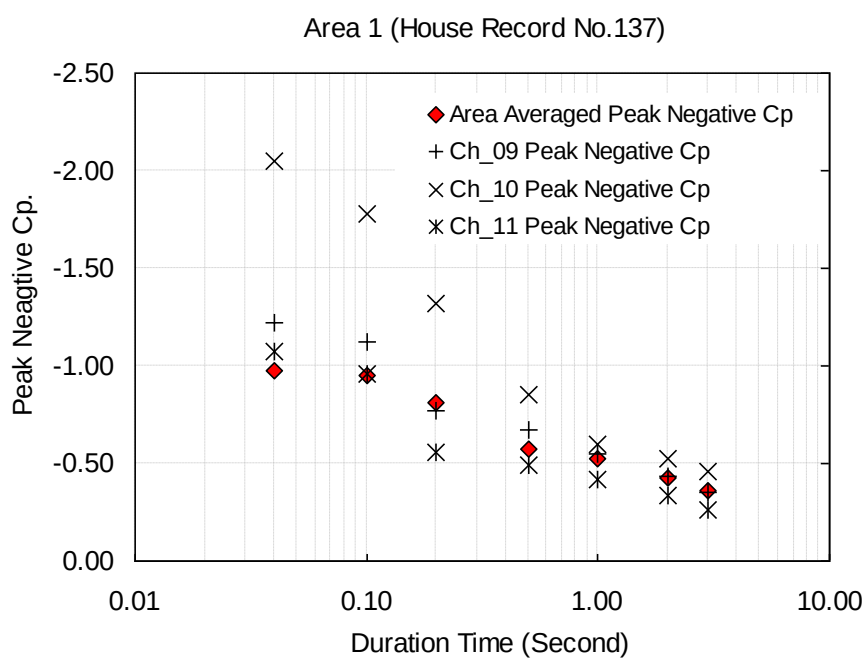

Figure 5.8(a) Comparison of Area-averaged Negative Peak Pressure Coefficients to The Corresponding Values of Individual Channels within Area 1

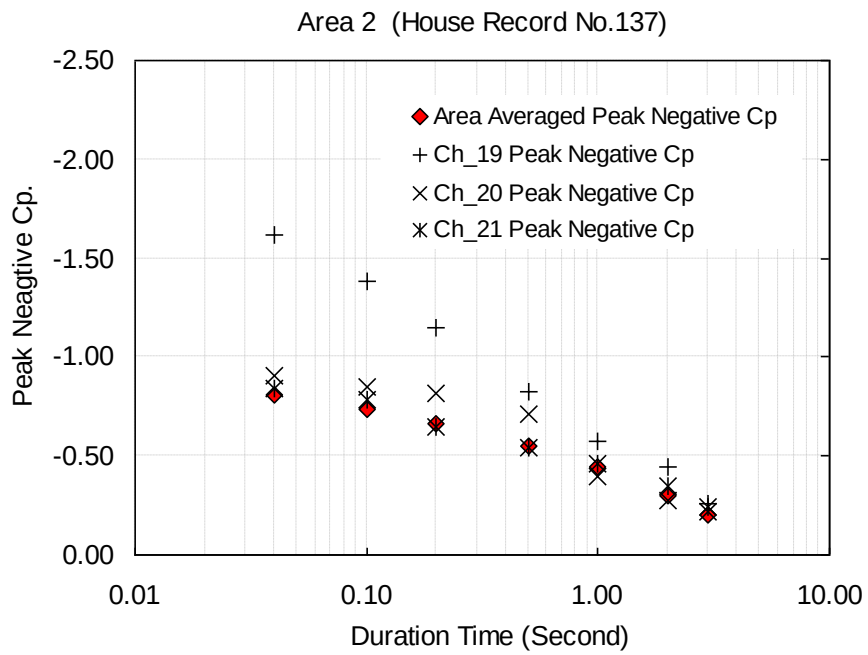

Figure 5.8(b) Comparison of Area-averaged Negative Peak Pressure Coefficients to The Corresponding Values of Individual Channels within Area 2

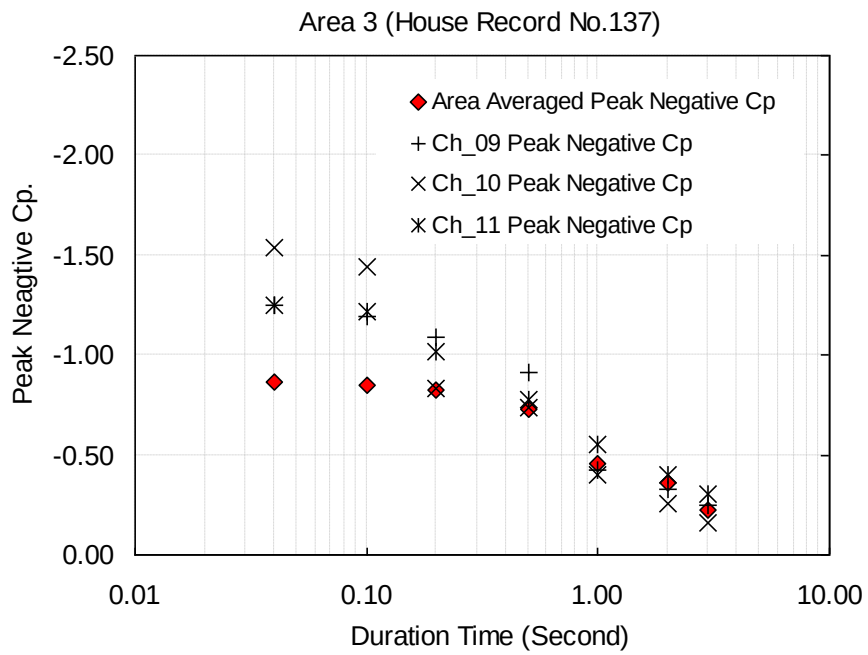

Figure 5.8(c) Comparison of Area-averaged Negative Peak Pressure Coefficients to The Corresponding Values of Individual Channels within Area 3

Based on four 15-minute full-scale measurement records of House FL-27 in Hurricane Ivan, the effect of time-averaged on area-averaged peak factor g is investigated. For each area, 15-minute peak gust factors of 25 Hz data, which are filtered from 100 Hz full-scale test records, are chosen as the reference value and named as $g(0)$. The peak gust factors $g(T)$ of each area for special averaging period T are calculated and compared with the reference value $g(0)$ that has no moving average. In Figures 5.9(a), (b), and (c), the ratio of the peak factors $g(T)$ to the reference value $g(0)$ of an area is plotted against the averaging period T. As shown in these figures mentioned above, the ratio of $g(T)$ to $g(0)$ generally decreases with increasing of averaging period T .The gust factors $g(0)$ of Area 2 and Area 3, as shown in Figures 5.9 (b) and (c), are found to remain near unity up to an averaging time of 0.2 seconds. This means that the negative peak wind pressure is frequently exerted for at least 0.2 seconds on these corner areas.

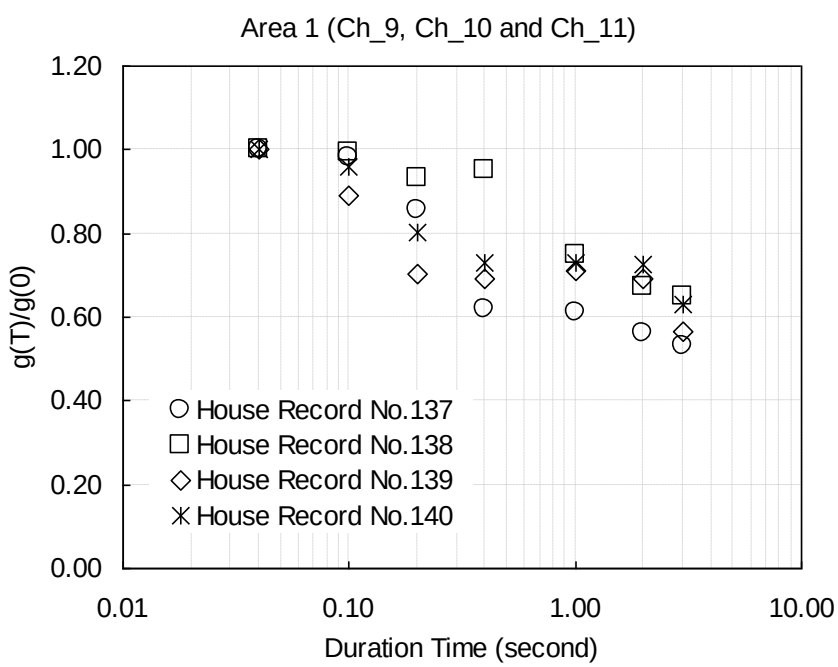

Figure 5.9(a) Effect of Averaging Period on the Peak Factor of Area 1

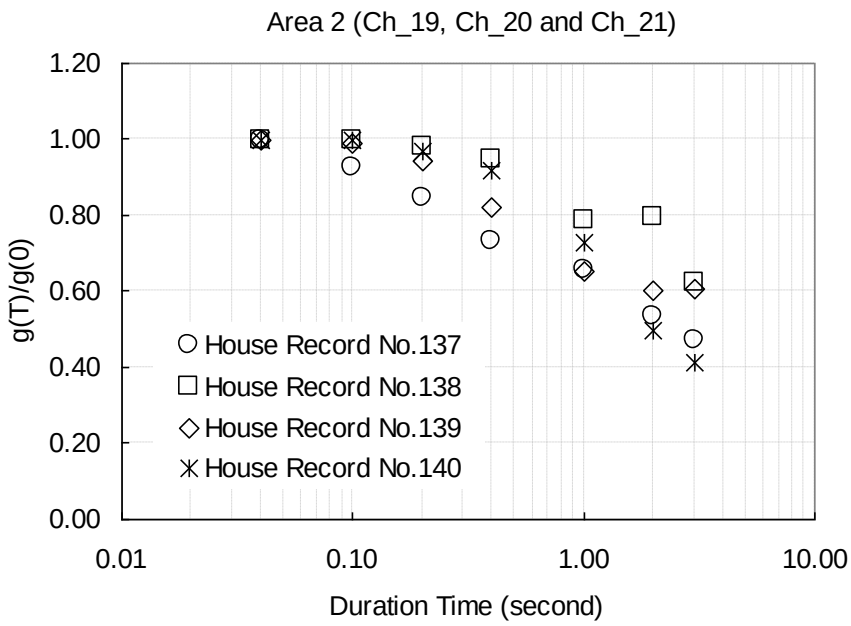

Figure 5.9(b) Effect of Averaging Period on the Peak Factor of Area 2

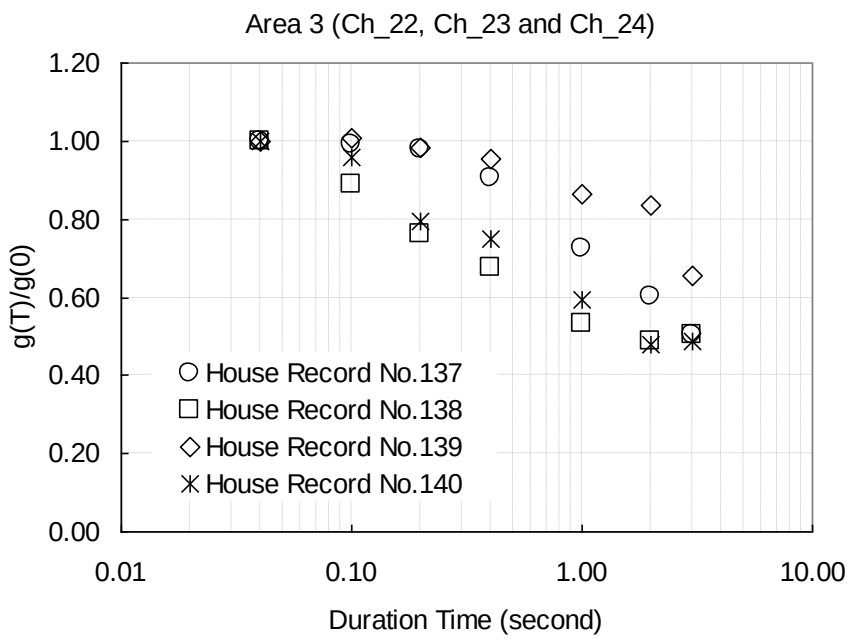

Figure 5.9(c) Effect of Averaging Period on the Peak Factor of Area 3

.

5.6 Summary

Wind loads measured by the House Instrumentation System are validated in this chapter. Estimates of uncertainties associated with reference pressures, temperature variations, and calibration errors are less than +/- 2.7 psf with 95% confidence level. This indicates that the House Instrumentation System has the capability to capture and record the extreme wind loads on experimental buildings.

The 15-minute PDF of the fluctuating wind pressures on the experimental building roof are calculated. Analysis results show that PDF of external negative pressure coefficients calculated using the Equation (5-9c) matches well the negative part of the measured PDF of wind pressure.

The spatial and time-averaged effects on peak pressures were also investigated in this chapter. It is found that negative peak wind load generally decreases with the increasing of the averaging period T . The negative peak wind pressure force on a single point can occur for 1 second and an area-averaged negative peak wind pressure can occur for 0.2 seconds at a roof corner area. The area-averaged negative peak pressure coefficient for an area is apparently less than the corresponding worst of the negative peak pressure coefficients of individual channels within this area. However, the effect of area-averaging on negative peak wind loads can be neglected when the averaging period T exceeds 1 second.

CHAPTER 6

WIND TUNNEL SIMULATION OF HURRICANE WIND LOADS ON HOUSE FL-27

The Full-scale wind pressure results collected from House FL-27 during Tropical Storm Isidore and Hurricane Ivan provide high resolution field data of hurricane wind loads occurring on a single family house. These results now provide wind engineers with an opportunity to validate current scale-model wind tunnel simulation methods by evaluating the ability to reproduce hurricane wind loads in areas of flow separation and flow reattachment on roofs near the corners and leading edges.

In this chapter, wind tunnel tests for House FL-27 model are described. The comparisons of wind tunnel and full-scale test results that have been presented previously in Chapter 5 are used to determine the ability of wind tunnel techniques to reproduce full-scale hurricane wind loads measured. In addition, wind tunnel and the full-scale test results are compared with the wind load design code provision values. The influences of terrain exposures and surrounding houses are also investigated. By applying wind tunnel simulation results and a hurricane simulation model, design wind loads on the critical roof corner area of the subject house are calculated and compared with ASCE prescriptive wind loads.

6.1 House Model and Wind Tunnel Setting

Wind loads on low-rise buildings depend on factors such as building geometry, upstream flow characteristics, and the terrain surrounding the building. Therefore, the accuracy of simulating wind loads in a wind tunnel depends on precise field measurements, since changing parameters can cause significant differences in the observed behaviors (Melbourne, 1993). The choice of model scale and boundary layer simulation methods must also be carefully considered when conducting wind tunnel studies on low-rise buildings.

A 1:50 scale geometrically similar acrylic model of House FL-27 was fabricated and used in wind tunnel tests. Twenty-four pressure taps are installed in the roof of the house model corresponding to the locations of the full-scale pressure sensor described in Chapter 5. In addition, four hundred seventy-two additional taps were installed on the roof surface of the model as shown in Figure 6.1.

Figure 6.2 provides a photo of the 1:50 scale House FL-27 model and the arrangement plan of taps. Particular attention has been paid to the roof corner and roof edge areas with a high density of test taps. In these areas the wind flow may separate to form high local turbulence and vortices.

To sufficiently consider the effect of surrounding buildings on wind load, typical neighboring houses constructed from foam and scaled from the actual dimensions of the surrounding buildings were mounted on the turntable surrounding House FL-27 model, as shown in Figure 6.3.

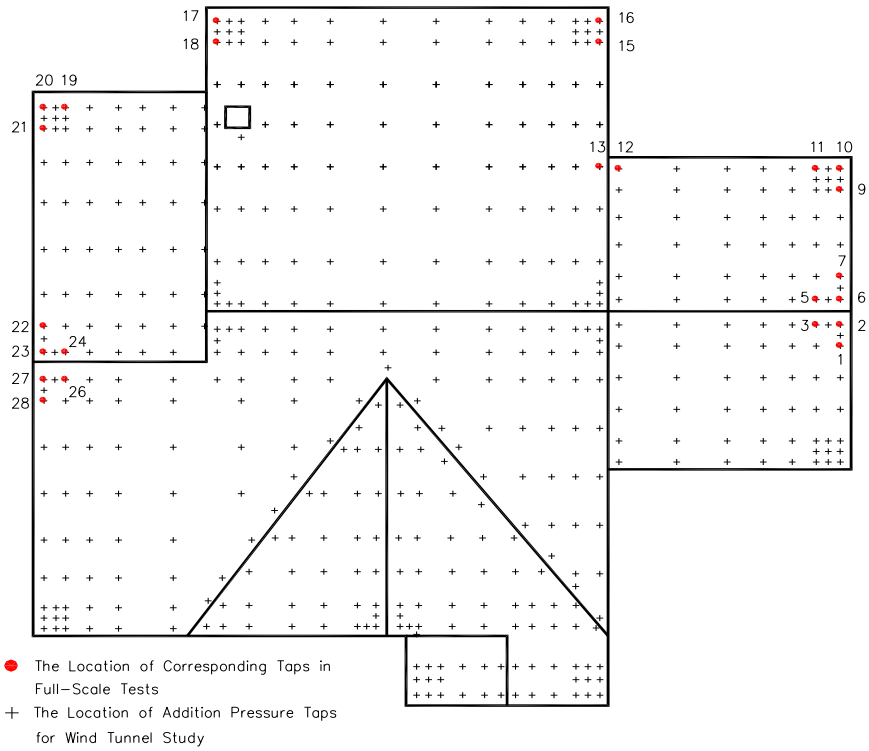

Figure 6.1 Arrangements of Taps on House FL-27 Model Roof

Figure 6.2 Photo of 1:50 Scale Model of House FL-27

Figure 6.3 House Model of FL-27 within Simulated Surrounding Houses Under 1:50 Suburban Terrain Exposure

FL-27 house model studies are conducted in the Boundary Layer Wind Tunnel at Clemson University. A 1:50 suburban terrain exposure is developed in the wind tunnel by combining spires, trip boards and roughness elements along 14.6 m of the upstream fetch, as shown in Figure 3.4. The wind velocity profile in the wind tunnel matches the log-law natural atmospheric boundary layer. Figure 3.5 shows that the mean wind speed profile matches well with the log-law relationship for the standard sparse density suburban terrain (roughness length z_0 =0.3 m) that reflects well the environment of House FL-27. The wind speed profile fits well with the log-law relationship at mean roof height. The mean turbulence intensity at mean roof height, which is generated by the upstream terrain exposure setting, is 22% which is less than the theoretical turbulence intensity of 30% for this roughness length of z_0 = 0.3 m. If considering the effect of surrounding houses, the

turbulence intensity at mean model roof height is expected to approach the roughly 30 to 35% turbulence intensity estimated from the anemometers above the roof of the house.

The mean wind speed in the wind tunnel at the height of the model roof height is 5.5 m/s. The maximum 15-minute mean wind speed measured at FL-27 roof height was 8 m/s during Tropical Storm Isidore and 16 m/s during Hurricane Ivan. Full-scale test results which are used for comparing with wind tunnel simulation results are calculated by using down sampled 10 Hz full-scale data, and then the minimum sampling frequency of wind tunnel test should be 172 Hz applying the similarity rule expressed as Equation (3-12). Considering the Nyquist's Sampling Theorem (Oppenheim, 1999), the minimum wind tunnel sampling frequency should be 350 Hz. Pressures on the model are simultaneously sampled at 500 Hz, and the pressure signal is low-pass filtered with a frequency cut-off of 200 Hz. At a relatively high sample rate of 500 Hz, this tubing system is adequate to capture all the peak pressure coefficient data. House Instrumentation System recorded wind pressure with a sampling rate of 100 Hz during a 15-minute recording duration. Applying the similarity rule, the corresponding sampling period of wind tunnel tests are 30 seconds for Tropical Storm Isidore and 48 seconds for Hurricane Ivan, respectively. Table 6.1 summarizes the test parameters for wind tunnel simulation tests.

Table 6.1 Measurement Configurations and Data Acquisition of Wind Tunnel Model Study of House FL-27.

Model scale	1:50
Sampling frequency	500Hz
Low pass filter cut-off frequency	200Hz
Sampling period	All direction (0°-360°):120s Special directions (125°): 30s (Isidore) and 48s (Ivan)
Wind angles (degree)	All directions: every 10° over a 360° range Incident direction for simulation: 125°
Upstream exposure	1:50 suburban terrain exposure
Mean wind speed at model roof height	5.5 m/s

6.2 Wind Tunnel Simulation Results of House FL-27 Model

In the full-scale tests of House FL-27, house anemometers and mobile towers are used to monitor the changes in wind speed and wind direction. Considering that the house anemometers are unavoidably disturbed by both the experimental house itself and the surrounding structures, the anemometers mounted on the experimental house may not accurately record the actual incident wind directions. However, the nearby mobile towers provide additional data to obtain confidence in incident wind flow information around House FL-27. Figure 4.4 presents the aerial photos of locations where mobile towers were erected during Tropical Storm Isidore and Hurricane Ivan. Thus, the incident wind directions at House FL-27 roof height are determined by mobile towers records. Table 6.2(a) and (b) summarizes the wind directions with the highest 15-minute mean wind speed at 10-meter height measured by mobile towers in Tropical Storm Isidore and Hurricane Ivan.

Table 6.2(a) 15-minute Mean Incident Wind Directions and Wind Speeds at House FL-27 Roof Height in Tropical Storm Isidore

Tropical Storm Isidore		
House Record No.49	15-minute Mean Wind Direction	
	House Anemometers (at 6.5m Height)	Mobile Towers (at 10m Height)
15-minute mean incident wind directions	130°	125°
15-minute mean wind speed (m/s)	7.8	18.9

Table 6.2(b) 15-minute Mean Incident Wind Directions and Wind Speeds at House FL-27 Roof Height in Hurricane Ivan

Hurricane Ivan		
House Record No.137	15-minute Mean Wind Direction	
	House Anemometers (at 6.5m Height)	Mobile Towers (at 10m Height)
15-minute mean incident wind directions	114°	124°
15-minute mean wind speed (m/s)	15.5	37.1

Table 6.2(a) and (b) shows that the maximum 15-minute mean wind speed measured at the 10-meter height by mobile towers in Tropical Storm Isidore and Hurricane Ivan corresponds to a wind direction of 125˚. Therefore, the experimental model is tested under a wind incident angle of 125˚ in wind tunnel. To record a good representation of the surface pressures for the given flow condition, the experimental model is tested sixteen times. For each time, the sampling period is 30 seconds or 48 seconds. 30 seconds corresponds to 15-minute sampling period of the full-scale test in Tropical Storm Isidore, and 48 seconds corresponds to 15-minute sampling period of the full-scale test in Hurricane Ivan. The House FL-27 model was also tested for a full 360˚ to obtain data records for 120 second duration for every 10˚ increment. These data

records are used to determine the wind directions that created the most severe wind loads for each roof tap location.

For the equivalent full-scale tap locations, the average statistics of the peak minimum, mean, and peak maximum pressure coefficients from 16 trials at wind incident angle of 125˚ were plotted in Figures 6.4 (a) and (b) with the corresponding most extreme statistics for all wind directions. Pressure tap recordings show larger magnitude peak pressure coefficients from wind directions other than the 125˚ angle. This indicates that the worst pressure coefficients observed in full-scale tests might not be the worst values possible considering all directions.

Figure 6.5 shows the contour maps of peak negative pressure coefficients plotted for the wind incident angle of 125˚ (6.5a) and all wind directions (6.5b). Figure 6.5(a) shows that the leading edge and corner areas of the house model experienced suction forces at the wind incident angle of 125˚, which coincides with the full-scale tests from House FL-27 in Hurricane Ivan. The extreme peak suctions are found to occur at corner and edge areas (Area 19, 20, and 21), as shown in Figure 6.5(a). This indicates that the full-scale sensors were not installed in the worst pressure locations. Based on this, we predict that the worst peak pressure coefficients on the House FL-27 roof during these two extreme events.

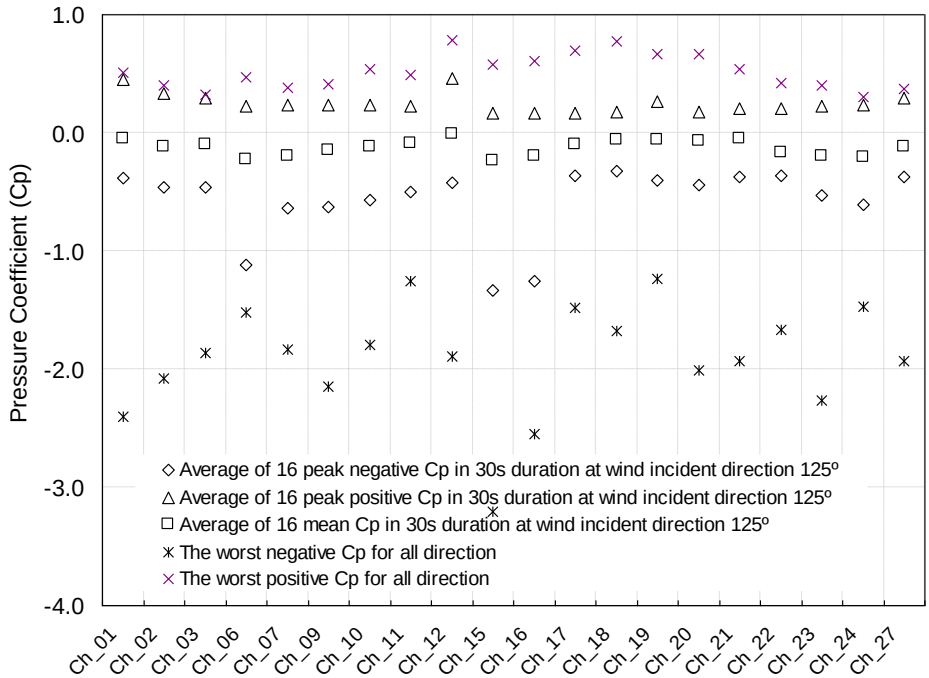

Figure 6.4(a) Pressure Coefficients of the House FL-27 Model Tests to Simulate the Wind Loads of Tropical Storm Isidore

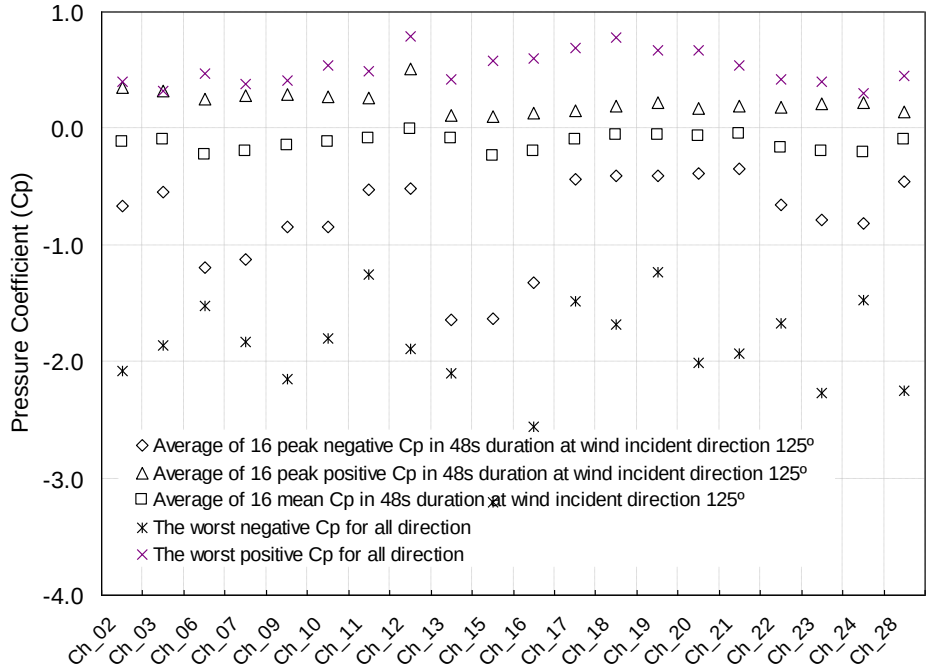

Figure 6.4(b) Pressure Coefficients of the House FL-27 Model Tests to Simulate the Wind Loads of Hurricane Ivan

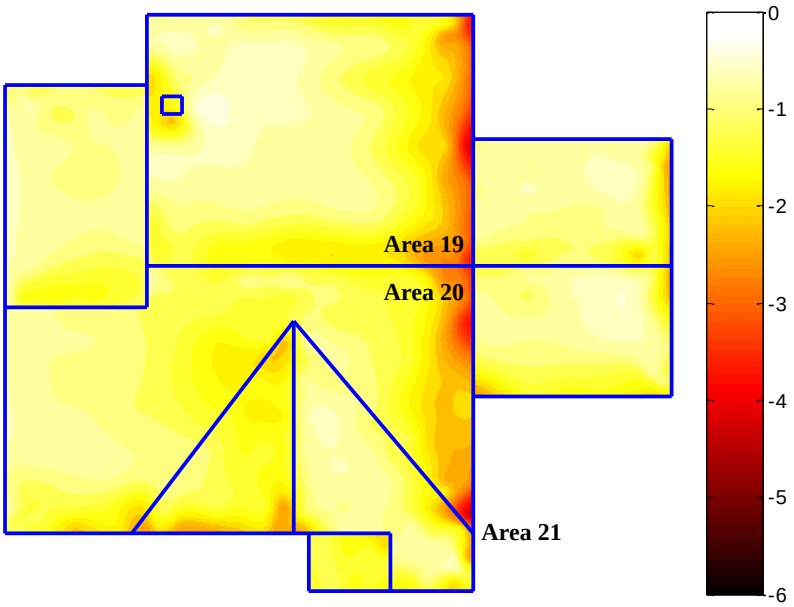

(a) Wind incident direction =125°

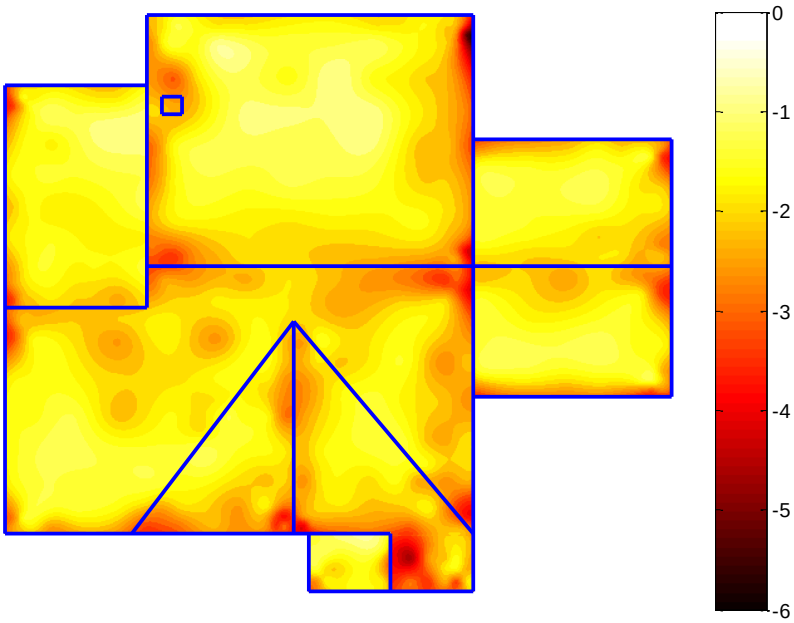

(b) All direction = 0°-360°

Figure 6.5 Peak Negative Pressure Coefficients on House FL-27 Model Roof

6.3 Comparison of Wind Tunnel Simulation with Field Measurement Results

Figures 6.6(a) and (b) compare the pressure coefficients obtained from the full-scale and model tests. There is good agreement between the pressure coefficients obtained at full-scale and wind tunnel results for the mean, peak positive, and standard deviation of pressure coefficients. However, marked differences are observed between full-scale during Hurricane Ivan and wind tunnel results for the peak negative pressure coefficients ranging from a maximum of 98% difference at Channel 16 and to a minimum of 0.1% difference at Channel 9. These differences may however expected, because the comparisons are based on a single observation of peak negative pressure coefficients at full-scale tests rather than an expected value calculated using several observations (i.e. mean and standard deviation calculations). These results are consistent with previous wind tunnel tests that consistently underestimate the peak negative pressure coefficient at full-scale tests (Levitan and Mehta, 1992; Tieleman, 1998; Dearhart, 2003).

A regression analysis was performed to identify relationships between the full-scale and wind tunnel data to determine if the wind tunnel studies adequately simulated extreme wind loads on the experimental building, and whether adjustments to the full-scale data can be rationally imposed. The linear regression analysis results are displayed for the peak negative, mean, peak positive, and standard deviation in Figures 6.7(a), (b), (c), and (d) respectively. The linear regression analyses of the standard deviation of pressure coefficients show that the wind tunnel results closely match the corresponding full-scale results. The difference of the standard deviation between wind tunnel and full-scale values recorded during Tropical Storm Isidore averaged across all taps is 0.03. This

small difference suggests that the model study was able to faithfully reproduce the pressure coefficient fluctuations.

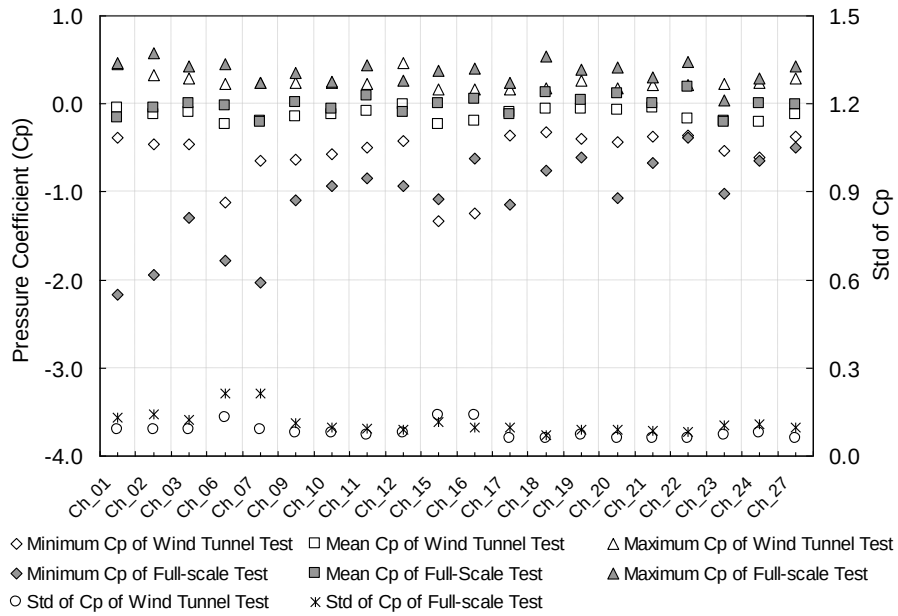

Figure 6.6(a) Comparison of Pressure Coefficients of Full-scale Tests (Tropical Storm Isidore) with Wind Tunnel Tests at Wind Incident Direction = 125°

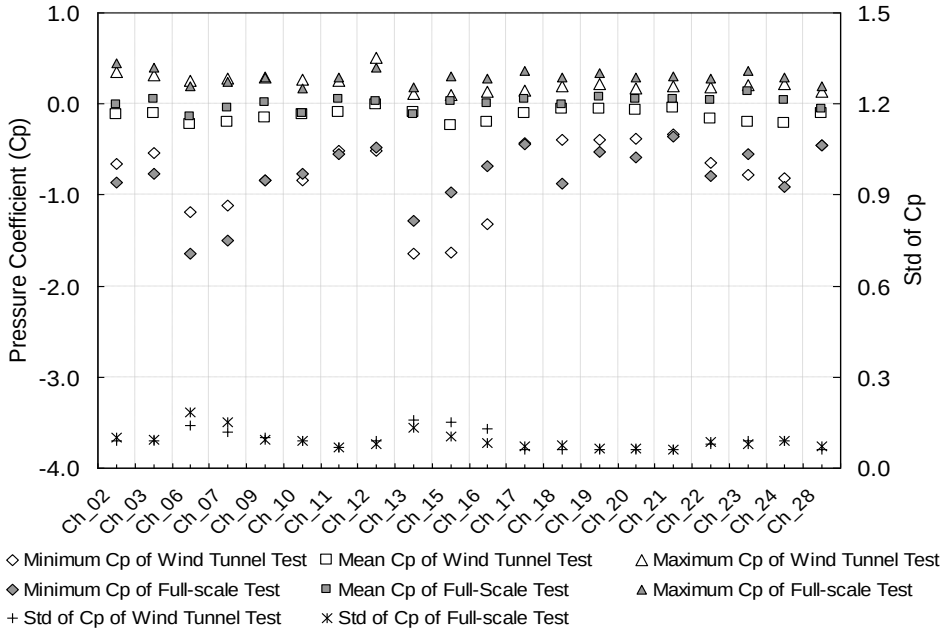

Figure 6.6(b) Comparison of Pressure Coefficients of Full-scale Tests (Hurricane Ivan) with Wind Tunnel Tests at Wind Incident Direction = 125°

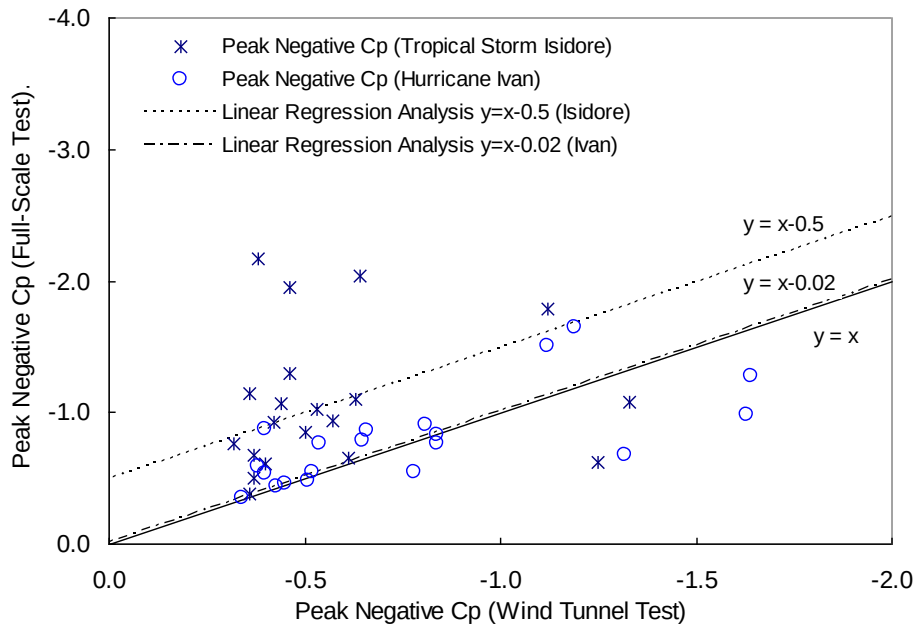

Figure 6.7(a) Linear Regression Analyses of Peak Negative Pressure Coefficients of Full-Scale and Wind Tunnel Simulation Tests

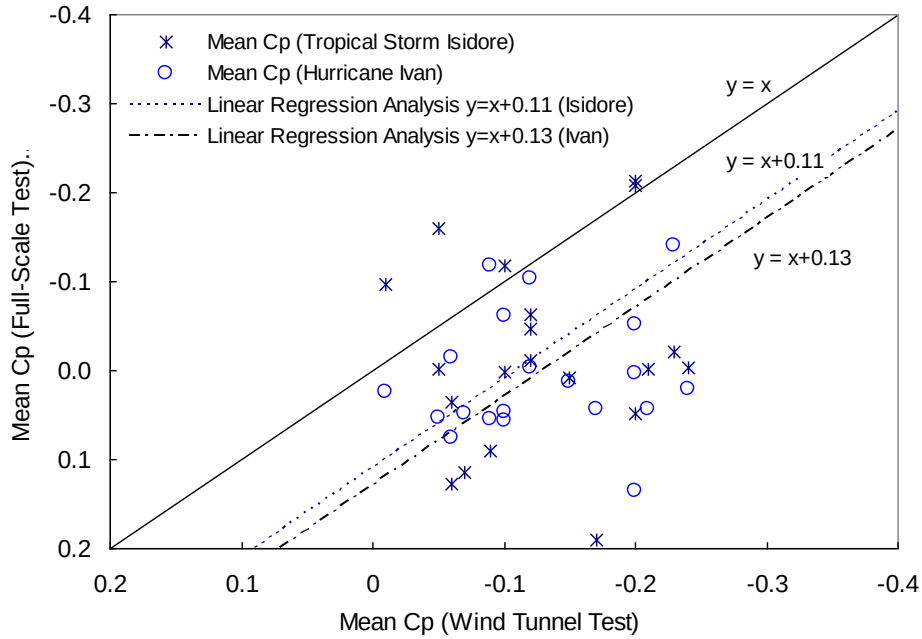

Figure 6.7(b) Linear Regression Analyses of Mean Pressure Coefficients of Full-Scale and Wind Tunnel Simulation Tests

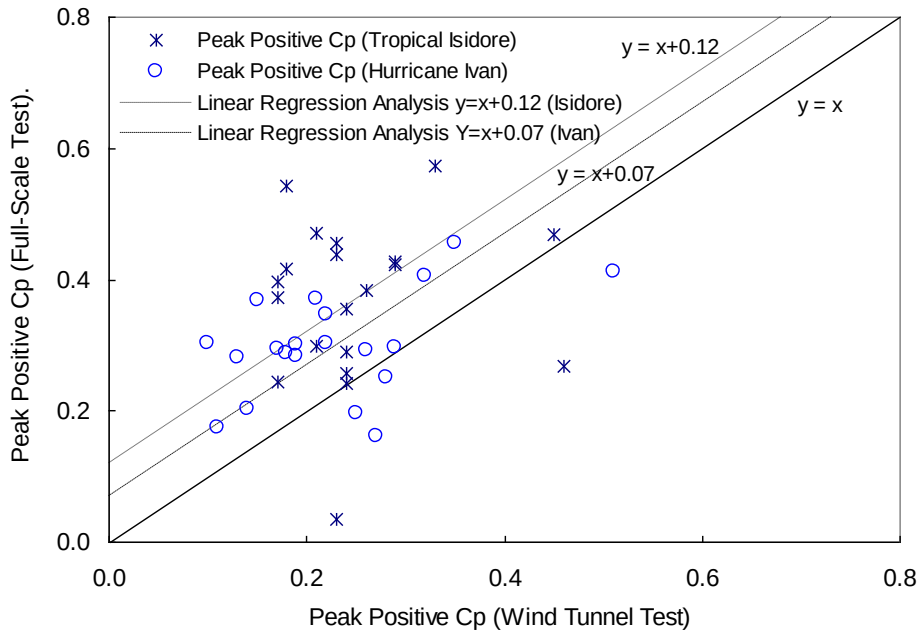

Figure 6.7(c) Linear Regression Analyses of Peak Positive Pressure Coefficients of Full-Scale and Wind Tunnel Simulation Tests

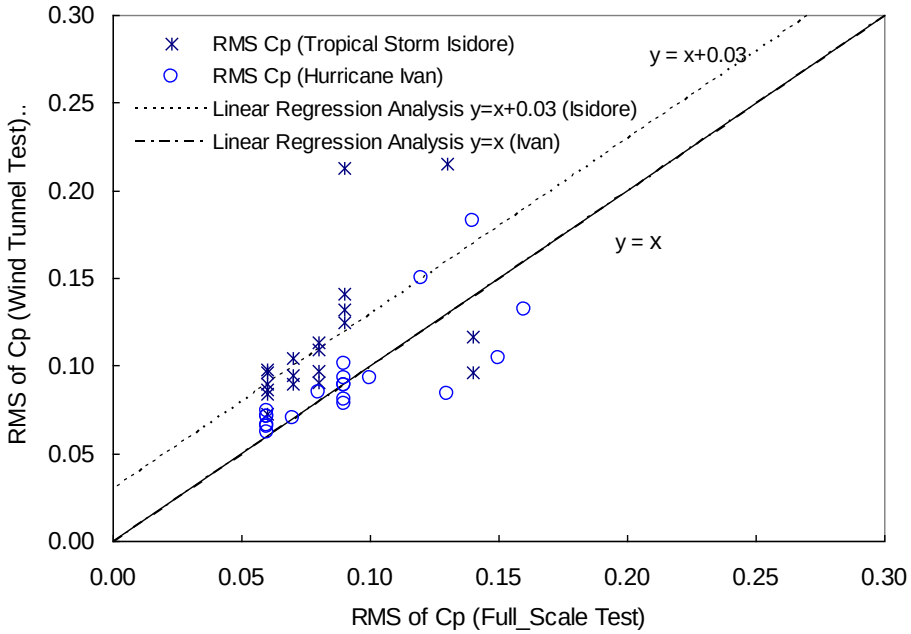

Figure 6.7(d) Linear Regression Analyses of RMS of Pressure Coefficients of Full-Scale and Wind Tunnel Simulation Tests

The linear regression analysis of the mean, peak negative and peak positive pressure coefficients show a shift between the house model and full-scale test results. Table 6.3 summarizes the averaged difference across all taps of the mean, peak minimum and maximum pressure coefficients and the corresponding averaged difference of wind pressures between the model and house tests.

Table 6.3 Averaged difference across all taps of the mean, peak minimum and maximum pressure coefficients between the model and House FL-27

Tropical Storm Isidore	Averaged difference of Cp	Averaged difference of wind pressure (psf)	3-second gust wind speed at mean roof height (m/s)
Peak Negative Cp	-0.5	-1.83	16.9
Mean Cp	0.11	0.40	
Peak Positive Cp	0.12	0.44	
Hurricane Ivan	**Averaged difference of Cp**	**Averaged difference of wind pressure (psf)**	**3-second gust wind speed at mean roof height (m/s)**
Peak Negative Cp	-0.02	-0.31	34.8
Mean Cp	0.13	2.02	
Peak Positive Cp	0.07	1.09	

The largest mean shift is approximately 0.5Cp, which occurs when comparing the peak negative pressure coefficients between model and full-scale data recorded during Tropical Storm Isidore. A shift of 0.5Cp in the full-scale values in Tropical Storm Isidore represents a change of about 1.8 psf of wind pressure for the maximum 3-second gust wind speed of 16.9 m/s at the mean house roof height observed during this storm. Based on uncertainty analysis of full-scale data presented in Chapter 5, estimates of the maximum uncertainties associated with corrections for reference pressures, temperature variations, and calibration errors are less than +/- 2.7 psf with a 95% confidence level. This relatively large shift is based on a single observed peak value. However, it does not

utilize the statistics contained in the thousands of full-scale instantaneous measurements of pressure. It is more rational to propose that any shift in the full-scale coefficients based on a comparison of expected value-based statistics such as mean or standard deviation, which contain information from all observed samples. Therefore, it is reasonable to suggest that the pressure coefficients of full-scale results can be slightly adjusted according to the shift of mean pressure coefficient between model and full-scale results.

Adjusted pressure coefficients from full-scale tests for both storms are calculated by subtracting 0.11 from pressure coefficient values of full-scale tests from Tropical Storm Isidore and subtracting 0.13 from pressure coefficient values from Hurricane Ivan. The averaged differences across all taps of the adjusted mean pressure coefficients between the model and adjusted full-scale test results are zero. Figures 6.8(a) and (b) show that the mean and peak positive pressure coefficients of the wind tunnel tests match the corresponding adjusted full-scale test results. However, there remains disagreement between the peak negative pressure coefficients measured at full-scale and wind tunnel model.

One explanation of this deviation in peak negative pressure coefficient values between full-scale and model may be differences in turbulence intensity between full-scale and wind tunnel tests. The turbulence intensity of full-scale at House FL-27 roof height was 30 to 40% (see Table 4.3(a)) and in the wind tunnel it was estimated around 30%. Prior studies (Tieleman, 2003) found that lower wind tunnel turbulence intensity produces smaller peak negative pressure coefficients. He suggested that simulation of the turbulence intensity value is necessary in order to obtain reasonable relationships between the peak minimum and peak maximum pressure coefficients between wind

tunnel and full scale test results. However, this explanation in this case is not convincing in light of how well the standard deviations of Cp match between full-scale and model, as shown in Figures 6.8(a) and (b). Two different random processes with identical second order moments but differing extreme values generally exhibit differences in the tail of the associated probability density functions. The probability density functions (PDFs) obtained from the wind tunnel tests (16 repeats) and the full-scale data (1 repeat) are shown in Figures 6.9(a), (b), and (c) for Channel location 2, 3, and 9 respectively. It is found that the PDF of the full-scale data is more skewed than the PDF for the wind tunnel data. Perhaps it represents a departure between full-scale and scaled model in the behavior of the dynamics in the separation regions where the taps are located. On the other hand, the error of model scaling and the determination of reference velocity can also cause the deviation of test results between the full scale and wind tunnel model.

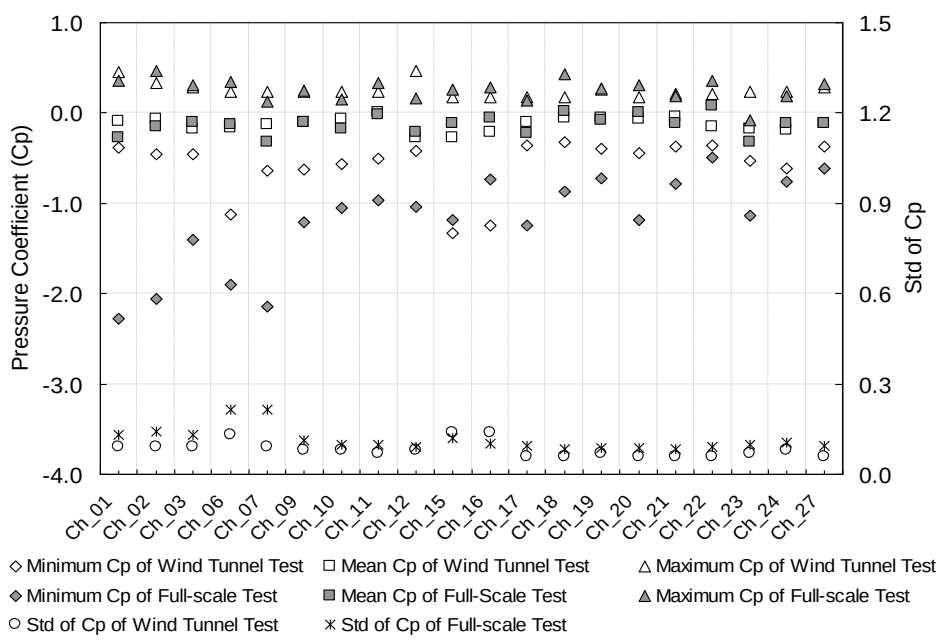

Figure 6.8(a) Comparison of Adjusted Pressure Coefficients of Full-scale Tests (Tropical Storm Isidore) with Wind Tunnel Tests at Wind Incident Direction = 125°

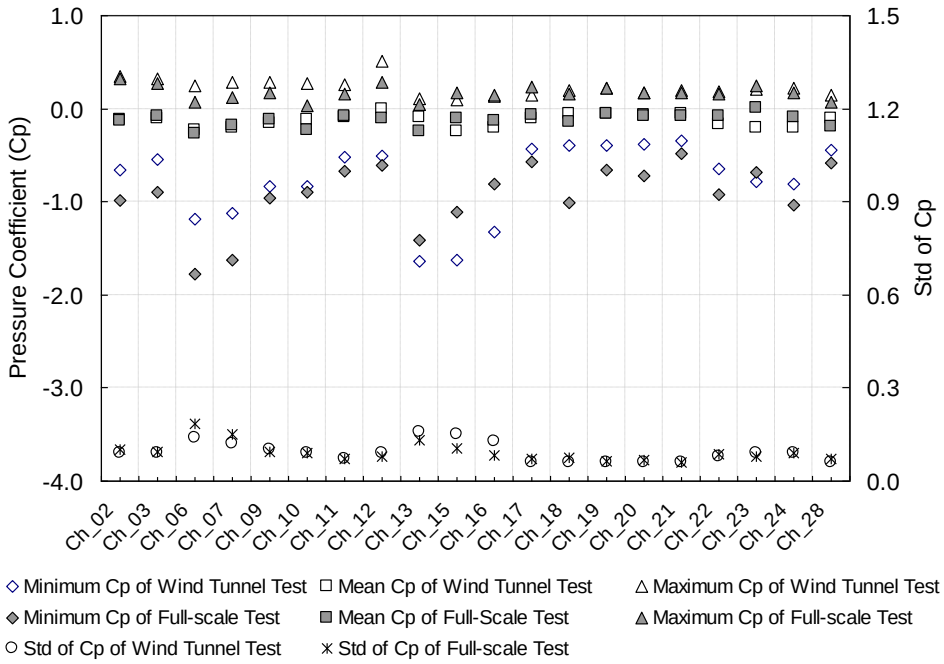

Figure 6.8(b) Comparison of Adjusted Pressure Coefficients of Full-scale Tests (Hurricane Ivan) with Wind Tunnel Tests at Wind Incident Direction = 125°

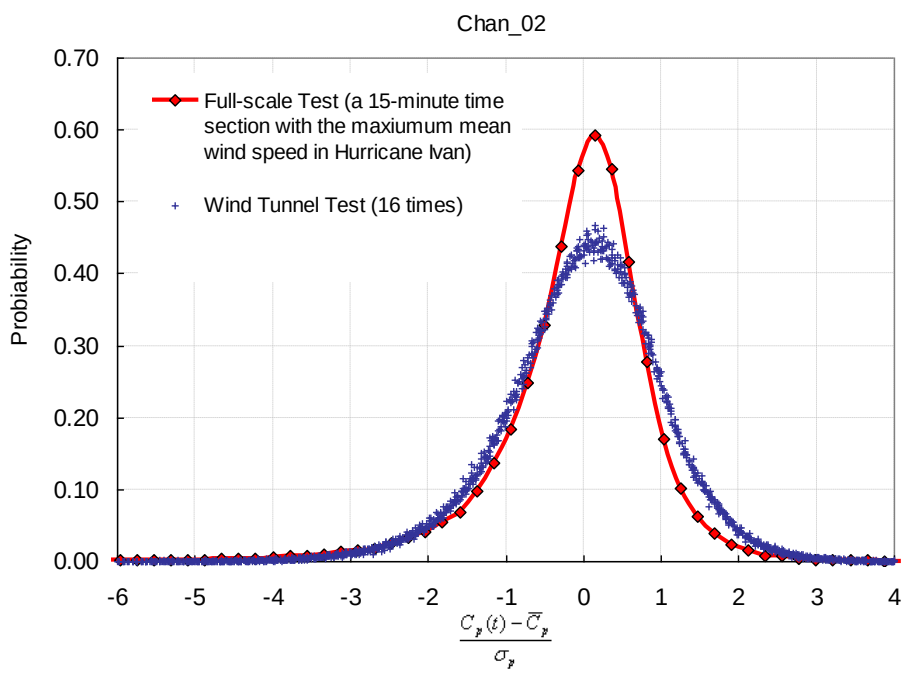

Figure 6.9(a) Comparison of PDF of Channel 2 of Full-Scale test (Hurricane Ivan) with Wind Tunnel Simulation at Wind Incident Direction = 125°

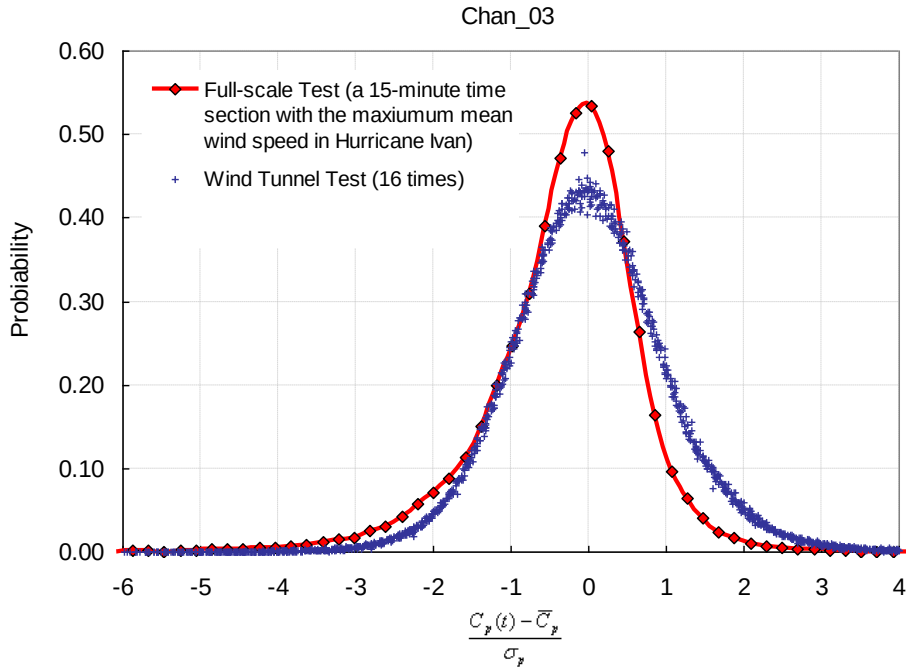

Figure 6.9(b) Comparison of PDF of Channel 3 of Full-scale Test (Hurricane Ivan) with Wind Tunnel Simulation at Wind Incident Direction = 125°

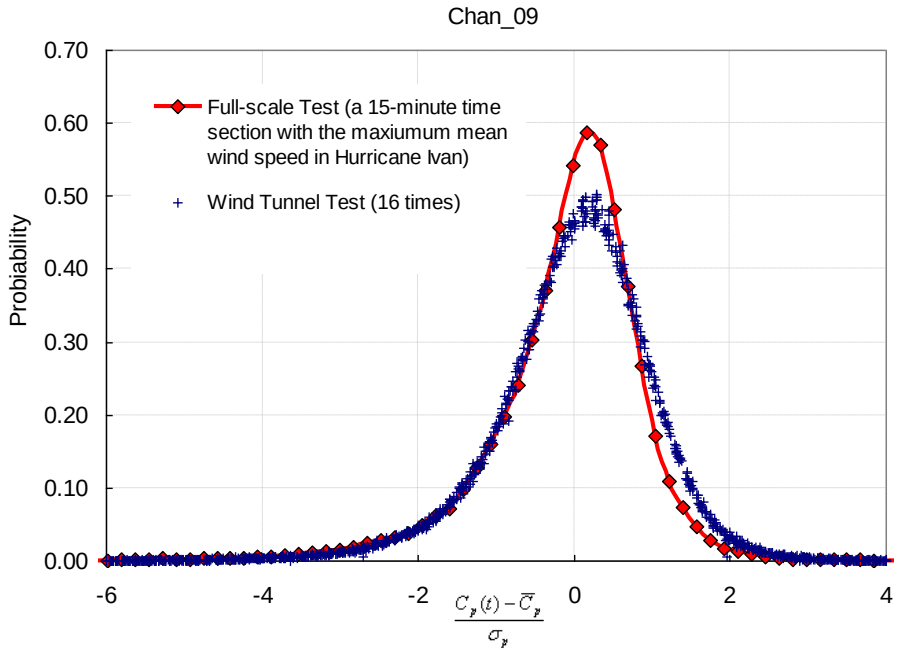

Figure 6.9(c) Comparison of PDF of Channel 9 of Full-scale Test (Hurricane Ivan) with Wind Tunnel Simulation at Wind Incident Direction = 125°

6.4 Influences of Neighborhood Houses and Terrain Exposures on Wind Loads

Wind loads on low-rise buildings depend on building geometry, dimensions, surroundings, terrain exposure, and wind flow characteristics. In order to investigate the influence of surrounding houses, the House FL-27 model was tested in isolation for suburban terrain exposure, with no roughness elements placed on the turntable. The peak wind pressure coefficients ($\breve{C}_p$ and $\widehat{C}_p$ respectively) for all wind directions measured without surrounding houses are compared with the corresponding peak values measured with surrounding houses under the same test terrain exposure (suburban and open country). The location of surrounding houses were presented in Figure 6.3.

As shown in Figure 6.10 (a) and (b), the influence of surrounding houses is weak for the peak positive pressure coefficients ($\widehat{C}_p$). The peak negative pressure coefficients ($\breve{C}_p$) measured with no surroundings are generally decreased when surrounding houses are added, except at Channel 12 can 15. For the incident wind direction of 125°, the peak negative pressure coefficients ($\breve{C}_p$) of channel 15, channel 23, and channel 24 are found to be increased by surrounding houses.

To investigate the influence of terrain exposures, the House FL-27 model was arranged on the turntable in isolation and tested under 1:50 suburban terrain and open country exposure. The worst peak pressure coefficients ($\breve{C}_p$ and $\widehat{C}_p$) for all directions measured under these two exposure settings are compared in Figure 6.11. This shows that the worst peak coefficients ($\breve{C}_p$) measured under suburban terrain exposure exceed the corresponding values measured under open country exposure. Historically, wind load on components and cladding for low-rise buildings in ASCE 7 were determined assuming an

"open country" wind exposure. Currently ASCE 7 uses one set of pressure coefficients regardless of the wind exposure, but allows wind loads to be determined for components and cladding using the actual terrain roughness at the site. Therefore, the comparison results presented in Figure 6.11 raise questions about the validity of using one set of pressure coefficients regardless of the terrain exposures for design wind loads on low-rise buildings.

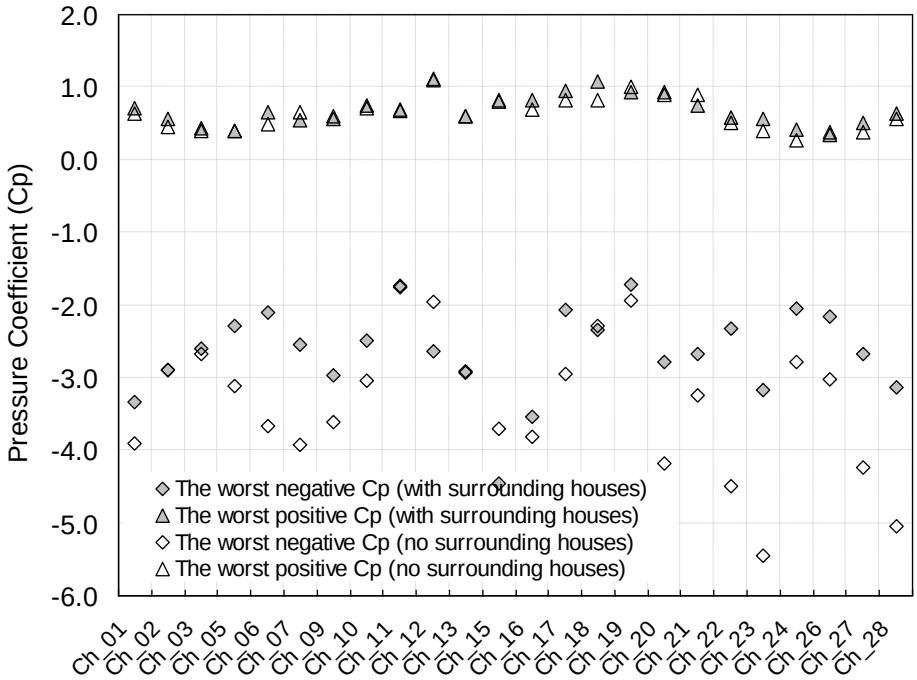

Figure 6.10(a) Comparison of Largest Peak Pressure Coefficients with and without Surrounding Houses for All Directions (Suburban Exposure)

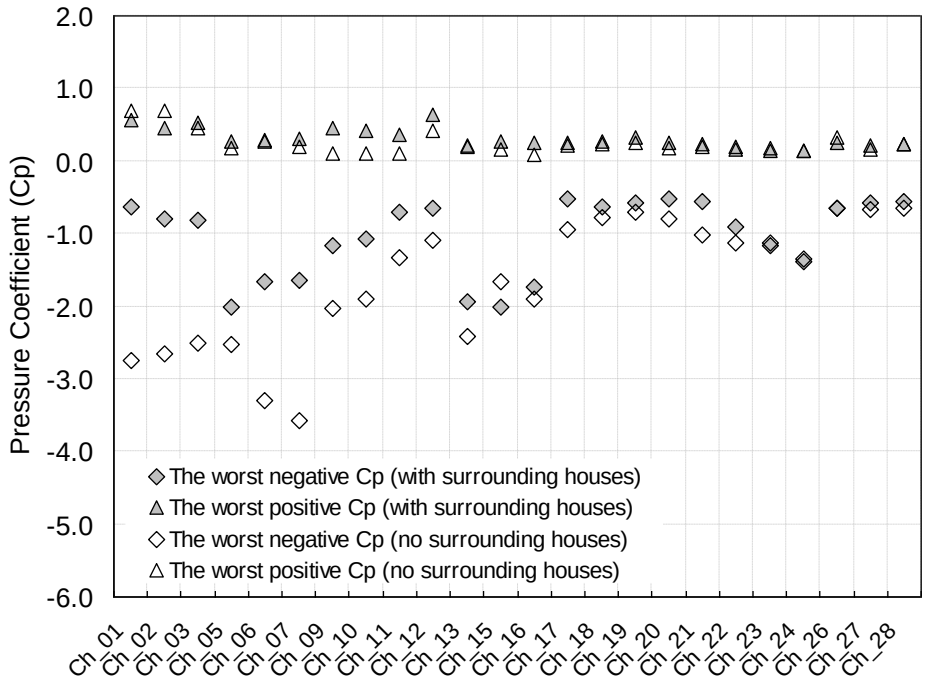

Figure 6.10(b) Comparison of Peak Pressure Coefficients with and without Surrounding Houses for Wind Incident Directions = 125° (Suburban Exposure)

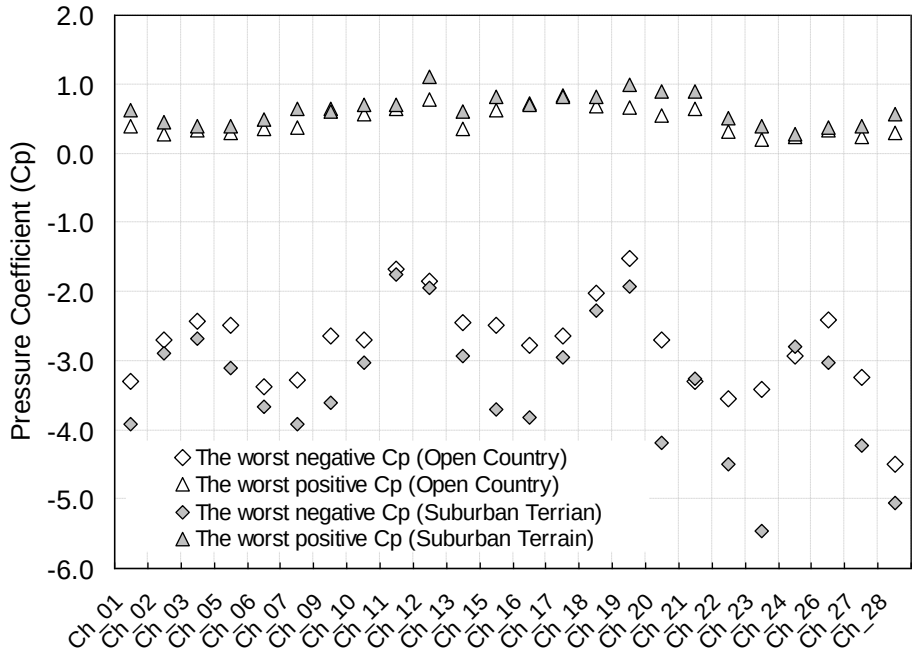

Figure 6.11 Comparison of Largest Peak Pressure Coefficients for All Directions Measured Under 1:50 Suburban Terrain and Open Country Exposures

6.5 Design Wind loads on House FL-27

Design wind load for the components and cladding (C&C) system of low-rise buildings are calculated by the following equations (ASCE 7-05, 2005):

$$q_h = 0.00256 \cdot K_z \cdot K_d \cdot K_{zt} \cdot U^2 \cdot I \tag{6-1a}$$

$$p = q_h \cdot [(GC_p) - (GC_{pi})] \tag{6-1b}$$

where, q_h is the velocity pressure at mean roof height (psf); K_z is the velocity pressure exposure coefficient defined in ASCE 7-05 Section 6.5.6.6; K_d is the wind directionality factor defined in ASCE 7-05 Section 6.5.4.4; K_{zt} is the topographic factor defined in ASCE 7-05 Section 6.5.7.2, U is the basic design wind speed (unit: mph) defined in ASCE 7-05 Figure 6-1, GC_p is the external pressure coefficient given in ASCE 7-05 Figure 6-11 through Figure 6-16, GC_{pi} is the internal pressure coefficient defined in ASCE 7-05 Figure 6-5.

As shown in Equations (6-1a) and (6-1b), design wind loads on a specific low-rise building basically depend on the values of basic wind speed and pressure coefficients. For the basic wind speed, ASCE 7-05 states in Section 6.5.4 that "*the design wind speed for buildings in hurricane prone regions shall not be less than the resulting 500-year return period wind speed divided by* $\sqrt{1.5}$."

In this section, the design wind loads on the critical roof corner areas of House FL-27 are calculated. Pressure coefficients are generated from the wind tunnel tests. The basic design wind speed is derived from a hurricane simulation program provided by Peter Vickery (Vickery, 2000).

6.5.1 Pressure Coefficients of Single Points on House FL-27

In full-scale tests of House FL-27, most of the pressure sensors are located at the roof eave and ridge corner areas where it is expected that the extreme wind pressures are most likely to occur. The ASCE 7-05 wind design negative pressure coefficients for the roof corner areas are -2.6 for negative pressure and 0.5 for positive pressure for areas less than 1.0 square meter.

In Figure 6.12, the largest peak pressure coefficients ($\breve{C}_p$ and $\widehat{C}_p$) of the twenty-four sensors from full-scale tests of House FL-27 are compared with the ASCE 7-05 design values. This comparison is plotted with respect to the changes in load time duration. The comparison shows that the largest positive peak pressure coefficients ($\widehat{C}_p$) of full scale test results exceed the code value. For the negative peak pressure coefficients ($\breve{C}_p$), the largest values measured in Tropical Storm Isidore exceed the code value when the load duration times are less than or equal to 1 second.

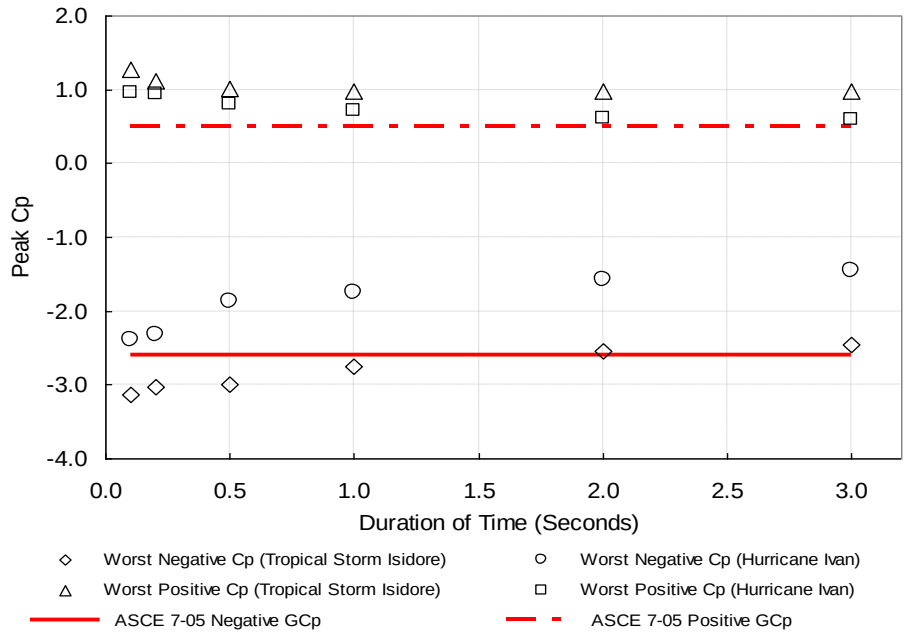

Figure 6.12 Comparison of Largest Peak Pressures of Twenty Four Sensors of Full-scale Test Results with ASCE 7-05 Provision Values

6.5.2 Area-averaged Wind Loads on House FL-27

The peak positive and negative pressure coefficients shown previously in Figure 6.12 are single point pressures, and they therefore do not represent wind loads over the roof corner areas. The area-averaged peak pressure coefficients of full-scale tests for the specific roof corner areas shown in Figure 5.7 are calculated by using Equation (5-12) and (5-13). Because the effective tributary areas of three pressure taps in these corners are less than 1.0 square meter, the design pressure coefficients for these areas are -2.6 for the negative peak pressure coefficient and 0.5 for the positive pressure coefficient.

The area-averaged peak pressure coefficients of a specific area, which are calculated based on full-scale records, are compared with ASCE 7-05 code values in Figures 6.13(a) and (b). It is observed that the area-averaged peak negative pressure coefficients are significantly less than the ASCE 7-05 design value, but the area-averaged

positive peak pressure coefficients still exceed the ASCE 7-05 design value. By comparing Figure 6.12 and Figure 6.13(a) and (b), we find that the area-averaged negative peak pressure coefficient is less than the single point values in this area. However, the area-averaged effects are small for the peak positive pressure coefficients on roof corner areas.

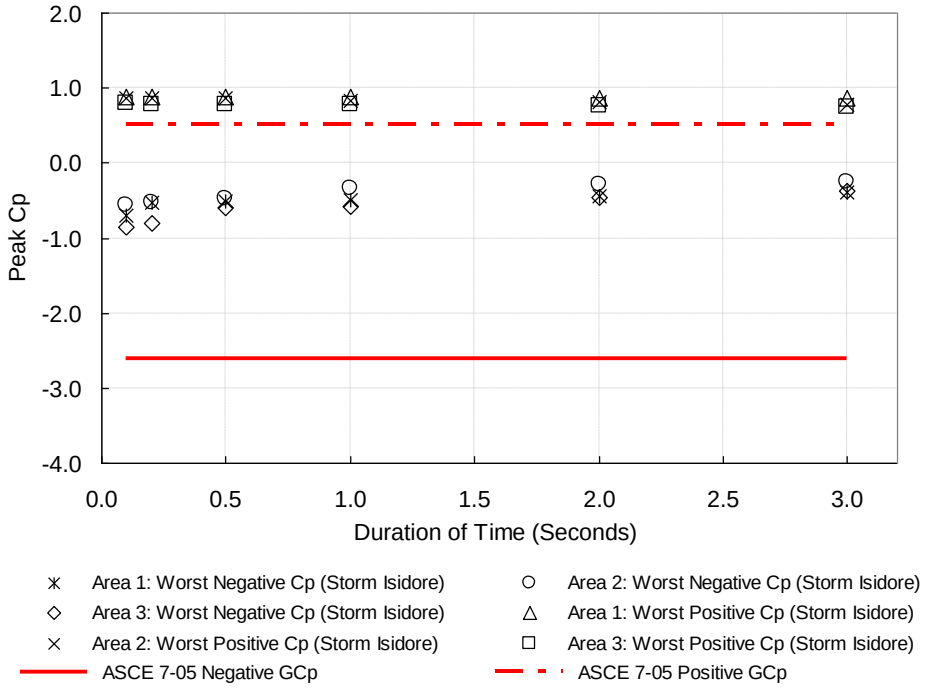

Figure 6.13(a) Comparison of Area-averaged Peak Pressures of the Specific Areas (Tropical Storm Isidore) with ASCE 7-05 Provision Values

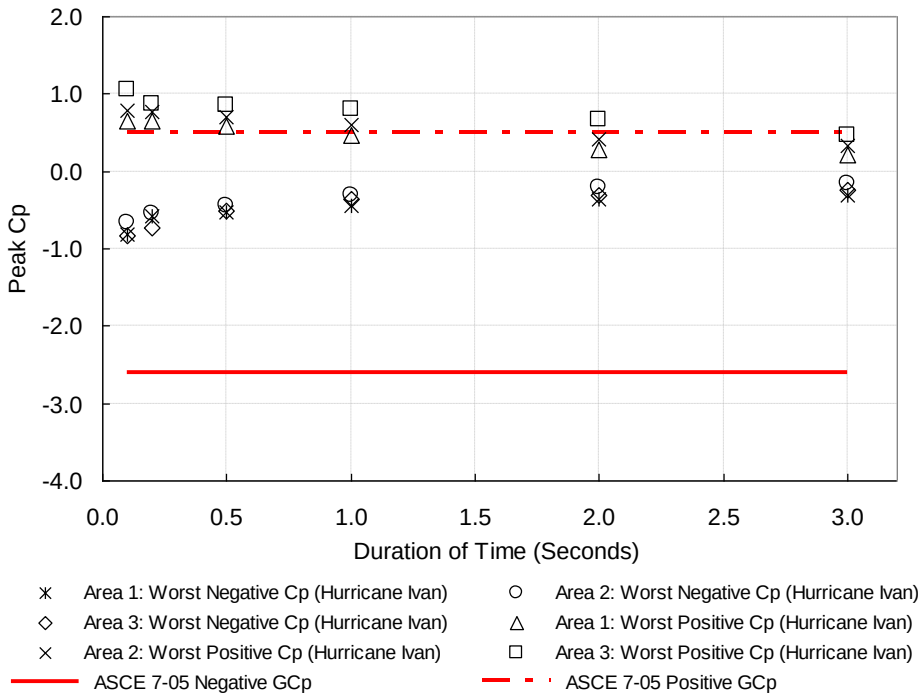

Figure 6.13(b) Comparison of Area-averaged Peak Pressures of Specific Areas (Hurricane Ivan) with ASCE 7-05 Provision Values

Although the area-averaged negative pressure coefficients for full-scale tests are less than ASCE 7-05 design value, the results of full-scale tests can only represent the values for specific incident wind directions from 120° to 130° and not peak pressure for all wind directions. Wind tunnel tests of House FL-27 model indicate that the peak pressure coefficients observed in full-scale tests are not be the largest values for all directions, and the larger area-averaged negative pressure coefficients on House FL-27 can be expected at other directions. The largest area-averaged pressure coefficients of three roof corner areas (shown in Figure 5.7) for all directions are calculated and compared to ASCE 7-05 code values in Figure 6.14. This comparison shows that the largesr area-averaged negative peak pressure coefficients three roof corner areas (shown in Figure 5.7) for all directions exceed the ASCE 7-05 code value for short time durations (less than 0.5

second). It is also observed that the largest area-averaged positive peak pressure coefficients exceed the ASCE 7-05 code value for all directions but approaches the code value asymptotically for duration greater than 2.0 seconds.

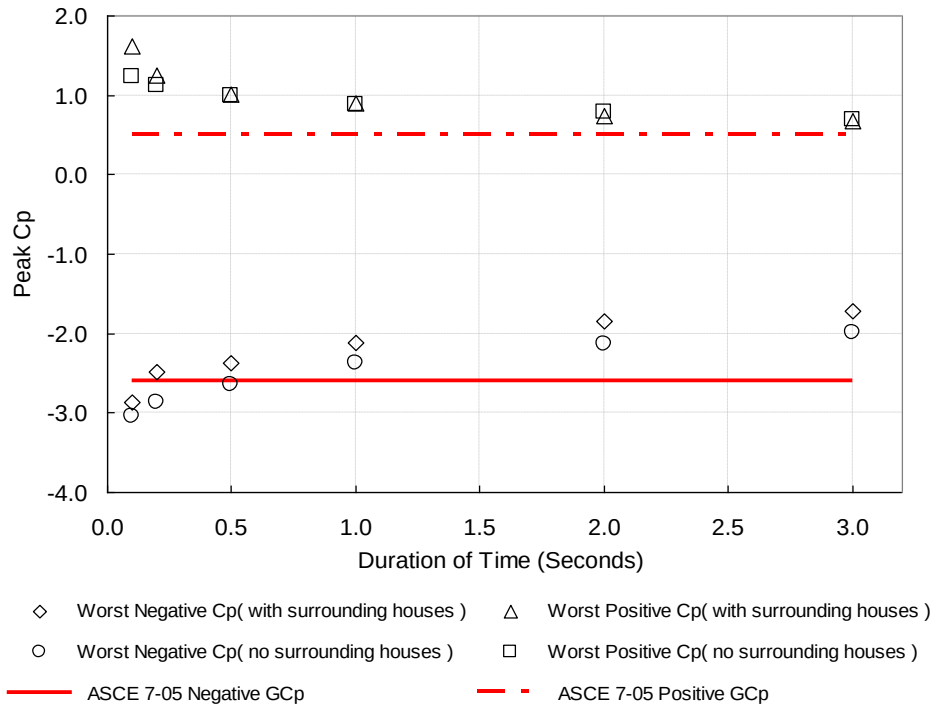

Figure 6.14 Comparison Largest Peak Pressures of Twenty Four Sensors for All Directions (Wind tunnel tests) with ASCE 7-05 Provision Values

6.5.3 Design Wind Loads on Critical Corner Areas of House FL-27

In this section the design wind loads on the critical roof corner areas of House FL-27 are calculated. The division of the critical roof corner areas of House FL-27 model is shown in Figure 6.15. The equivalent tributary area of each corner is about 1 m^2. Each of the corners has 6 to 9 taps distributed in them. Based on Equations (6-1a) and (6-1b),

ASCE 7-05 external design wind loads on House FL-27 critical corner areas are calculated and listed on Table 6.4.

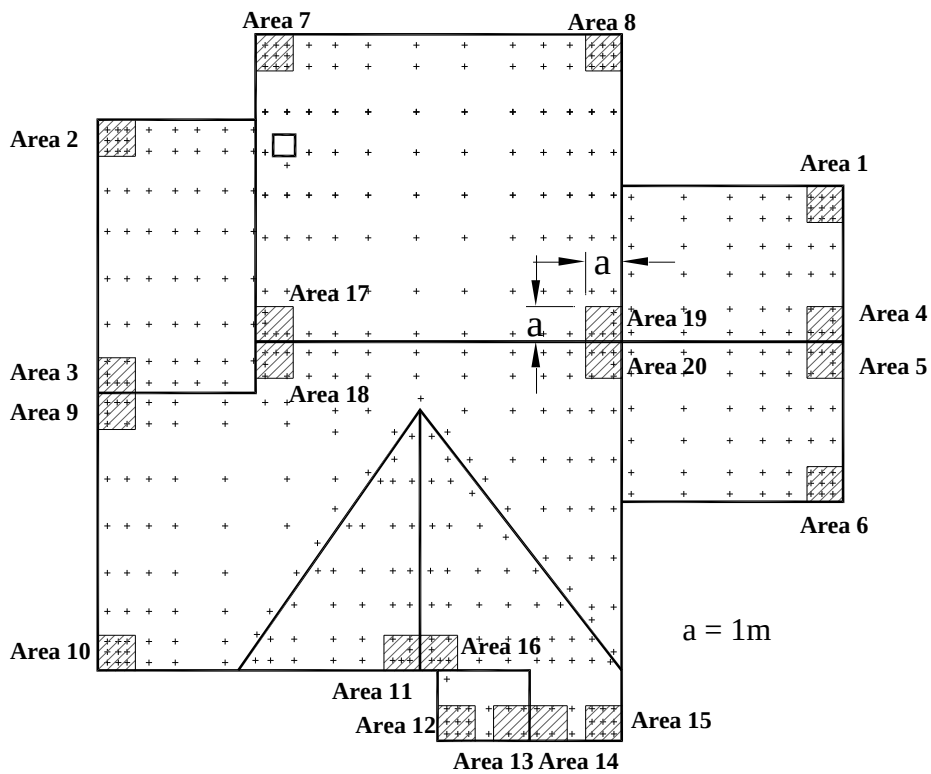

Figure 6.15 Divisions of Critical Roof Corner Areas of House FL-27 Model

Table 6.4 ASCE 7-05 Design Wind Loads on House FL-27 at Critical Roof Corner Areas

Basic Wind Speed (mph)	130	The Design External Wind Load	
		Negative Wind Pressure(psf)	Positive Wind Pressure(psf)
External Negative GC_p	-2.6	67	13
External Positive GC_p	0.5		
Directionality factor K_d	0.85		

The results presented earlier in Section 6.3 show that, although the peak negative pressure coefficients may be underestimated, wind tunnel tests can be considered to

effectively reproduce hurricane wind loads measured in full-scale tests of House FL-27. Therefore, these wind tunnel results are used to evaluate the design wind loads on House FL-27 through combining a hurricane simulation model provided by Peter Vickery (Vickery, 2000). The area-averaged peak pressure coefficients GC_p of wind tunnel tests are listed in Appendix F. The design wind speeds are derived from the hurricane simulation model. This hurricane simulation model is used to generate the 500-year return period of the mean hourly wind speed at 10-meter height at House FL-27 location for open country exposure for each direction. Then, the design 3-second gust wind speed at mean roof height for each direction is calculated as explained in Section 4.4 using Equations (4-4a) and (4-4b).

Combining wind tunnel GC_p values and simulated design wind speed, the area-averaged external design wind load for critical roof corner areas of House FL-27 (see Figure 6.15) are calculated. Two methods are used to calculate area-averaged external design wind loads, and these methods are summarized in Table 6.4.

Method 1 uses the largest peak external pressure coefficients for all directions (from 0° to 360°) and the largest simulated design wind speed for all directions (from 0° to 360°) to calculates design wind load by combining a directionality factor. Method 2 uses the peak external pressure coefficients and the simulated design wind speed for a wind direction to calculate external wind load in this wind direction. Then, the largest external peak wind loads for all directions (from 0° to 360°) are chosen as the final external design wind loads. The external design wind loads on House FL-27 critical roof corner areas based on Method 1 and Method 2 are presented in Figure 6.16 and compared with ASCE 7-05 design values.

Table 6.4 Summary of Methods for Calculating External Design Wind Loads on House FL-27 Roof Corner Areas

	Equation
Method 1	Negative External Design Wind Load: $p_{-} = 0.00256 \cdot K_d \cdot U^2_{\text{Largest}} \cdot (GC_p)^{-}_{\text{Largest}}$ Positive External Design Wind Load: $p_{+} = 0.00256 \cdot K_d \cdot U^2_{\text{Largest}} \cdot (GC_p)^{+}_{\text{Largest}}$ where, $(GC_p)^{-}_{\text{Largest}}$: the largest peak negative pressure coefficients for all directions; $(GC_p)^{-}_{\text{Largest}}$: the largest peak positive pressure coefficients for all directions; U_{Largest} : the largest simulated design wind speed for all direction; K_d : directionality factor = 0.85.
Method 2	Negative External Design Wind Load: $p_{-} = \min[0.00256 \cdot U(\theta)^2 \cdot GC_p^{-}(\theta)]$ Positive External Design Wind Load: $p_{+} = \max[0.00256 \cdot U(\theta)^2 \cdot GC_p^{+}(\theta)]$ where, $GC_p^{-}(\theta)$: the peak negative pressure coefficients for wind direction θ; $GC_p^{+}(\theta)$: the peak positive pressure coefficients for wind direction θ; $U(\theta)$: the simulated design wind speed for wind direction θ.

In Figure 6.16, the negative external design wind load of Area 14, which is calculated through Method 1, is 71 psf. This value has exceeded the ASCE 7-05 design value by 6%. The largest external negative design wind load calculated by Method 2 is 54psf, which occurs at Area 20 for wind incident direction of 22.5° (North is 0° and the wind direction shifts clockwise). This value is 81% of ASCE 7-05 design wind value.

As shown in Figure 6.16, the positive external design wind loads of Area 1, 2, 6, 7, 8 , 12, 13, and 15, which are calculated through both of Method 1 and Method 2, exceed ASCE 7-05 design value. For Method 1, the largest positive value is 40 psf, which

occurs at Area 12. This value exceeds ASCE 7-05 design value by 210%. For Method 2, the largest positive value is 29 psf, which occurs at Area 12. This value exceeds ASCE 7-05 design value by 25%.

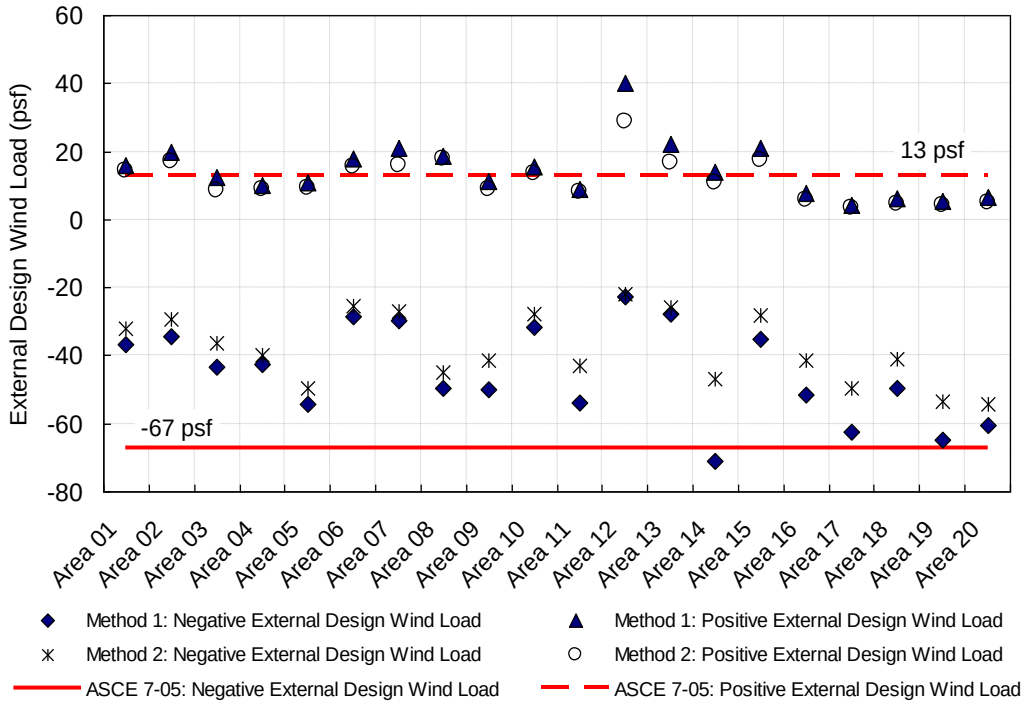

Figure 6.16 Comparison of the External Negative Simulated Design Wind Loads on Roof Corner Areas with ASCE 7-05 Design Load

6.6 Summary

Through such a validation of widely-used wind tunnel techniques, researchers will gain greater confidences that wind tunnel test accurately defines wind loads on low-rise structures.

In this chapter, wind tunnel model tests of House FL-27 are described. The comparisons of full-scale and wind tunnel test results are conducted. The results indicate that wind tunnel tests can reproduce the mean, peak positive, and standard deviation of pressure coefficients that were measured in two tropical cyclones. The results also show some divergences of peak negative pressure coefficients between full-scale and wind tunnel experiments. For almost all tap locations, the peak negative Cp wind tunnel values are lower full-scale test results. The probability density function of wind pressure of full-scale and wind tunnel experiments show that the full-scale data exhibits more skewed distributions than the wind tunnel data and some differences in the tail of the associated probability density functions compared with the wind tunnel data.

Full-scale and wind tunnel test results are compared with ASCE 7-05 code values. The comparison results shows that ASCE 7-05 underestimates wind pressure coefficients on critical roof corner areas. The largest area-averaged peak negative pressure coefficient is -3.8 (listed in Appendix F), which exceeds ASCE 7-05 wind design pressure coefficient value by 46%. The largest area-averaged positive pressure coefficient is 2.1 (listed in Appendix F) which exceeds ASCE 7-05 code value by 320%. Combining wind tunnel model test results and hurricane wind speed simulating results, the design wind loads on the critical roof corner areas are calculated and compared with ASCE 7 design values. The largest external negative design wind load is 71 psf which value has

exceeded the ASCE 7-05 design value by 6%, and the largest positive value is 40 psf which value exceeds ASCE 7-05 design value by 210%. These results further indicate that ASCE 7 is non-conservative to design wind pressures occurring at roof corner areas.

Wind tunnel model tests for House FL-27 indicate that surrounding houses can apparently decrease wind loads on a house roof. However, the wind load at some individual tap locations is found to be increased by the surrounding houses. The investigation of the effects of terrain exposures show that peak negative pressure coefficients measured under suburban terrain are larger than values measured under open country exposure. Since 1995, ASCE 7 has used one set of pressure coefficients for wind load design regardless of the wind exposure. Wind tunnel tests of House FL-27 indicate that this method underestimates wind loads on house roof corner areas which are located in suburban terrain.

CHAPTER 7

INVESTIGATION OF THE INFLUENCES OF TERRAIN EXPOSURES AND NEIGHBORHOODS ON WIND LOADS ON LOW-RISE BUILDINGS

Wind load design code ASCE 7 uses one set of pressure coefficients regardless of wind exposure to calculate the design wind load on components and cladding system (C&C system) of low-rise buildings. This set of pressure coefficients was historically determined by assuming an “open country” wind exposure and until 1995 all low-rise building components and cladding wind loads were based on open terrain assumptions. Beginning in 1995 ASCE 7 allows components and cladding wind loads to be calculated for the actual terrain where the low-rise building is sited but still used one set of pressure coefficients. Results of full-scale and wind tunnel tests for House FL-27 presented in Chapter 6 show that this current ASCE 7 wind design method underestimates components and cladding wind loads on low-rise buildings located at suburban terrain exposure and wind pressure coefficients of components and cladding are apparently affected by terrain exposure and surrounding houses.

In this chapter, the influences of the terrain exposure and surrounding houses on components and cladding wind loads are further examined using a study of these neighborhood house configurations. At the beginning of this chapter, descriptions of the models and wind tunnel set-up for this study are presented. Then, the influence of terrain exposure and surrounding houses on pressure coefficients are presented in the second and third sections.

7.1 Experimental Models and Set-up

Three residential houses are selected as representation of homes built in the state of Florida. 1:50 scale models of the three houses (see Figures 7.1(a), (b), and (c)), named as the FIU series models, are constructed by the Florida International University and Clemson University. Based on the method described in ASCE 7-05 Figure 6-11B-Figure 6-11D (ASCE 7-05, 2005), each of the model roofs is divided into three zones categories, Zone 1 - interior, Zone 2 – edge, and Zone 3 - corner. The investigation of the influences of terrain exposures and surrounding houses on components and cladding wind loads is conducted according to the different divisions of roofs.

To investigate the influences of terrain exposures, Wind tunnel tests were conducted and each house model was set on the turntable in isolation in open country and suburban terrain exposures. Wind tunnel test setup was as described in Chapter 3. Table 7.1 summarizes the main test parameters for the investigation of the influence of terrain exposures.

To investigate the influences of surrounding houses on wind loads, three sets of neighboring houses are modeled on a 1:50 scale. They are arranged on the turntable to represent the typical high density, medium density, and sparse density of surrounding situations, respectively. Each of the experimental house models is separately tested with each of the sets of neighboring houses. The detailed information of the three sets of neighboring houses is given in Figures 7.2(a), (b), and (c). Table 7.2 summarizes the main test parameters for the investigation of the influence of the surrounding houses.

Table 7.1 Main Test Parameters of Wind Tunnel Tests for the Investigating Influences of Terrain Exposures

Model Name	FIU Model 1, FIU Model 2 and FIU Model 3
Model Scale	1:50
Sampling Frequency	300 Hz
Low Pass Filter Cut-off Frequency	100 Hz
Sampling period	120 seconds
Wind Angles (deg)	Every 10° over a 360° range
Upstream Exposure	1:50 Open and Suburban
Reference Tunnel Wind Speed	11 m/s
Arrangement of Turntable	Only Isolated Experimental Model

Table 7.2 Main Test Parameters of Wind Tunnel Tests for the Investigating Influences of Surrounding Houses

Model Name	FIU Model 1, FIU Model 2 and FIU Model 3
Model Scale	1:50
Sampling Frequency	300 Hz
Low Pass Filter Cut-off Frequency	100 Hz
Sampling period	120 seconds
Wind Angles (deg)	Every 45° over a 360° range
Upstream Exposure	1:50 Open and Suburban
Reference Tunnel Wind Speed	11 m/s
Arrangement of Turntable	High Density, Medium Density, and Sparse Density Of Surrounding Buildings

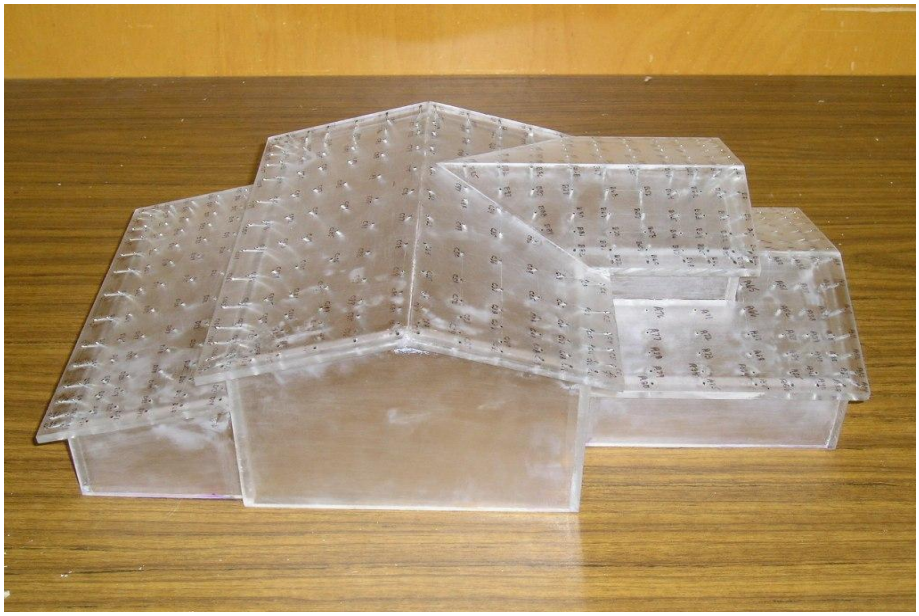

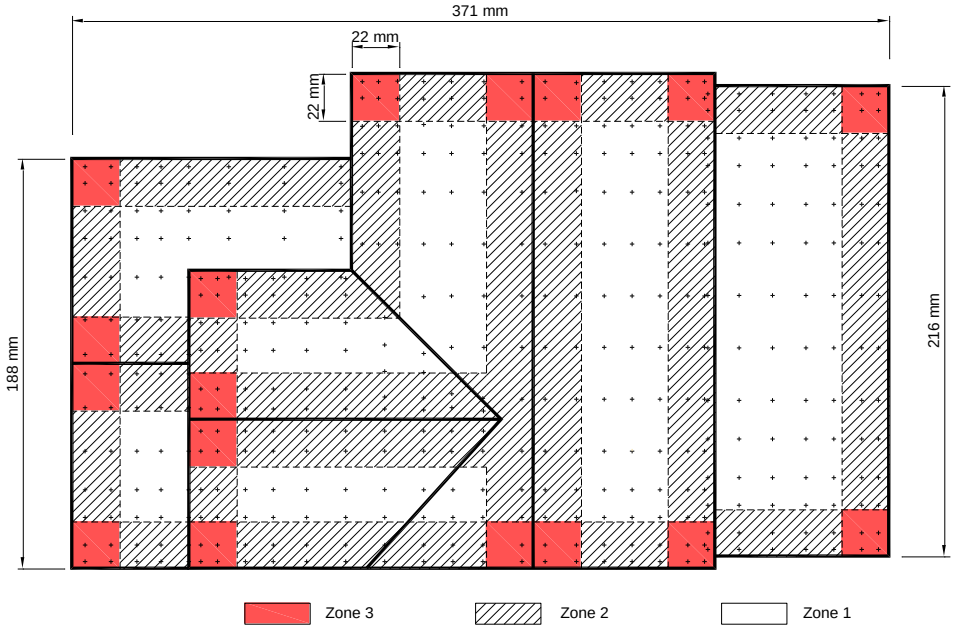

Figure 7.1(a) Photo, Arrangement of Test Points and Divisions of Roof of 1:50 Scale FIU Model 1 (Model Basic Size: L × W × H = 371 mm × 218 mm × 114 mm, and 445 Test Points Arranged on the Model Roof)

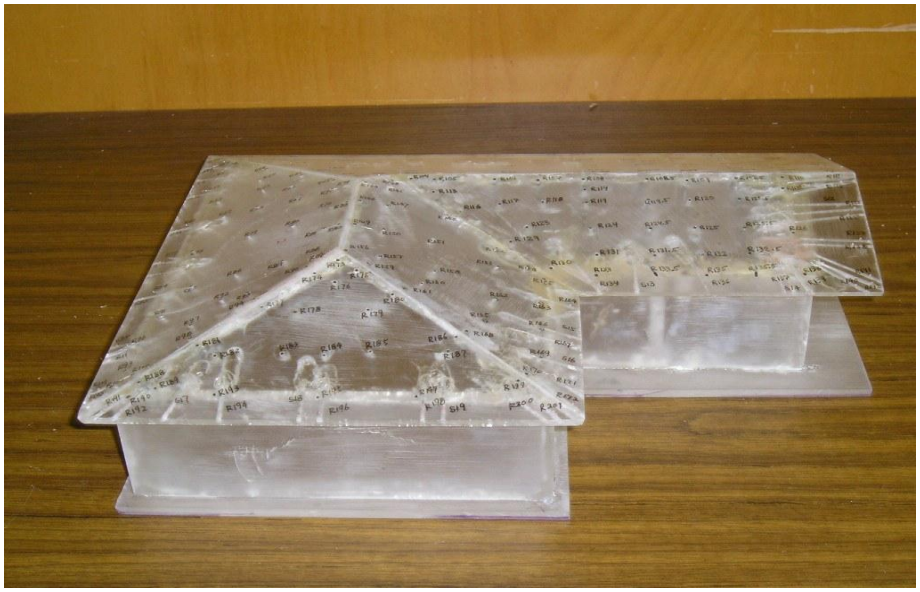

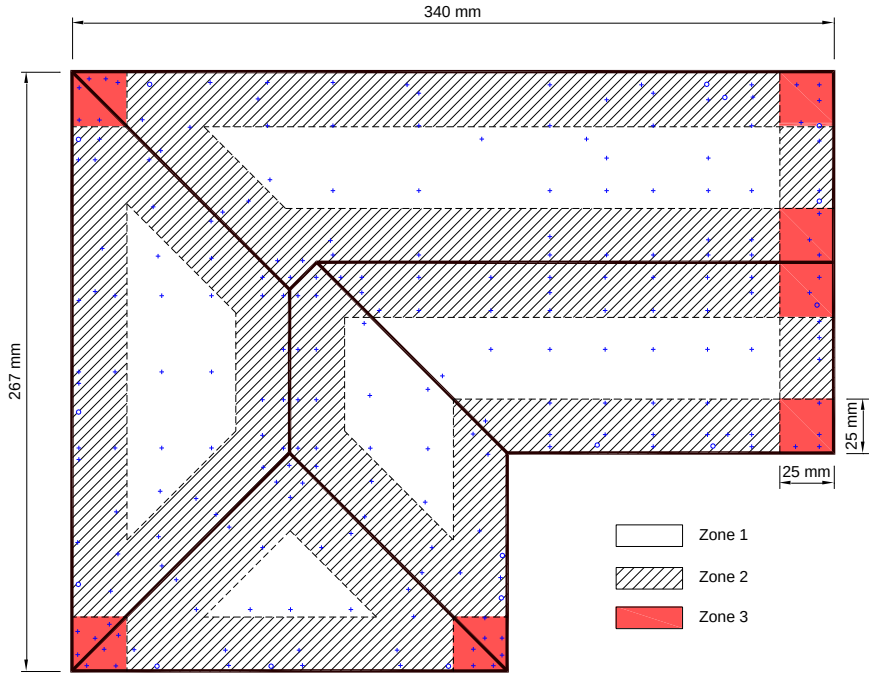

Figure 7.1(b) Photo, Arrangement of Test Points and Divisions of Roof of 1:50 Scale FIU Model 2 (Model Basic Size: L × W × H = 340 mm × 267 mm × 76 mm and 218 Test Points Arranged on the Model Roof)

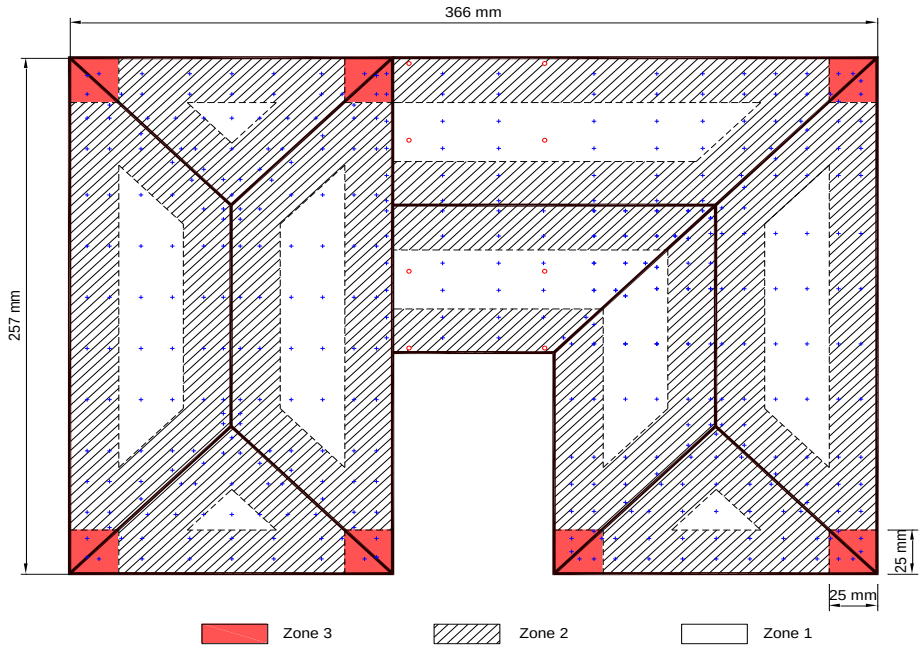

Figure 7.1(c) Photo, Arrangement of Test Points and Divisions of Roof of 1:50 Scale FIU Model 3 (Model Basic Size: L × W × H = 366 mm × 257 mm × 122 mm and 404 Test Points Arranged on the Model Roof)

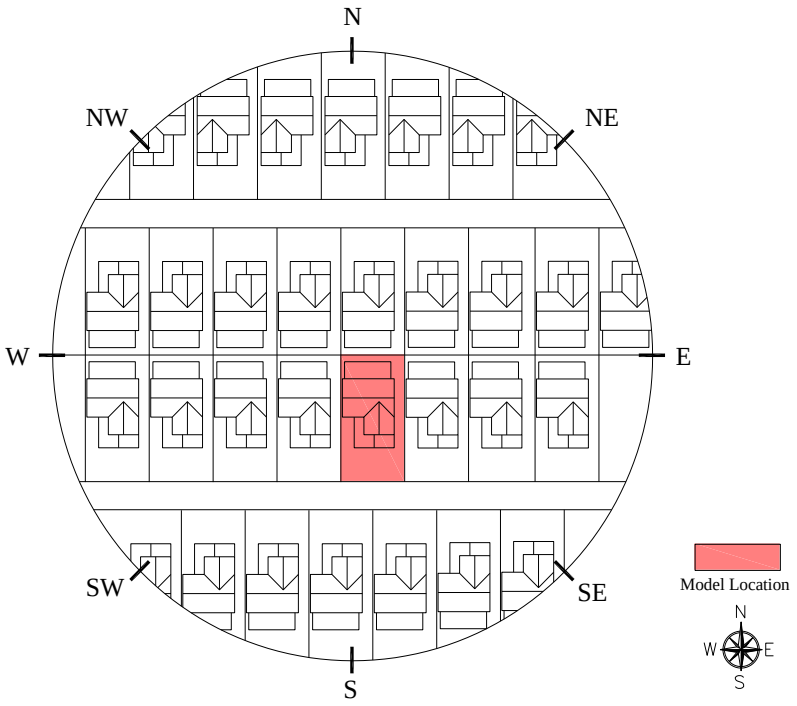

Figure 7.2(a) Arrangement of Turntable for High Density Surrounding Houses

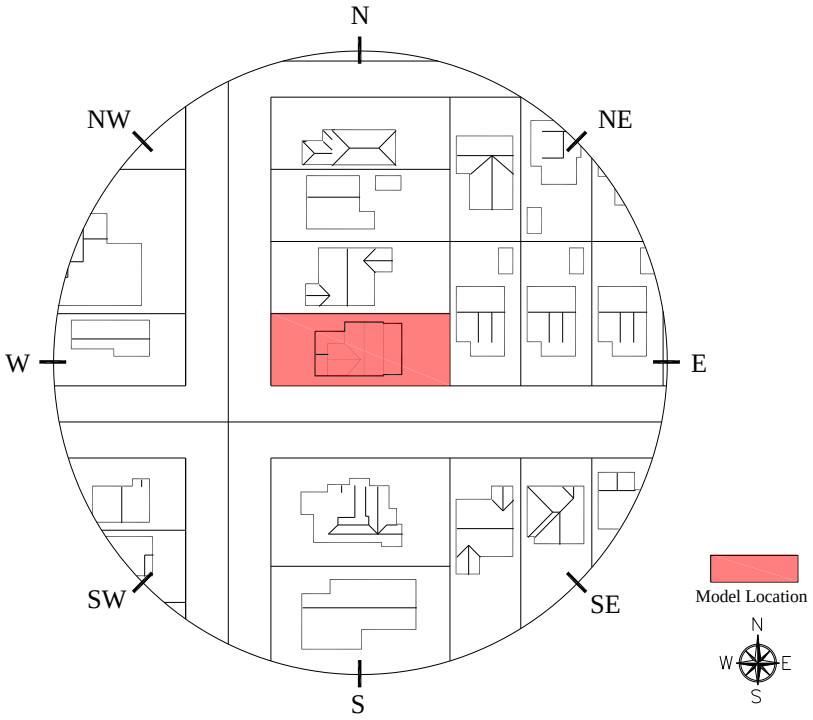

Figure 7.2(b) Arrangement of Turntable for Medium Density Surrounding Houses

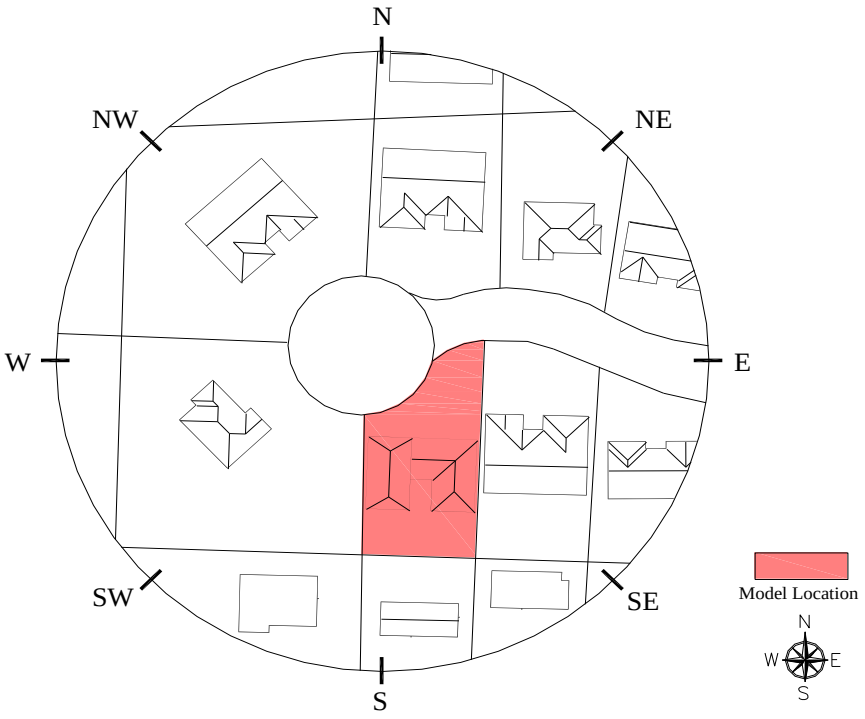

Figure 7.2(c) Arrangement of Turntable for Low Density Surrounding Houses

7.2 The Influences of Terrain Exposures

Three FIU house models were tested in isolation under open country and suburban terrain exposures, respectively. The results of this study concern the peak pressure coefficients for all wind directions. The pressure coefficients measured under suburban terrain exposure are compared with the corresponding results from open country exposure. Based on these comparisons, a linear regression analysis was conducted for different zones.

The comparison shown in Figure 7.3(a) indicates that the worst negative pressure coefficients on the roof corner areas, which are measured under the suburban terrain condition, on average exceed the corresponding results measured under the open country exposure by 5 percent. For the other roof areas (Zone 2 and Zone 3), there are no apparent differences between the worst negative pressure coefficients measured under the open country and the suburban terrain exposure, as shown in Figure 7.3(b) and Figure 7.3(c). Figure 7.4 shows that there are no apparent differences between the worst positive pressure coefficients measured under the open country and the suburban terrain exposure.

Wind load design code ASCE 7 uses one set of pressure coefficients regardless of terrain exposures to calculate the design wind loads on the C&C system of low-rise buildings. This set of pressure coefficients was historically determined by assuming an “open country” wind exposure. In this investigation, this method is further proven to be non-conservative when calculating the negative C&C wind loads on roof corners and positive C&C wind loads on the whole house roof which is located in a suburban terrain.

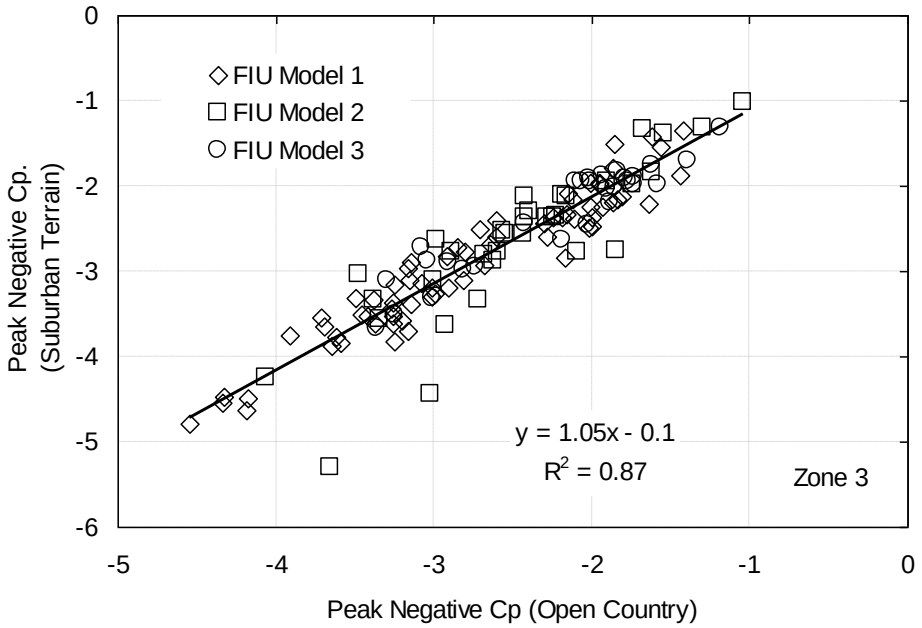

Figure 7.3(a) Comparisons and Linear Regression Analysis of Peak Negative Pressure Coefficients on Zone 3 of FIU Series House Models

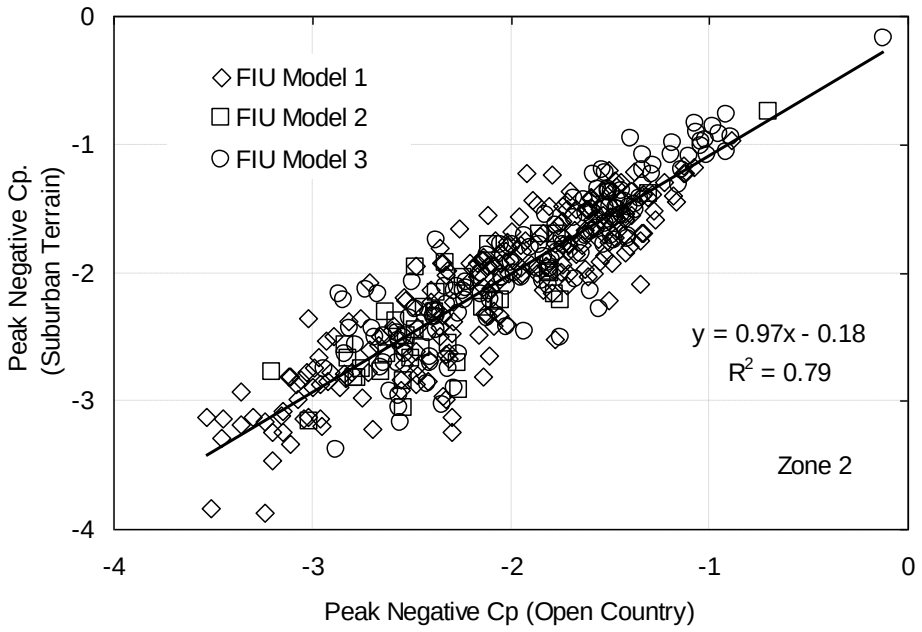

Figure 7.3(b) Comparisons and Linear Regression Analysis of Peak Negative Pressure Coefficients on Zone 2 of FIU Series House Models

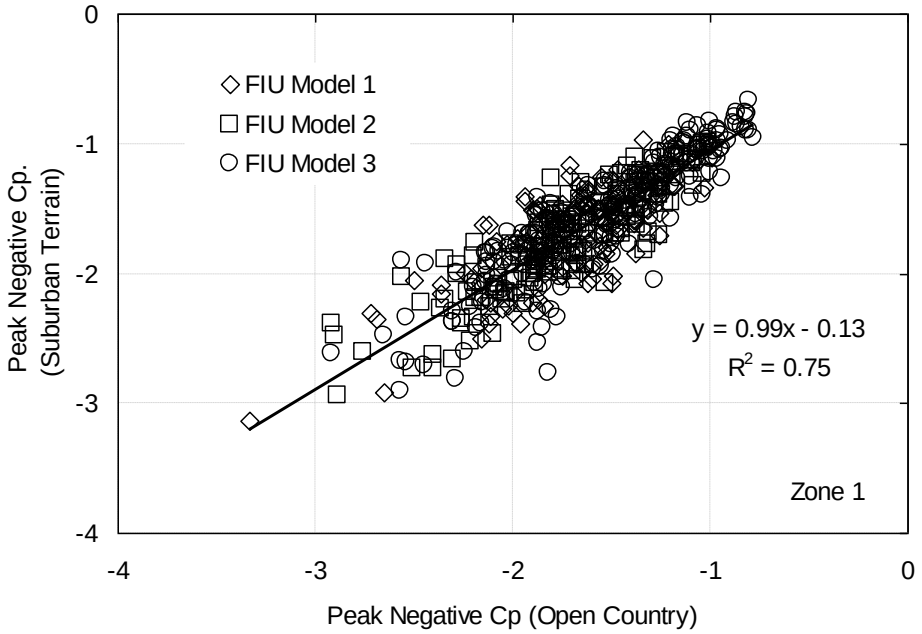

Figure 7.3(c) Comparisons and Linear Regression Analysis of Peak Negative Pressure Coefficients on Zone 1 of FIU Series House Models

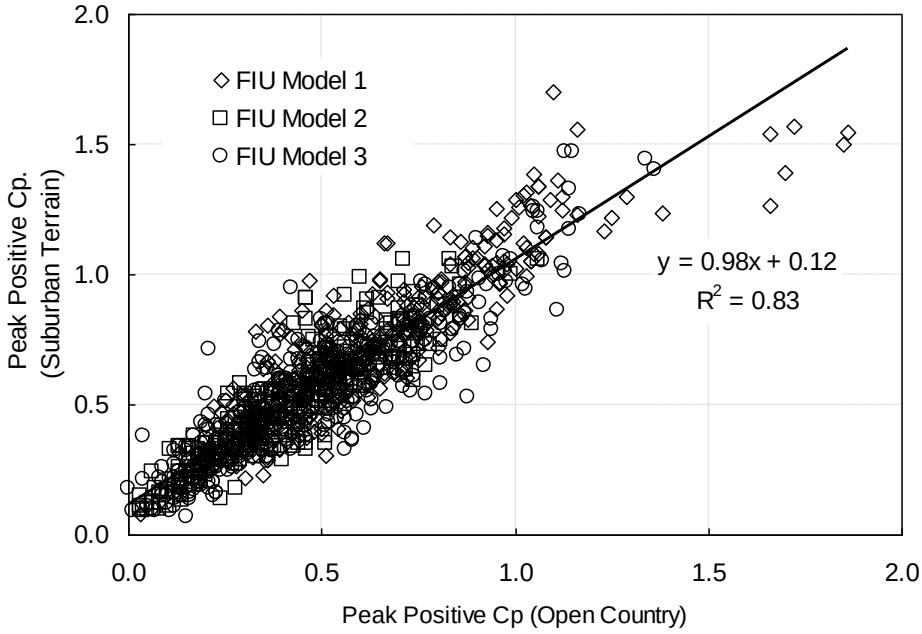

Figure 7.4 Comparisons and Linear Regression Analysis of Peak Positive Pressure Coefficients on Roofs of FIU Series House Models

7.3 The Influence of Surrounding Houses

In general, low-rise buildings are usually surrounded by surrounding houses, and wind loads on low-rise buildings are definitely affected by these neighboring houses. However, the current wind load design code ASCE 7-05 only considers the effect of roughness of the upwind terrain but neglects the direct effect of neighboring houses. The primary study goal described in this section is to better understand and quantify the effect of surrounding buildings on wind load on low-rise buildings.

Three FIU house models, as shown in Figures 6.1(a), (b), and (c), are used for this research. Each of the experimental models is set on the turntable in isolation and tested under open country and suburban terrain exposure settings. These test settings are called isolation test cases. The test results of the isolation test cases are referred to as the standard values. Three sets of neighboring houses, shown in Figures 7.2(a), (b), and (c), are modeled to represent the typical high density, medium density, and sparse density of surrounding houses, respectively. Each experimental model is also tested separately with three sets of surrounding houses under open country or suburban terrain settings, and the test results are compared with the standard values to examine the effect of the density of surrounding houses.

Jia and Sill (1998) systematically studied the influence of roughness element space density on the wind flow characteristics and the pressure distribution on a single cube block embedded in a uniform roughness field. In general, surroundings houses can be treated as the roughness elements with the same size of the subject structure. Therefore, the roughness element spacing density is chosen as the main parameter to examine the effect of surrounding houses on wind load on low-rise buildings in this

study. The roughness element spacing density is scaled by a dimensionless ratio A_f / s, which is defined as the ratio of frontal area (A_f) of the element to tributary area (s) of this element. In this study, the ranges of the dimensionless ratio A_f / s, which represent the different densities of surrounding houses, are selected and summarized in Table 7.3.

Table 7.3 Range of Ratio A_f / s of Roughness Element Spacing Density for Different Density of Surrounding Houses

	High Density Neighborhoods	**Medium Density Neighborhoods**	**Sparse Density Neighborhoods**
Roughness Element Spacing Density	> 0.12	0.8 – 0.12	< 0.8

The ratio of $\hat{C}_{p.S} / \hat{C}_{p.0}$, which represents the changes of peak pressure coefficients caused by surrounding buildings, is expressed as the symbol ϕ. The ratio of ϕ can be written as the function of the dimensionless ratio A_f / s by:

$$\phi = \frac{\hat{C}_{p.S}}{\hat{C}_{p.0}} = f\left(\Delta\left(\frac{A_f}{s}\right)\right) = f\left(\left(\frac{A_f}{s}\right)_S - \left(\frac{A_f}{s}\right)_0\right) = f\left(\left(\frac{A_f}{s}\right)_S\right) \tag{7-1}$$

where, $\hat{C}_{p.S}$ is the peak pressure coefficients measured under the experimental model surrounded by neighboring houses; $\hat{C}_{p.0}$ is the peak pressure coefficient obtained under the isolation test case, in which the experimental model is arranged on the turntable in isolation; $(A_f / s)_s$ is the ratio of frontal area of element to tributary area. When an experimental model is set on the turntable in isolation, the ratio of frontal area of the element to tributary area of the element is expressed as $(A_f / s)_0$ and this value is equal to

zero. The dimensionless ratios A_f / s of three sets of surroundings in eight directions are calculated and listed on Table 7.3. The ratio of ϕ for every test point for each wind direction is calculated. For each of the specific roof zone divisions, which are shown in Figures 7.1(a), (b), and (c), the mean ratio of $\bar{\phi}$ for a zone division is plotted against the dimensionless ratio A_f / s and shown in Figures 7.5(a), (b), (c), and Figure 7.6.

Table 7.4 Dimensionless Ratio A_f / s of Roughness Element Spacing Density for Three Sets of Surrounding Houses for Eight Wind Directions

Wind Direction	**High Density Neighborhoods**	**Medium Density Neighborhoods**	**Sparse Density Neighborhoods**
N	0.15	0.10	0.06
NE	0.20	0.12	0.07
E	0.19	0.09	0.05
SE	0.11	0.08	0.07
S	0.13	0.07	0.08
SW	0.11	0.03	0.06
W	0.19	0.03	0.01
NW	0.20	0.02	0.01
Average	0.16	0.08	0.05

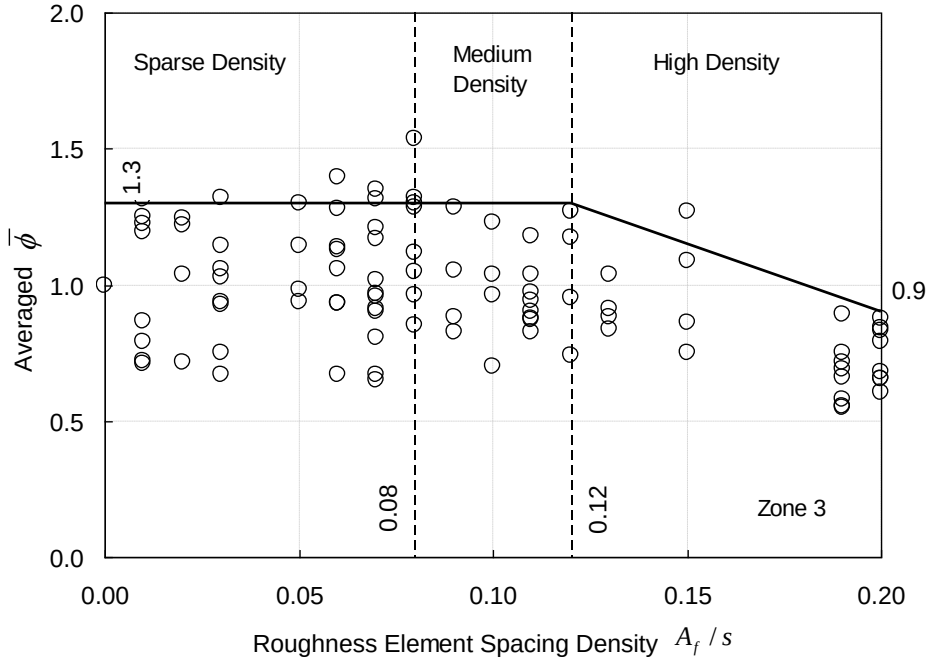

Figure 7.5(a) Envelope Line of $\bar{\phi}$ of the Negative Peak Pressure Coefficients against the Dimensionless Ratio A_f / s for Zone 3 of FIU Series House Models

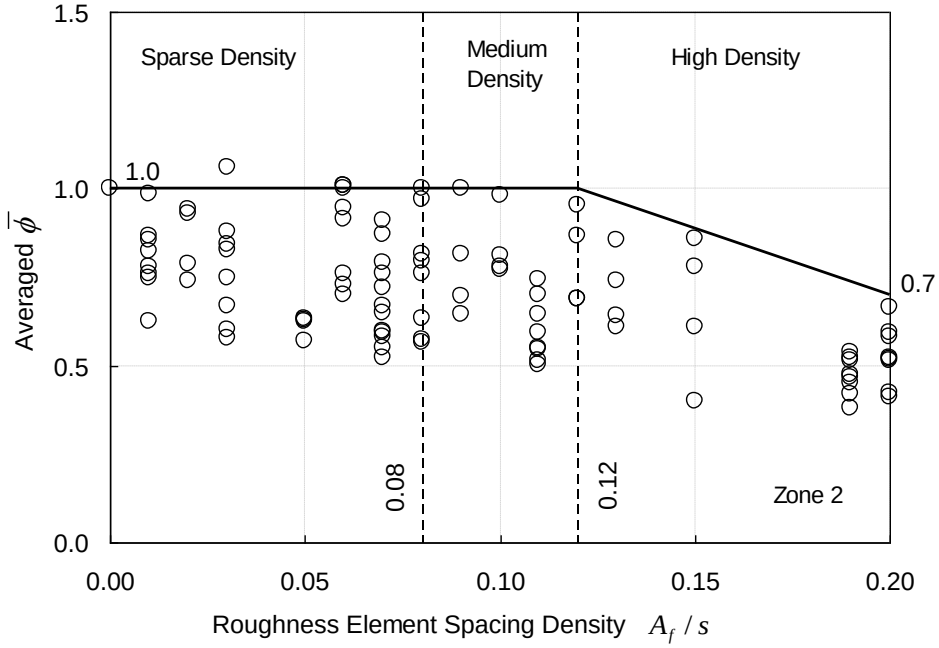

Figure 7.5(b) Envelope Line of $\bar{\phi}$ of the Negative Peak Pressure Coefficients against the Dimensionless Ratio A_f / s for Zone 2 of FIU Series House Models

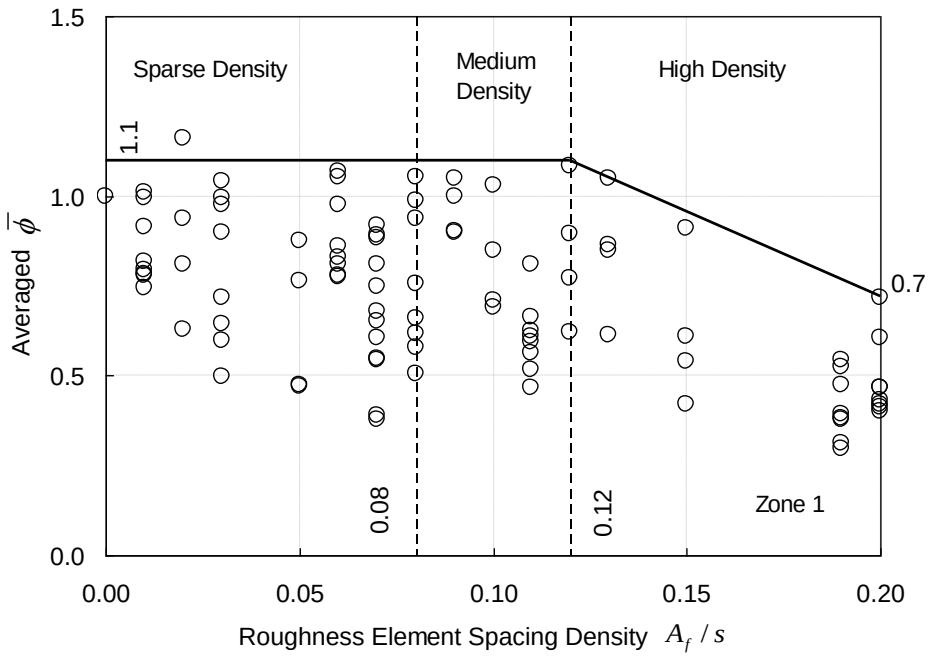

Figure 7.5(c) Envelope Line of $\bar{\phi}$ of the Negative Peak Pressure Coefficients against the Dimensionless Ratio A_f / s for Zone 1 of FIU Series House Models

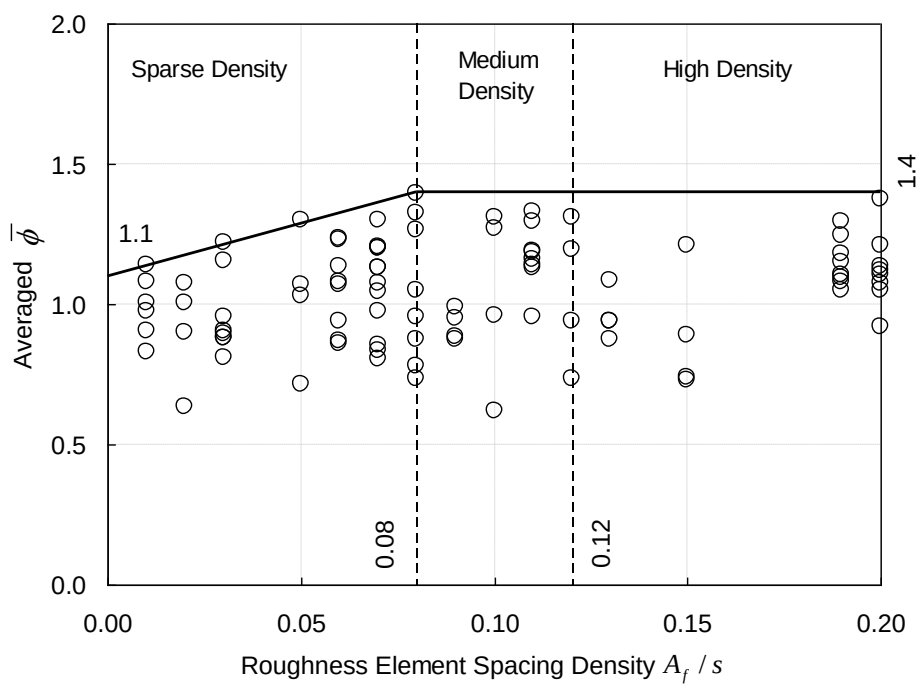

Figure 7.6 Envelope Line of $\bar{\phi}$ of the Positive Peak Pressure Coefficients against the Dimensionless Ratio A_f / s for Roof Areas of FIU Series House Models

Figures 7.5(a), (b), and (c) indicate that density of surrounding buildings does affect the peak negative wind pressure coefficients on the subject model roof. As the density of surrounding buildings increases, the average peak negative wind pressure coefficients on roof Zone 1 and Zone 2 decreases. For the average peak negative wind pressure coefficients on roof Zone 3, the average peak negative wind pressure coefficients are also apparently decreased in the high density of surrounding settings. However, under the sparse and medium density of surrounding houses, the average peak negative wind pressure coefficients can be increased by up to 30% when the dimensionless ratio A_f / s of roughness element spacing density is less than 0.12. The effect of surrounding houses on the peak wind positive pressure coefficients is displayed in Figure 7.6. The peak positive wind pressure coefficients are increased with the increase of the density of surrounding buildings.

Under the sparse density of the surrounding houses, the distances between houses are enough to ensure the wake and separation of air flow will fully develop. This makes the air flow more complicated and increases the turbulence of flow. In general, the higher turbulence intensity will result in increased wind pressure fluctuations on the separation area and will cause the higher peak pressures. This may be a justifiable explanation for the increase of the peak negative wind pressure with the increasing of A_f / s under medium density of surroundings. For the high density of the surroundings, wind speed will be reduced. When the density of surroundings increases enough, the distances between surrounding buildings are too close and the wake and separation of air flow do not have enough space to develop, therefore the turbulence and vortices in flow become stable. With the wind speed reduced, the wind pressure on the buildings will decrease.

7.4 Summary

Wind tunnel studies of FIU series house models show that the peak negative pressure coefficients on roof corner areas measured in a suburban terrain exposure setting exceed the corresponding peak negative pressure coefficients measured in a open country exposure setting. The current wind load design code uses one set of pressure coefficients that is historically determined assuming an “open country” wind exposure. It is non-conservative to design wind load on roof corner areas of low-rise buildings located at suburban exposure with this set of coefficients.

In general, surrounding houses can decrease the wind load on buildings. However, wind tunnel studies of FIU series models show that wind pressures on roof corner areas have a tendency to be enlarged under the medium density of surrounding houses. ASCE 7 does not take into account the effect of surrounding structures. This approach has been found to be non-conservative for the determination of design wind load on critical roof corner areas of buildings which are located in a medium density of surroundings.

CHAPTER 8

CONCLUSIONS AND RECOMMENDATIONS

In this dissertation, the hurricane extreme wind loads on a residential house, House FL-27, were investigated though full-scale pressure measurements during tropical cyclone events and tests in a boundary layer wind tunnel. The analysis of high resolution data collected during Tropical Strom Isidore (2002) and Hurricane Ivan (2004) have provided pressure coefficients at critical roof corner areas of House FL-27 that were compared with wind tunnel test values. Results of both full-scale and wind tunnel tests were also compared with ASCE 7 wind design provisions. Specific conclusions can be made as follows:

8.1 Conclusion

- The House Instrumentation System of the Florida Coastal Monitoring Program successfully recorded high-resolution wind pressures on House FL-27 from Tropical Storm Isidore (2002) and Hurricane Ivan (2004). The uncertainty of the measurement results of the House Instrumentation System associated with reference pressures, temperature variations, and calibration errors is less than +/- 2.7 psf with a confidence interval of 95% for full-scale records during Hurricane Ivan. This indicates that the House Instrumentation System captures and records hurricane wind load behaviors on prototype buildings with reasonable accuracy.
- Wind tunnel tests for the House FL-27 model show strong agreement between wind tunnel and full-scale data when comparing means, positive peak and

standard deviations of pressure coefficients. Wind tunnel simulation tests underestimate the peak negative pressure coefficients, although the comparisons indicate that the wind tunnel simulation methods can generally reproduce the extreme wind loads measured in full-scale tests of House FL-27.

- Equation (5-9c) effectively represents the negative part of the measured probability density function (PDF) of wind pressure measured in full-scale tests. The comparison of the PDF of wind pressures from full-scale and wind tunnel tests show that the full-scale data exhibits a more skewed distribution and some differences in the tail of the associated probability density functions compared with the wind tunnel data. This can be used to explain the phenomenon that the wind tunnel tests underestimate the negative peak pressure coefficients from full-scale tests.
- Investigation of spatial and time-averaged effects on peak pressures shows peak wind loads generally decrease with an increasing averaging period. The negative peak wind pressure at a single point can occur for 1 second. An area-averaged negative peak wind pressure can occur for 0.2 seconds at a roof corner area. The area-averaged negative peak pressure coefficient for an area is less than the corresponding negative peak pressure coefficients of individual channels within this area. However, the effect of area-averaging on negative peak wind loads can be neglected when the averaging period T exceeds 1 second.
- Comparisons of full-scale and wind tunnel results with ASCE 7-05 wind design provisions show that the pressure coefficients measured in full-scale and wind tunnel test of House FL-27 have exceeded ASCE 7-05 wind design provisions.

These results indicate that ASCE 7 wind design code underestimates wind pressures occurring at roof corner areas.

- Wind tunnel tests on House FL-27 and the FIU-series house models show that the negative pressure coefficients on the roof corner areas, which are measured under the suburban terrain condition, on average exceed the corresponding results measured under the open country exposure by 6 percent. These indicate that one set of pressure coefficients used in ASCE 7 is non-conservative when calculating the negative C&C wind loads on roof corners and positive C&C wind loads on the whole house roof which is located in a suburban terrain.
- Wind tunnel studies for FIU series models show that wind pressure coefficients on roof corner areas are increased under the sparse and medium density of surrounding houses. If the effect of surrounding houses is neglected, then the effect of wind loads on roof corner areas of buildings which are located in surroundings of medium density will be underestimated.

8.2 Recommendations for Future Research

This study suggests the following areas where continued investigation should be pursued:

- Analysis and investigation of lateral turbulence scale on wind loads based on full-scale tests;
- More detailed comparisons of probability density function of models with full-scale test results;

- More detailed comparisons of area averaging effects on wind loads measured by model and full-scale tests;
- Increased turbulence intensity of flow simulation more than 30% to effectively reproduce the peak negative wind loads in wind tunnel testing;
- Investigation of effects of lateral turbulence intensity on simulating peak wind loads measured from full-scale tests.

APPENDICES

Appendix A

Lists of 15-minute Records of House FL-27 Full-scale Tests during Tropical Storm Isidore (2002) and Hurricane Ivan (2004)

Tropical Storm Isidore		Hurricane Ivan	
House Record Number	Start Time	House Record Number	Start Time
1	9-25-2002 21:45:20	15	9-14-2004 23:36:32
2	9-25-2002 22:00:31	16	9-14-2004 23:51:41
3	9-25-2002 22:15:41	17	9-15-2004 00:06:49
4	9-25-2002 22:30:52	18	9-15-2004 00:21:58
5	9-25-2002 22:46:04	19	9-15-2004 00:37:06
6	9-25-2002 23:01:14	20	9-15-2004 00:52:15
7	9-25-2002 23:16:25	21	9-15-2004 01:07:23
8	9-25-2002 23:31:36	22	9-15-2004 01:22:31
9	9-25-2002 23:46:46	23	9-15-2004 01:37:40
10	9-26-2002 00:01:57	24	9-15-2004 01:52:48
11	9-26-2002 00:17:08	25	9-15-2004 02:07:57
12	9-26-2002 00:32:19	26	9-15-2004 02:23:05
13	9-26-2002 00:47:29	27	9-15-2004 02:38:14
14	9-26-2002 01:02:40	28	9-15-2004 02:53:22
15	9-26-2002 01:17:52	29	9-15-2004 03:08:31
16	9-26-2002 01:33:03	30	9-15-2004 03:23:39
17	9-26-2002 01:48:13	31	9-15-2004 03:38:48
18	9-26-2002 02:03:24	32	9-15-2004 03:53:56
19	9-26-2002 02:18:35	33	9-15-2004 04:09:04
20	9-26-2002 02:33:46	34	9-15-2004 04:24:13
21	9-26-2002 02:48:57	35	9-15-2004 04:39:21
22	9-26-2002 03:04:08	36	9-15-2004 04:54:30
23	9-26-2002 03:19:19	37	9-15-2004 05:09:38
24	9-26-2002 03:34:29	38	9-15-2004 05:24:47
25	9-26-2002 03:49:41	39	9-15-2004 05:39:55
26	9-26-2002 04:04:51	40	9-15-2004 05:55:04
27	9-26-2002 04:20:02	41	9-15-2004 06:10:12
28	9-26-2002 04:35:13	42	9-15-2004 06:25:21
29	9-26-2002 04:50:24	43	9-15-2004 06:40:29
30	9-26-2002 05:05:34	44	9-15-2004 06:55:37

Tropical Storm Isidore		Hurricane Ivan	
House Record Number	Start Time	House Record Number	Start Time
31	9-26-2002 05:20:45	45	9-15-2004 07:10:46
32	9-26-2002 05:35:56	46	9-15-2004 07:25:54
33	9-26-2002 05:51:07	47	9-15-2004 07:41:03
34	9-26-2002 06:06:18	48	9-15-2004 07:56:11
35	9-26-2002 06:21:29	49	9-15-2004 08:11:20
36	9-26-2002 06:36:40	50	9-15-2004 08:26:28
37	9-26-2002 06:51:51	51	9-15-2004 08:41:37
38	9-26-2002 07:07:02	52	9-15-2004 08:56:45
39	9-26-2002 07:22:13	53	9-15-2004 09:11:53
40	9-26-2002 07:37:24	54	9-15-2004 09:27:02
41	9-26-2002 07:52:35	55	9-15-2004 09:42:10
42	9-26-2002 08:07:46	56	9-15-2004 09:57:19
43	9-26-2002 08:22:57	57	9-15-2004 10:12:27
44	9-26-2002 08:38:09	58	9-15-2004 10:27:36
45	9-26-2002 08:53:19	59	9-15-2004 10:42:44
46	9-26-2002 09:08:31	60	9-15-2004 10:57:52
47	9-26-2002 09:23:41	61	9-15-2004 11:13:01
48	9-26-2002 09:38:52	62	9-15-2004 11:28:09
49	9-26-2002 09:54:03	63	9-15-2004 11:43:18
50	9-26-2002 10:09:14	64	9-15-2004 11:58:26
51	9-26-2002 10:24:25	65	9-15-2004 12:13:35
52	9-26-2002 10:39:36	66	9-15-2004 12:28:43
53	9-26-2002 10:54:47	67	9-15-2004 12:43:51
54	9-26-2002 11:09:58	68	9-15-2004 12:59:00
55	9-26-2002 11:25:09	69	9-15-2004 13:14:08
56	9-26-2002 11:40:20	70	9-15-2004 13:29:17
57	9-26-2002 11:55:30	71	9-15-2004 13:44:25
58	9-26-2002 12:10:41	72	9-15-2004 13:59:34
59	9-26-2002 12:25:52	73	9-15-2004 14:14:42
60	9-26-2002 12:41:03	74	9-15-2004 14:29:51
61	9-26-2002 12:56:14	75	9-15-2004 14:44:59
62	9-26-2002 13:11:25	76	9-15-2004 15:00:07
63	9-26-2002 13:26:36	77	9-15-2004 15:15:16
64	9-26-2002 13:41:47	78	9-15-2004 15:30:24
65	9-26-2002 13:56:58	79	9-15-2004 15:45:33
66	9-26-2002 14:12:09	80	9-15-2004 16:00:41
67	9-26-2002 14:27:20	81	9-15-2004 16:15:49

Tropical Storm Isidore		Hurricane Ivan	
House Record Number	Start Time	House Record Number	Start Time
68	9-26-2002 14:42:30	82	9-15-2004 16:30:58
69	9-26-2002 14:57:41	83	9-15-2004 16:46:06
70	9-26-2002 15:12:52	84	9-15-2004 17:01:15
71	9-26-2002 15:28:03	85	9-15-2004 17:16:23
72	9-26-2002 15:43:15	86	9-15-2004 17:31:32
73	9-26-2002 15:58:26	87	9-15-2004 17:46:40
74	9-26-2002 16:13:37	88	9-15-2004 18:01:48
75	9-26-2002 16:28:48	89	9-15-2004 18:16:57
76	9-26-2002 16:43:58	90	9-15-2004 18:32:05
77	9-26-2002 16:59:09	91	9-15-2004 18:47:13
78	9-26-2002 17:14:20	92	9-15-2004 19:02:22
79	9-26-2002 17:29:30	93	9-15-2004 19:17:30
80	9-26-2002 17:44:41	94	9-15-2004 19:32:38
81	9-26-2002 17:59:52	95	9-15-2004 19:47:47
82	9-26-2002 18:15:04	96	9-15-2004 20:02:55
83	9-26-2002 18:30:15	97	9-15-2004 20:18:03
84	9-26-2002 18:45:26	98	9-15-2004 20:33:11
85	9-26-2002 19:00:36	99	9-15-2004 20:48:20
86	9-26-2002 19:15:47	100	9-15-2004 21:03:28
87	9-26-2002 19:30:58	101	9-15-2004 21:18:36
88	9-26-2002 19:46:09	102	9-15-2004 21:33:45
89	9-26-2002 20:01:20	103	9-15-2004 21:48:53
90	9-26-2002 20:16:30	104	9-15-2004 22:04:02
91	9-26-2002 20:31:42	105	9-15-2004 22:19:10
92	9-26-2002 20:46:53	106	9-15-2004 22:34:18
93	9-26-2002 21:02:03	107	9-15-2004 22:49:27
94	9-26-2002 21:17:14	108	9-15-2004 23:04:35
95	9-26-2002 21:32:25	109	9-15-2004 23:19:44
96	9-26-2002 21:47:36	110	9-15-2004 23:34:52
97	9-26-2002 22:02:47	111	9-15-2004 23:50:00
98	9-26-2002 22:17:58	112	9-16-2004 00:05:09
99	9-26-2002 22:33:09	113	9-16-2004 00:20:17
100	9-26-2002 22:48:19	114	9-16-2004 00:35:25
101	9-26-2002 23:03:30	115	9-16-2004 00:50:34
102	9-26-2002 23:18:41	116	9-16-2004 01:05:42
103	9-26-2002 23:33:52	117	9-16-2004 01:20:50
104	9-26-2002 23:49:03	118	9-16-2004 01:35:59

Tropical Storm Isidore		Hurricane Ivan	
House Record Number	Start Time	House Record Number	Start Time
105	9-27-2002 00:04:14	119	9-16-2004 01:51:07
106	9-27-2002 00:19:25	120	9-16-2004 02:06:15
107	9-27-2002 00:34:36	121	9-16-2004 02:21:24
108	9-27-2002 00:49:47	122	9-16-2004 02:36:32
109	9-27-2002 01:04:58	123	9-16-2004 02:51:41
110	9-27-2002 01:20:09	124	9-16-2004 03:06:49
111	9-27-2002 01:35:20	125	9-16-2004 03:21:57
112	9-27-2002 01:50:31	126	9-16-2004 03:37:06
113	9-27-2002 02:05:42	127	9-16-2004 03:52:14
114	9-27-2002 02:20:53	128	9-16-2004 04:07:22
115	9-27-2002 02:36:03	129	9-16-2004 04:22:31
116	9-27-2002 02:51:15	130	9-16-2004 04:37:39
117	9-27-2002 03:06:26	131	9-16-2004 04:52:48
118	9-27-2002 03:21:37	132	9-16-2004 05:07:56
119	9-27-2002 03:36:47	133	9-16-2004 05:23:04
120	9-27-2002 03:51:58	134	9-16-2004 05:38:13
121	9-27-2002 04:07:10	135	9-16-2004 05:53:21
122	9-27-2002 04:22:20	136	9-16-2004 06:08:29
123	9-27-2002 04:37:31	137	9-16-2004 06:23:38
124	9-27-2002 04:52:42	138	9-16-2004 06:38:46
125	9-27-2002 05:07:53	139	9-16-2004 06:53:55
126	9-27-2002 05:23:04	140	9-16-2004 07:09:03
127	9-27-2002 05:38:14	141	9-16-2004 07:24:12
128	9-27-2002 05:53:25	142	9-16-2004 07:39:21
129	9-27-2002 06:08:36	143	9-16-2004 07:54:29
130	9-27-2002 06:23:47	144	9-16-2004 08:09:37
131	9-27-2002 06:38:57	145	9-16-2004 08:24:46
132	9-27-2002 06:54:09	146	9-16-2004 08:39:54
133	9-27-2002 07:09:20	147	9-16-2004 08:55:03
134	9-27-2002 07:24:31	148	9-16-2004 09:10:11
135	9-27-2002 07:39:42	149	9-16-2004 09:25:20
136	9-27-2002 07:54:53	150	9-16-2004 09:40:28
137	9-27-2002 08:10:04	151	9-16-2004 09:55:37
138	9-27-2002 08:25:15	152	9-16-2004 10:10:45
139	9-27-2002 08:40:26	153	9-16-2004 10:25:53
140	9-27-2002 08:55:37	154	9-16-2004 10:41:02
141	9-27-2002 09:10:48	155	9-16-2004 10:56:10

Tropical Storm Isidore		Hurricane Ivan	
House Record Number	Start Time	House Record Number	Start Time
142	9-27-2002 09:25:59	156	9-16-2004 11:11:19
143	9-27-2002 09:41:10	157	9-16-2004 11:26:28
144	9-27-2002 09:56:20	158	9-16-2004 11:41:36
145	9-27-2002 10:11:31	159	9-16-2004 11:56:44
146	9-27-2002 10:26:42	160	9-16-2004 12:11:53
147	9-27-2002 10:41:53	161	9-16-2004 12:27:01
148	9-27-2002 10:57:04	162	9-16-2004 12:42:10
149	9-27-2002 11:12:15	163	9-16-2004 12:57:18
150	9-27-2002 11:27:26	164	9-16-2004 13:12:27
151	9-27-2002 11:42:36	165	9-16-2004 13:27:35
152	9-27-2002 11:57:47	166	9-16-2004 13:42:44
153	9-27-2002 12:12:58	167	9-16-2004 13:57:52
154	9-27-2002 12:28:09	168	9-16-2004 14:13:01
155	9-27-2002 12:43:20	169	9-16-2004 14:28:09
156	9-27-2002 12:58:30	170	9-16-2004 14:43:18
157	9-27-2002 13:13:41	171	9-16-2004 14:58:26
158	9-27-2002 13:28:52	172	9-16-2004 15:13:35
159	9-27-2002 13:44:03	173	9-16-2004 15:28:43
160	9-27-2002 13:59:14	174	9-16-2004 15:43:52
161	9-27-2002 14:14:25	175	9-16-2004 15:59:00
162	9-27-2002 14:29:36	176	9-16-2004 16:14:08
163	9-27-2002 14:44:47	177	9-16-2004 16:29:17
164	9-27-2002 14:59:58	178	9-16-2004 16:44:25
165	9-27-2002 15:15:09	179	9-16-2004 16:59:33
		180	9-16-2004 17:14:42
		181	9-16-2004 17:29:50
		182	9-16-2004 17:44:59
		183	9-16-2004 18:00:07
		184	9-16-2004 18:15:15
		185	9-16-2004 18:30:24
		186	9-16-2004 18:45:33
		187	9-16-2004 19:00:41
		188	9-16-2004 19:15:49
		189	9-16-2004 19:30:58
		190	9-16-2004 19:46:06

Appendix B

Source Program for Analyzing Full-scale Records of the House Instrumentation System (10Hz Down-Sampling Records)

```
clear all
format compact;
filename = ['SensorCalibration.txt'];
fid = fopen(filename,'r');
del = fscanf(fid,'%c',19);
TempVal = fscanf(fid,'%f');
L = length(TempVal);
SensorNumber = TempVal(1:2:(L-1));
SensitivityFactors = TempVal(2:2:L);
fclose(fid);
DeltaTemp = House_Temperature_F(13:188);
DeltaTemp = DeltaTemp-DeltaTemp(1);
DeltaPressure_Tower = House_RefPressure_PSF(13:188);
DeltaPressure_Tower = DeltaPressure_Tower - DeltaPressure_Tower(1);
WDirection_10m = Direction_10m(13:188);
Time_Stamp = Time_Stamp(13:188);
Prefixion = ['Ivan_2004_Hubbard_10Hz_'];
load('Ivan_2004_Hubbard_10Hz_015.mat');
ch_0_PreStorm_Mean = mean(pressure);
Channel_RefMean(1) = mean(ch_01);
Channel_RefMean(2) = mean(ch_02);
Channel_RefMean(3) = mean(ch_03);
Channel_RefMean(4) = mean(ch_04);
Channel_RefMean(5) = mean(ch_05);
Channel_RefMean(6) = mean(ch_06);
Channel_RefMean(7) = mean(ch_07);
Channel_RefMean(8) = mean(ch_08);
Channel_RefMean(9) = mean(ch_09);
Channel_RefMean(10) = mean(ch_10);
Channel_RefMean(11) = mean(ch_11);
```

```
Channel_RefMean(12) = mean(ch_12);
Channel_RefMean(13) = mean(ch_13);
Channel_RefMean(14) = mean(ch_14);
Channel_RefMean(15) = mean(ch_15);
Channel_RefMean(16) = mean(ch_16);
Channel_RefMean(17) = mean(ch_17);
Channel_RefMean(18) = mean(ch_18);
Channel_RefMean(19) = mean(ch_19);
Channel_RefMean(20) = mean(ch_20);
Channel_RefMean(21) = mean(ch_21);
Channel_RefMean(22) = mean(ch_22);
Channel_RefMean(23) = mean(ch_23);
Channel_RefMean(24) = mean(ch_24);
Channel_RefMean(25) = mean(ch_25);
Channel_RefMean(26) = mean(ch_26);
Channel_RefMean(27) = mean(ch_27);
Channel_RefMean(28) = mean(ch_28);
for i = 135:140;
   disp(i);
   FileNumber = num2str(i);
   FileName = [Prefixion, FileNumber,'.mat'];
   load(FileName);
   Meanspeed(i-124) = mean(speed_1);
   GustSpeed(i-124) = Meanspeed(i-124)*2.126;

   Ch_0 = mean(pressure)-ch_0_PreStorm_Mean;
   ch_0_Temp=Ch_0*SensitivityFactors(1)+DeltaTemp(i14)*0.0144*SensitivityFactors(1)*SensitivityFact
                    ors(1)/20.6;
   ChannelTemp(:,1)=(ch_01-Channel_RefMean(1))*SensitivityFactors(2)-ch_0_Temp+DeltaTemp(i-
                    14)*0.0144*(SensitivityFactors(2)^2)/20.6;
   ChannelTemp(:,2)=(ch_02-Channel_RefMean(2))*SensitivityFactors(3)-ch_0_Temp+DeltaTemp(i-
                    14)*0.0144*(SensitivityFactors(3)^2)/20.6;
   ChannelTemp(:,3)=(ch_03-Channel_RefMean(3))*SensitivityFactors(4)-ch_0_Temp+DeltaTemp(i-
                    14)*0.0144*(SensitivityFactors(4)^2)/20.6;
   ChannelTemp(:,4)=(ch_04-Channel_RefMean(4))*SensitivityFactors(5)-ch_0_Temp+DeltaTemp(i-
                    14)*0.0144*(SensitivityFactors(5)^2)/20.6;
```

```
ChannelTemp(:,5)=(ch_04-Channel_RefMean(5))*SensitivityFactors(6)-ch_0_Temp+DeltaTemp(i-
        14)*0.0144*(SensitivityFactors(6)^2)/20.6;
ChannelTemp(:,6)=(ch_06-Channel_RefMean(6))*SensitivityFactors(7)-ch_0_Temp+DeltaTemp(i-
        14)*0.0144*(SensitivityFactors(7)^2)/20.6;
ChannelTemp(:,7)=(ch_07-Channel_RefMean(7))*SensitivityFactors(8)-ch_0_Temp+DeltaTemp(i-
        14)*0.0144*(SensitivityFactors(8)^2)/20.6;
ChannelTemp(:,8)=(ch_08-Channel_RefMean(8))*SensitivityFactors(9)-ch_0_Temp+DeltaTemp(i-
        14)*0.0144*(SensitivityFactors(9)^2)/20.6;
ChannelTemp(:,9)=(ch_09-Channel_RefMean(9))*SensitivityFactors(10)-ch_0_Temp+DeltaTemp(i-
        14)*0.0144*(SensitivityFactors(10)^2)/20.6;
ChannelTemp(:,10)=(ch_10-Channel_RefMean(10))*SensitivityFactors(11)-ch_0_Temp+DeltaTemp(i-
        14)*0.0144*(SensitivityFactors(11)^2)/20.6;
ChannelTemp(:,11)=(ch_11-Channel_RefMean(11))*SensitivityFactors(12)-ch_0_Temp+DeltaTemp(i-
        14)*0.0144*(SensitivityFactors(12)^2)/20.6;
ChannelTemp(:,12)=(ch_12-Channel_RefMean(12))*SensitivityFactors(13)-ch_0_Temp+DeltaTemp(i-
        14)*0.0144*(SensitivityFactors(13)^2)/20.6;
ChannelTemp(:,13)=(ch_13-Channel_RefMean(13))*SensitivityFactors(14)-ch_0_Temp+DeltaTemp(i-
        14)*0.0144*(SensitivityFactors(14)^2)/20.6;
ChannelTemp(:,14)=(ch_14-Channel_RefMean(14))*SensitivityFactors(15)-ch_0_Temp+DeltaTemp(i-
        14)*0.0144*(SensitivityFactors(15)^2)/20.6;
ChannelTemp(:,15)=(ch_15-Channel_RefMean(15))*SensitivityFactors(16)-ch_0_Temp+DeltaTemp(i-
        14)*0.0144*(SensitivityFactors(16)^2)/20.6;
ChannelTemp(:,16)=(ch_16-Channel_RefMean(16))*SensitivityFactors(17)-ch_0_Temp+DeltaTemp(i-
        14)*0.0144*(SensitivityFactors(17)^2)/20.6;
ChannelTemp(:,17)=(ch_17-Channel_RefMean(17))*SensitivityFactors(18)-ch_0_Temp+DeltaTemp(i-
        14)*0.0144*(SensitivityFactors(18)^2)/20.6;
ChannelTemp(:,18)=(ch_18-Channel_RefMean(18))*SensitivityFactors(19)-ch_0_Temp+DeltaTemp(i-
        14)*0.0144*(SensitivityFactors(19)^2)/20.6;
ChannelTemp(:,19)=(ch_19-Channel_RefMean(19))*SensitivityFactors(20)-ch_0_Temp+DeltaTemp(i-
        14)*0.0144*(SensitivityFactors(20)^2)/20.6;
ChannelTemp(:,20)=(ch_20-Channel_RefMean(20))*SensitivityFactors(21)-ch_0_Temp+DeltaTemp(i-
        14)*0.0144*(SensitivityFactors(21)^2)/20.6;
ChannelTemp(:,21)=(ch_21-Channel_RefMean(21))*SensitivityFactors(22)-ch_0_Temp+DeltaTemp(i-
        14)*0.0144*(SensitivityFactors(22)^2)/20.6;
ChannelTemp(:,22)=(ch_22-Channel_RefMean(22))*SensitivityFactors(23)-ch_0_Temp+DeltaTemp(i-
        14)*0.0144*(SensitivityFactors(23)^2)/20.6;
```

```
    ChannelTemp(:,23)=(ch_23-Channel_RefMean(23))*SensitivityFactors(24)-ch_0_Temp+DeltaTemp(i-
                    14)*0.0144*(SensitivityFactors(24)^2)/20.6;
    ChannelTemp(:,24)=(ch_24-Channel_RefMean(24))*SensitivityFactors(25)-ch_0_Temp+DeltaTemp(i-
                    14)*0.0144*(SensitivityFactors(25)^2)/20.6;
    ChannelTemp(:,25)=(ch_25-Channel_RefMean(25))*SensitivityFactors(26)-ch_0_Temp+DeltaTemp(i-
                    14)*0.0144*(SensitivityFactors(26)^2)/20.6;
    ChannelTemp(:,26)=(ch_26-Channel_RefMean(26))*SensitivityFactors(27)-ch_0_Temp+DeltaTemp(i-
                    14)*0.0144*(SensitivityFactors(27)^2)/20.6;
    ChannelTemp(:,27)=(ch_27-Channel_RefMean(27))*SensitivityFactors(28)-ch_0_Temp+DeltaTemp(i-
                    14)*0.0144*(SensitivityFactors(28)^2)/20.6;
    ChannelTemp(:,28)=(ch_28-Channel_RefMean(28))*SensitivityFactors(29)-ch_0_Temp+DeltaTemp(i-
    MinCp10Hz((i-124),:) = min(ChannelTemp)/(0.00256*GustSpeed(i-124)^2);
    MeanCp10Hz((i-124),:) = mean(ChannelTemp)/(0.00256*GustSpeed(i-124)^2);
    MaxCp10Hz((i-124),:) = max(ChannelTemp)/(0.00256*GustSpeed(i-124)^2);
    stdCp10Hz((i-124),:) = std(ChannelTemp/((0.00256*GustSpeed(i-124)^2)));
    clear ch_0_Temp ChannelTemp
end

WorstNegativeCp(:,1) = min(MinCp10Hz);
WorstPositiveCp(:,1) = max(MaxCp10Hz);
save('House_Cp_10Hz_Luis','MinCp10Hz','MeanCp10Hz','MaxCp10Hz','stdCp10Hz')
```

Appendix C

Uncertainty Analysis of the Wind Loads Measured Hurricane Ivan

Table C.1 Simulated Mean Values and Standard Deviations of Peak Negative Wind Pressure Measured in Hurricane Ivan Considering the Effects of Random Variables. (Unit: psf)

House Record	Channel 2		Channel 3		Channel 6	
	$E(\cdot)$	σ	$E(\cdot)$	σ	$E(\cdot)$	σ
No.135	-22.26	1.05	-15.96	1.13	-35.85	1.28
No.136	-23.25	1.08	-22.21	1.19	-27.73	1.24
No.137	-22.52	1.10	-11.92	1.15	-34.20	1.31
No.138	-21.06	1.10	-17.76	1.20	-26.84	1.27
No.139	-19.34	1.11	-16.32	1.20	-30.08	1.30
No.140	-17.98	1.11	-12.33	1.18	-22.70	1.25
The Range of σ	1.05 ~1.11		1.13 ~ 1.20		1.24 ~ 1.31	
House Record	Channel 7		Channel 9		Channel 10	
	$E(\cdot)$	σ	$E(\cdot)$	σ	$E(\cdot)$	σ
No.135	-31.01	1.26	-18.26	1.17	-27.34	1.23
No.136	-20.33	1.19	-15.95	1.18	-17.66	1.16
No.137	-34.61	1.33	-29.02	1.28	-19.22	1.20
No.138	-20.25	1.23	-17.97	1.23	-14.67	1.17
No.139	-26.58	1.29	-18.15	1.24	-17.42	1.21
No.140	-18.68	1.23	-17.70	1.24	-16.41	1.20
The Range of σ	1.26 ~ 1.33		1.17 ~ 1.28		1.16 ~ 1.25	
House Record	Channel 11		Channel 12		Channel 13	
	$E(\cdot)$	σ	$E(\cdot)$	σ	$E(\cdot)$	σ
No.135	-16.68	1.11	-11.09	1.26	-26.02	1.03
No.136	-9.12	1.07	-8.77	1.27	-26.33	1.05
No.137	-13.39	1.13	-11.97	1.32	-21.60	1.03
No.138	-8.08	1.10	-9.42	1.32	-24.40	1.07
No.139	-8.86	1.12	-9.27	1.33	-23.29	1.07
No.140	-8.61	1.12	-7.96	1.32	-17.63	1.02
The Range of σ	1.10~ 1.15		1.26 ~ 1.33		1.03 ~ 1.08	
House Record	Channel 15		Channel 16		Channel 17	
	$E(\cdot)$	σ	$E(\cdot)$	σ	$E(\cdot)$	σ
No.135	-24.65	1.17	-16.27	1.08	-17.25	0.83
No.136	-22.92	1.17	-17.30	1.11	-7.33	0.79
No.137	-24.53	1.21	-18.12	1.14	-9.30	0.82
No.138	-19.73	1.19	-17.16	1.14	-7.40	0.82
No.139	-22.50	1.22	-21.28	1.19	-9.85	0.84

No.140	-14.53	1.16	-19.42	1.17	-17.96	0.89
The Range of σ	1.17 ~ 1.22		1.08~ 1.19		0.83 ~ 0.84	
House Record	Channel 18		Channel 19		Channel 20	
	$E(\cdot)$	σ	$E(\cdot)$	σ	$E(\cdot)$	σ
No.135	-14.21	1.03	-21.21	1.09	-12.02	1.18
No.136	-12.90	1.04	-7.37	1.02	-8.14	1.18
No.137	-16.67	1.08	-9.30	1.06	-12.69	1.23
No.138	-21.04	1.10	-12.15	1.09	-8.79	1.22
No.139	-18.42	1.11	-8.64	1.08	-9.91	1.24
No.140	-18.87	1.11	-5.61	1.06	-9.03	1.24
The Range of σ	1.03 ~ 1.11		1.02 ~ 1.09		1.18 ~ 1.25	
House Record	Channel 21		Channel 22		Channel 23	
	$E(\cdot)$	σ	$E(\cdot)$	σ	$E(\cdot)$	σ
No.135	-10.53	1.16	-18.15	1.12	-21.82	1.09
No.136	-8.14	1.16	-11.27	1.09	-13.84	1.07
No.137	-5.99	1.18	-16.37	1.16	-14.66	1.10
No.138	-6.87	1.20	-18.77	1.19	-11.03	1.09
No.139	-8.55	1.22	-15.59	1.18	-12.13	1.11
No.140	-7.43	1.21	-20.98	1.23	-11.79	1.11
The Range of σ	1.16 ~ 1.22		1.12 ~ 1.23		1.09 ~ 1.12	
House Record	Channel 24		Channel 28			
	$E(\cdot)$	σ	$E(\cdot)$	σ		
No.135	-18.19	1.11	-10.71	1.17		
No.136	-20.71	1.16	-13.72	1.21		
No.137	-14.01	1.13	-11.94	1.23		
No.138	-25.18	1.25	-8.86	1.23		
No.139	-16.39	1.18	-12.88	1.25		
No.140	-24.35	1.24	-9.96	1.25		
The Range of σ	1.11 ~ 1.24		1.17 ~ 1.25			

Table C.2 Simulated Mean Values and Standard Deviations of Mean Wind Pressure Measured in Hurricane Ivan Considering the Effects of Random Variables. (Unit: psf)

House Record	Channel 2		Channel 3		Channel 6	
	$E(\cdot)$	σ	$E(\cdot)$	σ	$E(\cdot)$	σ
No.135	-0.12	0.99	0.63	1.02	-2.39	1.04
No.136	-0.14	1.01	0.63	1.04	-2.39	1.06
No.137	-0.02	1.03	0.84	1.06	-2.03	1.08
No.138	-0.02	1.04	0.83	1.07	-1.78	1.09
No.139	-0.28	1.06	0.61	1.09	-2.05	1.11
No.140	-0.62	1.06	0.49	1.09	-1.82	1.10
The Range of σ	0.99 ~ 1.06		1.02 ~ 1.09		1.04 ~ 1.11	
House Record	Channel 7		Channel 9		Channel 10	
	$E(\cdot)$	σ	$E(\cdot)$	σ	$E(\cdot)$	σ
No.135	-0.86	1.03	-0.10	1.07	-1.86	1.02
No.136	-0.77	1.05	-0.14	1.09	-1.97	1.04
No.137	-0.48	1.08	-0.05	1.12	-1.99	1.06
No.138	-0.26	1.09	-0.08	1.13	-2.10	1.07
No.139	-0.50	1.10	-0.11	1.15	-2.18	1.09
No.140	-0.33	1.10	-0.10	1.15	-2.24	1.09
The Range of σ	1.03 ~ 1.10		1.07 ~1.15		1.02 ~ 1.09	
House Record	Channel 11		Channel 12		Channel 13	
	$E(\cdot)$	σ	$E(\cdot)$	σ	$E(\cdot)$	σ
No.135	0.93	0.98	0.74	1.23	-1.57	0.83
No.136	0.94	1.00	0.61	1.26	-1.62	0.85
No.137	1.09	1.02	0.55	1.29	-1.52	0.87
No.138	1.12	1.03	0.46	1.31	-1.41	0.88
No.139	0.84	1.05	0.34	1.33	-1.38	0.89
No.140	0.11	1.05	0.15	1.33	-1.11	0.88
The Range of σ	0.98 ~1.05		1.23 ~ 1.33		0.83 ~ 0.88	
House Record	Channel 15		Channel 16		Channel 17	
	$E(\cdot)$	σ	$E(\cdot)$	σ	$E(\cdot)$	σ
No.135	0.93	0.99	-0.12	0.97	0.96	0.73
No.136	0.91	1.01	-0.19	0.99	0.86	0.75
No.137	1.12	1.03	-0.05	1.01	0.97	0.76
No.138	1.20	1.05	-0.02	1.02	0.87	0.77
No.139	1.17	1.06	-0.08	1.04	0.84	0.78
No.140	1.30	1.06	-0.05	1.04	0.73	0.78
The Range of σ	0.99 ~ 1.06		0.97 ~ 1.04		0.73 ~ 0.78	
House Record	Channel 18		Channel 19		Channel 20	
	$E(\cdot)$	σ	$E(\cdot)$	σ	$E(\cdot)$	σ
No.135	-0.14	0.99	1.32	0.95	0.83	1.11
No.136	-0.19	1.01	1.33	0.97	0.79	1.13
No.137	-0.20	1.03	1.36	1.00	0.84	1.16
No.138	-0.24	1.04	1.37	1.01	0.81	1.17

No.139	-0.37	1.06	1.24	1.02	0.67	1.19
No.140	-0.55	1.06	1.16	1.02	0.56	1.19
The Range of σ	0.99 ~ 1.06		0.95 ~ 1.02		1.11 ~ 1.19	
House Record	Channel 21		Channel 22		Channel 23	
	$E(\cdot)$	σ	$E(\cdot)$	σ	$E(\cdot)$	σ
No.135	0.61	1.08	-3.15	1.17	-0.56	0.98
No.136	0.60	1.10	-3.22	1.19	-0.63	1.00
No.137	0.64	1.13	-3.37	1.22	-0.69	1.02
No.138	0.64	1.14	-3.43	1.23	-0.68	1.03
No.139	0.51	1.16	-3.62	1.25	-0.83	1.05
No.140	0.43	1.16	-3.78	1.25	-0.96	1.05
The Range of σ	1.08 ~ 1.16		1.17 ~ 1.25		0.98 ~ 1.05	
House Record	Channel 24		Channel 28			
	$E(\cdot)$	σ	$E(\cdot)$	σ		
No.135	-2.20	1.17	-4.94	1.13		
No.136	-2.30	1.19	-5.29	1.15		
No.137	-2.37	1.22	-5.12	1.18		
No.138	-2.38	1.24	-5.26	1.19		
No.139	-2.54	1.24	-5.74	1.21		
No.140	-2.63	1.25	-6.20	1.21		
The Range of σ	1.17 ~ 1.24		1.13 ~ 1.21			

Table C.3 Simulated Mean Values and Standard Deviations of Peak Positive Wind Pressure Measured in Hurricane Ivan Considering the Effects of Random Variables. (Unit: psf)

House Record	Channel 2		Channel 3		Channel 6	
	$E(\cdot)$	σ	$E(\cdot)$	σ	$E(\cdot)$	σ
No.135	9.63	0.96	11.11	0.98	9.53	0.99
No.136	10.99	0.98	11.77	0.99	10.06	1.02
No.137	9.46	1.01	8.38	1.02	8.06	1.04
No.138	8.38	1.02	8.32	1.04	6.43	1.06
No.139	10.12	1.04	10.97	1.06	10.12	1.07
No.140	6.50	1.03	7.42	1.01	4.33	1.07
The Range of σ	0.96 ~ 1.04		0.98 ~ 1.06		0.99~ 1.07	
House Record	Channel 7		Channel 9		Channel 10	
	$E(\cdot)$	σ	$E(\cdot)$	σ	$E(\cdot)$	σ
No.135	10.33	0.99	7.59	1.04	5.82	0.97
No.136	10.31	1.01	11.57	1.07	10.03	0.98
No.137	8.74	1.04	10.00	1.10	5.96	1.03
No.138	7.08	1.05	7.51	1.11	6.03	1.03
No.139	10.88	1.07	10.66	1.12	8.40	1.05
No.140	5.60	1.07	6.27	1.12	4.96	1.05
The Range of σ	0.99 ~ 1.07		1.04 ~ 1.12		0.97 ~ 1.03	
House Record	Channel 11		Channel 12		Channel 13	
	$E(\cdot)$	σ	$E(\cdot)$	σ	$E(\cdot)$	σ
No.135	7.42	0.95	11.89	1.15	9.54	0.79
No.136	11.69	0.97	11.52	1.19	9.72	0.81
No.137	8.86	1.00	11.25	1.22	5.95	0.83
No.138	8.44	1.00	9.42	1.25	7.44	0.84
No.139	10.90	1.02	9.69	1.27	7.72	0.85
No.140	7.29	1.03	8.84	1.27	5.23	0.85
Mean value of σ	0.95 ~ 1.02		1.15 ~ 1.27		0.79 ~ 0.85	
House Record	Channel 15		Channel 16		Channel 17	
	$E(\cdot)$	σ	$E(\cdot)$	σ	$E(\cdot)$	σ
No.135	10.37	0.96	9.13	0.94	12.61	0.71
No.136	11.71	0.98	11.26	0.95	11.22	0.71
No.137	8.25	1.00	7.58	0.99	8.77	0.74
No.138	8.26	1.01	7.93	1.00	9.90	0.75
No.139	10.47	1.03	9.44	1.01	10.04	0.76
No.140	6.36	1.03	5.65	1.01	8.14	0.76
The Range of σ	0.96 ~ 1.03		0.94 ~ 1.01		0.71 ~ 0.76	
House Record	Channel 18		Channel 19		Channel 20	
	$E(\cdot)$	σ	$E(\cdot)$	σ	$E(\cdot)$	σ
No.135	11.72	0.97	11.31	0.94	11.10	1.09
No.136	10.37	0.99	11.56	0.94	11.26	1.10
No.137	7.88	1.02	8.50	0.98	8.02	1.14

No.138	8.59	1.03	9.93	0.98	9.30	1.15
No.139	9.30	1.04	9.84	1.00	9.49	1.17
No.140	6.32	1.05	8.17	1.00	7.19	1.17
The Range of σ	0.97 ~ 1.04		0.94 ~ 1.00		1.09 ~ 1.17	
House Record	Channel 21		Channel 22		Channel 23	
	$E(\cdot)$	σ	$E(\cdot)$	σ	$E(\cdot)$	σ
No.135	10.87	1.06	12.13	1.17	13.58	0.96
No.136	11.13	1.07	11.63	1.20	13.69	0.97
No.137	7.71	1.09	8.92	1.22	9.51	0.99
No.138	9.40	1.11	8.56	1.25	9.76	1.02
No.139	9.64	1.13	10.50	1.25	12.03	1.02
No.140	7.64	1.14	7.27	1.25	9.69	1.02
The Range of σ	1.06 ~ 1.13		1.17 ~ 1.25		0.96 ~ 1.02	
House Record	Channel 24		Channel 28			
	$E(\cdot)$	σ	$E(\cdot)$	σ		
No.135	12.16	1.13	10.76	1.11		
No.136	11.82	1.13	10.31	1.13		
No.137	8.09	1.17	6.48	1.16		
No.138	8.68	1.21	7.61	1.17		
No.139	9.70	1.22	8.48	1.19		
No.140	7.24	1.21	5.65	1.20		
The Range of σ	1.13 ~ 1.22		1.11 ~ 1.19			

Appendix D

Measured and Predicted 15-minute PDF of Pressure coefficient of Individual Channels Measured in Hurricane Ivan

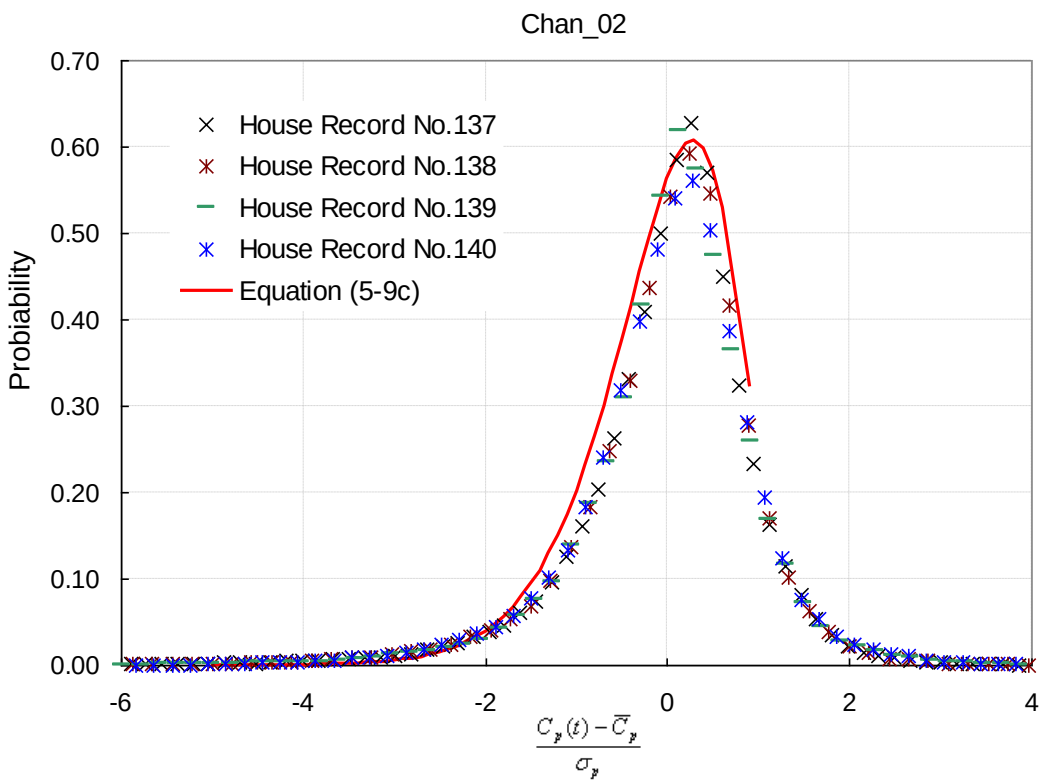

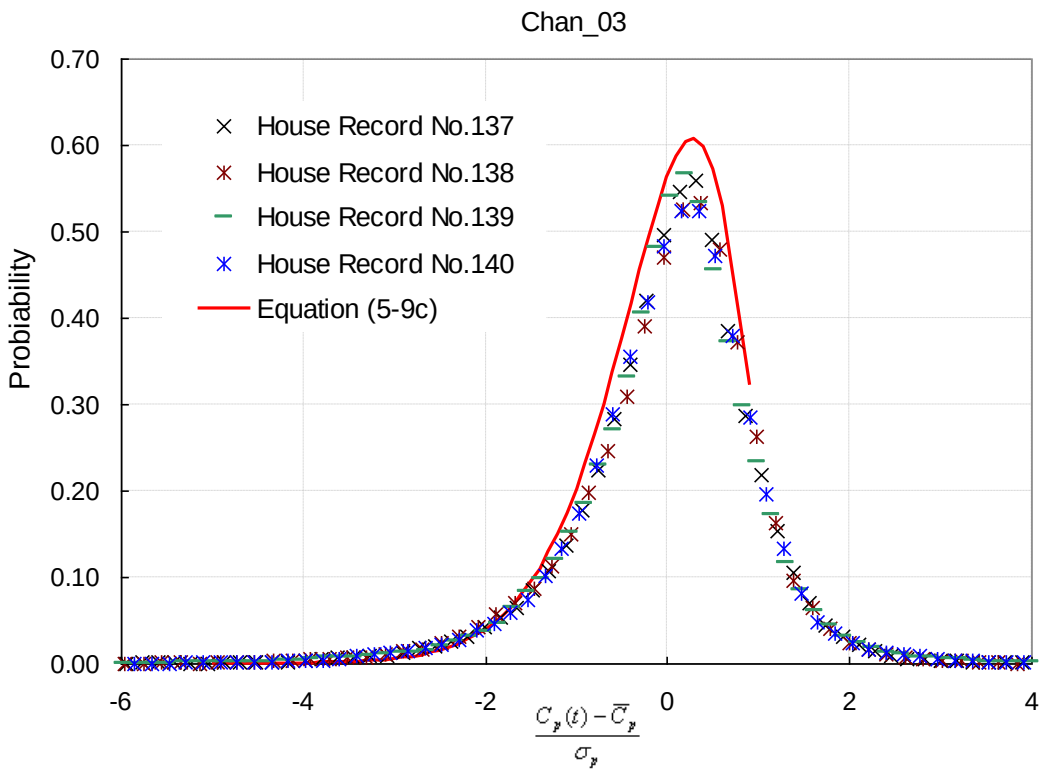
Chan_03
Probiability
0.70
0.60
0.50
0.40
0.30
0.20
0.10
0.00
-6
-4
-2
0
2
4
House Record No.137
House Record No.138
House Record No.139
House Record No.140
Equation (5-9c)
$\frac{C_p(t)-\overline{C}_p}{\sigma_p}$

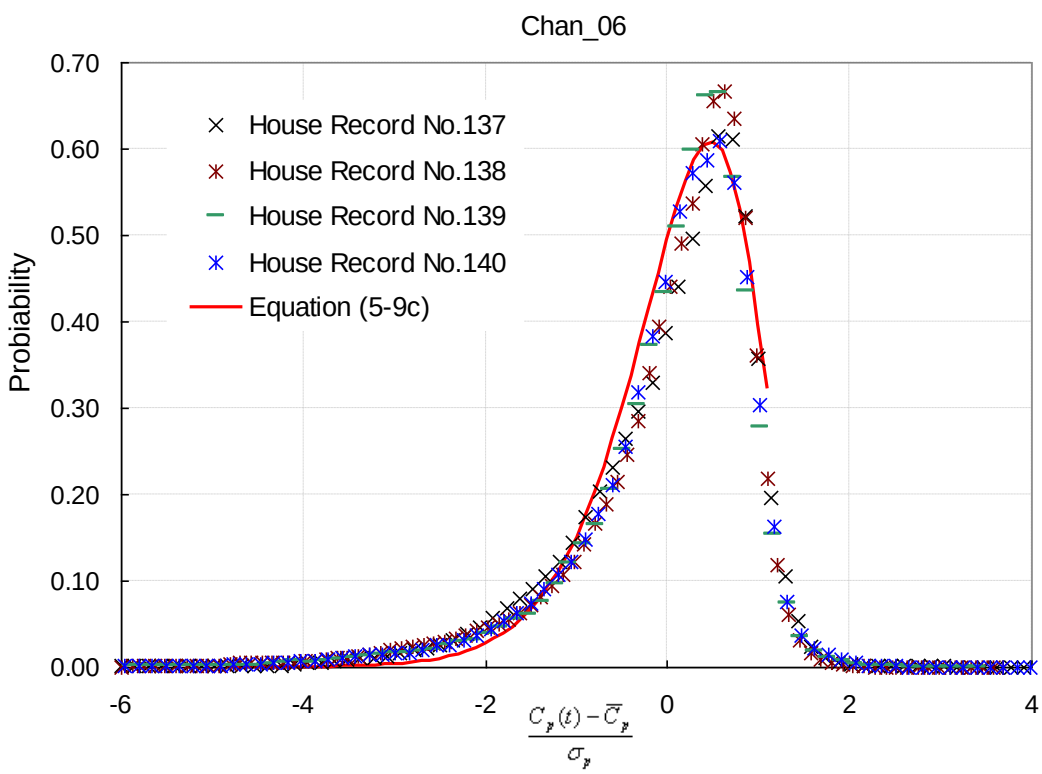
Chan_06
Probiability
0.70
0.60
0.50
0.40
0.30
0.20
0.10
0.00
-6
-4
-2
0
2
4
House Record No.137
House Record No.138
House Record No.139
House Record No.140
Equation (5-9c)
$\frac{C_p(t)-\overline{C}_p}{\sigma_p}$

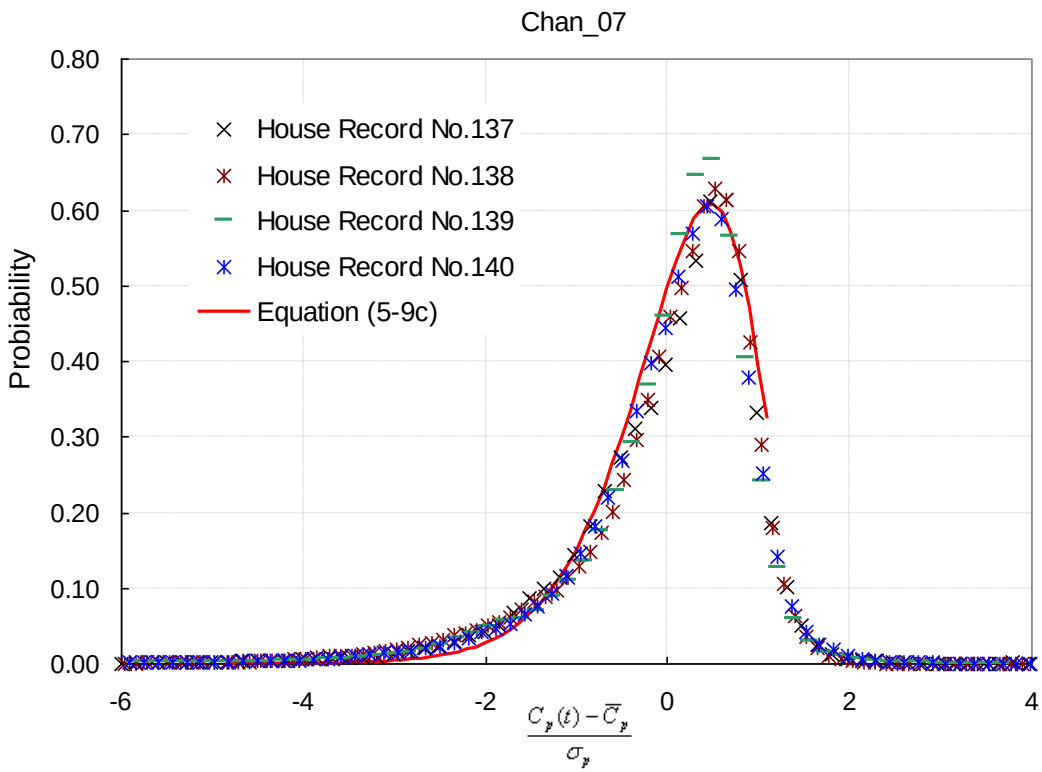
Chan_07
Probiability
0.80
0.70
0.60
0.50
0.40
0.30
0.20
0.10
0.00
-6
-4
-2
0
2
4
House Record No.137
House Record No.138
House Record No.139
House Record No.140
Equation (5-9c)
$\frac{C_p(t)-\overline{C}_p}{\sigma_p}$

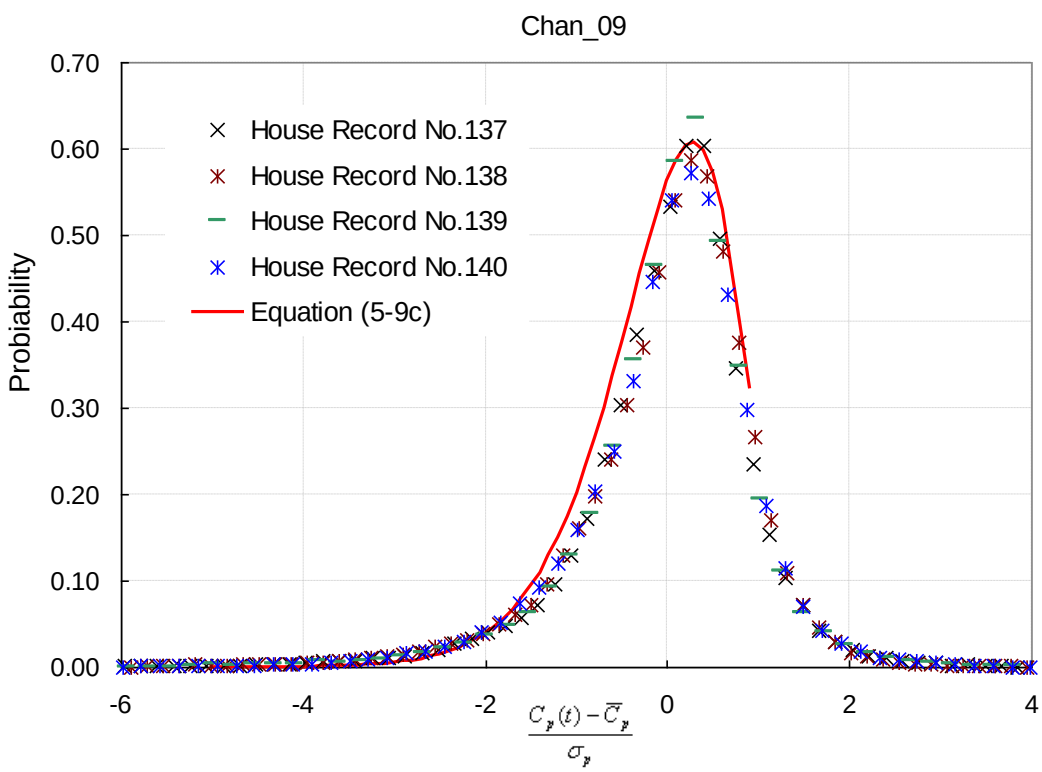
Chan_09
Probiability
0.70
0.60
0.50
0.40
0.30
0.20
0.10
0.00
-6
-4
-2
0
2
4
House Record No.137
House Record No.138
House Record No.139
House Record No.140
Equation (5-9c)
$\frac{C_p(t)-\overline{C}_p}{\sigma_p}$

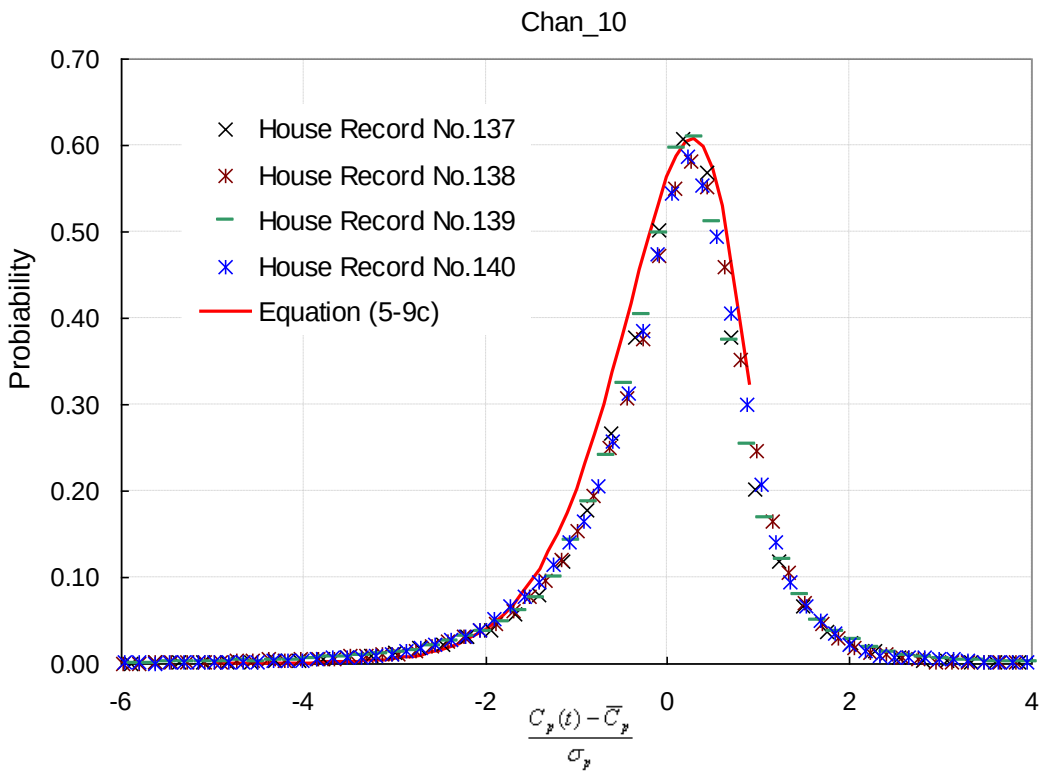
Chan_10
Probiability
0.70
0.60
0.50
0.40
0.30
0.20
0.10
0.00
-6
-4
-2
0
2
4
House Record No.137
House Record No.138
House Record No.139
House Record No.140
Equation (5-9c)
$\frac{C_p(t)-\overline{C}_p}{\sigma_p}$

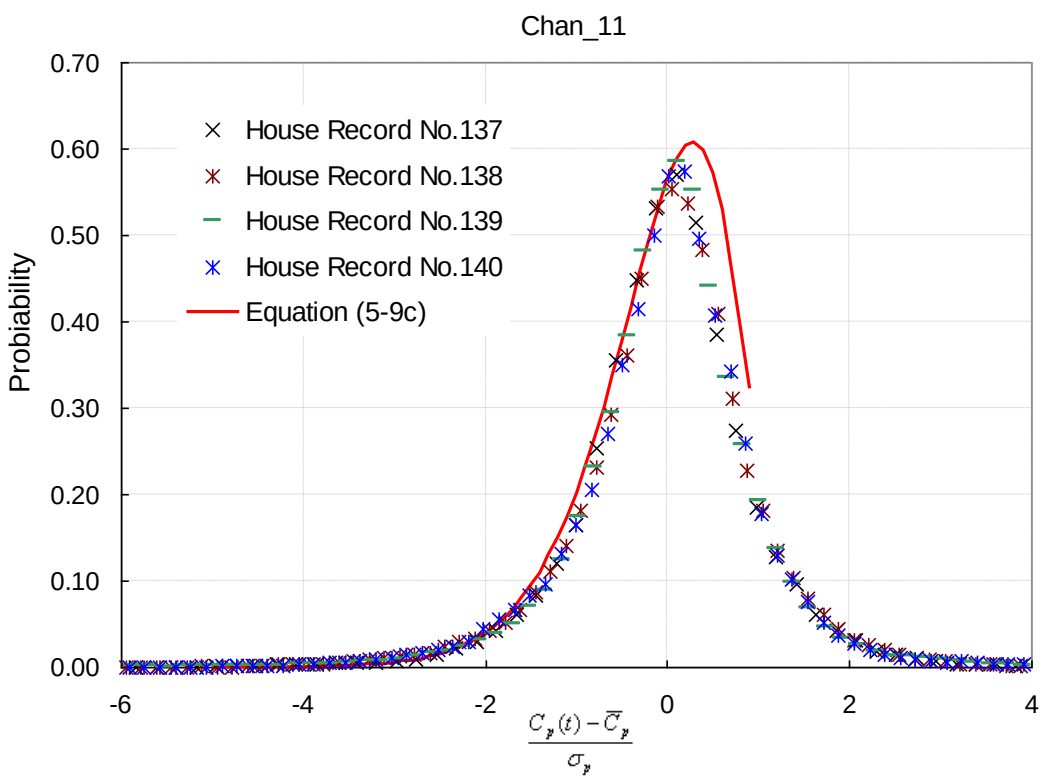
Chan_11
Probiability
0.70
0.60
0.50
0.40
0.30
0.20
0.10
0.00
-6
-4
-2
0
2
4
House Record No.137
House Record No.138
House Record No.139
House Record No.140
Equation (5-9c)
$\frac{C_p(t)-\overline{C}_p}{\sigma_p}$

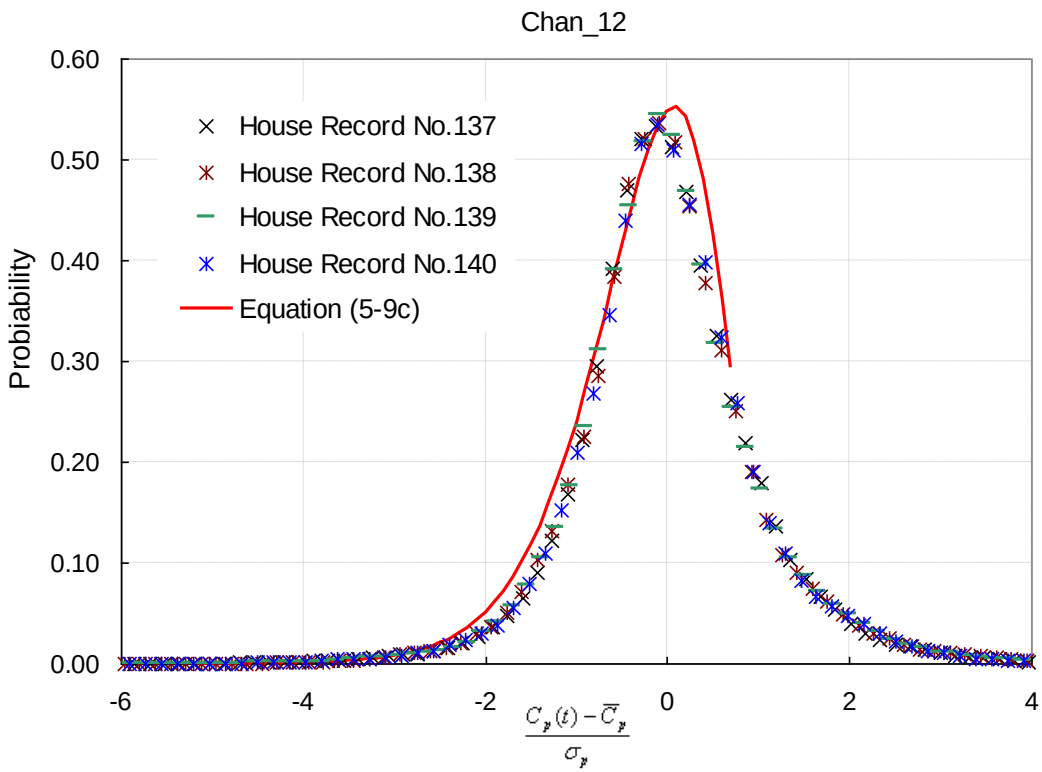
Chan_12
Probiability
0.60
0.50
0.40
0.30
0.20
0.10
0.00
-6
-4
-2
0
2
4
House Record No.137
House Record No.138
House Record No.139
House Record No.140
Equation (5-9c)
$\frac{C_y(t)-\overline{C}_y}{\sigma_y}$

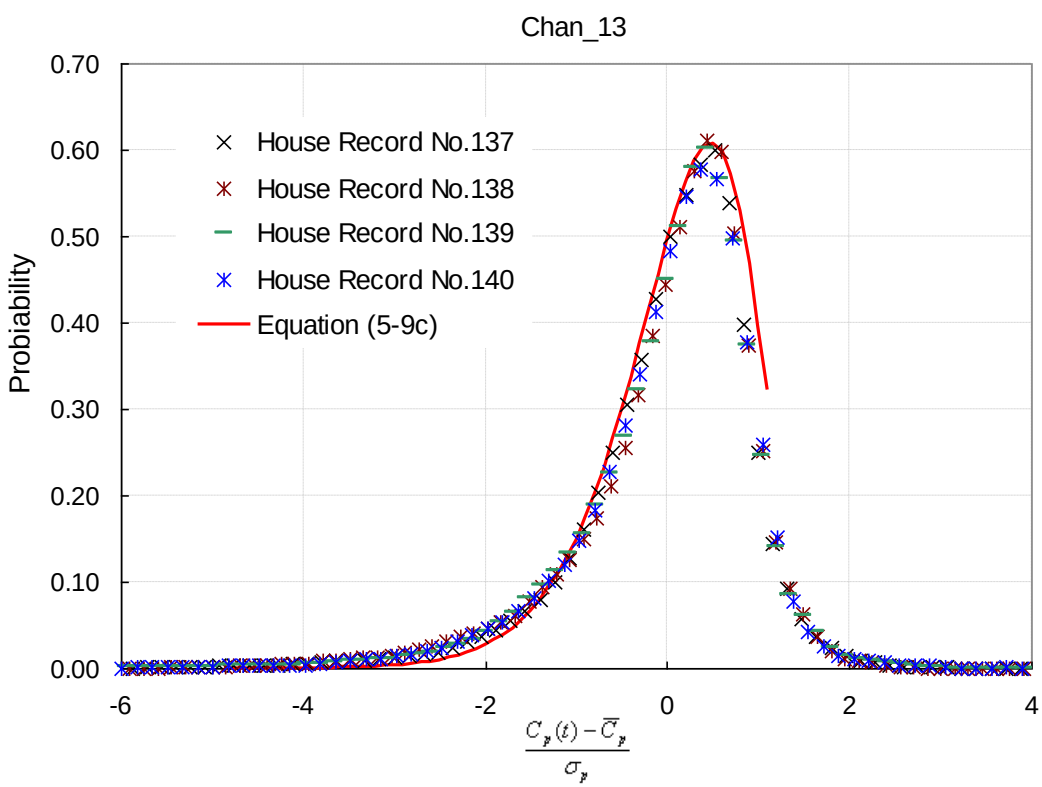
Chan_13
Probiability
0.70
0.60
0.50
0.40
0.30
0.20
0.10
0.00
-6
-4
-2
0
2
4
House Record No.137
House Record No.138
House Record No.139
House Record No.140
Equation (5-9c)
$\frac{C_y(t)-\overline{C}_y}{\sigma_y}$

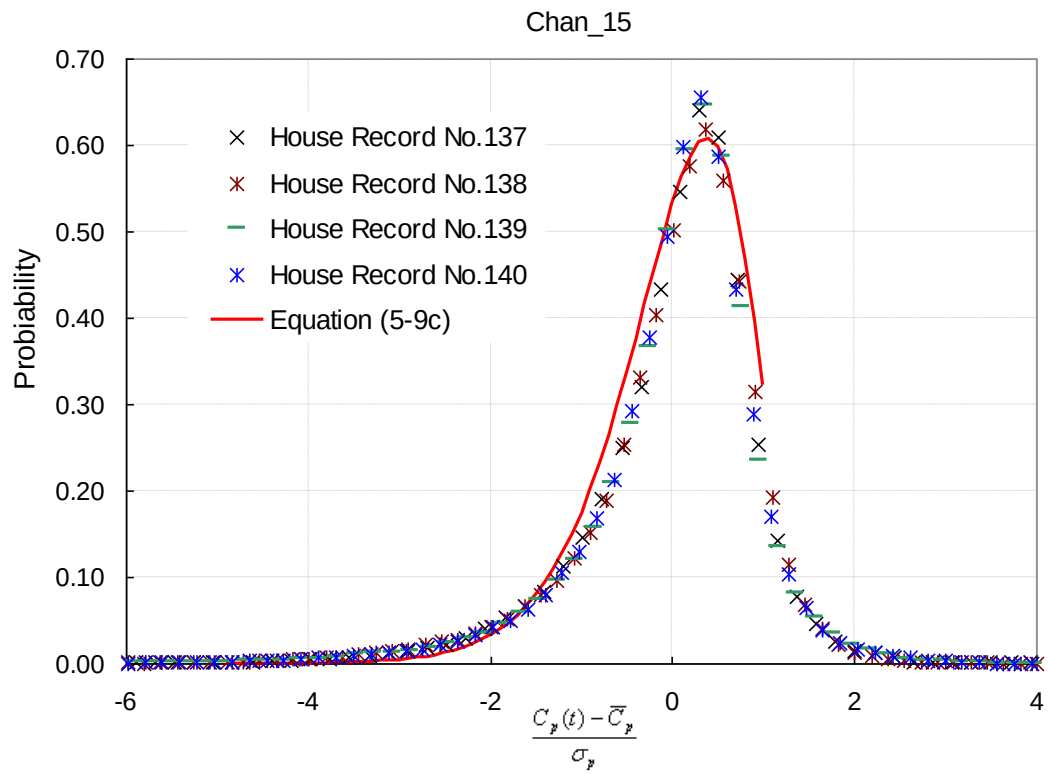
Chan_15
Probiability
0.70
0.60
0.50
0.40
0.30
0.20
0.10
0.00
-6
-4
-2
0
2
4
House Record No.137
House Record No.138
House Record No.139
House Record No.140
Equation (5-9c)
$\frac{C_p(t)-\overline{C}_p}{\sigma_p}$

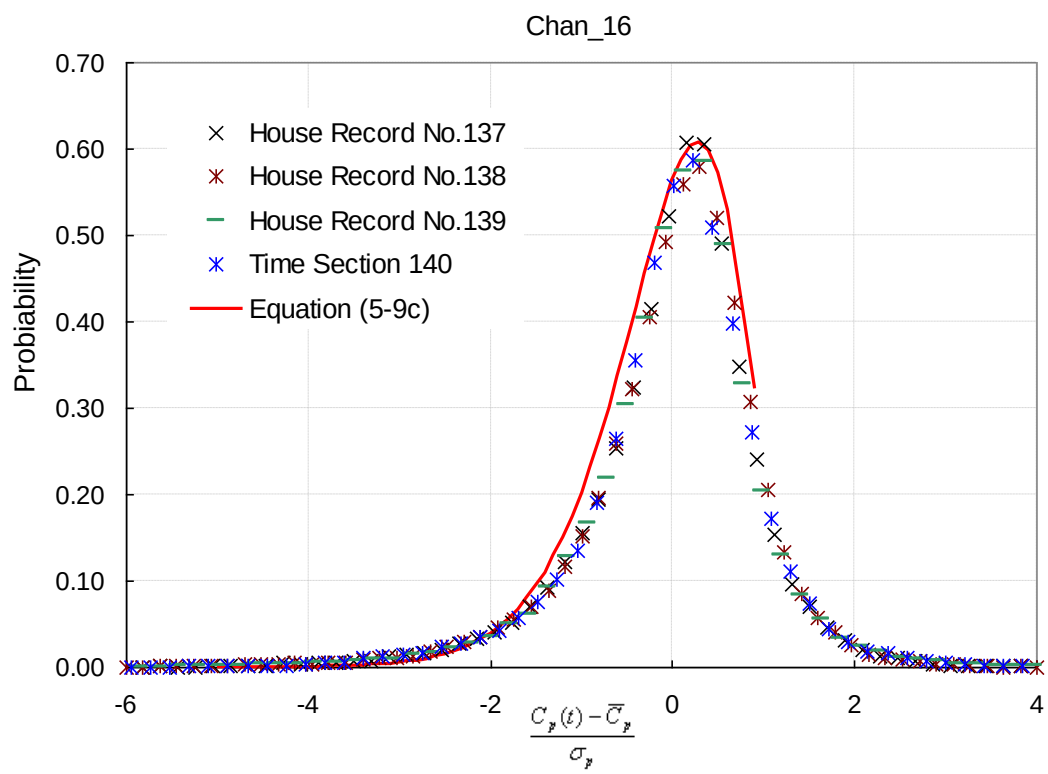
Chan_16
Probiability
0.70
0.60
0.50
0.40
0.30
0.20
0.10
0.00
-6
-4
-2
0
2
4
House Record No.137
House Record No.138
House Record No.139
Time Section 140
Equation (5-9c)
$\frac{C_p(t)-\overline{C}_p}{\sigma_p}$

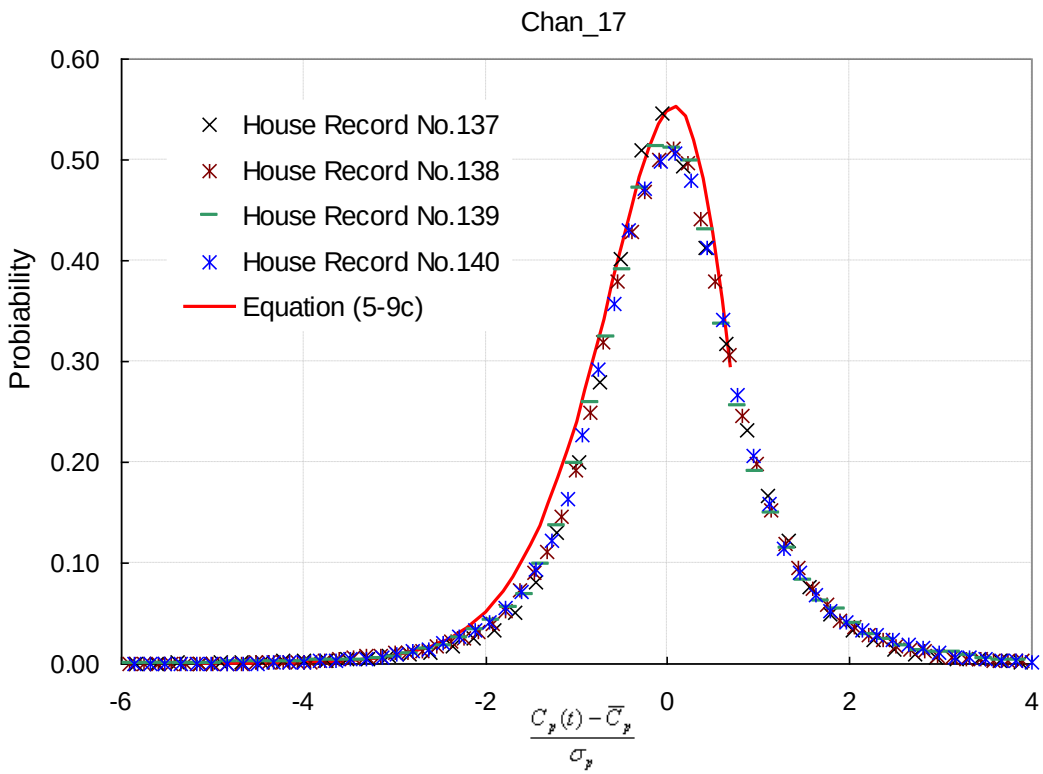
Chan_17
Probiability
0.60
0.50
0.40
0.30
0.20
0.10
0.00
-6
-4
-2
0
2
4
House Record No.137
House Record No.138
House Record No.139
House Record No.140
Equation (5-9c)
$\frac{C_p(t)-\overline{C}_p}{\sigma_p}$

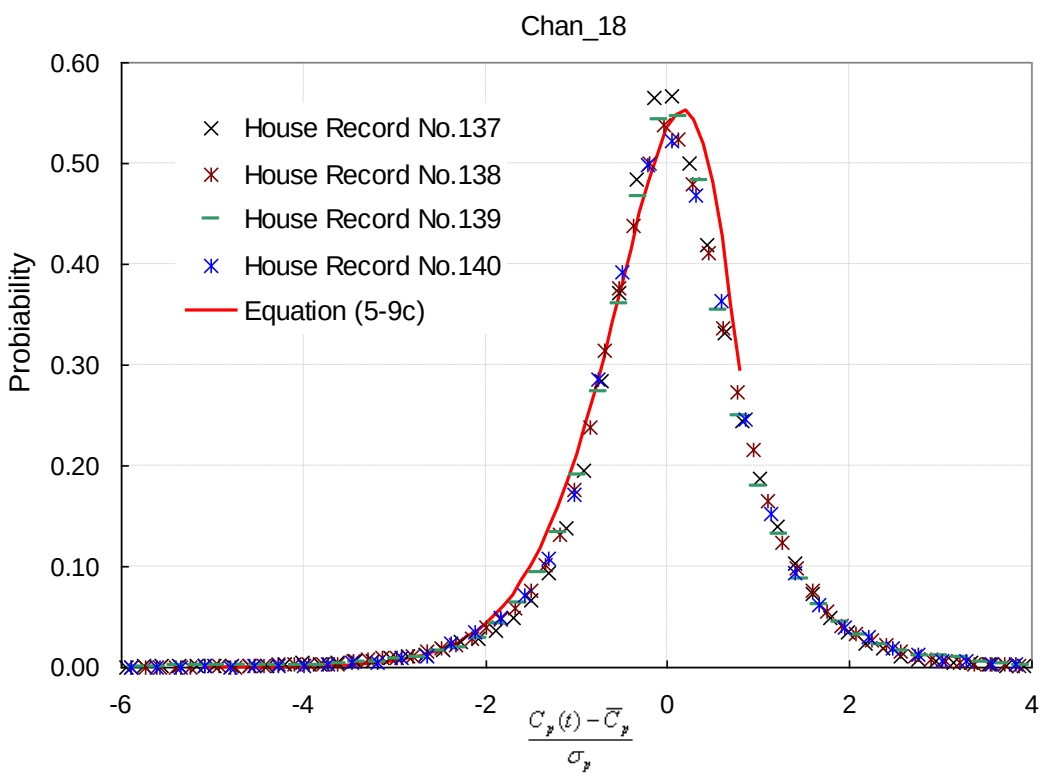
Chan_18
Probiability
0.60
0.50
0.40
0.30
0.20
0.10
0.00
-6
-4
-2
0
2
4
House Record No.137
House Record No.138
House Record No.139
House Record No.140
Equation (5-9c)
$\frac{C_p(t)-\overline{C}_p}{\sigma_p}$

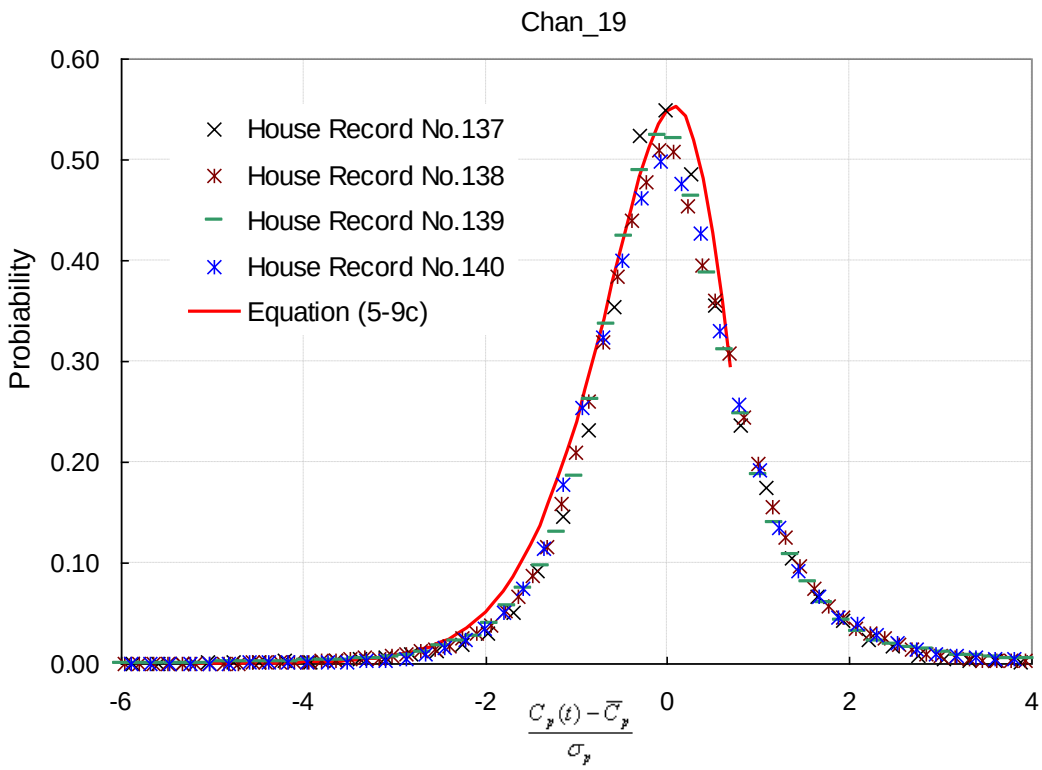
Chan_19
Probiability
0.60
0.50
0.40
0.30
0.20
0.10
0.00
-6
-4
-2
0
2
4
House Record No.137
House Record No.138
House Record No.139
House Record No.140
Equation (5-9c)
$\frac{C_p(t)-\overline{C}_p}{\sigma_p}$

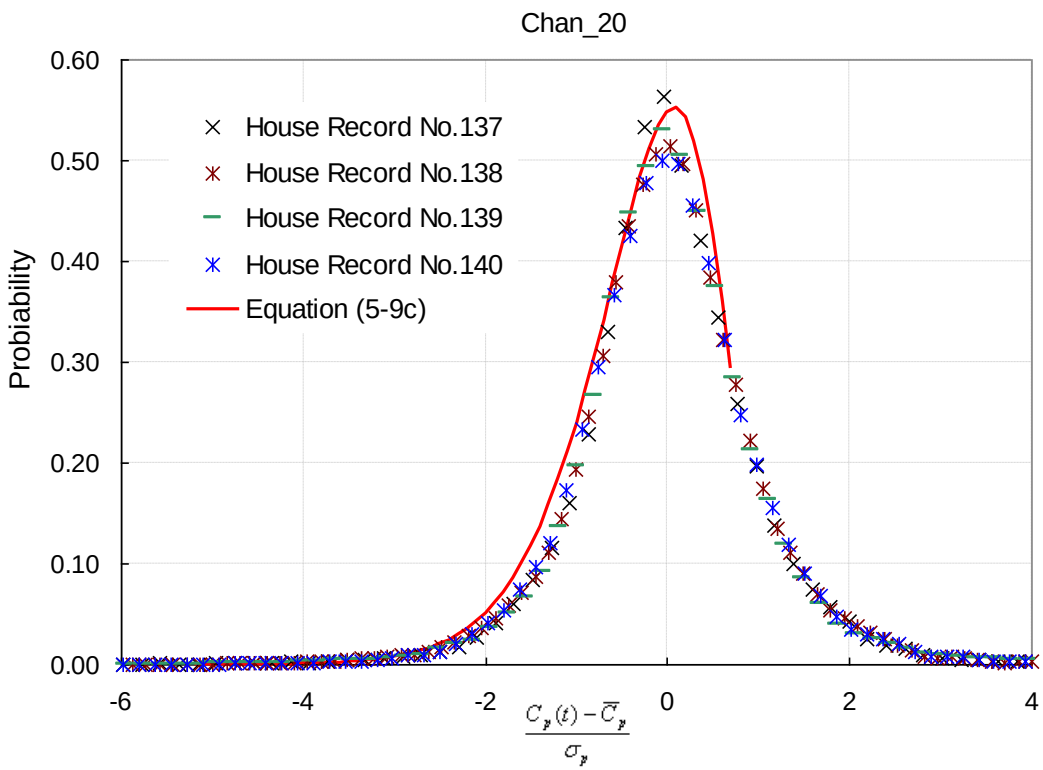
Chan_20
Probiability
0.60
0.50
0.40
0.30
0.20
0.10
0.00
-6
-4
-2
0
2
4
House Record No.137
House Record No.138
House Record No.139
House Record No.140
Equation (5-9c)
$\frac{C_p(t)-\overline{C}_p}{\sigma_p}$

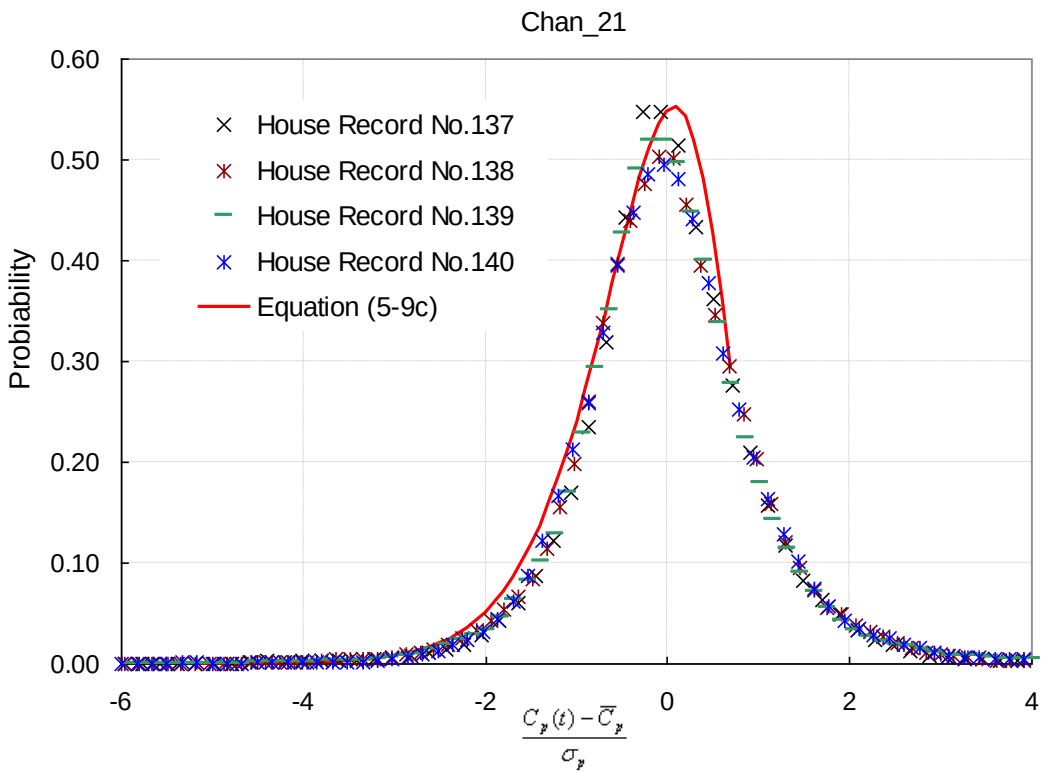
Chan_21
0.60
0.50
0.40
0.30
0.20
0.10
0.00
Probiability
House Record No.137
House Record No.138
House Record No.139
House Record No.140
Equation (5-9c)
-6
-4
-2
0
2
4
$\frac{C_y(t)-\overline{C}_y}{\sigma_y}$

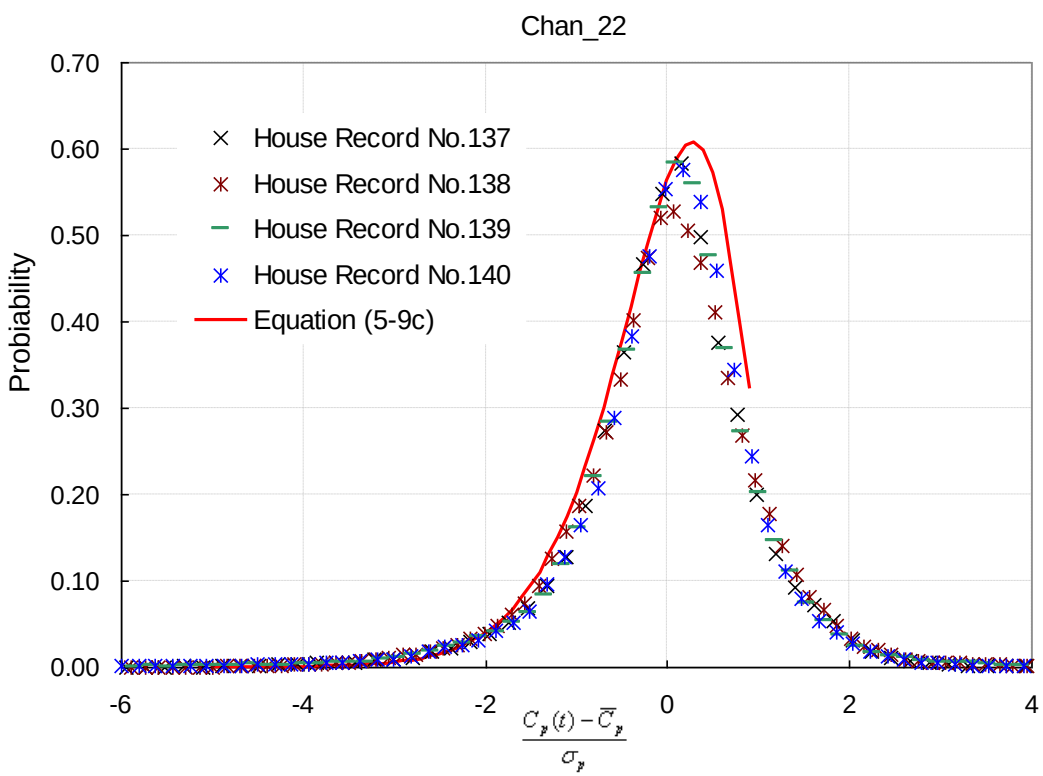
Chan_22
0.70
0.60
0.50
0.40
0.30
0.20
0.10
0.00
Probiability
House Record No.137
House Record No.138
House Record No.139
House Record No.140
Equation (5-9c)
-6
-4
-2
0
2
4
$\frac{C_y(t)-\overline{C}_y}{\sigma_y}$

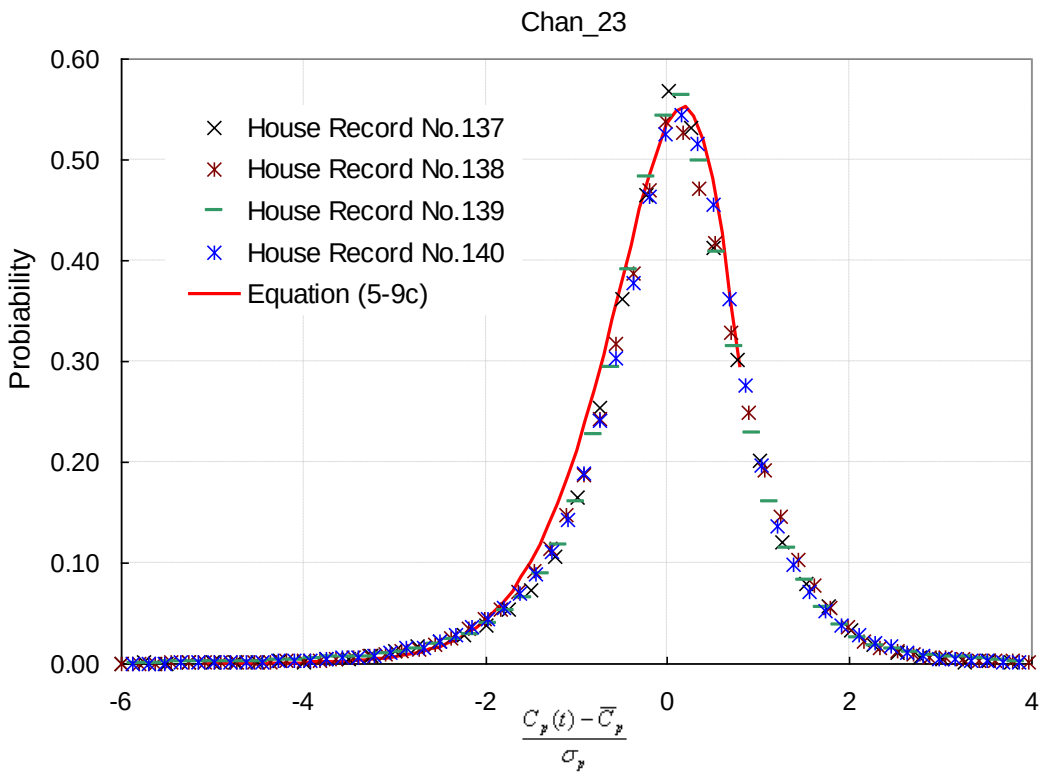
Chan_23
Probiability
0.60
0.50
0.40
0.30
0.20
0.10
0.00
-6
-4
-2
0
2
4
House Record No.137
House Record No.138
House Record No.139
House Record No.140
Equation (5-9c)
$\frac{C_p(t)-\overline{C}_p}{\sigma_p}$

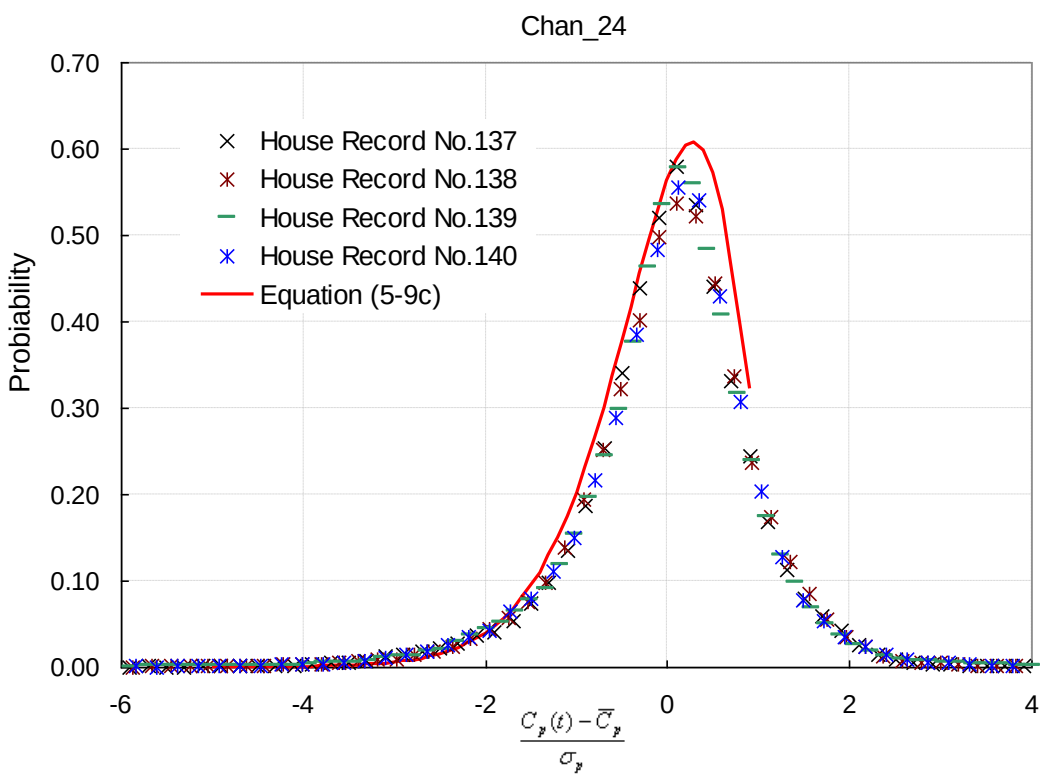
Chan_24
Probiability
0.70
0.60
0.50
0.40
0.30
0.20
0.10
0.00
-6
-4
-2
0
2
4
House Record No.137
House Record No.138
House Record No.139
House Record No.140
Equation (5-9c)
$\frac{C_p(t)-\overline{C}_p}{\sigma_p}$

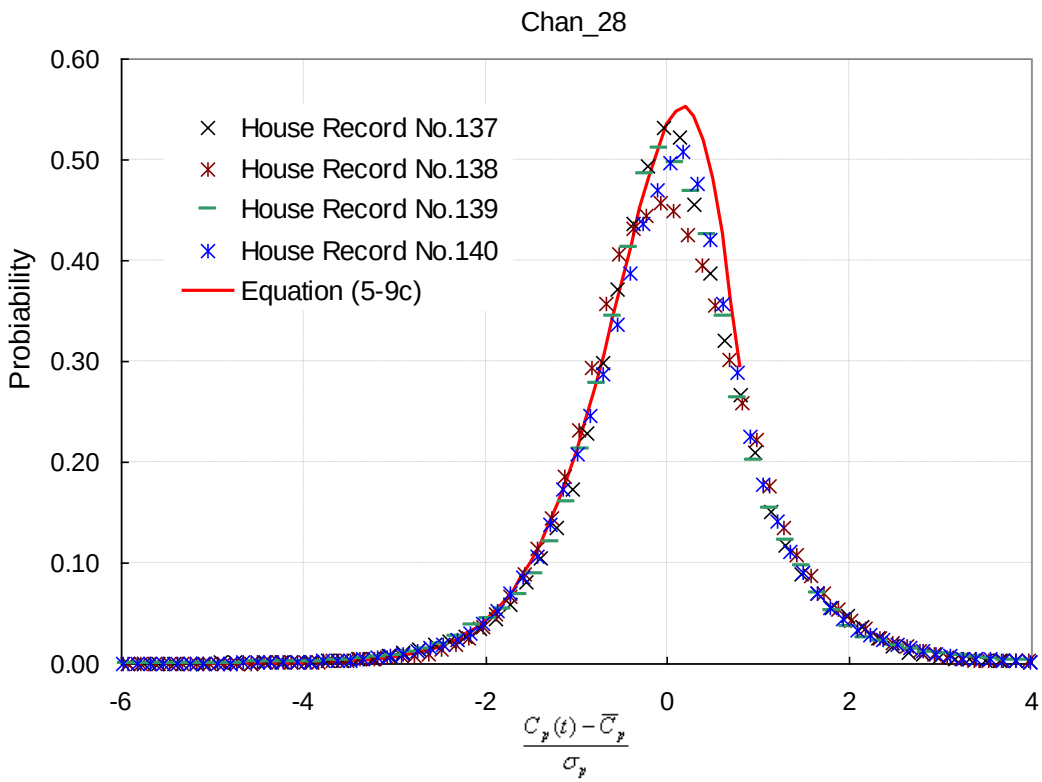
Chan_28
0.60
0.50
0.40
0.30
0.20
0.10
0.00
Probiability
House Record No.137
House Record No.138
House Record No.139
House Record No.140
Equation (5-9c)
-6
-4
-2
0
2
4
$\frac{C_y(t)-\overline{C}_y}{\sigma_y}$

Appendix E

Effect of Averaging Period on the Peak Factors of Individual Channels

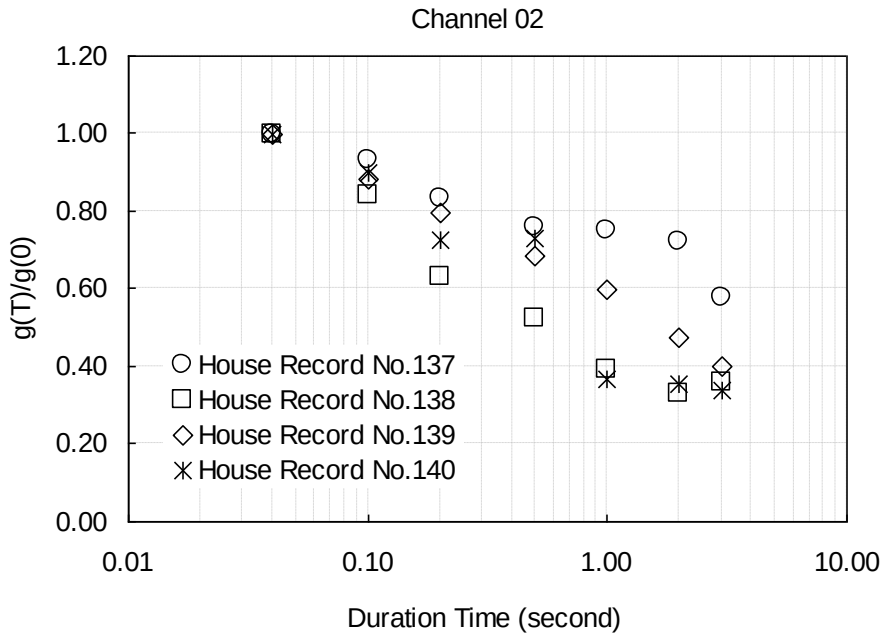

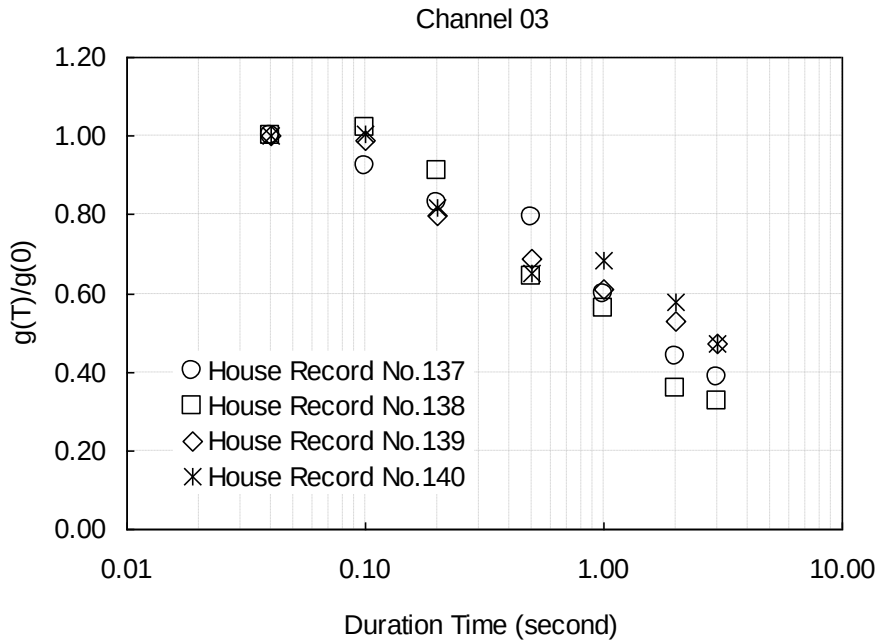
Channel 03
1.20
1.00
0.80
0.60
0.40
0.20
0.00
g(T)/g(0)
House Record No.137
House Record No.138
House Record No.139
House Record No.140
0.01
0.10
1.00
10.00
Duration Time (second)

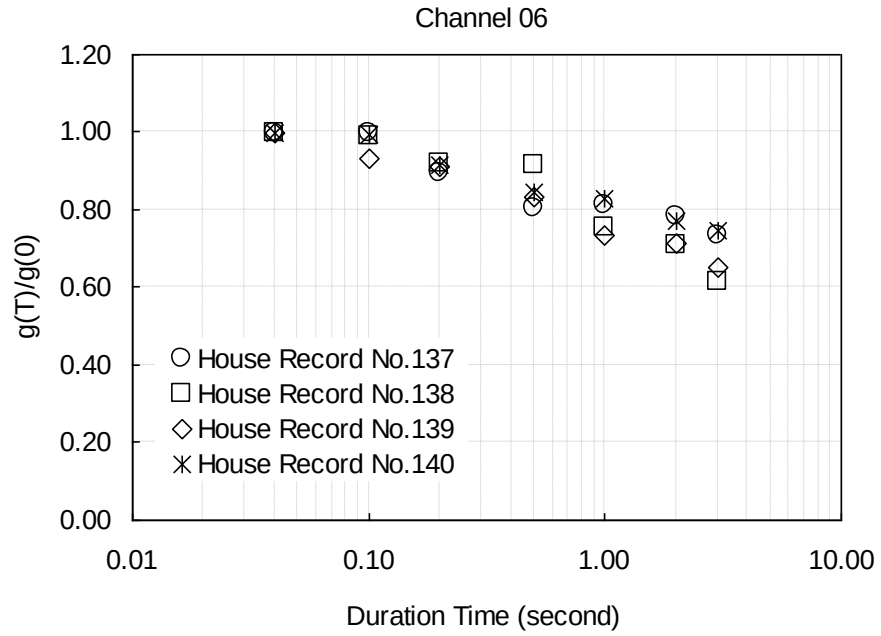
Channel 06
1.20
1.00
0.80
0.60
0.40
0.20
0.00
g(T)/g(0)
House Record No.137
House Record No.138
House Record No.139
House Record No.140
0.01
0.10
1.00
10.00
Duration Time (second)

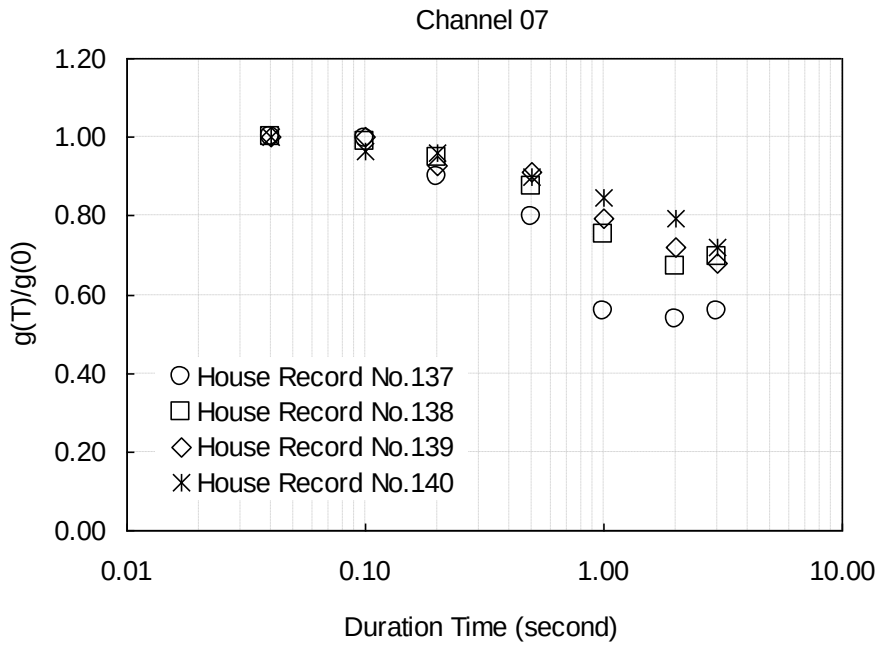
Channel 07
1.20
1.00
0.80
0.60
0.40
0.20
0.00
g(T)/g(0)
House Record No.137
House Record No.138
House Record No.139
House Record No.140
0.01
0.10
1.00
10.00
Duration Time (second)

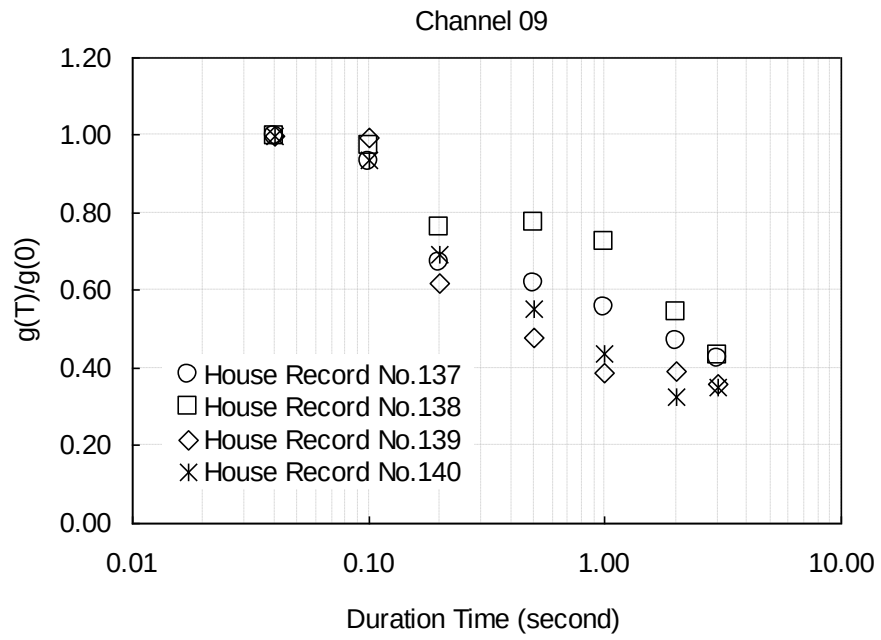
Channel 09
1.20
1.00
0.80
0.60
0.40
0.20
0.00
g(T)/g(0)
House Record No.137
House Record No.138
House Record No.139
House Record No.140
0.01
0.10
1.00
10.00
Duration Time (second)

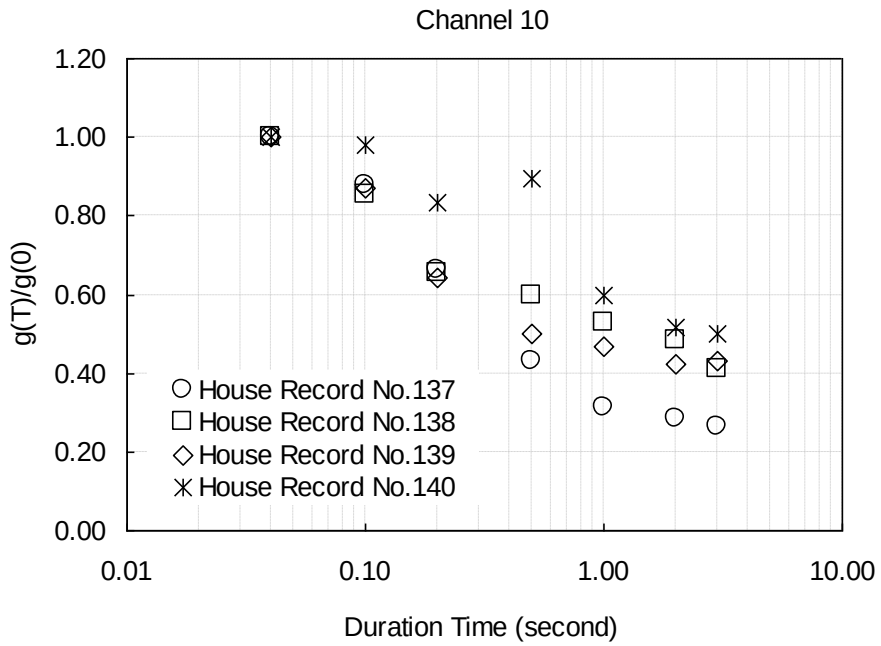
Channel 10
1.20
1.00
0.80
0.60
0.40
0.20
0.00
g(T)/g(0)
House Record No.137
House Record No.138
House Record No.139
House Record No.140
0.01
0.10
1.00
10.00
Duration Time (second)

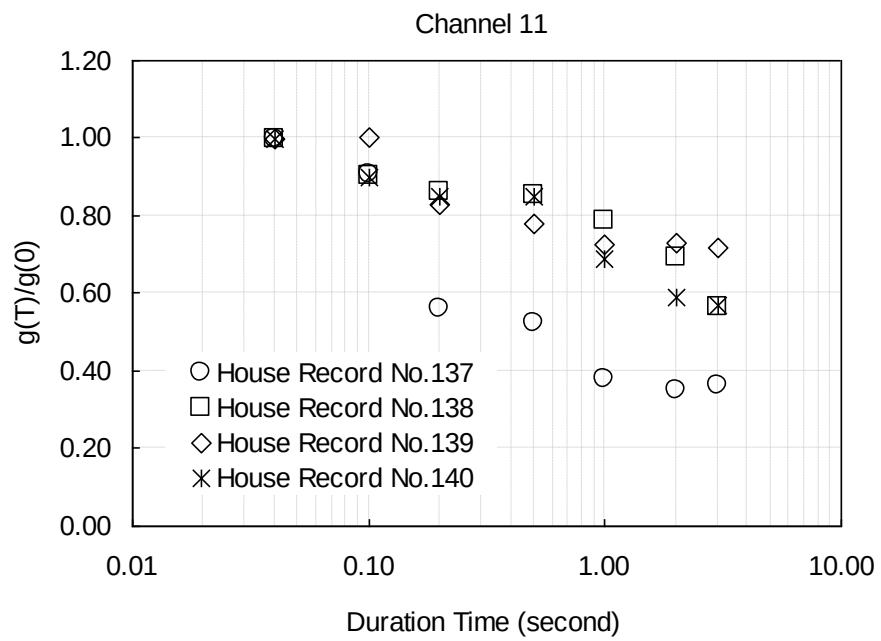
Channel 11
1.20
1.00
0.80
0.60
0.40
0.20
0.00
g(T)/g(0)
House Record No.137
House Record No.138
House Record No.139
House Record No.140
0.01
0.10
1.00
10.00
Duration Time (second)

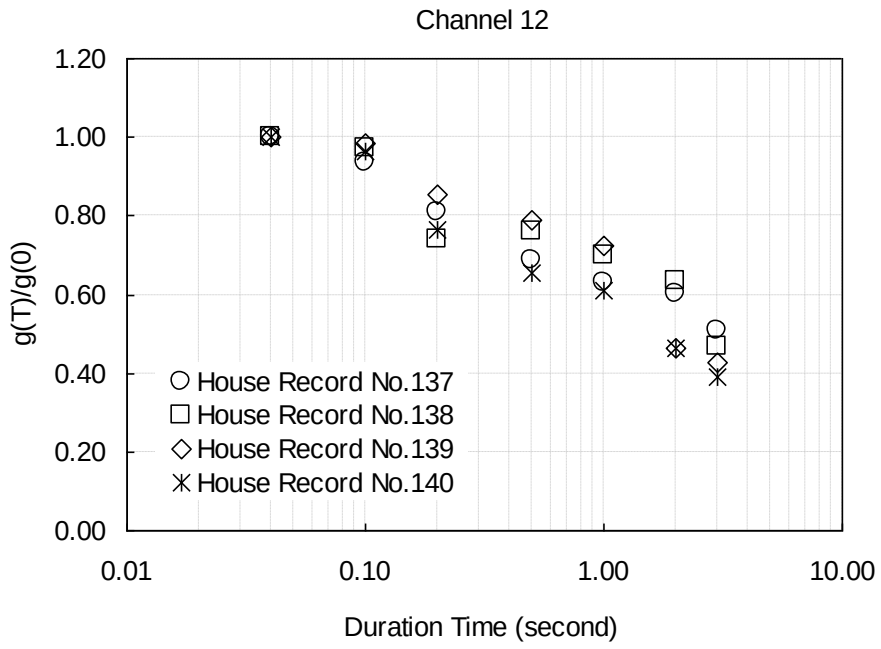
Channel 12
1.20
1.00
0.80
0.60
0.40
0.20
0.00
g(T)/g(0)
House Record No.137
House Record No.138
House Record No.139
House Record No.140
0.01
0.10
1.00
10.00
Duration Time (second)

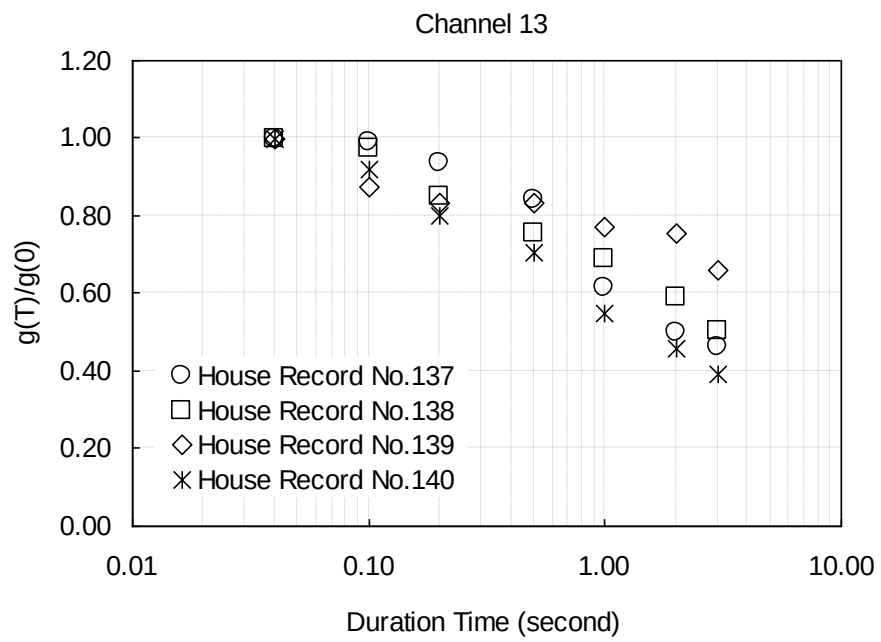
Channel 13
1.20
1.00
0.80
0.60
0.40
0.20
0.00
g(T)/g(0)
House Record No.137
House Record No.138
House Record No.139
House Record No.140
0.01
0.10
1.00
10.00
Duration Time (second)

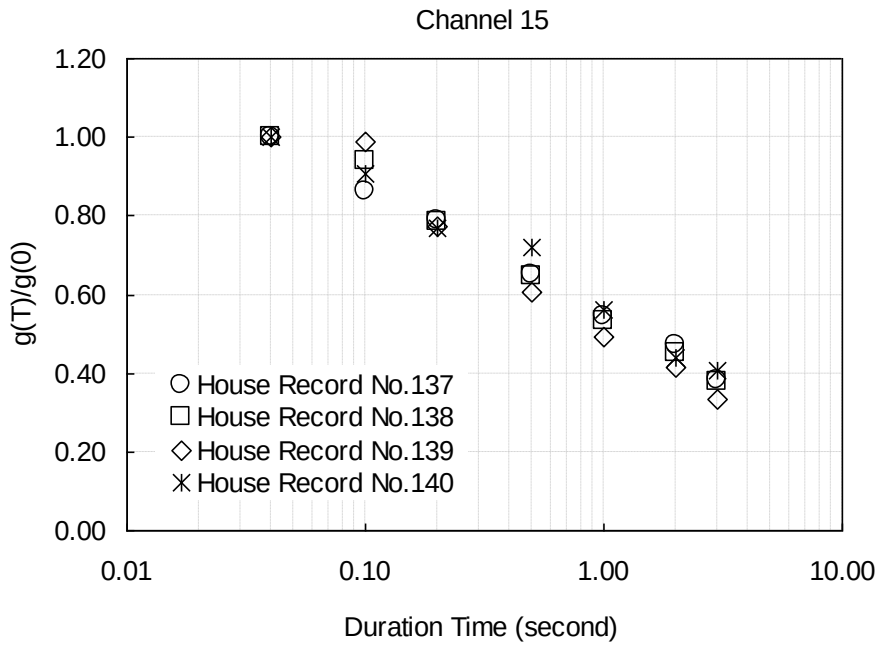
Channel 15
1.20
1.00
0.80
0.60
0.40
0.20
0.00
g(T)/g(0)
House Record No.137
House Record No.138
House Record No.139
House Record No.140
0.01
0.10
1.00
10.00
Duration Time (second)

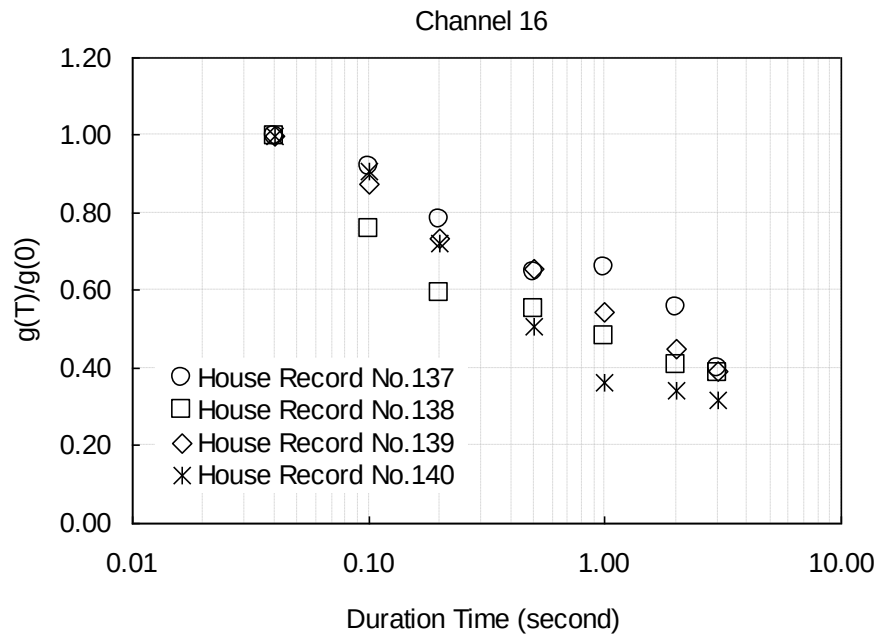
Channel 16
1.20
1.00
0.80
0.60
0.40
0.20
0.00
g(T)/g(0)
House Record No.137
House Record No.138
House Record No.139
House Record No.140
0.01
0.10
1.00
10.00
Duration Time (second)

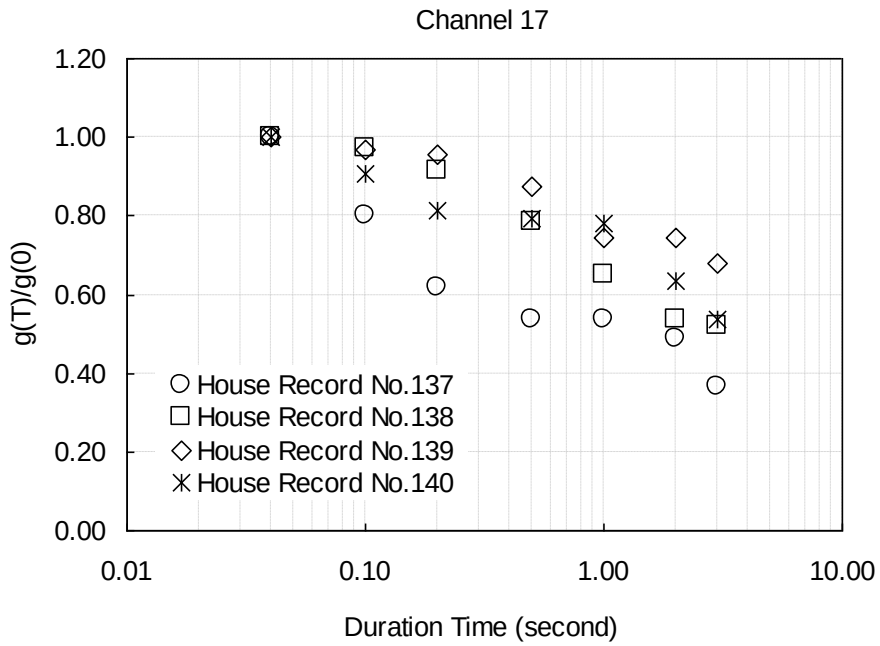
Channel 17
1.20
1.00
0.80
0.60
0.40
0.20
0.00
g(T)/g(0)
House Record No.137
House Record No.138
House Record No.139
House Record No.140
0.01
0.10
1.00
10.00
Duration Time (second)

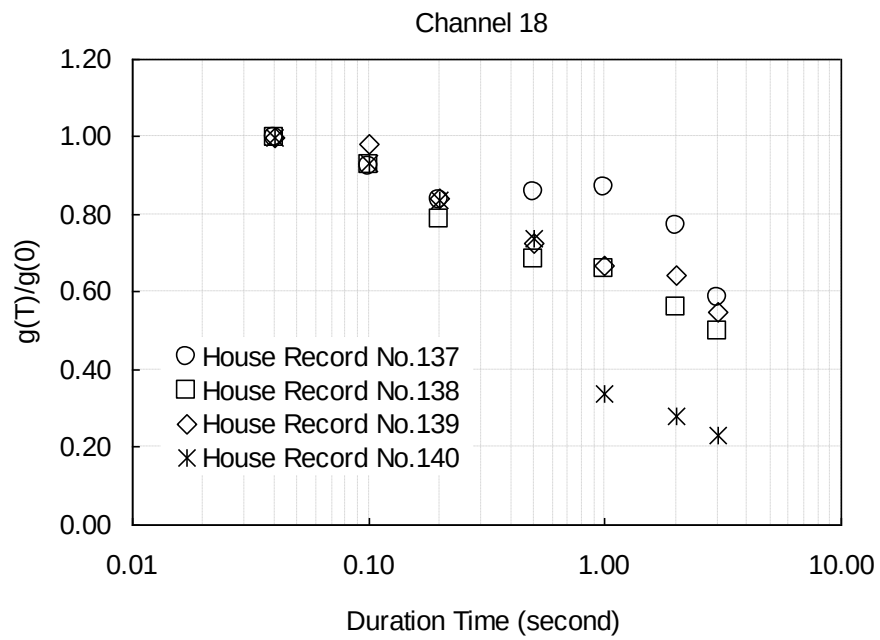
Channel 18
1.20
1.00
0.80
0.60
0.40
0.20
0.00
g(T)/g(0)
House Record No.137
House Record No.138
House Record No.139
House Record No.140
0.01
0.10
1.00
10.00
Duration Time (second)

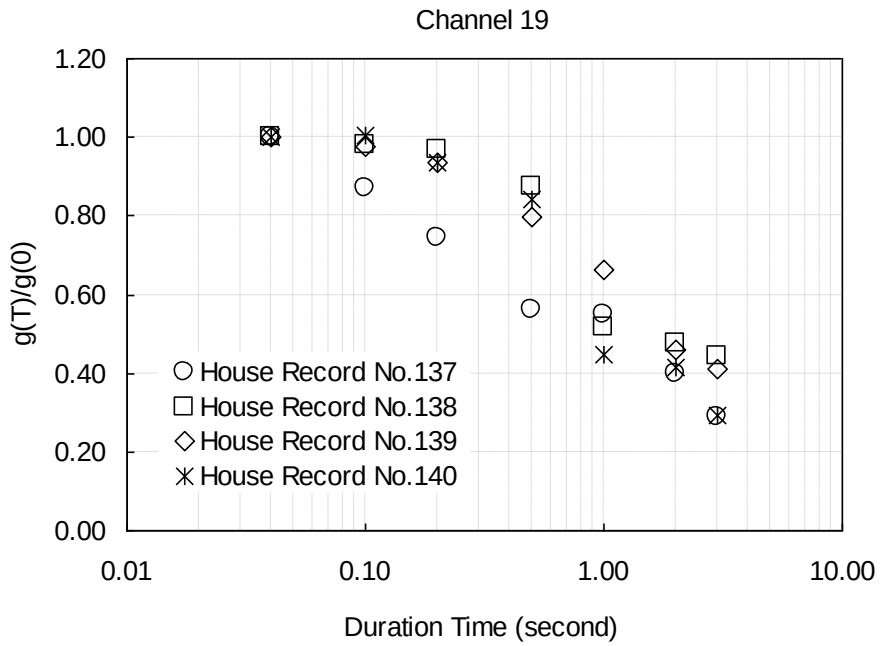
Channel 19
1.20
1.00
0.80
0.60
0.40
0.20
0.00
g(T)/g(0)
House Record No.137
House Record No.138
House Record No.139
House Record No.140
0.01
0.10
1.00
10.00
Duration Time (second)

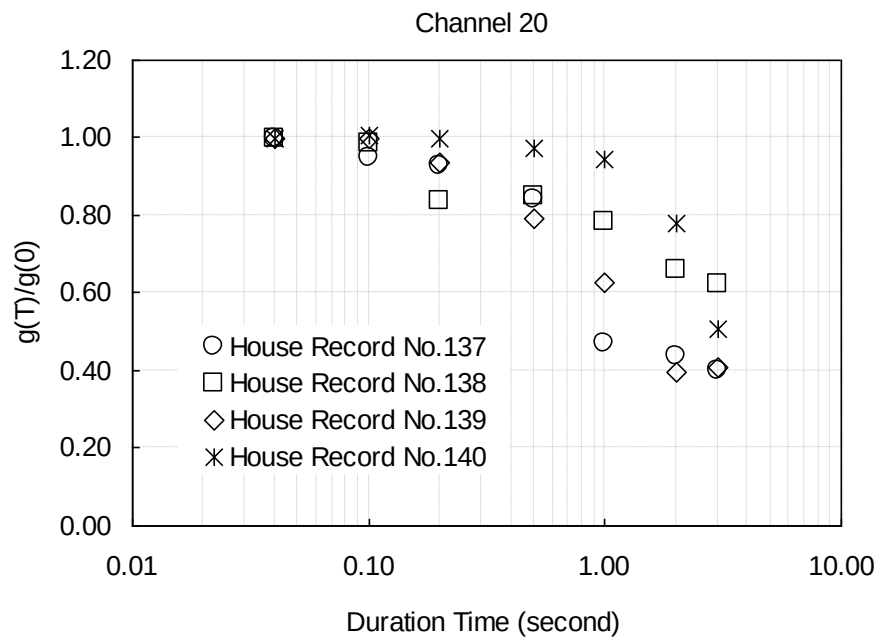
Channel 20
1.20
1.00
0.80
0.60
0.40
0.20
0.00
g(T)/g(0)
House Record No.137
House Record No.138
House Record No.139
House Record No.140
0.01
0.10
1.00
10.00
Duration Time (second)

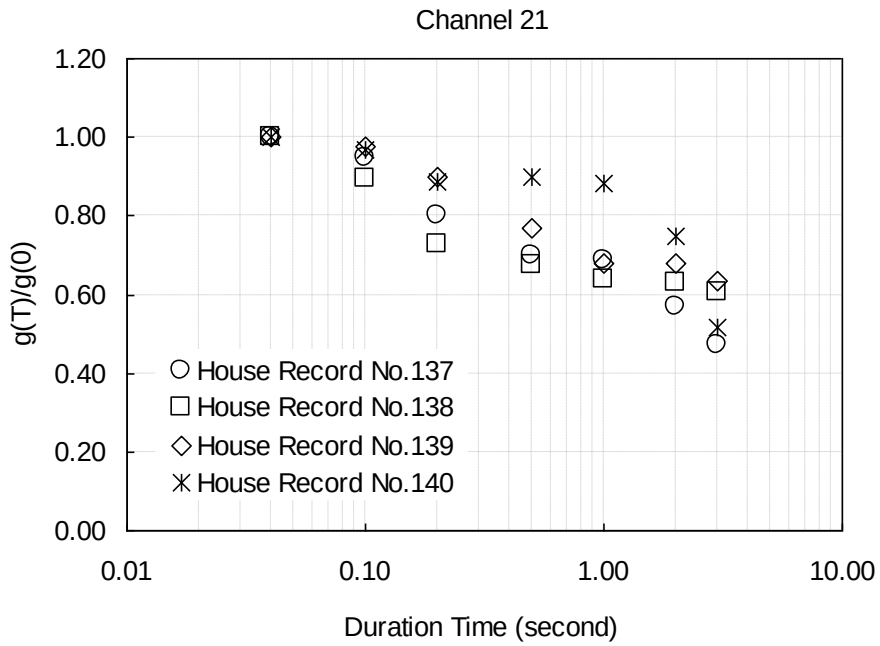
Channel 21
1.20
1.00
0.80
0.60
0.40
0.20
0.00
g(T)/g(0)
House Record No.137
House Record No.138
House Record No.139
House Record No.140
0.01
0.10
1.00
10.00
Duration Time (second)

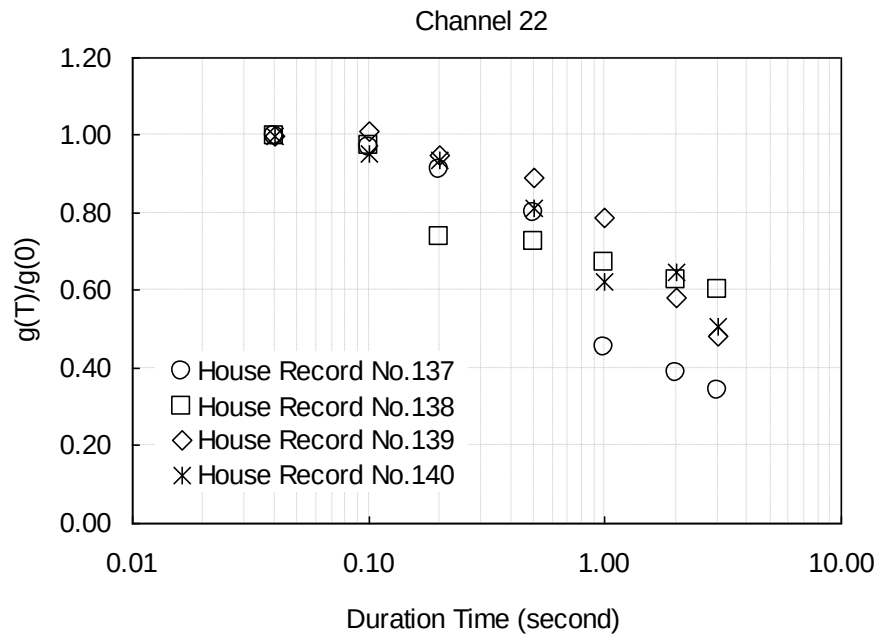
Channel 22
1.20
1.00
0.80
0.60
0.40
0.20
0.00
g(T)/g(0)
House Record No.137
House Record No.138
House Record No.139
House Record No.140
0.01
0.10
1.00
10.00
Duration Time (second)

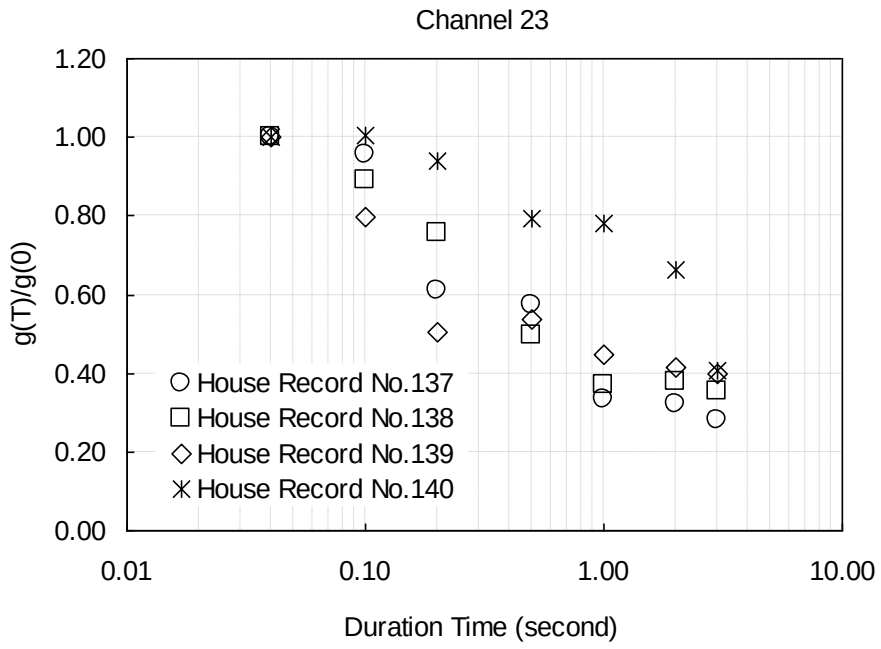
Channel 23
1.20
1.00
0.80
0.60
0.40
0.20
0.00
g(T)/g(0)
House Record No.137
House Record No.138
House Record No.139
House Record No.140
0.01
0.10
1.00
10.00
Duration Time (second)

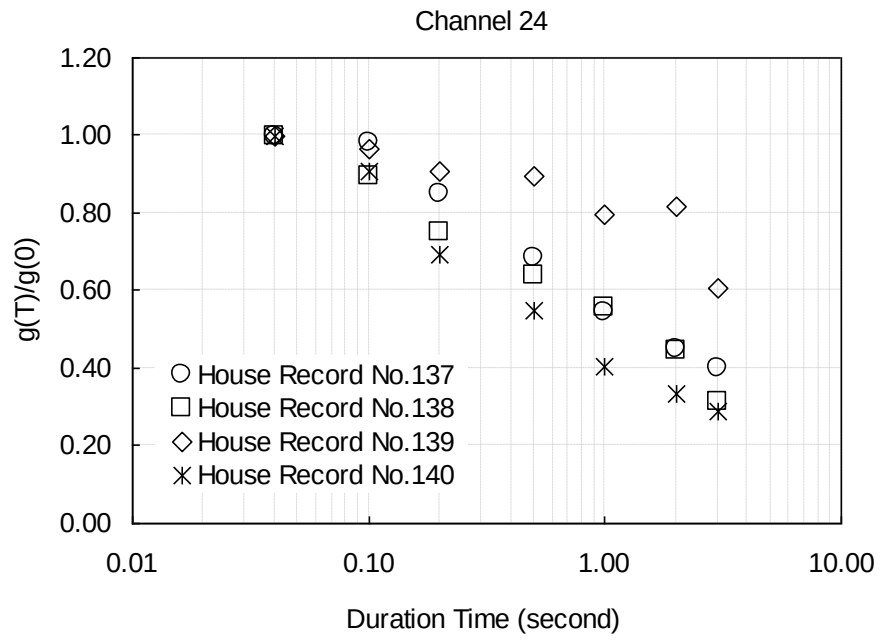
Channel 24
1.20
1.00
0.80
0.60
0.40
0.20
0.00
g(T)/g(0)
House Record No.137
House Record No.138
House Record No.139
House Record No.140
0.01
0.10
1.00
10.00
Duration Time (second)

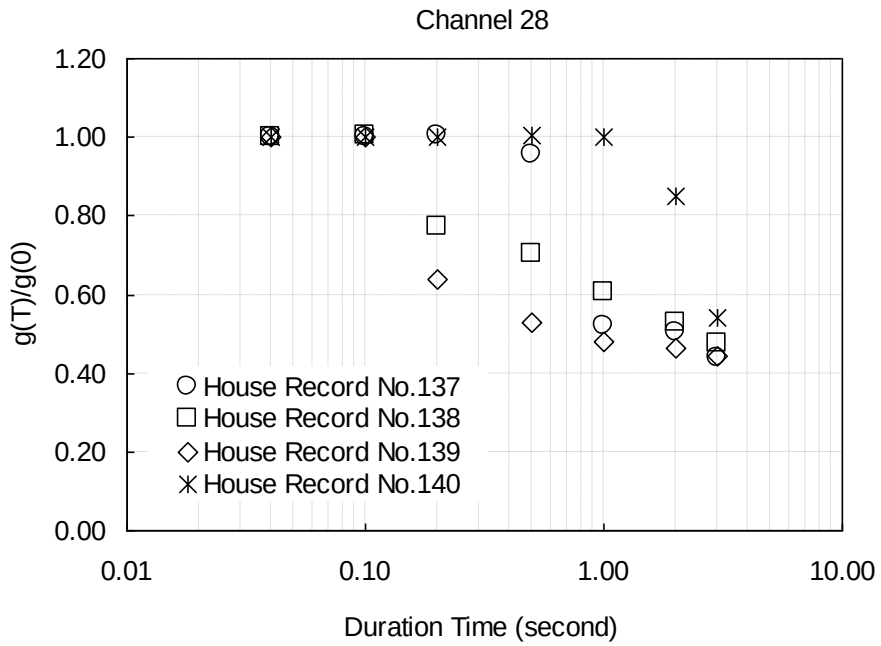
Channel 28
1.20
1.00
0.80
0.60
0.40
0.20
0.00
g(T)/g(0)
0.01
0.10
1.00
10.00
Duration Time (second)
House Record No.137
House Record No.138
House Record No.139
House Record No.140

Appendix F

Comparison of Area-Averaged Negative Peak Pressure Coefficients to the Corresponding Values of Individual Channels

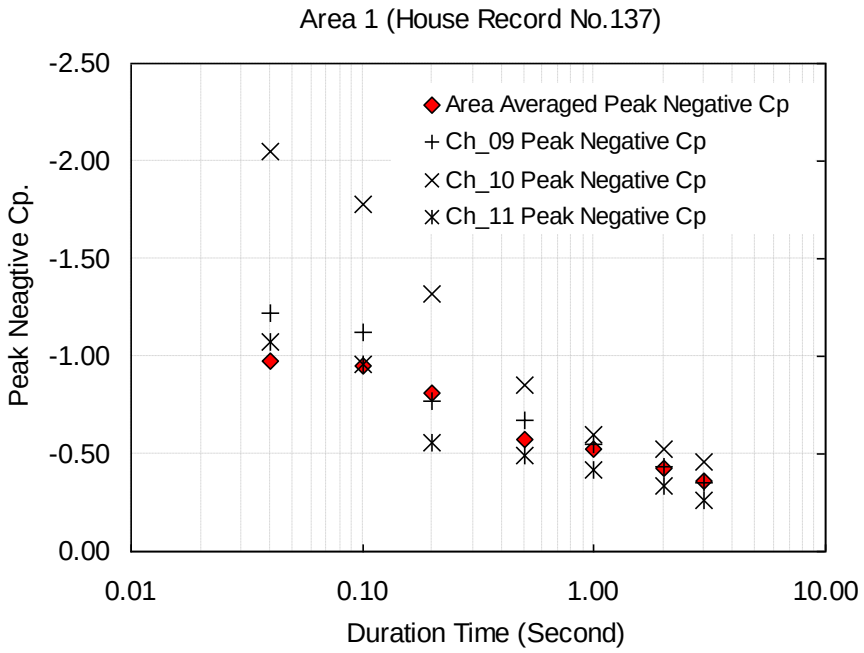

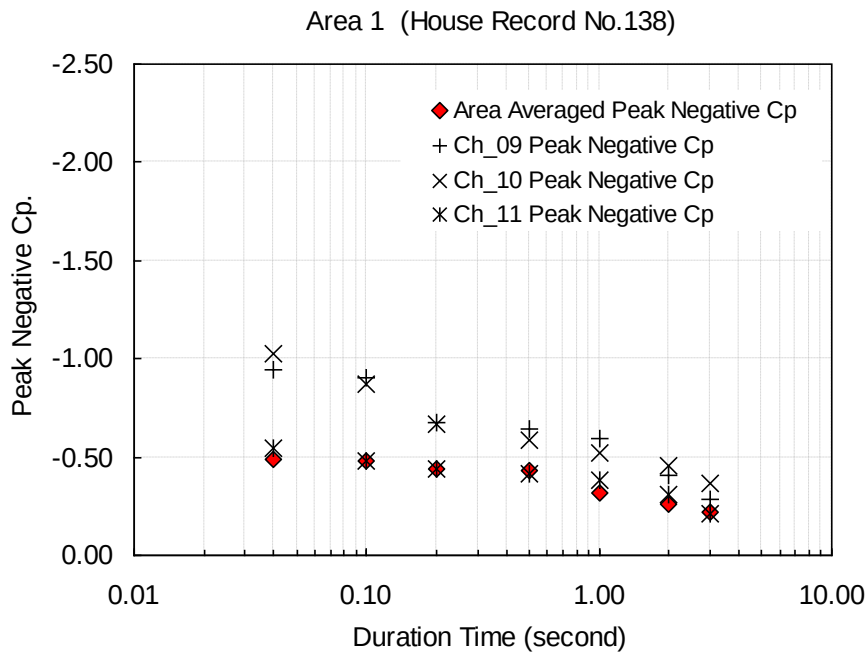
Area 1 (House Record No.138)
Area Averaged Peak Negative Cp
Ch_09 Peak Negative Cp
Ch_10 Peak Negative Cp
Ch_11 Peak Negative Cp
Peak Negative Cp.
-2.50
-2.00
-1.50
-1.00
-0.50
0.00
0.01
0.10
1.00
10.00
Duration Time (second)

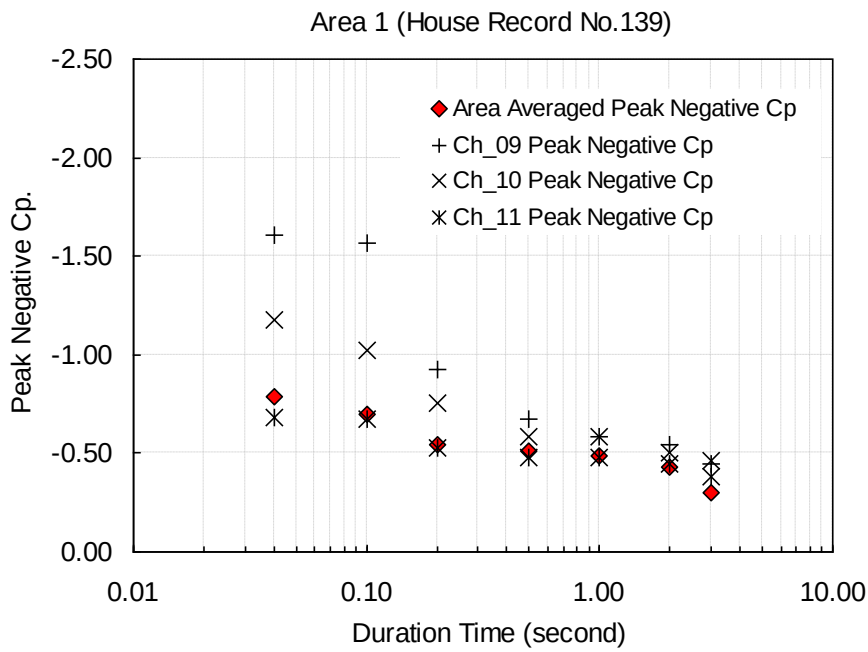
Area 1 (House Record No.139)
Area Averaged Peak Negative Cp
Ch_09 Peak Negative Cp
Ch_10 Peak Negative Cp
Ch_11 Peak Negative Cp
Peak Negative Cp.
-2.50
-2.00
-1.50
-1.00
-0.50
0.00
0.01
0.10
1.00
10.00
Duration Time (second)

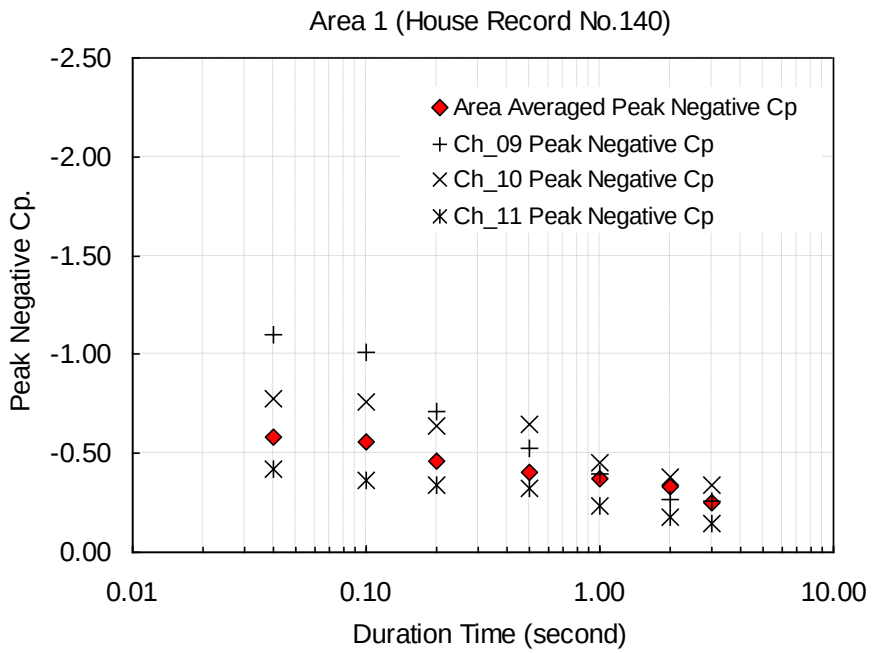
Area 1 (House Record No.140)
Area Averaged Peak Negative Cp
Ch_09 Peak Negative Cp
Ch_10 Peak Negative Cp
Ch_11 Peak Negative Cp
Peak Negative Cp.
-2.50
-2.00
-1.50
-1.00
-0.50
0.00
0.01
0.10
1.00
10.00
Duration Time (second)

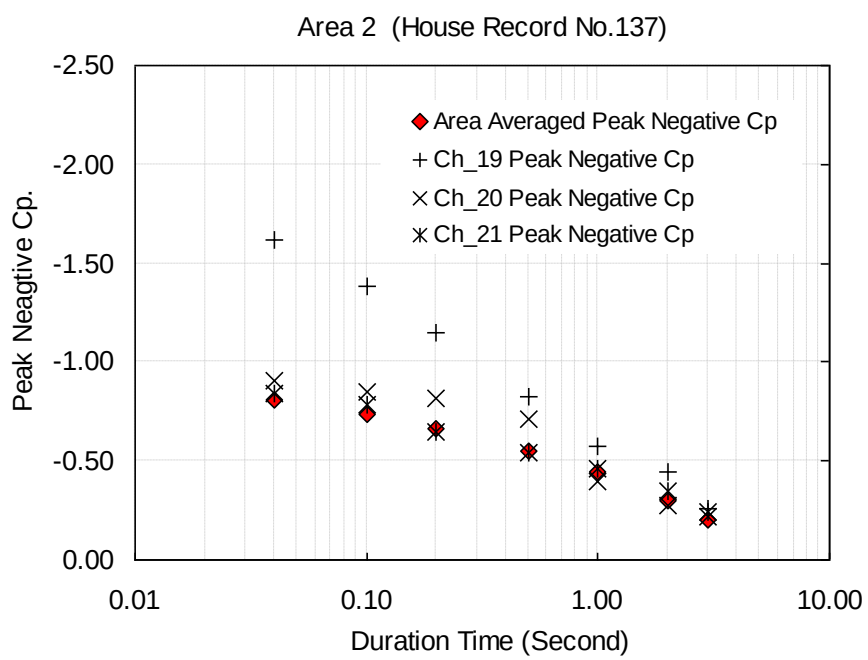
Area 2 (House Record No.137)
Area Averaged Peak Negative Cp
Ch_19 Peak Negative Cp
Ch_20 Peak Negative Cp
Ch_21 Peak Negative Cp
Peak Neagtive Cp.
-2.50
-2.00
-1.50
-1.00
-0.50
0.00
0.01
0.10
1.00
10.00
Duration Time (Second)

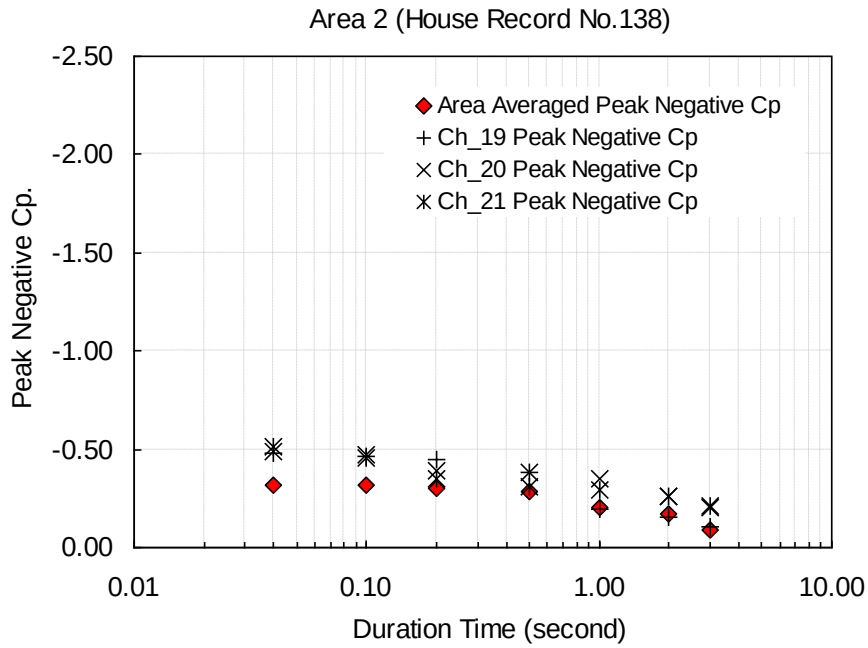
Area 2 (House Record No.138)
Area Averaged Peak Negative Cp
Ch_19 Peak Negative Cp
Ch_20 Peak Negative Cp
Ch_21 Peak Negative Cp
Peak Negative Cp.
-2.50
-2.00
-1.50
-1.00
-0.50
0.00
0.01
0.10
1.00
10.00
Duration Time (second)

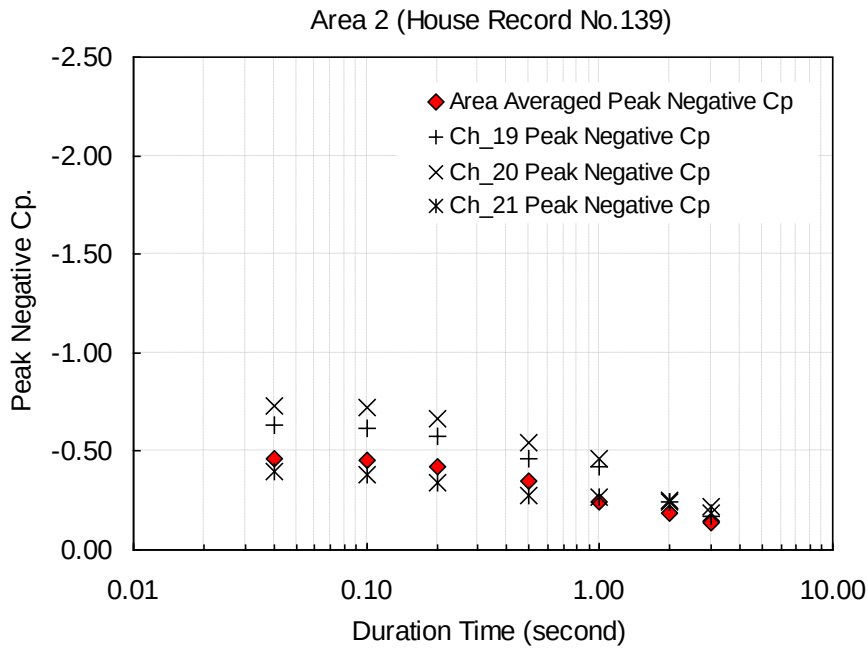
Area 2 (House Record No.139)
Area Averaged Peak Negative Cp
Ch_19 Peak Negative Cp
Ch_20 Peak Negative Cp
Ch_21 Peak Negative Cp
Peak Negative Cp.
-2.50
-2.00
-1.50
-1.00
-0.50
0.00
0.01
0.10
1.00
10.00
Duration Time (second)

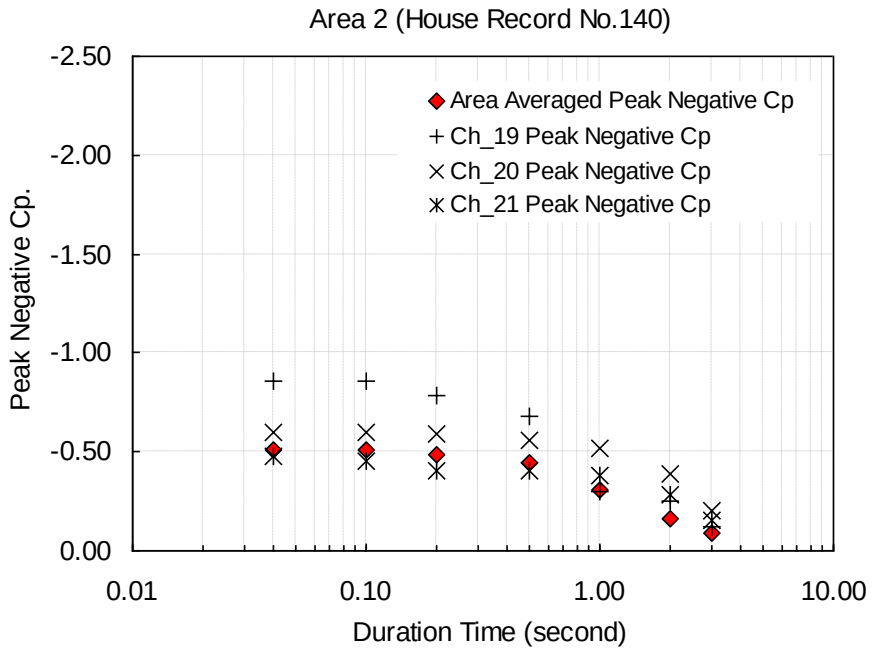
Area 2 (House Record No.140)
Area Averaged Peak Negative Cp
Ch_19 Peak Negative Cp
Ch_20 Peak Negative Cp
Ch_21 Peak Negative Cp
Peak Negative Cp.
-2.50
-2.00
-1.50
-1.00
-0.50
0.00
0.01
0.10
1.00
10.00
Duration Time (second)

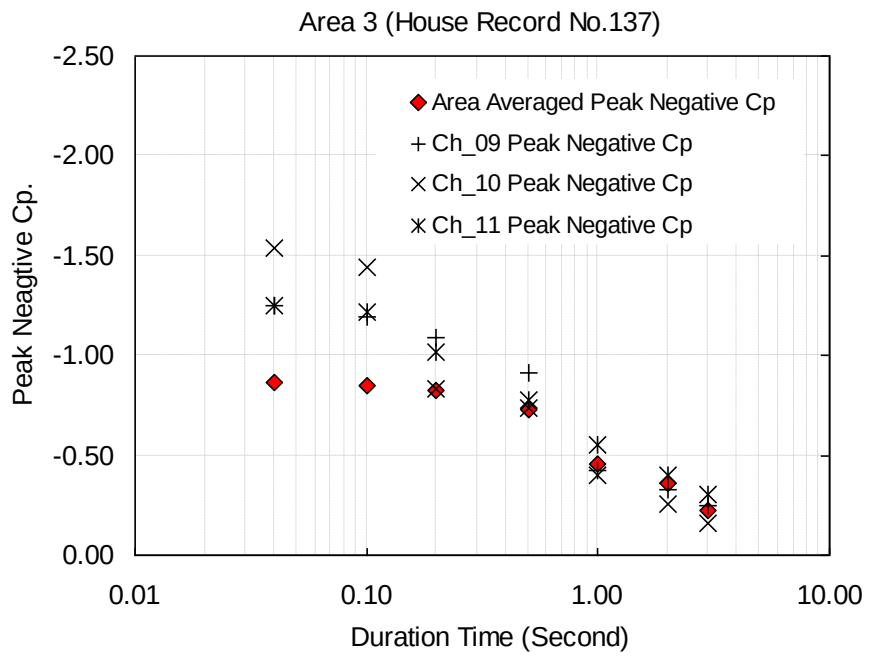
Area 3 (House Record No.137)
Area Averaged Peak Negative Cp
Ch_09 Peak Negative Cp
Ch_10 Peak Negative Cp
Ch_11 Peak Negative Cp
Peak Neagtive Cp.
-2.50
-2.00
-1.50
-1.00
-0.50
0.00
0.01
0.10
1.00
10.00
Duration Time (Second)

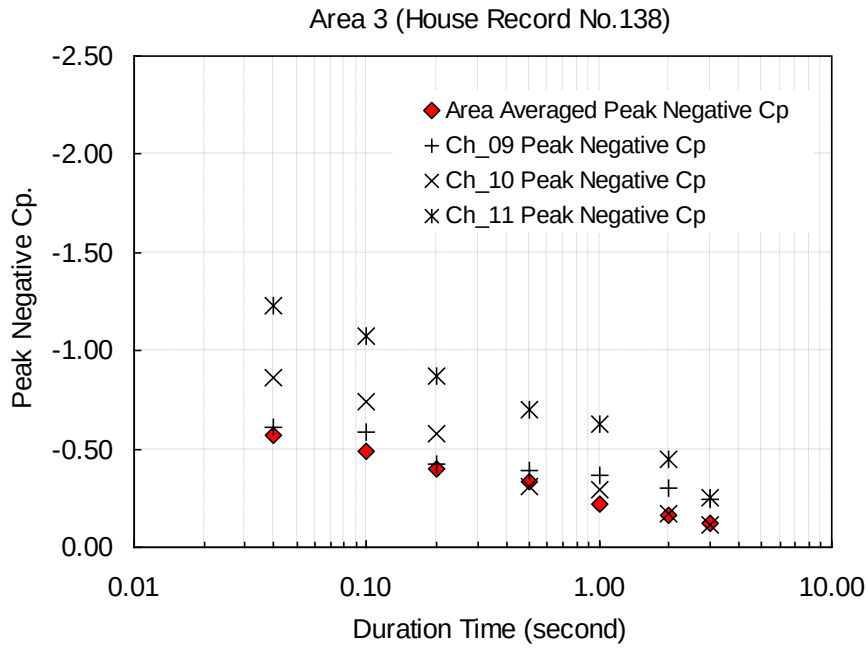
Area 3 (House Record No.138)
Area Averaged Peak Negative Cp
Ch_09 Peak Negative Cp
Ch_10 Peak Negative Cp
Ch_11 Peak Negative Cp
Peak Negative Cp.
-2.50
-2.00
-1.50
-1.00
-0.50
0.00
0.01
0.10
1.00
10.00
Duration Time (second)

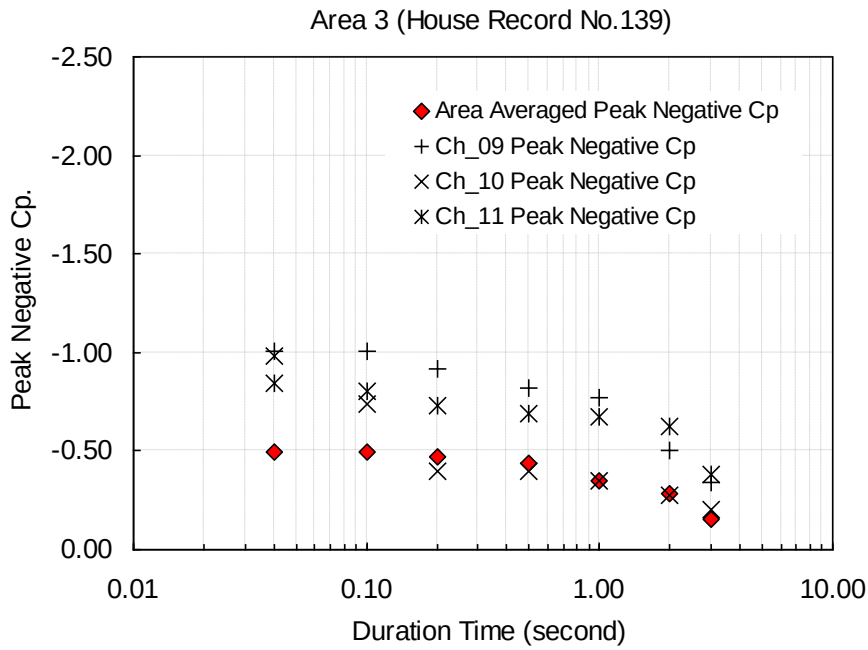
Area 3 (House Record No.139)
Area Averaged Peak Negative Cp
Ch_09 Peak Negative Cp
Ch_10 Peak Negative Cp
Ch_11 Peak Negative Cp
Peak Negative Cp.
-2.50
-2.00
-1.50
-1.00
-0.50
0.00
0.01
0.10
1.00
10.00
Duration Time (second)

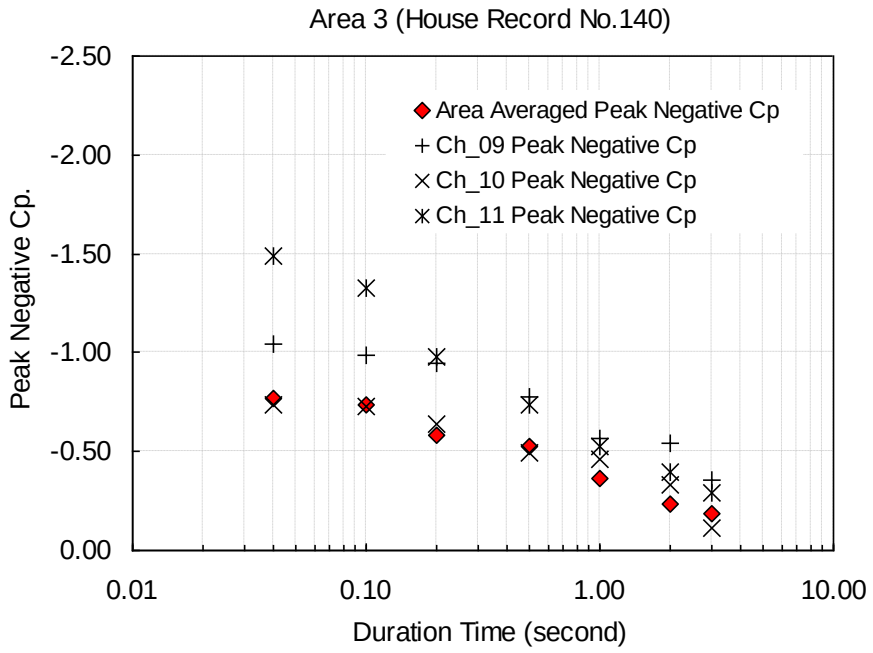
Area 3 (House Record No.140)
Area Averaged Peak Negative Cp
Ch_09 Peak Negative Cp
Ch_10 Peak Negative Cp
Ch_11 Peak Negative Cp
Peak Negative Cp.
-2.50
-2.00
-1.50
-1.00
-0.50
0.00
0.01
0.10
1.00
10.00
Duration Time (second)

Appendix G

Area-Averaged Pressure Coefficients of Critical Roof Corner Areas

Wind Direction	Areas	Mean Cp	Min Cp	Max Cp	Areas	Mean Cp	Min Cp	Max Cp
10	Area 1	-0.16	-1.17	0.70	Area 11	-0.18	-0.77	0.28
20	Area 1	-0.14	-1.98	0.85	Area 11	-0.22	-1.09	0.20
30	Area 1	-0.14	-1.88	0.77	Area 11	-0.27	-1.18	0.11
40	Area 1	-0.15	-1.58	0.74	Area 11	-0.33	-1.28	0.06
50	Area 1	-0.18	-1.52	0.59	Area 11	-0.38	-1.60	0.01
60	Area 1	-0.21	-1.50	0.67	Area 11	-0.39	-1.35	0.02
70	Area 1	-0.19	-1.56	0.70	Area 11	-0.38	-1.48	-0.02
80	Area 1	-0.15	-1.22	0.46	Area 11	-0.34	-1.37	0.00
90	Area 1	-0.10	-0.82	0.67	Area 11	-0.30	-1.22	0.06
100	Area 1	-0.12	-0.93	0.60	Area 11	-0.36	-1.43	-0.03
110	Area 1	-0.13	-0.97	0.40	Area 11	-0.46	-1.82	0.01
120	Area 1	-0.15	-0.94	0.38	Area 11	-0.63	-2.08	-0.11
130	Area 1	-0.21	-0.89	0.33	Area 11	-0.75	-2.47	-0.13
140	Area 1	-0.26	-0.93	0.31	Area 11	-0.67	-2.49	0.04
150	Area 1	-0.33	-1.17	0.18	Area 11	-0.60	-2.89	-0.02
160	Area 1	-0.35	-1.03	0.09	Area 11	-0.50	-2.04	0.06
170	Area 1	-0.36	-1.06	0.14	Area 11	-0.45	-1.93	0.26
180	Area 1	-0.35	-0.95	0.00	Area 11	-0.39	-2.10	0.24
190	Area 1	-0.32	-1.00	0.02	Area 11	-0.36	-1.65	0.33
200	Area 1	-0.21	-1.00	0.14	Area 11	-0.34	-1.73	0.47
210	Area 1	-0.15	-0.72	0.13	Area 11	-0.44	-1.96	0.30
220	Area 1	-0.13	-0.62	0.21	Area 11	-0.47	-1.94	0.34
230	Area 1	-0.12	-0.63	0.22	Area 11	-0.43	-1.81	0.30
240	Area 1	-0.11	-0.61	0.27	Area 11	-0.34	-1.66	0.44
250	Area 1	-0.09	-0.57	0.35	Area 11	-0.26	-1.46	0.44
260	Area 1	-0.07	-0.77	0.32	Area 11	-0.18	-1.23	0.43
270	Area 1	-0.06	-1.08	0.37	Area 11	-0.14	-0.98	0.37
280	Area 1	-0.04	-0.56	0.44	Area 11	-0.13	-0.93	0.37

Wind Direction	Areas	Mean Cp	Min Cp	Max Cp	Areas	Mean Cp	Min Cp	Max Cp
290	Area 1	-0.03	-0.53	0.38	Area 11	-0.14	-0.64	0.26
300	Area 1	-0.04	-0.98	0.49	Area 11	-0.16	-0.66	0.37
310	Area 1	-0.06	-1.11	0.47	Area 11	-0.16	-0.67	0.25
320	Area 1	-0.09	-0.79	0.44	Area 11	-0.16	-0.79	0.28
330	Area 1	-0.11	-0.98	0.33	Area 11	-0.15	-0.70	0.36
340	Area 1	-0.14	-0.95	0.55	Area 11	-0.17	-0.78	0.49
350	Area 1	-0.17	-1.30	0.52	Area 11	-0.16	-0.79	0.23
360	Area 1	-0.17	-1.38	0.67	Area 11	-0.15	-0.66	0.22
10	Area 2	-0.08	-1.20	0.78	Area 12	-0.19	-0.62	0.11
20	Area 2	-0.13	-1.02	0.80	Area 12	-0.21	-0.57	0.05
30	Area 2	-0.21	-0.91	0.58	Area 12	-0.23	-0.65	0.06
40	Area 2	-0.32	-0.99	0.36	Area 12	-0.26	-0.67	0.06
50	Area 2	-0.37	-1.15	0.14	Area 12	-0.29	-0.91	0.01
60	Area 2	-0.35	-1.04	0.10	Area 12	-0.30	-0.73	0.04
70	Area 2	-0.31	-0.98	0.09	Area 12	-0.32	-1.00	0.08
80	Area 2	-0.26	-0.79	0.13	Area 12	-0.33	-0.97	0.07
90	Area 2	-0.17	-0.75	0.19	Area 12	-0.30	-1.11	0.07
100	Area 2	-0.23	-0.66	0.14	Area 12	-0.32	-1.17	0.09
110	Area 2	-0.21	-0.65	0.11	Area 12	-0.28	-1.00	0.24
120	Area 2	-0.19	-0.59	0.26	Area 12	-0.23	-1.14	0.24
130	Area 2	-0.21	-0.60	0.09	Area 12	-0.18	-1.05	0.43
140	Area 2	-0.22	-0.61	0.09	Area 12	-0.14	-0.90	0.91
150	Area 2	-0.24	-0.67	0.07	Area 12	-0.10	-1.22	0.76
160	Area 2	-0.24	-1.14	0.13	Area 12	-0.02	-0.88	1.10
170	Area 2	-0.25	-0.91	0.12	Area 12	0.02	-0.79	1.21
180	Area 2	-0.21	-0.78	0.15	Area 12	0.05	-0.77	1.31
190	Area 2	-0.26	-0.97	0.16	Area 12	0.04	-0.75	1.48
200	Area 2	-0.24	-0.89	0.13	Area 12	0.11	-0.54	2.15
210	Area 2	-0.21	-1.14	0.27	Area 12	0.19	-0.58	1.47
220	Area 2	-0.19	-0.81	0.25	Area 12	0.21	-0.47	1.70
230	Area 2	-0.20	-1.00	0.22	Area 12	0.16	-0.49	1.48
240	Area 2	-0.19	-0.79	0.37	Area 12	0.13	-0.89	1.37
250	Area 2	-0.18	-0.76	0.32	Area 12	0.09	-0.61	1.08
260	Area 2	-0.15	-0.83	0.64	Area 12	0.06	-0.98	1.11
270	Area 2	-0.13	-1.22	0.50	Area 12	0.02	-0.88	1.05
280	Area 2	-0.13	-1.07	0.86	Area 12	-0.07	-0.93	0.85
290	Area 2	-0.16	-1.10	0.47	Area 12	-0.19	-1.02	0.52

Wind Direction	Areas	Mean Cp	Min Cp	Max Cp	Areas	Mean Cp	Min Cp	Max Cp
300	Area 2	-0.20	-1.84	0.60	Area 12	-0.26	-0.87	0.24
310	Area 2	-0.19	-1.75	0.67	Area 12	-0.27	-1.06	0.23
320	Area 2	-0.13	-1.73	0.77	Area 12	-0.25	-1.05	0.12
330	Area 2	-0.07	-1.57	1.07	Area 12	-0.22	-0.69	0.07
340	Area 2	-0.05	-1.44	0.93	Area 12	-0.24	-1.01	0.06
350	Area 2	-0.04	-1.60	0.91	Area 12	-0.22	-0.88	0.10
360	Area 2	-0.07	-1.45	1.04	Area 12	-0.19	-0.79	0.16
10	Area 3	-0.31	-1.32	0.10	Area 13	-0.18	-0.61	0.26
20	Area 3	-0.29	-0.97	0.16	Area 13	-0.20	-0.61	0.11
30	Area 3	-0.29	-0.92	0.11	Area 13	-0.22	-0.71	0.10
40	Area 3	-0.28	-0.77	0.10	Area 13	-0.26	-0.79	0.11
50	Area 3	-0.24	-0.73	0.19	Area 13	-0.30	-0.99	0.02
60	Area 3	-0.20	-0.63	0.27	Area 13	-0.33	-0.82	0.03
70	Area 3	-0.16	-0.71	0.18	Area 13	-0.37	-1.37	-0.01
80	Area 3	-0.13	-0.54	0.23	Area 13	-0.38	-1.22	0.03
90	Area 3	-0.09	-0.86	0.26	Area 13	-0.35	-1.41	0.02
100	Area 3	-0.14	-0.60	0.23	Area 13	-0.38	-1.20	0.01
110	Area 3	-0.19	-0.69	0.23	Area 13	-0.36	-1.37	0.12
120	Area 3	-0.25	-1.01	0.22	Area 13	-0.34	-1.26	0.20
130	Area 3	-0.33	-1.02	0.04	Area 13	-0.30	-1.36	0.41
140	Area 3	-0.36	-1.11	0.00	Area 13	-0.24	-1.34	0.51
150	Area 3	-0.41	-1.45	-0.03	Area 13	-0.17	-1.49	0.54
160	Area 3	-0.46	-1.56	-0.05	Area 13	-0.09	-1.10	0.84
170	Area 3	-0.48	-1.70	-0.03	Area 13	-0.06	-1.02	0.75
180	Area 3	-0.54	-1.70	-0.06	Area 13	-0.04	-0.94	0.88
190	Area 3	-0.64	-2.33	-0.16	Area 13	-0.06	-0.99	0.92
200	Area 3	-0.66	-2.00	-0.08	Area 13	-0.03	-0.86	1.20
210	Area 3	-0.66	-1.89	-0.12	Area 13	-0.03	-0.74	0.94
220	Area 3	-0.57	-2.26	-0.05	Area 13	-0.05	-0.80	1.01
230	Area 3	-0.47	-1.80	0.20	Area 13	-0.09	-1.22	0.77
240	Area 3	-0.33	-1.73	0.23	Area 13	-0.09	-1.10	0.72
250	Area 3	-0.22	-1.37	0.29	Area 13	-0.10	-0.82	0.57
260	Area 3	-0.17	-1.20	0.31	Area 13	-0.11	-0.73	0.43
270	Area 3	-0.14	-1.06	0.44	Area 13	-0.13	-0.82	0.51
280	Area 3	-0.13	-0.84	0.67	Area 13	-0.15	-0.85	0.30
290	Area 3	-0.15	-0.82	0.42	Area 13	-0.20	-0.83	0.19
300	Area 3	-0.21	-1.48	0.42	Area 13	-0.23	-0.92	0.19

Wind Direction	Areas	Mean Cp	Min Cp	Max Cp	Areas	Mean Cp	Min Cp	Max Cp
310	Area 3	-0.26	-1.33	0.36	Area 13	-0.23	-0.82	0.16
320	Area 3	-0.29	-1.63	0.22	Area 13	-0.20	-0.77	0.21
330	Area 3	-0.30	-1.60	0.24	Area 13	-0.18	-0.99	0.26
340	Area 3	-0.33	-1.44	0.14	Area 13	-0.19	-0.76	0.31
350	Area 3	-0.34	-1.41	0.21	Area 13	-0.18	-0.58	0.26
360	Area 3	-0.33	-1.56	0.17	Area 13	-0.18	-0.63	0.23
10	Area 4	-0.37	-1.63	0.10	Area 14	-0.15	-0.65	0.30
20	Area 4	-0.40	-2.13	0.22	Area 14	-0.16	-0.56	0.21
30	Area 4	-0.41	-1.69	0.11	Area 14	-0.17	-0.58	0.19
40	Area 4	-0.44	-1.60	0.19	Area 14	-0.19	-0.69	0.22
50	Area 4	-0.45	-2.01	0.17	Area 14	-0.20	-0.70	0.22
60	Area 4	-0.40	-1.50	0.29	Area 14	-0.22	-0.76	0.27
70	Area 4	-0.31	-1.88	0.42	Area 14	-0.21	-0.80	0.21
80	Area 4	-0.22	-1.17	0.41	Area 14	-0.20	-0.59	0.33
90	Area 4	-0.11	-1.14	0.55	Area 14	-0.15	-0.63	0.31
100	Area 4	-0.12	-1.13	0.44	Area 14	-0.16	-0.89	0.30
110	Area 4	-0.15	-1.13	0.48	Area 14	-0.15	-0.92	0.47
120	Area 4	-0.21	-1.44	0.40	Area 14	-0.13	-0.77	0.43
130	Area 4	-0.35	-1.60	0.26	Area 14	-0.12	-1.44	0.59
140	Area 4	-0.50	-2.02	0.16	Area 14	-0.11	-1.03	0.53
150	Area 4	-0.65	-2.19	0.09	Area 14	-0.12	-1.50	0.69
160	Area 4	-0.68	-1.98	-0.07	Area 14	-0.14	-1.33	0.66
170	Area 4	-0.67	-2.16	-0.09	Area 14	-0.15	-1.37	0.75
180	Area 4	-0.66	-2.21	-0.13	Area 14	-0.18	-1.60	0.67
190	Area 4	-0.64	-2.29	-0.09	Area 14	-0.25	-1.60	0.39
200	Area 4	-0.46	-2.15	0.00	Area 14	-0.32	-1.74	0.43
210	Area 4	-0.36	-1.39	0.09	Area 14	-0.48	-2.57	0.32
220	Area 4	-0.31	-1.12	0.07	Area 14	-0.55	-3.81	0.23
230	Area 4	-0.25	-1.07	0.19	Area 14	-0.53	-2.59	0.09
240	Area 4	-0.18	-0.95	0.23	Area 14	-0.44	-1.90	0.04
250	Area 4	-0.13	-0.62	0.25	Area 14	-0.36	-1.73	0.07
260	Area 4	-0.09	-0.57	0.32	Area 14	-0.29	-1.70	0.08
270	Area 4	-0.06	-0.94	0.32	Area 14	-0.27	-1.47	0.05
280	Area 4	-0.04	-0.49	0.42	Area 14	-0.23	-1.11	0.04
290	Area 4	-0.04	-0.65	0.34	Area 14	-0.21	-1.05	0.17
300	Area 4	-0.07	-0.50	0.34	Area 14	-0.20	-0.78	0.18
310	Area 4	-0.11	-0.60	0.23	Area 14	-0.19	-0.74	0.27

Wind Direction	Areas	Mean Cp	Min Cp	Max Cp	Areas	Mean Cp	Min Cp	Max Cp
320	Area 4	-0.17	-0.59	0.17	Area 14	-0.17	-0.79	0.28
330	Area 4	-0.22	-0.75	0.15	Area 14	-0.15	-0.83	0.28
340	Area 4	-0.27	-1.05	0.13	Area 14	-0.15	-0.82	0.20
350	Area 4	-0.30	-1.45	0.08	Area 14	-0.16	-0.68	0.23
360	Area 4	-0.33	-1.44	0.11	Area 14	-0.16	-0.72	0.27
10	Area 5	-0.76	-2.55	-0.17	Area 15	-0.15	-0.61	0.26
20	Area 5	-0.83	-2.90	-0.18	Area 15	-0.13	-0.54	0.35
30	Area 5	-0.82	-2.48	-0.10	Area 15	-0.13	-0.66	0.40
40	Area 5	-0.81	-2.91	-0.05	Area 15	-0.13	-0.81	0.47
50	Area 5	-0.74	-2.24	0.01	Area 15	-0.14	-0.68	0.68
60	Area 5	-0.54	-2.34	0.11	Area 15	-0.15	-0.88	0.56
70	Area 5	-0.38	-2.05	0.33	Area 15	-0.12	-1.02	0.83
80	Area 5	-0.25	-1.40	0.46	Area 15	-0.09	-0.86	0.66
90	Area 5	-0.10	-1.03	0.47	Area 15	-0.05	-0.67	0.69
100	Area 5	-0.07	-1.06	0.53	Area 15	-0.06	-0.68	0.70
110	Area 5	-0.07	-1.01	0.58	Area 15	-0.06	-0.73	0.95
120	Area 5	-0.08	-0.75	0.54	Area 15	-0.04	-0.83	0.86
130	Area 5	-0.17	-0.79	0.38	Area 15	-0.03	-0.93	0.93
140	Area 5	-0.25	-0.88	0.28	Area 15	-0.03	-0.97	1.13
150	Area 5	-0.33	-0.87	0.19	Area 15	-0.06	-1.06	0.97
160	Area 5	-0.36	-1.00	0.11	Area 15	-0.10	-1.21	0.75
170	Area 5	-0.36	-1.14	0.15	Area 15	-0.10	-0.90	0.62
180	Area 5	-0.35	-0.89	0.07	Area 15	-0.13	-1.13	0.62
190	Area 5	-0.36	-1.05	0.06	Area 15	-0.19	-1.89	0.44
200	Area 5	-0.26	-1.08	0.14	Area 15	-0.22	-1.35	0.40
210	Area 5	-0.23	-0.86	0.14	Area 15	-0.31	-1.30	0.41
220	Area 5	-0.21	-0.77	0.21	Area 15	-0.35	-1.77	0.20
230	Area 5	-0.19	-0.81	0.22	Area 15	-0.36	-1.42	0.32
240	Area 5	-0.13	-0.67	0.45	Area 15	-0.33	-1.44	0.22
250	Area 5	-0.09	-0.68	0.36	Area 15	-0.31	-1.38	0.15
260	Area 5	-0.07	-0.64	0.33	Area 15	-0.28	-1.26	0.08
270	Area 5	-0.06	-0.73	0.32	Area 15	-0.26	-1.22	0.27
280	Area 5	-0.06	-0.57	0.32	Area 15	-0.21	-1.05	0.10
290	Area 5	-0.07	-0.83	0.33	Area 15	-0.18	-0.74	0.14
300	Area 5	-0.12	-0.79	0.34	Area 15	-0.16	-0.64	0.32
310	Area 5	-0.19	-0.89	0.19	Area 15	-0.15	-0.62	0.20
320	Area 5	-0.30	-1.21	0.08	Area 15	-0.14	-0.66	0.22

Wind Direction	Areas	Mean Cp	Min Cp	Max Cp	Areas	Mean Cp	Min Cp	Max Cp
330	Area 5	-0.39	-1.16	0.05	Area 15	-0.15	-0.76	0.22
340	Area 5	-0.48	-1.79	-0.04	Area 15	-0.17	-0.75	0.16
350	Area 5	-0.58	-2.12	-0.02	Area 15	-0.17	-0.72	0.21
360	Area 5	-0.68	-2.16	-0.07	Area 15	-0.17	-0.66	0.29
10	Area 6	-0.38	-1.20	-0.02	Area 16	-0.15	-0.71	0.23
20	Area 6	-0.40	-1.23	-0.03	Area 16	-0.16	-0.70	0.24
30	Area 6	-0.40	-1.22	-0.04	Area 16	-0.18	-0.80	0.12
40	Area 6	-0.38	-1.19	0.07	Area 16	-0.21	-0.60	0.23
50	Area 6	-0.34	-1.02	0.04	Area 16	-0.23	-0.79	0.13
60	Area 6	-0.26	-0.92	0.22	Area 16	-0.25	-0.71	0.16
70	Area 6	-0.19	-0.87	0.45	Area 16	-0.23	-0.82	0.12
80	Area 6	-0.14	-0.72	0.48	Area 16	-0.21	-0.70	0.22
90	Area 6	-0.06	-0.59	0.63	Area 16	-0.17	-0.73	0.30
100	Area 6	0.00	-0.68	0.69	Area 16	-0.20	-0.77	0.26
110	Area 6	0.01	-1.08	0.96	Area 16	-0.22	-1.05	0.30
120	Area 6	-0.02	-0.80	0.77	Area 16	-0.28	-1.35	0.27
130	Area 6	-0.09	-1.03	0.63	Area 16	-0.33	-1.44	0.19
140	Area 6	-0.16	-1.20	0.62	Area 16	-0.35	-1.60	0.27
150	Area 6	-0.22	-1.10	0.64	Area 16	-0.39	-1.66	0.22
160	Area 6	-0.27	-1.19	0.53	Area 16	-0.42	-1.90	0.28
170	Area 6	-0.28	-1.54	0.74	Area 16	-0.40	-1.74	0.21
180	Area 6	-0.26	-1.11	0.45	Area 16	-0.36	-2.06	0.26
190	Area 6	-0.24	-1.13	0.71	Area 16	-0.38	-2.25	0.21
200	Area 6	-0.17	-1.46	0.67	Area 16	-0.39	-2.76	0.42
210	Area 6	-0.19	-1.26	0.53	Area 16	-0.50	-2.56	0.24
220	Area 6	-0.15	-1.16	0.63	Area 16	-0.54	-2.63	0.03
230	Area 6	-0.16	-1.16	0.83	Area 16	-0.56	-2.43	-0.04
240	Area 6	-0.17	-1.17	0.66	Area 16	-0.53	-2.34	-0.01
250	Area 6	-0.17	-0.87	0.49	Area 16	-0.50	-1.85	-0.03
260	Area 6	-0.14	-0.86	0.45	Area 16	-0.46	-1.77	-0.04
270	Area 6	-0.13	-0.69	0.42	Area 16	-0.46	-1.53	-0.02
280	Area 6	-0.12	-0.68	0.44	Area 16	-0.41	-1.54	-0.01
290	Area 6	-0.12	-0.61	0.29	Area 16	-0.37	-1.36	0.04
300	Area 6	-0.13	-0.68	0.29	Area 16	-0.38	-1.54	0.05
310	Area 6	-0.16	-0.68	0.19	Area 16	-0.38	-1.38	0.06
320	Area 6	-0.18	-0.77	0.17	Area 16	-0.32	-1.43	0.07
330	Area 6	-0.20	-0.79	0.14	Area 16	-0.27	-1.24	0.08

Wind Direction	Areas	Mean Cp	Min Cp	Max Cp	Areas	Mean Cp	Min Cp	Max Cp
340	Area 6	-0.24	-0.87	0.09	Area 16	-0.27	-1.41	0.11
350	Area 6	-0.29	-1.11	0.05	Area 16	-0.22	-1.17	0.16
360	Area 6	-0.33	-0.98	0.04	Area 16	-0.18	-0.84	0.22
10	Area 7	0.04	-0.63	0.88	Area 17	-0.30	-1.29	0.17
20	Area 7	-0.01	-0.63	0.72	Area 17	-0.29	-0.95	0.24
30	Area 7	-0.06	-0.62	0.60	Area 17	-0.30	-0.87	0.06
40	Area 7	-0.12	-0.89	0.56	Area 17	-0.34	-1.04	0.03
50	Area 7	-0.15	-0.80	0.44	Area 17	-0.33	-0.89	-0.02
60	Area 7	-0.18	-1.00	0.28	Area 17	-0.29	-0.82	0.07
70	Area 7	-0.18	-0.79	0.28	Area 17	-0.25	-0.73	0.10
80	Area 7	-0.17	-0.74	0.25	Area 17	-0.22	-0.72	0.05
90	Area 7	-0.12	-0.56	0.23	Area 17	-0.18	-0.82	0.13
100	Area 7	-0.15	-0.63	0.19	Area 17	-0.23	-0.72	0.10
110	Area 7	-0.15	-0.52	0.20	Area 17	-0.26	-1.06	0.05
120	Area 7	-0.16	-0.53	0.22	Area 17	-0.32	-1.31	0.08
130	Area 7	-0.17	-0.55	0.15	Area 17	-0.42	-1.43	-0.02
140	Area 7	-0.19	-0.68	0.18	Area 17	-0.48	-1.65	-0.04
150	Area 7	-0.19	-0.66	0.14	Area 17	-0.54	-1.79	0.00
160	Area 7	-0.18	-0.71	0.17	Area 17	-0.58	-1.89	-0.12
170	Area 7	-0.20	-0.77	0.21	Area 17	-0.62	-2.07	-0.12
180	Area 7	-0.17	-0.84	0.19	Area 17	-0.63	-2.16	-0.12
190	Area 7	-0.20	-0.80	0.22	Area 17	-0.69	-2.58	-0.14
200	Area 7	-0.17	-0.68	0.20	Area 17	-0.75	-2.66	-0.14
210	Area 7	-0.25	-0.87	0.13	Area 17	-0.81	-2.51	-0.16
220	Area 7	-0.25	-1.02	0.12	Area 17	-0.74	-3.35	-0.01
230	Area 7	-0.29	-0.97	0.07	Area 17	-0.69	-2.56	-0.05
240	Area 7	-0.33	-1.27	0.03	Area 17	-0.59	-2.28	0.01
250	Area 7	-0.38	-1.40	-0.01	Area 17	-0.51	-1.81	0.05
260	Area 7	-0.40	-1.41	0.07	Area 17	-0.43	-1.87	0.07
270	Area 7	-0.37	-1.36	0.35	Area 17	-0.43	-1.84	0.11
280	Area 7	-0.31	-1.57	0.35	Area 17	-0.44	-2.39	0.17
290	Area 7	-0.26	-1.42	0.47	Area 17	-0.45	-2.02	0.16
300	Area 7	-0.21	-1.53	0.75	Area 17	-0.47	-2.68	0.19
310	Area 7	-0.17	-1.46	0.79	Area 17	-0.48	-2.17	0.17
320	Area 7	-0.13	-1.44	0.76	Area 17	-0.46	-2.32	0.12
330	Area 7	-0.09	-1.59	0.77	Area 17	-0.43	-2.03	0.13
340	Area 7	-0.07	-1.04	0.93	Area 17	-0.46	-2.04	0.16

Wind Direction	Areas	Mean Cp	Min Cp	Max Cp	Areas	Mean Cp	Min Cp	Max Cp
350	Area 7	-0.03	-0.95	0.99	Area 17	-0.44	-2.08	0.08
360	Area 7	0.03	-0.90	1.13	Area 17	-0.36	-2.43	0.21
10	Area 8	0.00	-1.20	0.83	Area 18	-0.60	-1.88	-0.10
20	Area 8	-0.01	-1.54	0.98	Area 18	-0.53	-1.65	-0.01
30	Area 8	-0.01	-1.48	0.95	Area 18	-0.51	-1.59	-0.06
40	Area 8	-0.07	-1.84	0.88	Area 18	-0.52	-1.95	0.03
50	Area 8	-0.18	-2.48	0.88	Area 18	-0.48	-1.60	-0.01
60	Area 8	-0.31	-2.17	0.56	Area 18	-0.38	-1.34	0.04
70	Area 8	-0.45	-2.67	0.50	Area 18	-0.31	-1.07	0.08
80	Area 8	-0.49	-2.26	0.32	Area 18	-0.27	-0.82	0.05
90	Area 8	-0.46	-1.89	0.31	Area 18	-0.19	-0.97	0.12
100	Area 8	-0.50	-2.18	0.21	Area 18	-0.25	-0.87	0.11
110	Area 8	-0.47	-2.28	0.08	Area 18	-0.26	-0.89	0.17
120	Area 8	-0.39	-2.09	0.06	Area 18	-0.28	-0.93	0.14
130	Area 8	-0.33	-1.53	0.08	Area 18	-0.31	-1.06	0.09
140	Area 8	-0.29	-1.25	0.09	Area 18	-0.32	-1.48	0.04
150	Area 8	-0.27	-1.10	0.13	Area 18	-0.33	-1.17	0.10
160	Area 8	-0.25	-1.38	0.17	Area 18	-0.32	-0.97	0.06
170	Area 8	-0.25	-1.19	0.13	Area 18	-0.34	-0.99	0.04
180	Area 8	-0.21	-0.85	0.16	Area 18	-0.33	-0.99	0.11
190	Area 8	-0.17	-0.71	0.15	Area 18	-0.36	-1.05	0.09
200	Area 8	-0.14	-0.71	0.20	Area 18	-0.33	-1.05	0.13
210	Area 8	-0.17	-0.69	0.18	Area 18	-0.31	-1.14	0.07
220	Area 8	-0.15	-0.60	0.25	Area 18	-0.29	-1.23	0.15
230	Area 8	-0.15	-0.65	0.14	Area 18	-0.27	-1.01	0.19
240	Area 8	-0.15	-0.52	0.19	Area 18	-0.22	-0.92	0.31
250	Area 8	-0.15	-0.57	0.16	Area 18	-0.16	-1.00	0.28
260	Area 8	-0.15	-0.58	0.10	Area 18	-0.16	-1.06	0.33
270	Area 8	-0.15	-0.60	0.12	Area 18	-0.21	-1.09	0.24
280	Area 8	-0.15	-0.53	0.13	Area 18	-0.29	-1.67	0.27
290	Area 8	-0.15	-0.59	0.13	Area 18	-0.36	-1.63	0.11
300	Area 8	-0.16	-0.82	0.23	Area 18	-0.42	-2.01	0.08
310	Area 8	-0.17	-0.75	0.33	Area 18	-0.47	-2.03	0.05
320	Area 8	-0.16	-0.92	0.34	Area 18	-0.49	-2.08	0.08
330	Area 8	-0.13	-0.67	0.39	Area 18	-0.52	-2.10	0.04
340	Area 8	-0.12	-0.81	0.56	Area 18	-0.61	-2.08	-0.03
350	Area 8	-0.06	-0.71	0.84	Area 18	-0.67	-2.23	-0.04

Wind Direction	Areas	Mean Cp	Min Cp	Max Cp	Areas	Mean Cp	Min Cp	Max Cp
360	Area 8	-0.02	-1.13	1.00	Area 18	-0.65	-2.65	-0.04
10	Area 9	-0.58	-1.75	-0.14	Area 19	-0.45	-1.44	-0.03
20	Area 9	-0.50	-1.52	0.01	Area 19	-0.50	-1.70	0.11
30	Area 9	-0.47	-1.49	0.03	Area 19	-0.54	-1.83	-0.04
40	Area 9	-0.45	-1.51	0.02	Area 19	-0.57	-1.75	0.01
50	Area 9	-0.38	-1.10	0.04	Area 19	-0.60	-2.22	0.13
60	Area 9	-0.29	-1.07	0.10	Area 19	-0.57	-2.47	0.29
70	Area 9	-0.22	-0.76	0.11	Area 19	-0.58	-2.19	0.03
80	Area 9	-0.17	-0.70	0.17	Area 19	-0.57	-2.22	0.03
90	Area 9	-0.11	-0.58	0.19	Area 19	-0.53	-1.94	0.16
100	Area 9	-0.14	-0.53	0.25	Area 19	-0.58	-2.08	0.08
110	Area 9	-0.16	-0.62	0.32	Area 19	-0.60	-2.24	0.01
120	Area 9	-0.18	-0.62	0.33	Area 19	-0.69	-2.63	-0.03
130	Area 9	-0.22	-0.57	0.08	Area 19	-0.81	-3.02	-0.04
140	Area 9	-0.26	-0.73	0.04	Area 19	-0.89	-3.23	-0.15
150	Area 9	-0.29	-0.81	0.02	Area 19	-0.97	-3.47	-0.17
160	Area 9	-0.30	-0.87	0.06	Area 19	-0.88	-2.96	-0.18
170	Area 9	-0.29	-0.78	0.24	Area 19	-0.80	-2.85	-0.13
180	Area 9	-0.29	-0.89	0.17	Area 19	-0.70	-2.84	-0.07
190	Area 9	-0.30	-1.46	0.16	Area 19	-0.55	-1.98	-0.05
200	Area 9	-0.26	-0.93	0.31	Area 19	-0.46	-1.86	-0.03
210	Area 9	-0.27	-0.81	0.21	Area 19	-0.51	-1.95	-0.09
220	Area 9	-0.24	-1.10	0.31	Area 19	-0.45	-1.63	-0.02
230	Area 9	-0.20	-0.78	0.38	Area 19	-0.40	-1.34	0.05
240	Area 9	-0.15	-0.71	0.52	Area 19	-0.36	-1.18	0.01
250	Area 9	-0.11	-0.74	0.45	Area 19	-0.34	-1.27	-0.02
260	Area 9	-0.11	-0.89	0.60	Area 19	-0.29	-0.98	-0.02
270	Area 9	-0.12	-1.19	0.60	Area 19	-0.28	-0.86	0.03
280	Area 9	-0.17	-1.01	0.37	Area 19	-0.28	-0.70	-0.01
290	Area 9	-0.26	-1.68	0.39	Area 19	-0.28	-0.82	-0.03
300	Area 9	-0.40	-1.70	0.20	Area 19	-0.27	-0.63	0.07
310	Area 9	-0.56	-1.90	0.00	Area 19	-0.30	-0.78	-0.04
320	Area 9	-0.68	-1.96	-0.02	Area 19	-0.33	-0.76	-0.01
330	Area 9	-0.73	-2.68	-0.04	Area 19	-0.36	-0.86	-0.02
340	Area 9	-0.81	-2.32	-0.17	Area 19	-0.41	-0.99	-0.08
350	Area 9	-0.80	-2.54	-0.16	Area 19	-0.44	-1.23	-0.04
360	Area 9	-0.69	-2.29	-0.17	Area 19	-0.42	-1.15	0.02

Wind Direction	Areas	Mean Cp	Min Cp	Max Cp	Areas	Mean Cp	Min Cp	Max Cp
10	Area 10	-0.21	-0.62	0.12	Area 20	-0.70	-2.13	-0.21
20	Area 10	-0.20	-0.87	0.14	Area 20	-0.84	-3.25	-0.26
30	Area 10	-0.20	-0.86	0.13	Area 20	-0.90	-2.89	-0.23
40	Area 10	-0.19	-1.01	0.14	Area 20	-0.89	-3.07	-0.13
50	Area 10	-0.18	-0.74	0.18	Area 20	-0.79	-2.74	-0.17
60	Area 10	-0.17	-0.58	0.23	Area 20	-0.61	-2.80	0.24
70	Area 10	-0.15	-0.66	0.33	Area 20	-0.55	-2.11	0.07
80	Area 10	-0.13	-0.71	0.37	Area 20	-0.52	-1.87	-0.01
90	Area 10	-0.11	-0.82	0.27	Area 20	-0.49	-2.08	0.13
100	Area 10	-0.15	-0.83	0.29	Area 20	-0.47	-1.84	0.16
110	Area 10	-0.17	-1.04	0.20	Area 20	-0.49	-2.26	0.19
120	Area 10	-0.19	-0.74	0.21	Area 20	-0.53	-2.12	0.12
130	Area 10	-0.23	-0.94	0.26	Area 20	-0.54	-2.12	0.35
140	Area 10	-0.25	-1.00	0.35	Area 20	-0.54	-2.31	0.15
150	Area 10	-0.25	-0.90	0.40	Area 20	-0.56	-2.13	0.03
160	Area 10	-0.21	-1.43	0.74	Area 20	-0.50	-1.85	-0.06
170	Area 10	-0.17	-1.08	0.75	Area 20	-0.42	-1.51	0.12
180	Area 10	-0.14	-1.42	0.78	Area 20	-0.39	-1.45	0.00
190	Area 10	-0.13	-1.39	0.81	Area 20	-0.32	-1.54	0.08
200	Area 10	-0.05	-1.22	0.83	Area 20	-0.29	-0.97	0.15
210	Area 10	-0.07	-1.21	0.84	Area 20	-0.36	-1.25	0.06
220	Area 10	-0.11	-1.69	0.79	Area 20	-0.33	-0.94	0.06
230	Area 10	-0.11	-1.69	0.84	Area 20	-0.31	-0.87	0.12
240	Area 10	-0.10	-1.10	0.77	Area 20	-0.29	-0.85	0.08
250	Area 10	-0.12	-1.07	0.54	Area 20	-0.28	-0.83	0.04
260	Area 10	-0.13	-1.35	0.44	Area 20	-0.25	-0.74	0.06
270	Area 10	-0.15	-0.89	0.36	Area 20	-0.24	-0.79	0.05
280	Area 10	-0.19	-1.04	0.41	Area 20	-0.24	-0.69	0.02
290	Area 10	-0.25	-0.99	0.30	Area 20	-0.24	-0.95	0.02
300	Area 10	-0.29	-1.03	0.14	Area 20	-0.25	-0.96	0.14
310	Area 10	-0.31	-1.49	0.09	Area 20	-0.30	-1.16	0.03
320	Area 10	-0.31	-1.15	0.14	Area 20	-0.35	-1.17	0.02
330	Area 10	-0.31	-1.07	0.17	Area 20	-0.42	-1.25	0.02
340	Area 10	-0.33	-1.16	0.18	Area 20	-0.50	-1.63	-0.09
350	Area 10	-0.29	-0.96	0.09	Area 20	-0.56	-1.78	-0.09
360	Area 10	-0.24	-0.91	0.14	Area 20	-0.59	-1.95	-0.10

BIBLIOGRAPHY

AIR (2002), *Ten Years after Andrew: What Should We be Preparing for Now*, Technical Document_HASR_0208, AIR Worldwide Corporation Special Report.

ASCE (2005), *Minimum Design Loads for Buildings and Other Structures ASCE 7-05*, American Society of Civil Engineers.

ASCE (1999), *Wind Tunnel Studies of Buildings and Structures*, New York, American Society of Civil Engineers.

AME (2005), *Glossary of Meteorology*, http://amsglossary.allenpress.com/glossary/-browse, American Meteorological Society

Aponte, L. (2004), *Measurement, Validation and Dissemination of Hurricane Wind Data*. Department of Civil and Coastal Engineering. Gainsville, University of Florida. Master Thesis.

Banks, D., Meroney, R.N., Sarkar, P.P., Zhao, Z., and Wu, F. (2000), "Flow Visualization of Conical Vortices on Flat Roofs with Simultaneous Surface Pressure Measurement," *Journal of Wind Engineering and Industrial Aerodynamics*, Vol. 84, pp. 65-85.

Bendat, J. S. and Piersol, A.G., (2002), *Random Data: Analysis and Measurements Procedures*, New York, John Wiley and Sons.

Cermak, J. E. (1975), "Application of Fluid Mechanics to Wind Engineering-A Freeman Scholar Lecture," *Journal of Fluids Engineering, ASME*, Vol. 97, pp. 9-38.

Cermak, J. E. (2003), "Wind-tunnel Development and Trends in Applications to Civil Engineering," *Journal of Wind Engineering and Industrial Aerodynamics*, Vol. 91, pp. 355-370.

Chen, M. F. (2000), *Characterization of Wind Pressure Fluctuation on A Gable Roof House*, Department of Civil Engineering, Clemson, SC, Clemson University, Ph.D Dissertation.

Cheung, J. C. K., Holmes, J.D, Melbourne, W.H, Lakshmanan, N., and Bowditch, P. (1997), "Pressure on a 1/10 scale model of the Texas Tech Building," *Journal of Wind Engineering and Industrial Aerodynamics*, Vol. 69-71, pp. 529-538.

Choi, E. C. C. (1978). "Characteristics of Typhoons over the South China Sea," *Journal of Wind Engineering and Industrial Aerodynamics*, Vol. 3, pp. 353-365.

Cochran, L. S. and Cermak, J.E (1992), "Full--scale and Model Cladding Pressures on the Texas Tech University Experimental Building," *Journal of Wind Engineering and Industrial Aerodynamics*, Vol. 1-44; pp. 1589-1600.

Cook, N. J. (2002), "Discussion on: Influence of Incident Wind Turbulence on Pressure Fluctuations near Flat Roof Corners by F.Wu, P.P.Sarkar, K.C.Mehta, A.Zhao," *Journal of Wind Engineering and Industrial Aerodynamics*, Vol. 90, pp. 127-130.

Counihan, J. (1975), "Adiabatic Atmospheric Boundary Layers: A Review and Analysis of Data from the Period 1880-1972". *Atmos Environ.*, vol. 9, pp. 871-905.

Crossett, K. M., Culliton, T.J., Wiley,P.C. and Goodspeed, T.R. (2004), *Population Trends Along the Coastal United States*, National Oceanic and Atmospheric Administration.

Davenport, A. G. (1960), A Rationale for Determination of Design Wind Velocities, *Proc. ASCE 86*.

Davenport, A. G., Surry, D., and Stathopoulos, T. (1978), *Wind Loads on Low-rise Buildings: Final Report of Phase III*, University of West Ontario, Ontario, Canada,.

Dearhart, E. A. (2003), *Comparison of Field and Model Wind Pressure on Residential buildings in Tropical Storm Winds*, Department of Civil Engineering, Clemson University, Clemson, SC, Master Thesis.

Eaton, K. J. and Mayne, J.R (1975), "The Measurement of Wind Pressure on Two-story Houses at Aylesbury," *Journal of Wind Engineering and Industrial Aerodynamics* Vol. 1, pp. 67-109.

FCMP (2005), FCMP House Instrumentation System. *FCMP Website*: http://users.ce.ufl.edu/~fcmp/index.htm

FCMP (2005), FCMP Mobile Tower System. *FCMP Website:* http://users.ce.ufl.edu/~fcmp/index.htm

FEMA (1998), “Hurricane Georges Surpass Hurricane Andrew in Total Number of Disaster Applicant Registrations”, *US Federal Emergency Management Agency*.

Gumley, S. J. (1981), *Tubing Systems for the Measurement of Fluctuating Pressure in Wind Engineering*, University of Oxford, Ph.D Dissertation.

Gumley, S. J. (1983), "Tubing Systems for Pneumatic Averaging of Fluctuating Pressures," *Journal of Wind Engineering and Industrial Aerodynamics*, Vol. 12; pp. 189-228.

Gurley, K. R., Masters, F.J., Prevatt, D.O., and Reinhold, T.A. (2005), “Hurricane Data Collection: FCMP Deployments during the 2004 Atlantic Hurricane Season,” *10th Americas Conference on Wind Engineering*, Louisianan State University, Baton Rouge, Louisiana, USA.

Ho, T. C. E., (1992), *Variability of Low Building Wind Loads*, the University of Western Ontario London, Ontario, Canada, PhD Dissertation.

Ho, T. C. E., Surry, D., Morrish,D., and Kopp, G.A., (2005), "The UWO Contribution to NIST Aerodynamic Database for Wind Loads on Low Buildings: Part I. Archiving Format and Basic Aerodynamic Data," J*ournal of Wind Engineering and Industrial Aerodynamics*, Vol. 93, pp. 1-30.

Holmes, J. D., and Best, J.R., (1981). "An Approach to the Determination of Wind Load Effects on Low-rise Buildings," *Journal of Wind Engineering and Industrial Aerodynamics*, Vol. 7; pp. 273-287.

Holmes, J. D. (1982), *Comparison of Model and Full-scale Tests of the Aylesbury House. International Workshop on Wind Tunnel Modeling Criteria and Techniques in Civil Engineering Applications*, Gaithersburg, MD.

Holmes, J. D. (2001), *Wind Loading on Structures*, London, New York, Spon Press.

Jensen, M., and Franck, N. (1965), Model-Scale Tests in Turbulent Wind. Part II, *Danish Technical Press.*

Jia, Y. (1997), *The Effects of Roughness Element Spacing on Boundary Layer Velocity Profile and Pressure Distributions on a Cube*, Department of Civil Engineering, Clemson University, Clemson, SC, Phd Dissertation.

Jia, Y. and Sill, B. L. (1998), "Pressure on a Cube Embedded in a Uniform Roughness Field of Variable Spacing Desnsity, " *Journal of Wind Engineering and Industrial Aerodynamics*, Vol. 77&78, pp. 491-501.

King, R. O. (2005), “Hurricane Katrina: Insurance Losses and National Capacities for Financing Disaster Risk,” *CRS Report for Congress*.

Klotzbach, P. J. and Gray, W.M. (2006), *Extended Range Forecast of Atlantic Seasonal Hurricane Activity and U.S Landfall Strike Probability for 2006*, Department of Atmospheric Science,Colorado State University, Fort Collins, CO.

Krishna, P. (1995), "Wind Loads on Low Rise Buildings - A review," *Journal of Wind Engineering and Industrial Aerodynamics*, Vol. 54-55, pp. 383-396.

Levitan, M. L., and Mehta, K.C., (1992), "Texas Tech Field Experiments for Wind Loads Part II: Meteorological Instrumentation and Terrain Parameters," *Journal of Wind Engineering and Industrial Aerodynamics*, Vol. 41-44, pp. 1577-1588.

Marshall, R. D. (1977), *The Measurement of Wind Loads on Full-scale Mobile Home*, National Bureau of Standards. Washington, D.C.

Masters, F. J. (2004), *Measurement, Modeling and Simulation of Ground-Level Tropical Cyclone Winds*. Department of Civil and Coastal Engineering, University of Florida, Gainsville, Ph.D Dissertation.

Mehta, K. C., Levitan, M.L, and Iverson, R.E (1992), "Roof Corner Pressures Measured in the Field on a Low Building," *Journal of Wind Engineering and Industrial Aerodynamics*, Vol. 41-44, pp. 181-192.

Melbourne, W. H. (1993), "Turbulence and Leading Edge Phenomena," *Journal of Wind Engineering and Industrial Aerodynamics*, Vol. 49, pp. 45-64.

Michot, B. J. (1999), *Full-Scale Wind Pressure Measurement Utilizing Unobtrusive Absolute Pressure Transducer Technology*, Department of Civil Engineering, Clemson University, Clemson, SC, Master Thesis.

Monin, A. S., and Obukhov, A.M. (1954), "Basic laws of turbulent mixing in the atmosphere near the ground," *Tr. Akad. Nauk.*, SSSR Geophys. Inst., Vol. 24; pp. 1963-1987.

Monroe, J. S. (1996), “Wind Tunnel Modeling of Low Rise Structures in a Validated Open Country Simulation,” Civil Engineering Department, Clemson University, Clemson, SC, Master Thesis.

Oppenheim, A. V. (1999). Discrete-Time Signal Processing. USA, Prentice Hall.

Reinhold, T. A., Ed. (1982), *Wind tunnel modeling for civil engineering applications. International Workshop on Wind Tunnel Modeling for Civil Engineering Applications*, Gaithersburg, Maryland, Cambridge University Press.

Reinhold, T. A. (2005), *Assessing the Performance of Modern Building Codes & Standards in Reducing Hurricane Damage*, Presentation for Meeting of Task Force on Long-Term Solutions For Florida’s Hurricane Insurance Market.

Reinhold, T., Gurley, K and Buzbee, T. (2000), "Florida Coastal Monitoring Program: Home Instrumentation Project and Wind Field Monitoring”. *National Hurricane Conference*, New Orleans, LA.

Reinhold, T. A., Dearheart, E.A., Gurley, K., and Prevatt, D.O. (2005), “Wind Loads on Low-rise Buildings: Is one Set of Pressure Coefficients Sufficient for All Types of Terrain”, *International Structures and Wind Effects Conference*, Seoul, Korea.

Richardson, G. M., and Surry.D (1992), "The Silsoe building: A Comparison of Pressure Coefficients and Spectra at Model and Full-scale," *Journal of Wind Engineering and Industrial Aerodynamics*, Vol. 41-44, pp. 1653-1664.

Richardson, G. M., and Blackmore, P.A. (1995), "The Silsoe building: Comparison of 1:100 Model-scale Data with Full-scale Data, " *Journal of Wind Engineering and Industrial Aerodynamics*, Vol. 57, pp. 191-201.

Richardson, G. M. R., A.P. , Hoxey, R.P. and Surry, D. (1990), "Full-scale and Model Investigations of Pressures on An Industrial/Agricultural building," *Journal of Wind Engineering and Industrial Aerodynamics*, Vol. 36, pp. 1053–1062.

Robertson, A. P. (1992), "The Wind-Induced Response of A Full-Sscale Portal Framed Building," *Journal of Wind Engineering and Industrial Aerodynamics*, Vol. 41-44, pp. 1677-1688.

Scanivalve Corporation (2004), *The Manuel of RAD3200 System*, Scanivalve Corporation.

Scanivalve Corporation (2004), *The Manuel of ZOC33/64Px Electronic Pressure Scanning Module*, Scanivalve Corporation.

Sill, B. L., Cook, N. J. and Blackmore, P. A. (1989), "IAWE Aylesbury Comparative Experiment Preliminary Results of Wind tunnel Comparisons,” *Journal of Wind Engineering and Industrial Aerodynamics*, Vol. 32, pp. 285-302.

Sill, B. L., Cook, N. J. and Fang, C. (1992), "The Aylesbury Comparative Experiment: A Final Report," *Journal of Wind Engineering and Industrial Aerodynamics*, Vol. 41-44, pp. 1553-1564.

Simiu, E., and Scalan, R.H. (1992), *Wind Effects on Structures*, New York, John Wiley and Sons.

Smith, T.L., (2005), *The Hurricanes of 2004: An Overview of FEMA's Findings and Recommendations for Roof System Performance*, Professional Roofing Magazine.

Sparks, P. R., Schiff, S.D., and Reinhold, T.A. (1994), "Wind Damage to Envelopes of Houses and Consequent Insurance Losses," *Journal of Wind Engineering and Industrial Aerodynamics*, Vol. 53, pp. 145-155.

St. Pierre, L. M., Kopp, G.A., Surry, D., and Ho, T.C.E (2005), "The UWO Contribution to the NIST Aerodynamic Database for Wind Loads on Low Buildings: Part 2.

Comparison of Data with Wind Load Provisions," *Journal of Wind Engineering and Industrial Aerodynamics*, Vol. 93(n1), pp. 31-59.

Stathopoulos, T. (1979), *Turbulent Wind Action on Low-rise Buildings*, the University of Western Ontario, London, Ontario, Canada, PhD Dissertation.

Stathopoulos, T. (1984), "Wind Loads on Low-rise Buildings: State of the Art " *Engineering Structures*, Vol. 6, pp. 119-135.

Stathopoulos, T., and Saathoff, P. J. (1991), "Wind Pressure on Roofs of Various Geometries", *Journal of Wind Engineering and Industrial Aerodynamics*, Vol. 38, pp. 273-284.

Surry, D., and Stathopoulos, T. (1977), "An Experimental Approach to the Economical Measurement of Spatically-averaged Wind Loads," *Journal of Wind Engineering and Industrial Aerodynamics*, Vol. 2, pp. 385-397.

Surry, D. (1991a). "Pressure Measurements on the Texas Tech Buildings: Wind Tunnel Measurements and Comparisons with Full Scale." Journal of Wind Engineering and Industrial Aerodynamics, vol.38; pp.235-247.

Surry, D. (1991b), Wind Tunnel Simulation of the Texas Tech Building, *The Eighth International Conference on Wind Engineering*, University of Western Ontario, London, Canada.

Surry, D. (1999), “Wind Loads on Low-Rise Buildings: Past, Present and Future,” *10th International Conference on Wind Engineering*, Copenhagen, Denmark.

Ang, A.H.-S. and Tang, W.H. (1975), *Probability Concepts in Engineering Planning and Design*, New York, Wiley.

Tieleman, H. W. (1991), "Wind Tunnel Simulation of Surface Layer Flow for the Prediction of Wind Loads on Low-rise Structures," *Journal of Wind Engineering and Industrial Aerodynamics*, Vol. 38, pp. 151-160.

Tieleman, H. W., Reinhold, T.A, and Melbourne, W.H (1997), "Importance of Turbulence for the Prediction of Surface Pressure on Low-rise Structures," *Journal of Wind Engineering and Industrial Aerodynamics*, Vol. 69-71, pp. 519-528.

Tieleman, H. W., Hajj, M.R, and Reinhold, T.A (1998), "Wind Tunnel Simulation Requirements to Assess Wind Loads on Low-rise Buildings," *Journal of Wind Engineering and Industrial Aerodynamics*, Vol. 74-76, pp. 675-685.

Tieleman, H. W. (2003), "Wind Tunnel Simulation of Wind Loading on Low-rise Structures: A Review," *Journal of Wind Engineering and Industrial Aerodynamics*, Vol. 91, pp. 1627-1649.

Uematsu,Y., and Isyumov, N., (1998), "Peak Gust Pressures Acting on the Roof and Wall Edges of a Low-rise Building," *Journal of Wind Engineering and Industrial Aerodynamics*, Vol. 77-78, pp. 217-231.

Uematsu,Y., and Isyumov, N., (1999), "Review-Wind Pressure Acting on Low-rise Buildings," *Journal of Wind Engineering and Industrial Aerodynamics*, Vol. 82, pp. 1-25.

Vickery, P. J. (1984), *Wind Loads on the Aylesbury Experiment House: A Comparison Between Full Scale and Two Different Scale Models*, University of Western Ontario, London, Ontario, Canada, Master Thesis.

Vickery, P. J., Skerlj, P.F., Steckley, A.C., and Twisdale, L.A (2000), "Hurricane Wind Field Model for Use in Hurricane Simulation," *Journal of Wind Engineering and Industrial Aerodynamics*, Vol. 126, pp. 1203-1221.

von Karman, T., " Progress in the Statistical Theory of Turbulence", *Proc. Nat. Acad. Sci.*, Washington, DC (1948), 530-539